



Asphalt Research Consortium

Quarterly Technical Progress Report October 1-December 31, 2010

January 2011

Prepared for
Federal Highway Administration
Contract No. DTFH61-07-H-00009

By
Western Research Institute
Texas A&M University
University of Wisconsin-Madison
University of Nevada-Reno
Advanced Asphalt Technologies

www.westernresearch.org
www.ARC.unr.edu

TABLE OF CONTENTS

INTRODUCTION	1
GENERAL CONSORTIUM ACTIVITIES	3
PROGRAM AREA: MOISTURE DAMAGE.....	5
Category M1: Adhesion.....	5
Category M2: Cohesion.....	17
Category M3: Aggregate Surface	18
Category M4: Modeling.....	19
Category M5: Moisture Damage Prediction System	24
PROGRAM AREA: FATIGUE.....	27
Category F1: Material and Mixture Properties	27
Category F2: Test Method Development.....	46
Category F3: Modeling.....	65
PROGRAM AREA: ENGINEERED MATERIALS.....	87
Category E1: Modeling.....	87
Category E2: Design Guidance.....	106
PROGRAM AREA: VEHICLE-PAVEMENT INTERACTION.....	139
Category VP1: Workshop.....	139
Category VP2: Design Guidance.....	139
Category VP3: Modeling.....	143
PROGRAM AREA: VALIDATION.....	159
Category V1: Field Validation.....	159
Category V2: Accelerated Pavement Testing.....	160
Category V3: R&D Validation	161
PROGRAM AREA: TECHNOLOGY DEVELOPMENT.....	171
PROGRAM AREA: TECHNOLOGY TRANSFER.....	173
Category TT1: Outreach and Databases	173

INTRODUCTION

This document is the Quarterly Report for the period of October 1 to December 31, 2010 for the Federal Highway Administration (FHWA) Contract DTFH61-07-H-00009, the Asphalt Research Consortium (ARC). The Consortium is coordinated by Western Research Institute with partners Texas A&M University, the University of Wisconsin-Madison, the University of Nevada Reno, and Advanced Asphalt Technologies.

The Quarterly Report is grouped into seven areas, Moisture Damage, Fatigue, Engineered Paving Materials, Vehicle-Pavement Interaction, Validation, Technology Development, and Technology Transfer. The format of the report is based upon the Research Work Plan that is grouped by Work Element and Subtask.

This Quarterly Report summarizes the work accomplishments, data, and analysis for the various Work Elements and Subtasks. This report is being presented in a brief summary form. Please note that in many cases the report is briefer than in the past at the request of FHWA AOTR Mr. Eric Weaver. The Quarter of October 1 to December 31, 2010 is third quarter of the Year 4 contract year. Reviewers may want to reference the Year 4 Work Plan and perhaps the earlier Work Plans. There is also background information regarding the research plan contained in the Revised Year 2 Work Plan. The more detailed information about the research such as approaches to test method development, data collection, and analyses will be reported in research publications as part of the deliverables. All of the Work Plans, as well as many other documents, including quarterly reports, are posted on the ARC website, www.ARC.unr.edu.

SUPPORT OF FHWA AND DOT STRATEGIC GOALS

The Asphalt Research Consortium research is responsive to the needs of asphalt engineers and technologists, state DOT's, and supports the FHWA Strategic Goals and the Asphalt Pavement Road Map. More specifically, the research reported here supports the Strategic Goals of safety, mobility, and environmental stewardship. By addressing the causes of pavement failure and thus determining methods to improve asphalt pavement durability and longevity, this research will provide the motoring public with increased safety and mobility. The research directed at improved use of recycled asphalt pavement (RAP), warm mix asphalt, and cold mix asphalt supports the Strategic Goal of environmental stewardship.

GENERAL CONSORTIUM ACTIVITIES

PROGRESS THIS QUARTER

Asphalt Research Consortium members, Dr. Hussain Bahia, Dr. Elie Hajj, Dr. Eric Kalberer, and Mr. Michael Harnsberger attended the RAP Expert Task Group meeting in Oklahoma City, Oklahoma on October 26 & 27, 2010. An update on the RAP research being conducted by the ARC was presented. In addition to the above ARC members, Dr. Ramon Bonaquist attended the Warm-Mix Technical Working Group meeting being held in conjunction with the RAP ETG on October 27 & 28, 2010.

ARC members Dr. Dallas Little, Dr. Hussain Bahia, Dr. Peter Sebaaly, Dr. Ramon Bonaquist, Dr. Jean-Pascal Planche, and Mr. Michael Harnsberger met on December 20, 2010 to discuss the preparation of the Year 5 Work Plan, the schedule of planned contract deliverables, and the draft Technology Development products. During the meeting, a teleconference was held with the contract AOTR Mr. Eric Weaver of FHWA to discuss the above referenced items.

WORK PLANNED FOR NEXT QUARTER

Several ARC members are planning to attend and make presentations at the 90th Annual TRB Meeting in Washington DC during the week of January 23, 2011. ARC members also participate on TRB committees.

Dr. Jean-Pascal Planche and Dr. Eric Kalberer from WRI are planning on attending the Annual Association of Modified Asphalt Producers (AMAP) meeting in Kansas City, Missouri on February 15 – 17, 2011.

Several ARC members will attend and make presentations at the Binder, Mix & Construction, and Fundamental Properties & Advanced Models ETG meetings in Phoenix, Arizona during the week of March 14 – 18, 2011.

ARC members are planning to attend and participate in the Annual Association of Asphalt Paving Technologists (AAPT) meeting in Tampa, Florida on March 27 – 30, 2011.

Dr. Ramon Bonaquist of Advanced Asphalt Technologies will continue to work with Mr. Frank Fee of NuStar Energy to coordinate sampling of materials for the flow number study requested and approved by the Mixture and Construction ETG.

PROGRAM AREA: MOISTURE DAMAGE

CATEGORY M1: ADHESION

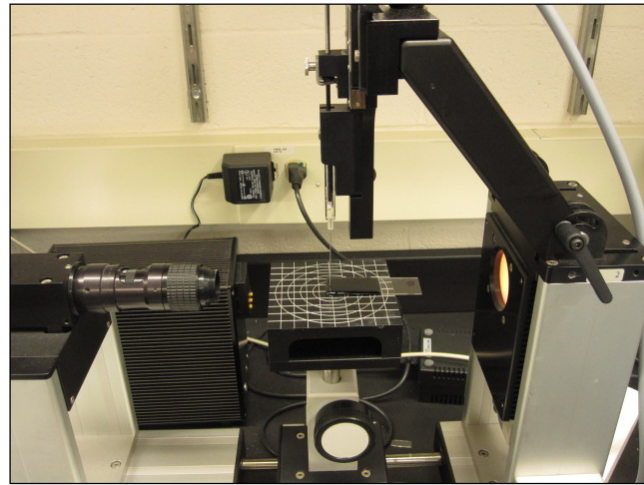
Work Element M1a: Affinity of Asphalt to Aggregate (UWM)

Work Done This Quarter

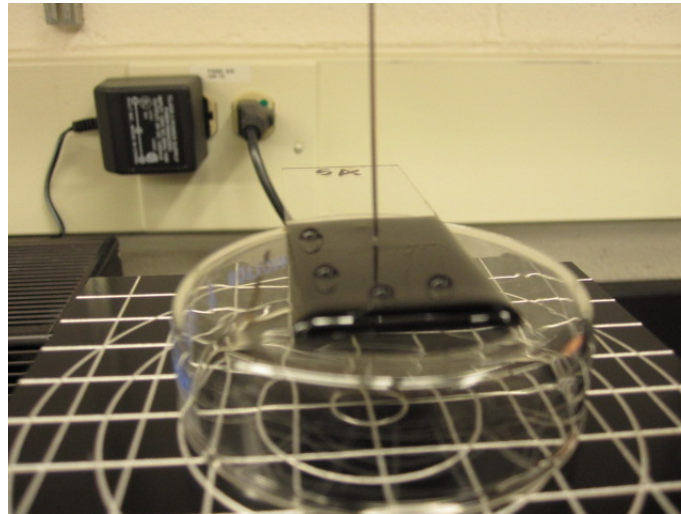
This quarter the research team explored the use of the sessile drop method to measure contact angle of asphalt binders and aggregates. Measurements of the contact angle at the surface of the binders and aggregates with three different liquids, with known surface energy, will allow for the estimation of surface energy. Efforts were focused on the development of an appropriate procedure for reliable contact angle measurements. Thus far, the team has used only distilled water for contact angle measurements, and future work will include the use of other liquids with known surface energy. Figure M1a.1 shows binders and aggregate samples and the equipment used for contact angle testing.



(a)



(b)



(c)

Figure M1a.1. Photographs. Contact angle testing: (a) binder and aggregate samples for sessile drop testing; (b) sessile drop test device; and (c) zoom-in of sessile drop testing of binders.

The materials used for sessile drop testing are described in table M1a.1. Two aggregate surfaces as well as two neat and five modified binders were tested.

Table M1a.1. Materials used for contact angle testing with sessile drop device.

Solution	Distilled Water
Aggregate	Limestone and Granite
Asphalt Binders	FH 64-22 and CRM 58-28
Modified Asphalt Binders	FH 64-22 + 1% Polyphosphoric Acid (PPA) FH 64-22 + 0.7% Elvaloy + 0.17% PPA CRM 58-28 + 1% PPA CRM 58-28 + 0.7% Elvaloy + 0.17% PPA CRM 58-28 + 2% Linear Styrene-Butadiene-Styrene (LSBS)

Figure M1a.2 shows typical results for binder CRM 58-28 neat and the limestone aggregate. Note that the contact angle is measured from the inside of the drop with respect to the horizontal base line. The contact angle is an indication of the potential wettability of the liquid (i.e., drop) in the surface (e.g., binder or aggregate). The lower the contact angle, the wider is the drop, and thus the better is the wettability of the liquid on that surface.

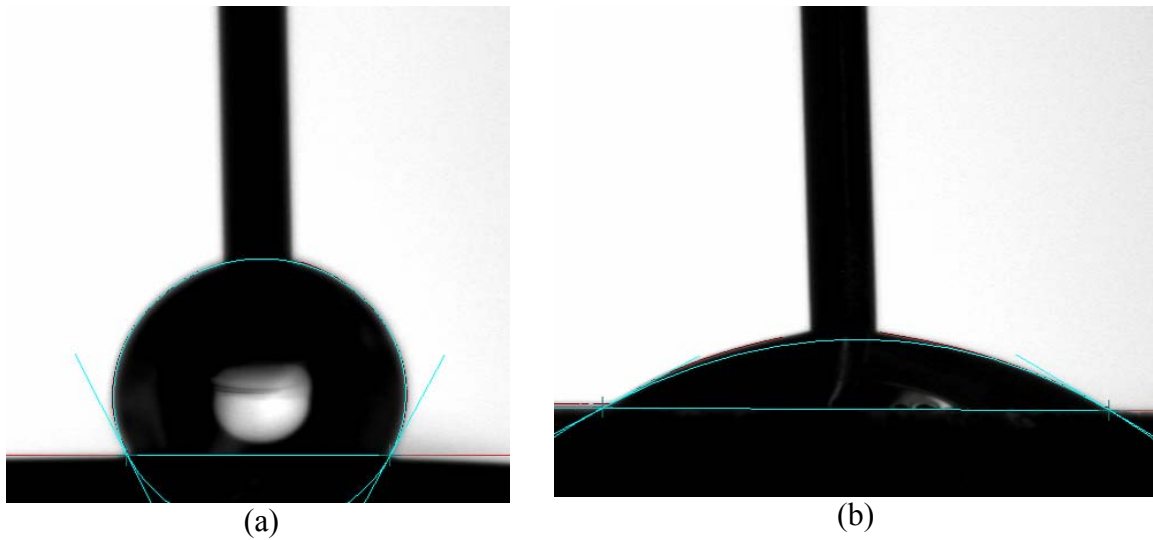


Figure M1a.2. Photographs. (a) Sessile drop testing of binder CRM 58-28 neat with distilled water; and (b) sessile drop testing of limestone with distilled water.

Significant Results

The research team obtained promising results with the sessile drop device. Tables M1a.2 and M1a.3 show the contact angle measurements with distilled water for the asphalt binders and aggregates, respectively. Testing for each material was done with five to 10 replicates (drops) on the same sample to evaluate variability of results. It can be seen that the coefficient of variation (CV) for one sample of material is relatively low for asphalt binders (i.e., < 5%) and acceptable

for aggregates (i.e., < 17%). The variation of the results for the aggregates is expected due to surface heterogeneity (i.e., different minerals).

Table M1a.2. Sessile drop results for asphalt binders.

Contact Angle (°)			
Sample	Average	Std	CV (%)
FH 64-22 Neat	113	1.69	1.49
FH 64-22 + 1% PPA	93	2.54	2.72
FH 64-22 + 0.7% Elvaloy + 0.17% PPA	98	2.39	2.45
CRM 58-28 Neat	117	2.87	2.46
CRM 58-28 + 1% PPA	105	5.95	5.68
CRM 58-28 + 0.7% Elvaloy + 0.17% PPA	106	4.48	4.24
CRM 58-28 + 2% LSBS	106	3.00	2.82

Table M1a.3. Sessile drop results for aggregates.

Contact Angle (°)			
Sample	Average	Std	CV (%)
Granite	65	8.33	12.76
Limestone	32	5.06	16.05

Figure M1a.3 shows a comparison of the results for contact angle of the asphalt binders and aggregates. It can be seen that neat binders have a significantly different contact angle compared to the modified binders. Furthermore, it seems that the addition of PPA increases the potential for wettability of the binders. Contact angle measurements for the aggregate indicate their hydrophilic (i.e., limestone) and hydrophobic (i.e., granite) nature. Lower contact angle with distilled water indicates more affinity of the limestone aggregate for water.

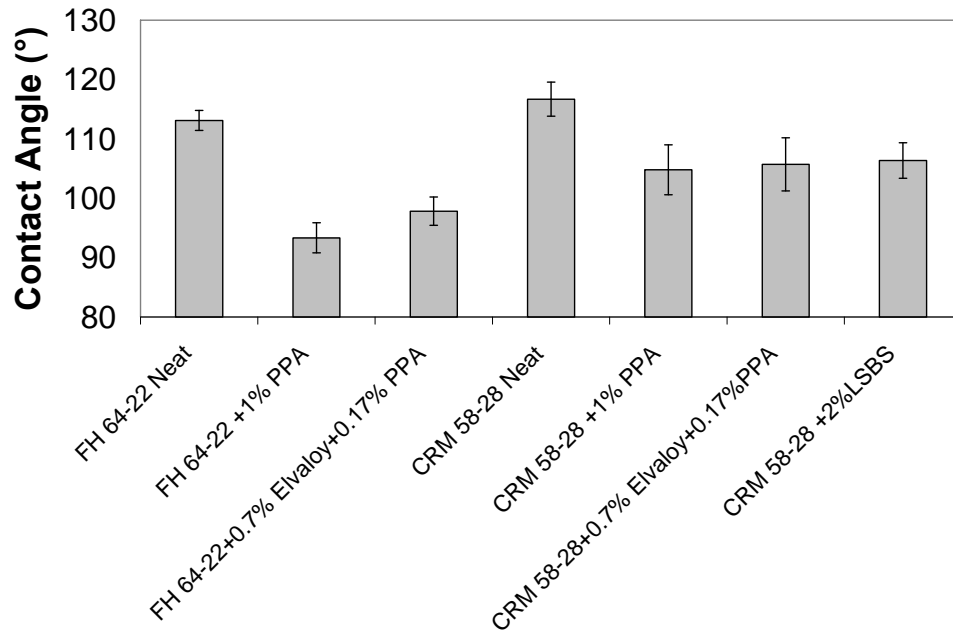


Figure M1a.3. Chart. Contact angle for binders using sessile drop with distilled water.

Significant Problems, Issues and Potential Impact on Progress

None.

Work Planned Next Quarter

Next quarter, efforts will focus on the indirect estimation of surface energy for both binders and aggregates with the contact angle measurements. Three different liquids with known surface energy will be used to estimate free surface energy. These measurements will then be compared with experimental results from the Bitumen Bond Strength (BBS) test to indicate that the BBS can be used as a surrogate test for surface energy measurements.

The research team will also continue working on the validation of the BBS procedure by performing moisture damage tests of mixtures by means of the Tensile Strength Ratio (TSR).

Work Element M1b: Work of Adhesion Based on Surface Energy

Subtask M1b-1: Surface Free Energy and Micro-Calorimeter Based Measurements for Work of Adhesion (TAMU)

Work Done This Quarter

The main goal of this subtask is to provide material property inputs required in other work elements as required. Any data obtained from this subtask will be included in the material properties database. In the last quarter surface free energy of some aggregates and asphalt binders that are being used to develop test methods were measured.

Significant Results

None.

Significant Problems, Issues and Potential Impact on Progress

None.

Work Planned Next Quarter

Work on this subtask will be conducted in conjunction with and as required by other work elements.

Subtask M1b-2: Work of Adhesion at Nano-Scale using AFM (WRI)

Work Done This Quarter

In this quarter we present evidence of stress induced micro-structuring on the fracture plane surface when a chilled asphalt film is mechanically stressed to the point of fracture. AFM images of fractured asphalt surfaces clearly show organized linear arrangements of sub-micron-sized particles, and other distinct features, which occur in repetitive patterns. Microstructure at several scales is observed on the fractured surfaces. Structures are typically organized in essentially parallel linear arrangements with perpendicular branching that is also composed of many parallel segments. The organized structuring observed at the fracture plane is very different from the familiar random “bee-structures” that are often observed on the surface of asphalt films. Even though the samples were fractured at a very low temperature, the fracture surfaces still exhibit characteristics of both ductile and brittle fracture.

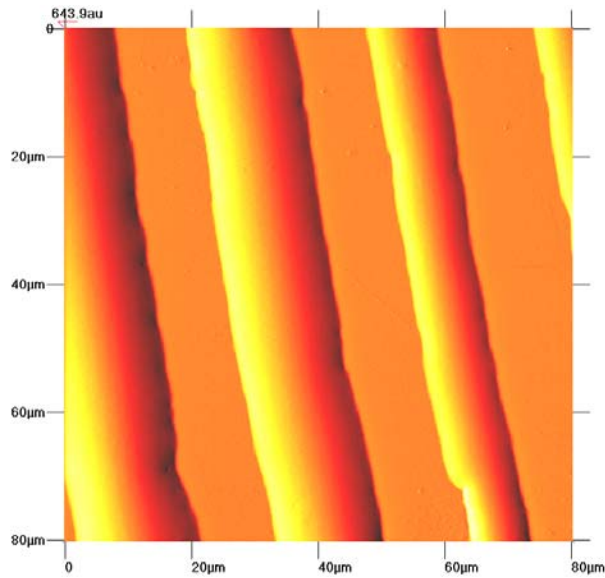
For the experiments reported this quarter glass microscope slides were bonded together with a thin film of asphalt to form a “sandwich” of asphalt between two glass substrates. The “sandwich” samples were then frozen by the application of a few drops of liquid nitrogen to the back of one slide, and the frozen “sandwich” was popped apart with a steady slow pulling motion applied to one of the slides while the other slide was held stationary. “Sandwich” samples were prepared using all eight of the SHRP core asphalts. Samples were prepared by placing a

small spot of asphalt on the center of a clean microscope slide, covering with a second clean slide and then heating in an oven at $\sim 120^{\circ}$ C for about one-half hour with a small weight on top of the stack. The prepared samples had an asphalt film thickness of $\sim 10\text{-}\mu\text{m}$. The samples were cooled to room temperature and stood for at least one hour before being chilled with liquid nitrogen and popped apart. The bond between the chilled “sandwich” components was strong and considerable pressure (unmeasured at this time) was required to fracture the samples. Once fracture was initiated it appeared to be essentially instantaneous.

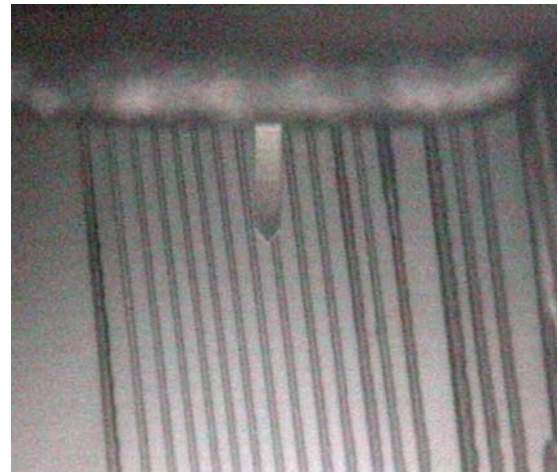
Significant Results

The following AFM images are presented as either “BB Wavemode” (enhanced non-contact topography) or “error” type images (essentially a derivative image that shows topography with better definition at the edges of features).

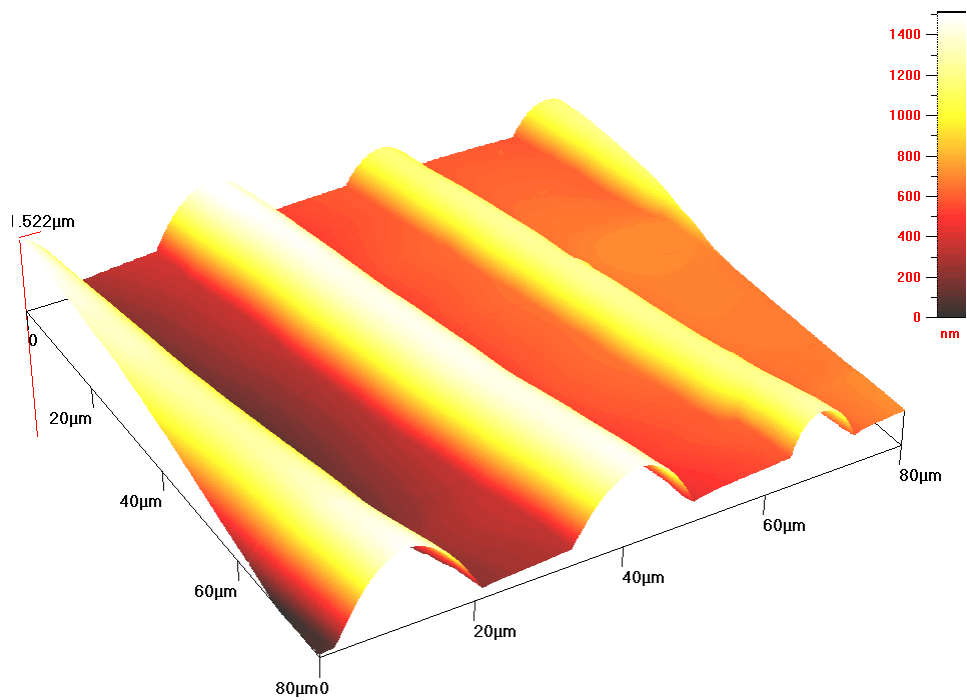
Figure M1b-2.1 shows an $80 \times 80\text{-}\mu\text{m}$ AFM error image, an optical microscope view, and a 3-dimensional rendering of the AFM image of the surface of a freeze/fractured sandwich made with SHRP core asphalt AAD-1. The optical microscope view, upper right, has a field of view that is 1.2-mm in width. The pointed object at the top center in this image is the AFM cantilever. Note that the width this cantilever is $\sim 40\text{-}\mu\text{m}$, which is half the width of the entire AFM image. As can be seen, the relative size and spacing of these bands extends over several length scales. Parallel bands as shown in this figure were evident on all of the freeze fractured samples. The banding typically appears as a comb-like arrangement with the “comb-teeth” diminishing in scale down the length of the comb. The “comb-teeth” at the larger end are of a scale that is easily visible with a low-powered optical microscope while at the opposite end they shrink to obscurity. This banded appearance indicates that the seemingly instantaneous fracture was actually a series of discrete events, and that, even at very low temperature, with a film thickness that is reasonable with respect to use in an asphalt pavement, the asphalt binder still exhibits some flow properties. This type of banded structuring was typically observed at the edge of the thicker material in an area in which the main fracture plane transferred from one glass slide to the other.



AAD-1 AFM 80-µm error image



AAD-1 Optical microscope 1.2-mm image



3-D rendering of AFM error image

Figure M1b-2.1 Parallel banding at different scales on the freeze/fractured surface of SHRP core asphalt AAD-1. Upper left, AFM error image, upper right, optical microscope image with 1.2-mm field of view, bottom, 3-d rendering of AFM image.

Figure M1b-2.2 shows a 40 X 40- μm image of the AAD-1 fracture surface where a similar comb-like arrangement is evident at a much smaller scale. In this image it can be seen that the “comb-teeth” are composed of many small particles with diameters of ~ 100 to 200-nm . Figure M1b-2.3 shows a 40 X 40- μm Wavemode image of the fracture surface of an AAK-1 “sandwich” sample where a similar arrangement of parallel bands is observed. In this figure the back of the comb is represented by a string of particles that extends across the entire image. The individual particles that make up this string appear to be $\sim 100\text{-nm}$ in diameter.

Figures M1b-2.4, M1b-2.5, and M1b-2.6 show 40 X 40- μm images of similar beaded arrangements as seen in freeze/fractured sandwich samples of SHRP core asphalts AAA-1, AAG-1, and AAM-1 respectively. Again we see long linear arrangements of small particles. The Wavemode image shown in figure M1b-2.4 shows particles that are clearly less than 50-nm in diameter arranged across a length of nearly $40\text{-}\mu\text{m}$. Some individual particles and circular arrangements of particles are evident in the lower right quadrant of the figure. Figure M1b-2.6 shows the beginning of the comb-like arrangements and another parallel beaded line (barely visible at the upper right side of the image).

Figure M1b-2.7 shows a 40 X 40- μm image of a freeze/fracture surface of asphalt AAC-1. This image clearly shows that the larger-scaled features are composed of apparently linear arrangements of particles at progressively finer scales. Figure M1b-2.8 shows a number of beaded structures with a more random orientation in a 40 X 40- μm image of a freeze/fracture surface of SHRP core asphalt AAG-1

We believe that images such as those shown in figure M1b-2.1 represent a waveform frozen in time, and that this waveform contains information about time-dependent flow properties associated with a nearly instantaneous fracture event. That is, these images present a mapping of strain localization during the fracture process. Similar patterns of strain localization (often referred to as shear banding) can be observed on the fractured faces of a broad range of ductile and quasi-brittle materials. Analysis of shear banding patterns has been conducted (e.g. Shawki and Clifton 1989, Rosakis et al. 2000) to help understand the phenomenon of strain localization in a variety of viscoplastic materials. Because the fracture event is nearly instantaneous, flow properties of quasi-brittle materials are extremely difficult to measure with more conventional methods. However, the contribution of this flow to the overall fracture energy may be significant even at very low temperatures.

It is well known that asphalts tend to harden as they age, and the chemistry associated with this increase in hardness is fairly well understood. It is also known that asphalts tend to become more brittle as they age. However, the conditions and chemistry associated with embrittlement in an asphalt pavement are much more poorly understood. Analysis of the pattern of localized strain left after the fracture of a chilled asphalt film can provide an important tool for the understanding of fracture damage in this apparently quasi-brittle material. Controlled freeze/fracture tests with subsequent imaging and analysis of the resulting waveform (or shear band pattern) may provide the tool that will allow us to understand the chemistry associated with embrittlement of asphalt pavements. When this chemistry is understood it should become possible to modify asphalt binders to minimize or delay the onset of embrittlement and thus significantly reduce highway degradation associated with cracking of the pavement.

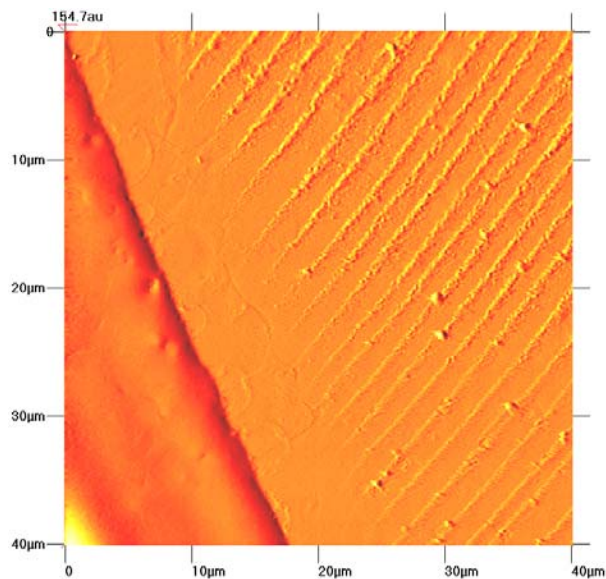


Figure M1b-2.2. AAD-1 freeze/fracture surface.

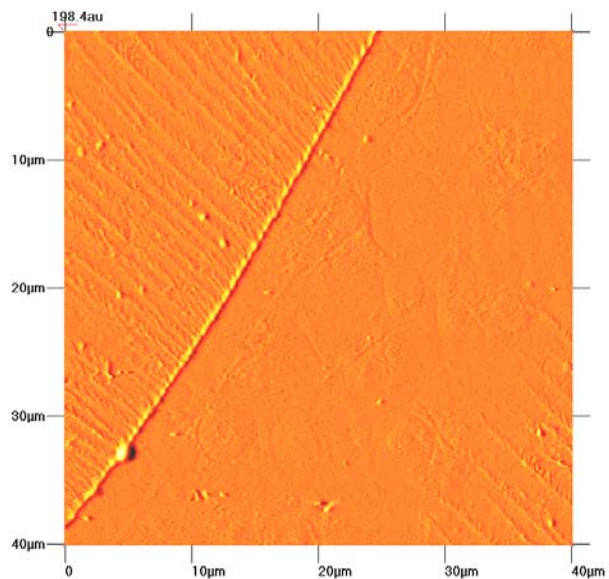


Figure M1b-2.3 AAK-1 freeze/fracture surface.

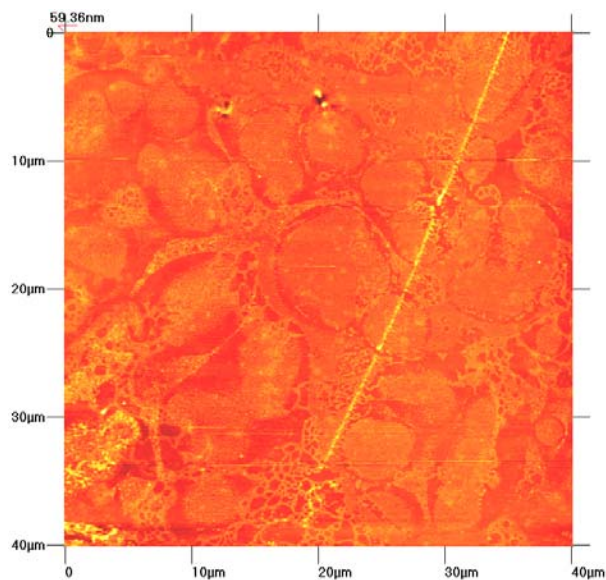


Figure M1b-2.4. AAA-1 freeze/fracture surface.

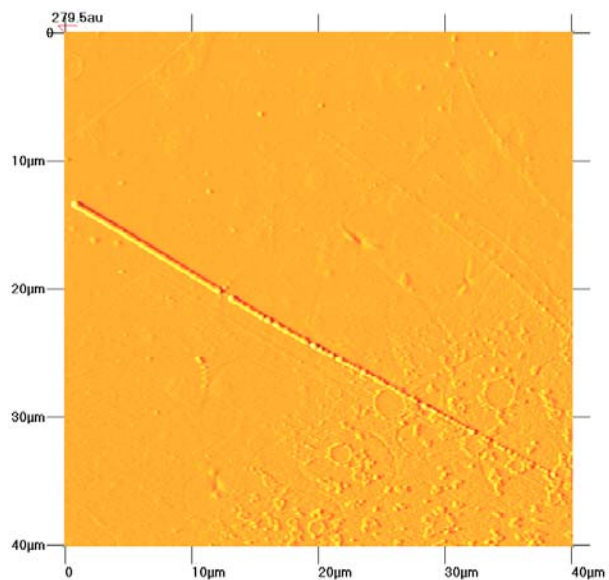


Figure M1b-2.5. AAG-1 freeze/fracture surface.

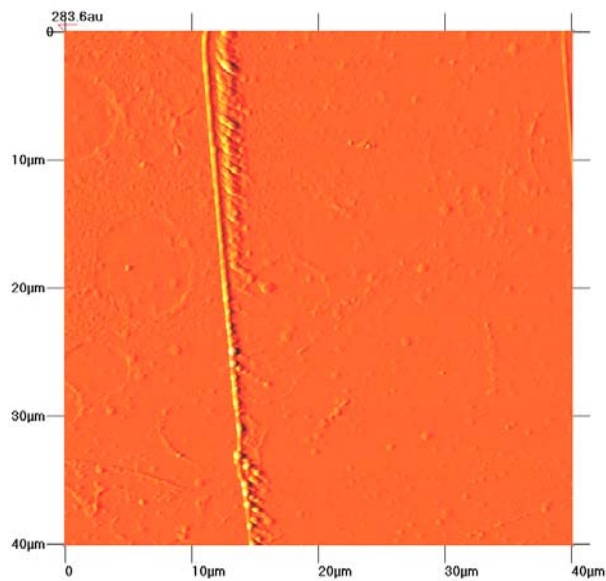


Figure M1b-2.6. AAM-1 freeze/fracture surface.

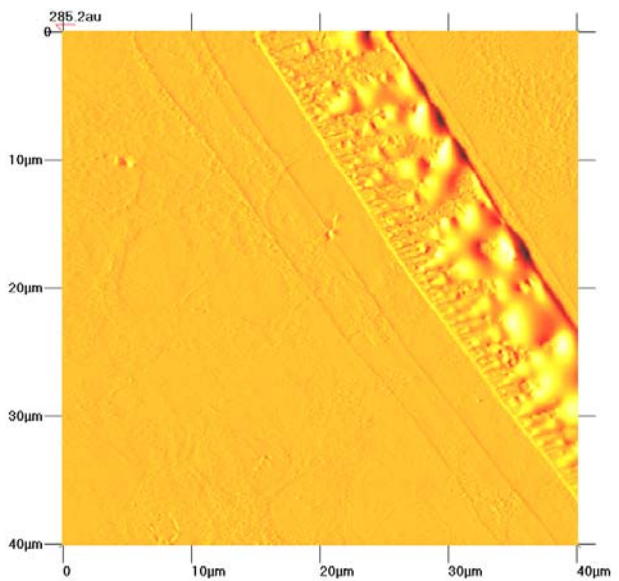


Figure M1b-2.7. AAC-1 freeze/fracture surface.

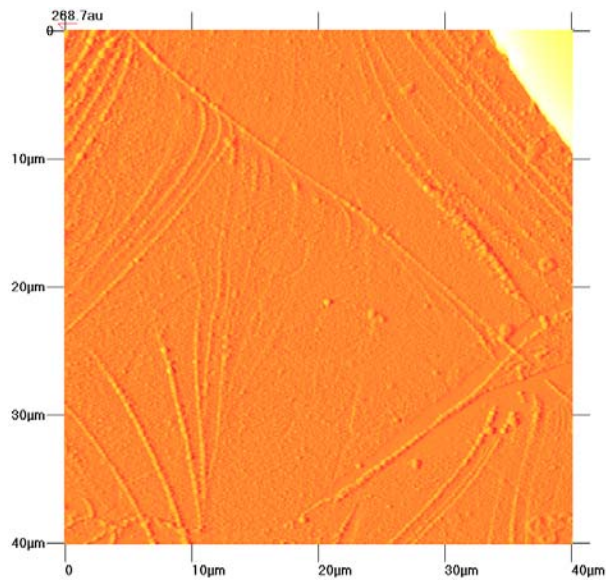


Figure M1b-2.8. AAG-1 freeze/fracture surface.

Significant Problems, Issues and Potential Impact on Progress

We still have not obtained polished aggregate slices that will be used in place of glass substrates for additional adhesion testing.

Work Planned Next Quarter

Experiments conducted this past quarter used a glass substrate as a surrogate for an aggregate surface. Next quarter we hope to obtain specimens of commonly used aggregate materials with different degrees of surface polish and to repeat freeze/fracture experiments using these materials. We plan to begin the design of freeze/fracture experiments in which the sample geometry, temperature, and separating force are carefully controlled. We will also continue the development of nano-rheological techniques which could lead to a much more thorough understanding of the asphalt/aggregate interface.

Cited References

Shawki, T. G., and R. J. Clifton, 1989, "Shear Band Formation in Thermal Viscoplastic Materials", *Mechanics of Materials*, 8, 13-43.

Rosakis, P., A. J. Rosakis, G. Ravichandran, and J. Hodowany, 2000, "A thermodynamic internal variable model for the partition of plastic work into heat and stored energy in metals", *Journal of the Mechanics and Physics of Solids*, 48, 581-607.

Subtask M1b-3: Identify Mechanisms of Competition Between Water and Organic Molecules for Aggregate Surface (TAMU)

Work Done This Quarter

This work element was completed and findings were reported in previous quarterly reports. There was no activity this quarter.

Work Planned Next Quarter

None.

Work Element M1c: Quantifying Moisture Damage Using DMA (TAMU)

Work Done This Quarter

This work element was completed and findings were reported in previous quarterly reports. There was no activity this quarter.

Work Planned Next Quarter

None.

CATEGORY M2: COHESION

Work Element M2a: Work of Cohesion Based on Surface Energy

Subtask M2a-1: Methods to Determine Surface Free Energy of Saturated Asphalt Binders (TAMU)

Work Done This Quarter

No activity was planned for this quarter.

Work Planned Next Quarter

The priority and need for this subtask will be evaluated and discussed in the Year 5 work plan.

Subtask M2a-2: Work of Cohesion Measured at Nano-Scale using AFM (WRI)

Work Done This Quarter

Work which is relevant to this subtask is reported under subtask heading M1b-2 “Work of adhesion at Nano-Scale using AFM”.

Significant Results

Please see results reported for subtask M1b-2.

Significant Problems, Issues and Potential Impact on Progress

None.

Work Planned Next Quarter

Work directed toward developing nano-rheology techniques will continue next quarter.

Work Element M2b: Impact of Moisture Diffusion in Asphalt Mixtures

Subtask M2b-1: Measurements of Diffusion in Asphalt Binders and Mixtures (TAMU)

Subtask M2b-2: Kinetics of Debonding at the Binder-Aggregate Interface (TAMU)

Work Done This Quarter

There was no activity this quarter.

Significant Results

None.

Significant Problems, Issues and Potential Impact on Progress

None.

Work Planned Next Quarter

We have accomplished significant portions of this work element including measurement of diffusion through binders and fine aggregate matrix. Further work will be conducted if prioritized based on the requirements from other work elements.

Work Element M2c: Measuring Thin Film Cohesion and Adhesion Using the PATTI Test and the DSR (UWM)

Most work is completed. The remaining activity is reported under Work Element M1a.

CATEGORY M3: AGGREGATE SURFACE

Work Element M3a: Aggregate Surface Characterization (TAMU)

Work Done This Quarter

This work element was completed and findings were reported in previous quarterly reports. There was no activity this quarter.

CATEGORY M4: MODELING

Work Element M4a: Micromechanics Model (TAMU)

A model for predicting and characterizing fracture damage of asphalt mixtures subject to moisture damage has been developed based on cohesive zone concept. This has been attempted by coupling the effect of moisture diffusion with the mechanical performance of asphalt mixtures by means of two key mechanisms: (1) stiffness reduction of the asphalt matrix (also referred to as fine aggregate matrix(FAM) phase; and (2) deterioration of the mechanical and fracture properties of the matrix-matrix interfaces (i.e., cohesive fracture) and matrix-aggregate interfaces (i.e., adhesive fracture); as a function of the amount of moisture present in the mixture.

In the model, different material constitutions (elastic, linear and nonlinear viscoelastic), mixture microstructure, and cohesive zone fracture characteristics are implemented within a commercial finite element software, *ABAQUS* in the form of UMAT (User MATerial) and UEL (User ELement), which is intended to simulate material-specific, nonlinear-inelastic microscale fracture and its propagation to complete failure incorporated with moisture damage in asphaltic composites with maximum versatility.

Work Done This Quarter

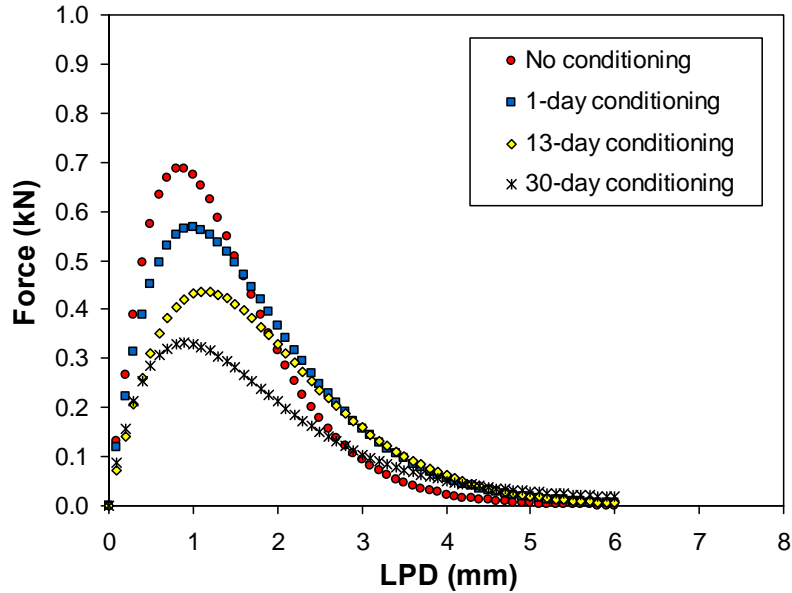
During this quarter we have mainly progressed validation of the model. Fracture test results of semi-circular bend (SCB) specimens with several different levels of moisture conditioning were incorporated with numerical simulations of the SCB fracture tests using sequentially coupled moisture diffusion-mechanical analysis. This provided moisture-dependent fracture characteristics of asphalt mixtures and resulting degradation characteristics of mixture properties (stiffness, cohesive zone strength, and cohesive zone fracture energy) due to moisture damage. The degradation characteristics of mixture properties were then applied to simulation of asphalt mixtures subjected to an arbitrary level of moisture saturation and mechanical loading for model validation. Work progress and significance of each activity can be summarized as follows:

Degradation characteristics due to moisture damage

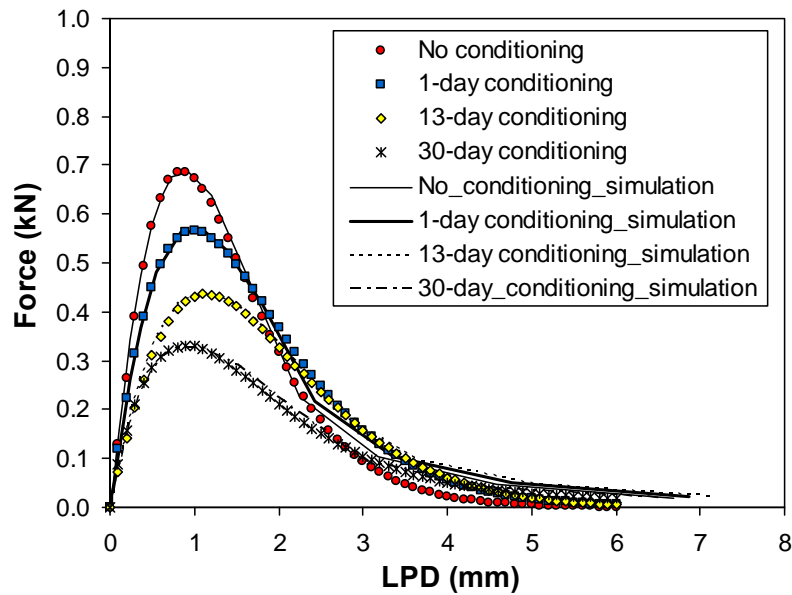
As presented in the last quarterly report, the SCB fracture tests were conducted with several different moisture conditioning levels in a water bath at 25°C. For each case, three SCB specimens were then tested at a constant loading rate: 50 mm/min. Test results in the form of applied force vs. line point displacement (LPD) at different levels of moisture conditioning are presented in figure M4a.1(a). The figure clearly demonstrates that all cases underwent damage due to moisture conditioning, and the level of damage increased as the conditioning time increased, which implies that the moisture infiltration in the specimens is detrimental to the integrity of asphalt mixtures.

The SCB test results were predicted by performing sequentially coupled (i.e., diffusion followed by mechanical loading) finite element (FE) simulations with two FE meshes: one SCB mesh without cohesive zone elements embedded to simulate moisture diffusion and the other SCB mesh whereas zero-thickness cohesive elements were inserted along the center of the mesh to

permit mode I crack growth. Figure M4a.1(b) illustrates a comparison between model simulations and test results plotting the applied load against line point displacements at several different moisture conditioning levels. As shown, model simulations could successfully predict the progressive degradation as the level of moisture damage increased, and generally correlate with the experimental data over the whole process from damage initiation to complete fracture.



(a)



(b)

Figure M4a.1. Force vs. LPD plots: (a) SCB test results; (b) SCB test results compared to FE simulations.

Good agreement between the modeling and testing resulted in material properties (i.e., mixture stiffness, cohesive zone strength, and cohesive zone fracture energy) that are degraded due to moisture conditioning. The three material properties identified at each level of moisture conditioning are presented in figure M4a.1. The degradation of material properties due to moisture saturation can then be formulated by equation M4a.1. The equation represents how the material property degrades as the level of saturation evolves by simply relating the normalized material property to the normalized value of moisture saturation through the exponential relationship.

$$\frac{\Omega_{wet}^o}{\Omega_{dry}^o} = \exp \left[-k \left(\frac{\phi}{\phi_{sat}} \right)^n \right] \quad (M4a-1)$$

where Ω_{dry}^o = any material property affected by moisture at unconditioned (dry) stage,
 Ω_{wet}^o = any material property affected by moisture at certain saturation level (wet),
 ϕ = a certain saturation level,
 ϕ_{sat} = fully saturated level, and
 k and n = model parameters.

The model parameter k -value in the equation represents the remaining property of sample at the stage of the complete saturation. Another model parameter, the exponent n -value, determines the shape of degrading trend. As the n -value decreases, samples lose the property at an early stage in a more sensitive manner than the case with a higher n -value. Thus, the two model parameters can be used as indicators to quantitatively assess the sensitivity to the presence of water in the asphalt mixtures. Figure M4a.2 also presents degradation curves of individual properties fitted by equation M4a.1.

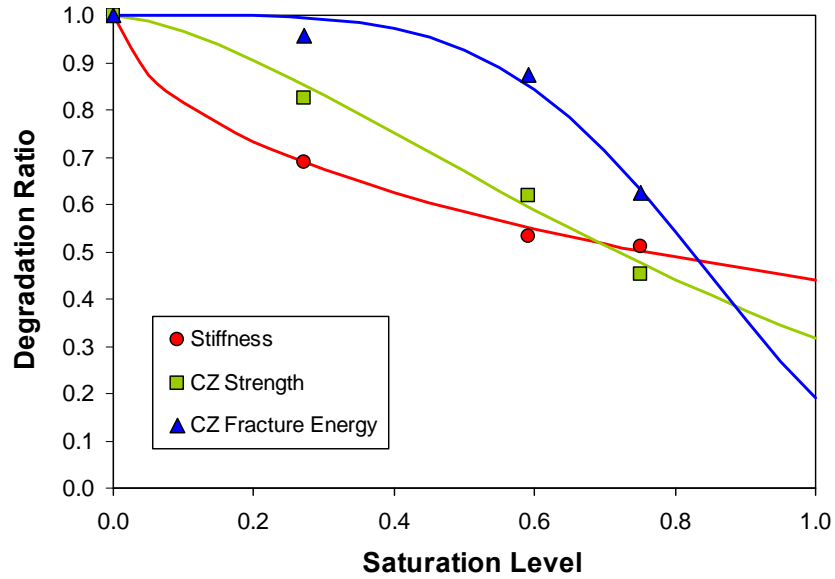


Figure M4a.2. Material properties degraded due to moisture conditioning.

Model validation

Using the moisture-dependent degradation characteristics of the mixture, model validation was conducted with SCB test results at an arbitrary level of moisture saturation (7-day conditioning) and SCB mechanical loading. The diffusion coefficient of the mixture and the degradation characteristic model parameters (i.e., k and n values) of individual material properties were applied to the validation. As shown in figure M4a.3, model simulation shows a good agreement with experimental data, which implies that the proposed sequentially coupled modeling approach incorporated with the degradation function can successfully predict the progressive damage behavior of asphalt mixtures when moisture damage is involved.

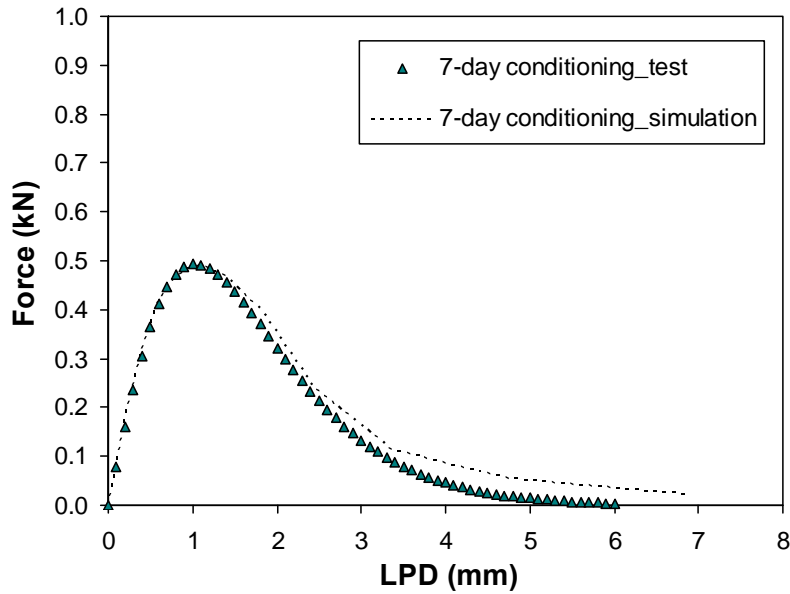


Figure M4a.3. Comparison between experimental result and model simulation.

Significant Problems, Issues and Potential Impact on Progress

None.

Work Planned Next Quarter

In the next quarter we will work on the following activities:

- Microstructure modeling of asphalt mixtures with moisture damage through the sequentially coupled moisture diffusion-mechanical analysis.
- Parametric analyses of the microstructure model incorporated with moisture damage characteristics.

Work Element M4b: Analytical Fatigue Model for Mixture Design (TAMU)

This work is addressed under Work Element F2b.

Work Element M4c: Unified Continuum Model (TAMU)

Work Done This Quarter

We developed thermodynamic framework for deriving constitutive equations for asphaltic materials by including moisture-induced damage effects. We used this thermodynamic

framework to derive constitutive equations that takes more complicated physical mechanisms that occur during moisture-induced damage. We also developed a systematic procedure for identifying the material parameters associated with the constitutive models based on well-designed experiments at TAMU. The experiments include moisture conditioned pull-off tests on mastic-aggregate systems using the materials from the ARC 2x2 matrix validation plan.

Significant Results

The significant result in the development of the framework for modeling moisture-induced damage and the development of the method to determine the parameters of this model.

Significant Problems, Issues and Potential Impact on Progress

None

Work Planned Next Quarter

The next quarter will focus on the experimental calibration and validation of the moisture damage model using the materials from the ARC 2x2 matrix validation plan.

CATEGORY M5: MOISTURE DAMAGE PREDICTION SYSTEM (All, TAMU lead)

Work on individual components such as test methods and micromechanics models required in the system is complete. The components will be put together in the form of a methodology towards the end of this project.

Moisture Damage Year 4		Year 4 (4/10-3/11)												Team
		4	5	6	7	8	9	10	11	12	1	2	3	
Adhesion														
M1a	Affinity of Asphalt to Aggregate - Mechanical Tests													
M1a-1	Select Materials													UWM
M1a-2	Conduct modified DSR tests													
M1a-3	Evaluate the moisture damage of asphalt mixtures	P					JP					P		
M1a-4	Correlate moisture damage between DSR and mix tests													
M1a-5	Propose a Novel Testing Protocol											JP		F
M1a-6	Standard Testing Procedure and Recommendation for Specifications								P					
M1b	Work of Adhesion													
M1b-1	Adhesion using Micro calorimeter and SFE													TAMU
M1b-2	Evaluating adhesion at nano scale using AFM													WRI
M1b-3	Mechanisms of water-organic molecule competition													TAMU
M1c	Quantifying Moisture Damage Using DMA						JP				D			F
Cohesion														
M2a	Work of Cohesion Based on Surface Energy													
M2a-1	Methods to determine SFE of saturated binders													TAMU
M2a-2	Evaluating cohesion at nano scale using AFM													WRI
M2b	Impact of Moisture Diffusion in Asphalt													
M2b-1	Diffusion of moisture through asphalt/mastic films				D				F					TAMU
M2b-2	Kinetics of debonding at binder-aggregate interface													
M2c	Thin Film Rheology and Cohesion													
M2c-1	Evaluate load and deflection measurements using the modified PATTI test													UWM
M2c-2	Evaluate effectiveness of the modified PATTI test for Detecting Modification													
M2c-3	Conduct Testing													
M2c-4	Analysis & Interpretation													
M2c-5	Standard Testing Procedure and Recommendation for Specifications													see Subtask M1a-6
Aggregate Surface														
M3a	Impact of Surface Structure of Aggregate													
M3a-1	Aggregate surface characterization					JP								TAMU
Modeling														
M4a	Micromechanics model development								JP					TAMU
M4b	Analytical fatigue model for use during mixture design													TAMU
M4c	Unified continuum model								JP			DP	M&A	TAMU
M5	Moisture Damage Prediction System													ALL

LEGEND

Deliverable codes

- D: Draft Report
- F: Final Report
- M&A: Model and algorithm
- SW: Software
- JP: Journal paper
- P: Presentation
- DP: Decision Point
- [x]

- Work planned
- Work completed
- Parallel topic

Deliverable Description

- Report delivered to FHWA for 3 week review period.
- Final report delivered in compliance with FHWA publication standards
- Mathematical model and sample code
- Executable software, code and user manual
- Paper submitted to conference or journal
- Presentation for symposium, conference or other
- Time to make a decision on two parallel paths as to which is most promising to follow through
- Indicates completion of deliverable x

Moisture Damage Year 2 - 5		Year 2 (4/08-3/09)				Year 3 (4/09-3/10)				Year 4 (04/10-03/11)				Year 5 (04/11-03/12)				Team
		Q1	Q2	Q3	Q4	Q1	Q2	Q3	Q4	Q1	Q2	Q3	Q4	Q1	Q2	Q3	Q4	
Adhesion																		
M1a	Affinity of Asphalt to Aggregate - Mechanical Tests																	
M1a-1	Select Materials		DP														UWM	
M1a-2	Conduct modified DSR tests		P															
M1a-3	Evaluate the moisture damage of asphalt mixtures				DP		P			P	JP		P					
M1a-4	Correlate moisture damage between DSR and mix tests						P			P								
M1a-5	Propose a Novel Testing Protocol				P					P, D					JP, F			
M1a-6	Standard Testing Procedure and Recommendation for Specifications											P						
M1b	Work of Adhesion																	
M1b-1	Adhesion using Micro calorimeter and SFE							JP									TAMU	
M1b-2	Evaluating adhesion at nano scale using AFM							JP								JP, F	WRI	
M1b-3	Mechanisms of water-organic molecule competition				JP												TAMU	
M1c	Quantifying Moisture Damage Using DMA											JP	D	F			TAMU	
Cohesion																		
M2a	Work of Cohesion Based on Surface Energy																	
M2a-1	Methods to determine SFE of saturated binders														JP		TAMU	
M2a-2	Evaluating cohesion at nano scale using AFM							JP								JP, F	WRI	
M2b	Impact of Moisture Diffusion in Asphalt																	
M2b-1	Diffusion of moisture through asphalt/mastic films							JP	D	F	D	F					TAMU	
M2b-2	Kinetics of debonding at binder-aggregate interface																	
M2c	Thin Film Rheology and Cohesion																	
M2c-1	Evaluate load and deflection measurements using the modified PATTI test	DP	JP	D	F												UWM	
M2c-2	Evaluate effectiveness of the modified PATTI test for Detecting Modification			D	DP, F													
M2c-3	Conduct Testing							JP										
M2c-4	Analysis & Interpretation				P					D								
M2c-5	Standard Testing Procedure and Recommendation for Specifications					D										see Subtask M1a-6		
Aggregate Surface																		
M3a	Impact of Surface Structure of Aggregate																	
M3a-1	Aggregate surface characterization									JP		P					TAMU	
Models																		
M4a	Micromechanics model development				JP				JP		JP			D	DP	F, SW	TAMU	
M4b	Analytical fatigue model for use during mixture design															M&A, D	F	
M4c	Unified continuum model								JP		JP	DP	M&A	D	DP	F, SW	TAMU	
M5	Moisture Damage Prediction System																ALL	

LEGEND

Deliverable codes

- D: Draft Report
- F: Final Report
- M&A: Model and algorithm
- SW: Software
- JP: Journal paper
- P: Presentation
- DP: Decision Point
- [x]

- Work planned
- Work completed
- Parallel topic

Deliverable Description

- Report delivered to FHWA for 3 week review period.
- Final report delivered in compliance with FHWA publication standards
- Mathematical model and sample code
- Executable software, code and user manual
- Paper submitted to conference or journal
- Presentation for symposium, conference or other
- Time to make a decision on two parallel paths as to which is most promising to follow through
- Indicates completion of deliverable x

PROGRAM AREA: FATIGUE

CATEGORY F1: MATERIAL AND MIXTURE PROPERTIES

Work Element F1a: Cohesive and Adhesive Properties (TAMU)

Work Done This Quarter

We prepared a comprehensive technical report documenting the work and results of this task. The report documents analytical models that describe the relationship between ideal and practical work of fracture as for different asphalt-aggregate systems.

Significant Results

The results demonstrated that a multiplicative relationship exists between the ideal and practical work of fracture. The relationship between these two quantities depends on binder compliance, loading rate, and temperature. This work has validated that the ideal work of fracture, which is calculated from surface energy, is a fundamental property than can be used to rank asphalt-aggregate systems based on their resistance to fracture under dry and wet conditions.

Significant Problems, Issues and Potential Impact on Progress

None

Work Planned Next Quarter

This subtask is completed.

Work Element F1b: Viscoelastic Properties (Year 1 start)

Subtask F1b-1: Viscoelastic Properties under Cyclic Loading (TAMU)

Work Done This Quarter

In this quarter we have completed significant work to validate, model, and document the presence of interaction nonlinearity in asphalt binders.

Significant Results

The findings thus far clearly demonstrate that: (i) the asphalt binder tends to dilate when subjected to shear loading, and (ii) the shear stiffness of the binder is strongly influenced by the stress state in the material, i.e. the shear stiffness of the binder changes due to the presence of axial loads on the binder specimen (figure F1b-1.1). These two findings are synthesized in the form of manuscripts for

two journal publications, one of which is currently under review with the journal, Mechanics of Time Dependent Materials. These findings clearly present a more accurate view of the viscoelastic properties of the asphalt binder under realistic stress states in asphalt pavements. The proposed constitutive model accommodates the multi-axial stress state and more accurately reflects the interaction effect (figure F1b-1.2).

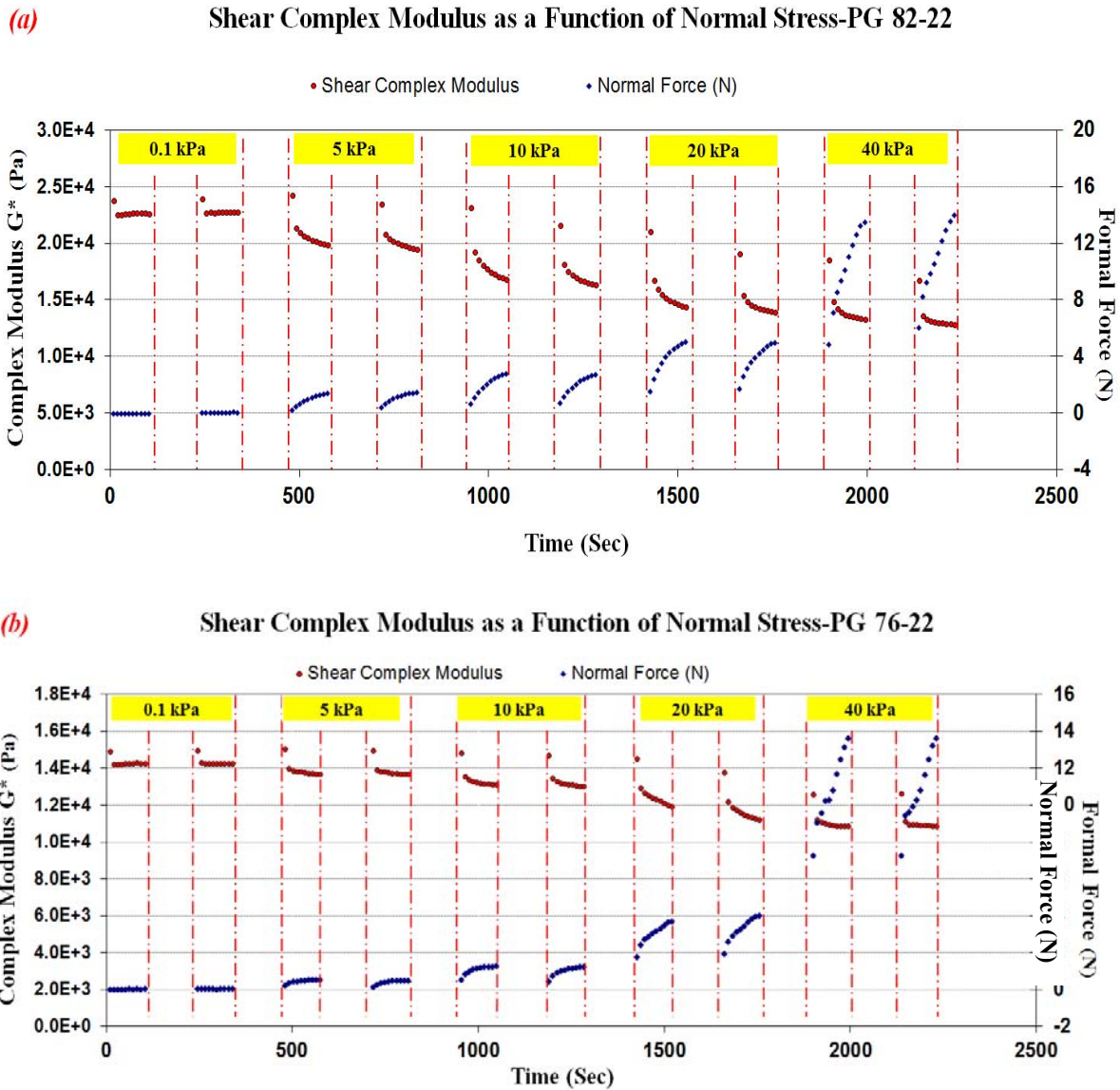


Figure F1b-1.1. Time sweep tests at different stress levels and 40°C; with two repeat at each stress level to detect any damage, with two minutes rest period between each time sweep – results show change in complex shear modulus due to interaction with the presence of axial normal force.

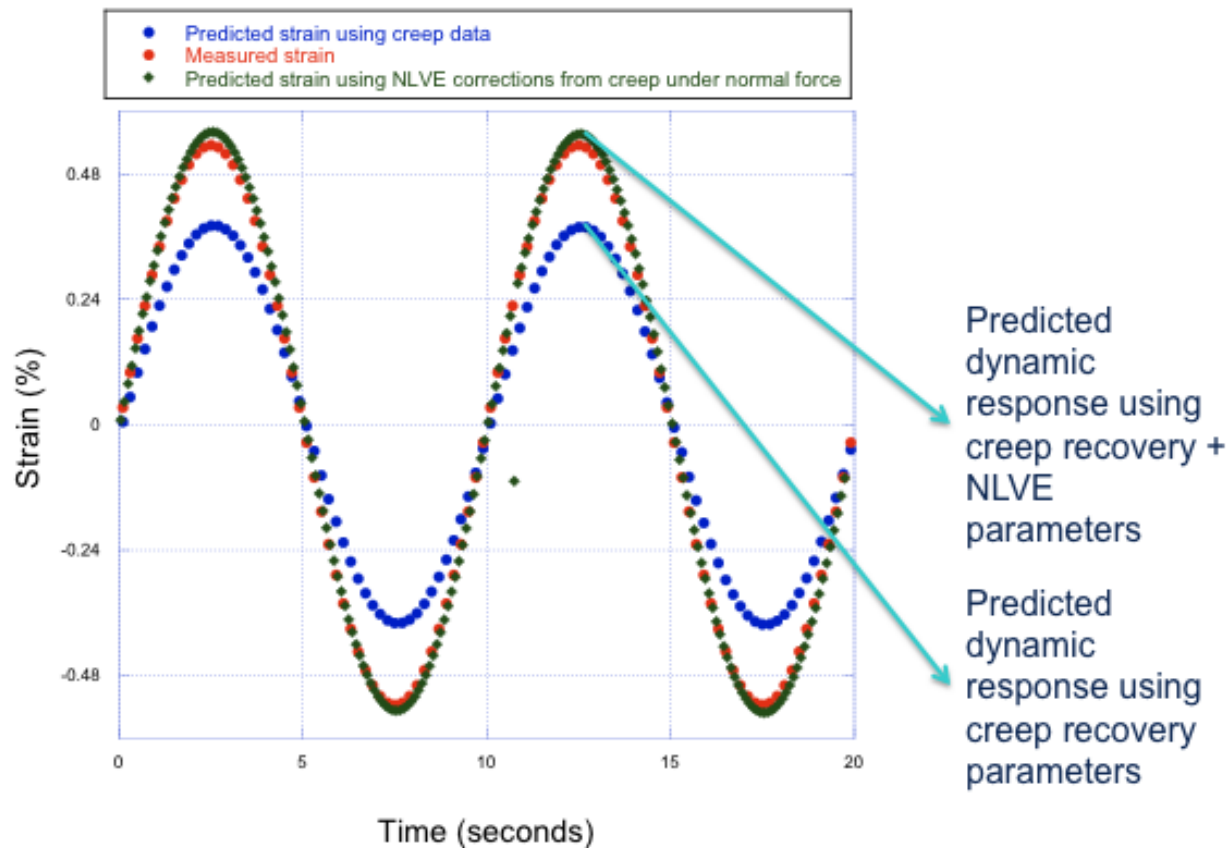


Figure F1b-1.2. Predicted versus measured shear strain under cyclic loading

Significant Problems, Issues and Potential Impact on Progress

None.

Work Planned Next Quarter

In the next quarter we plan to investigate the influence of time dependency of Poisson's ratio and applicability of this model to FAM specimens.

Subtask F1b-2: Separation of Nonlinear Viscoelastic Deformation from Fracture Energy under Repeated and Monotonic Loading (TAMU)

Work Done This Quarter

In this quarter, the characterization of the engineered properties is continued with the development work on the healing properties of asphalt mixtures. The measurement of healing and the prediction

of healing speed have been already studied using the repeated direct tension (RDT) test and documented in the last quarterly report. The advantage of the RDT test is the well-developed analysis method and obtainable results such as the damage density. However, it takes about 2 to 3 hours to obtain enough data points to construct a full healing curve, and the data processing is time-consuming. To improve the test efficiency, a more efficient test protocol with a fundamental analysis method is developed in this quarter to characterize the healing properties of asphalt mixtures.

Healing is a combination of two processes: crack closure (sometimes called “wetting”) and intrinsic healing (which involves molecular diffusion). In order to characterize the crack closure properties, the internal stresses in both the undamaged and damaged asphalt mixtures must be measured. The internal stress is the compressive load that drives the recovery of the deformation of the asphalt mixture specimen after removing the external tensile load. With the recovery of the bulk of the material, the cracks begin to close in the fracture process zone around each crack. A revised creep and recovery test is developed to measure the internal stress using the Material Testing System. A schematic plot of the stress and strain versus time in this test is shown in figure F1b-2.1. The creep phase of the test is the normal creep test with a constant creep load; the recovery phase of the test is incorporated with several three-step loadings to measure the internal stress. The strain keeps decreasing in the recovery phase, and the strain rate is not zero because of the presence of the internal stress. If an external load is applied to the material which makes the strain rate equal to zero, the material is in an equilibrium condition and the external load equals the internal stress.

According to this principle, the step loading is added to the recovery phase as shown in figure F1b-2.1. Three steps are required to determine the internal stress at one time point. For example, σ_1 , σ_2 , and σ_3 are added to determine the internal stress at t_1 . At the loading level σ_1 , the strain rate is less than zero ($\dot{\epsilon} < 0$), indicating that σ_1 is smaller than the internal stress at t_1 ; at the loading level σ_3 , the strain rate is greater than zero ($\dot{\epsilon} > 0$), indicating that σ_3 is larger than the internal stress at t_1 . When the strain rate is zero ($\dot{\epsilon} = 0$), the internal stress at t_1 equals to σ_2 . Then the internal stress can be obtained at t_2 , where a different level of the three-step loading is added, and so forth.

Normally, five points are needed to measure the internal stress at five different time points for the undamaged asphalt mixture, and seven points are required for the damaged asphalt mixture. Other details regarding the testing inputs are given in table F1b-2.1.

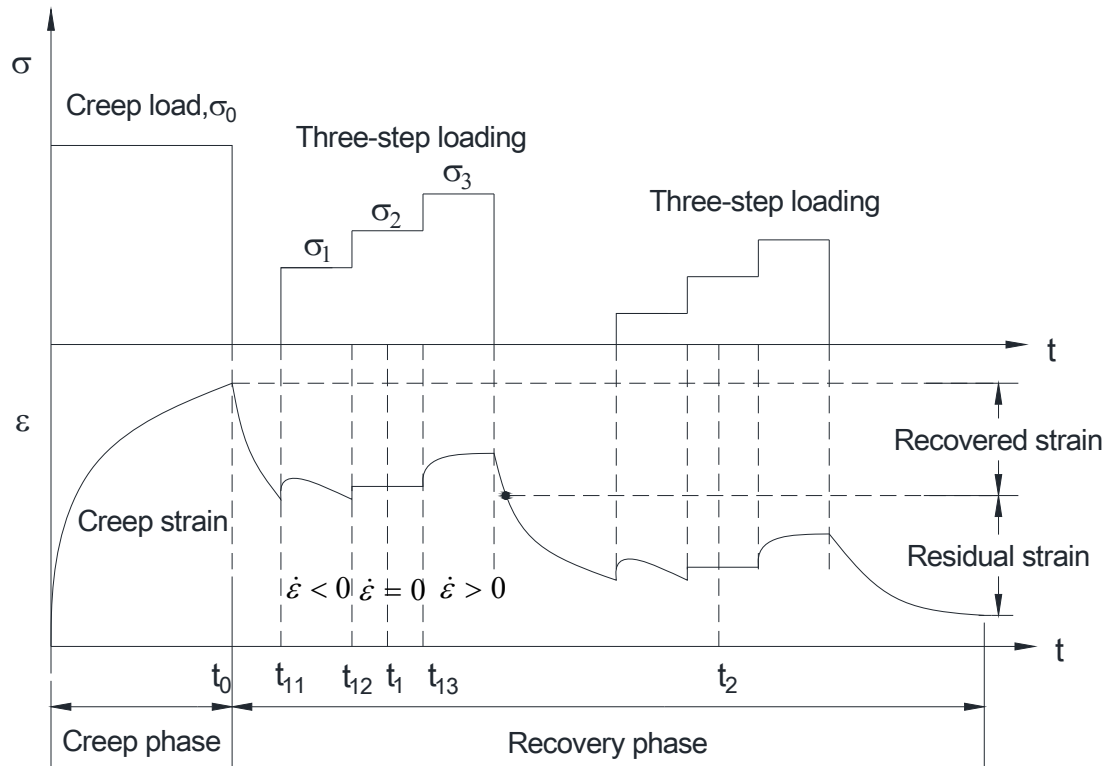


Figure F1b-2.1. Schematic plot of stress and strain in the revised creep and recovery test.

Table F1b-2.1. Testing inputs for the revised creep and recovery test in the MTS.

Specimen dimension	6 inches (150 mm) in height x 4 inches (100 mm) in diameter
LVDT mount	3 LVDTs, 120° apart
Gage length	3.54 inches (90 mm)
Temperature (°)	20
Loading time for the creep phase (sec)	40
Time of the recovery phase (sec)	150
Loading time for each step of three-step loading (sec)	2
Data acquisition	0.1 sec per point
Type of test	<ul style="list-style-type: none"> • Nondestructive test: the maximum strain at the end of the creep phase is controlled under 80 $\mu\epsilon$ • Destructive test: the maximum strain at the end of the creep phase is above 200 $\mu\epsilon$

The accuracy of the internal stress obtained from the revised creep and recovery test is verified by comparing the measured value to that calculated from the constitutive equation. The strain at the time interval $t \in [t_{12}, t_{13}]$ is calculated by the constitutive equation as follows:

$$\varepsilon(t) = \sigma_0 D(t) - \sigma_0 D(t - t_0) + \sigma_1 D(t - t_{11}) + (\sigma_2 - \sigma_1) D(t - t_{12}) \quad (\text{F1b-2.1})$$

where σ_0 is the constant creep load; $D(t)$ is the creep compliance of undamaged asphalt mixtures; t_0 is the end of the creep phase; t_{11} is the beginning of the loading level σ_1 ; t_{12} is the beginning of the loading level σ_2 ; and t_{13} is the beginning of the loading level σ_3 . Then the strain rate is given in equation F1b-2.2.

$$\dot{\varepsilon}(t) = \sigma_0 \dot{D}(t) - \sigma_0 \dot{D}(t - t_0) + \sigma_1 \dot{D}(t - t_{11}) + (\sigma_2 - \sigma_1) \dot{D}(t - t_{12}) \quad (\text{F1b-2.2})$$

Let $\dot{\varepsilon}(t) = 0$ and solve for σ_2 from equation F1b-2.2 to obtain:

$$\sigma_2 = \frac{\sigma_0 \dot{D}(t - t_0) - \sigma_0 \dot{D}(t) - \sigma_1 \dot{D}(t - t_{11})}{\dot{D}(t - t_{12})} + \sigma_1 \quad (\text{F1b-2.3})$$

Given σ_0 , σ_1 , $D(t)$, t_0 , t_{11} , and t_{12} , σ_2 calculated by equation F1b-2.3 is the theoretical value of the internal stress. Following the same procedure, the theoretical value of the internal stress at other time points can be calculated. The measured internal stress and the theoretical value calculated by equation F1b-2.3 for an undamaged asphalt mixture specimen are plotted in figure F1b-2.2. The measured value closely matches the theoretical value, suggesting the accuracy of the internal stress obtained from the revised creep and recovery test. This method to determine the internal stress is appropriate for undamaged asphalt mixtures only because the creep compliance of the undamaged material does not change so it can be predicted by simulating the creep compliance in the creep phase. The creep compliance of the damaged material cannot be obtained beyond the creep phase, i.e. after t_0 in figure F1b-2.1.

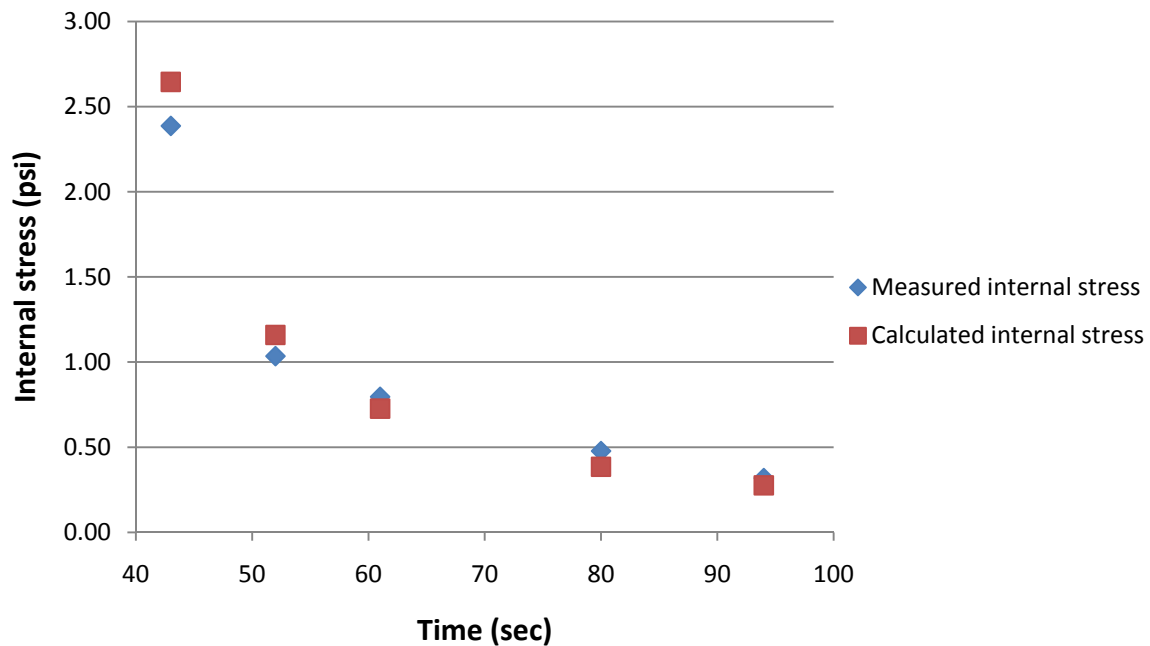


Figure F1b-2.2. Comparison of the measured and calculated internal stress.

Significant Results

The internal stress is proposed to characterize crack closure in damaged asphalt mixtures. The introduction of the internal stress makes it possible to study the material behavior during the period in which the healing actually occurs. Comparing to a phenomenological method like comparing the material stiffness before and after healing, it provides a more fundamental method to characterize healing directly using a mechanical approach.

The internal stress is measured by the revised creep and recovery test. This test has a normal creep phase with a constant load and a revised recovery phase incorporated with several three-step loadings. The three-step loading method is based on the principle of force equilibrium. It is verified by comparing the measured value of the internal stress to the theoretical value calculated by the constitutive equation. It has been proven that the measured value matches well with the theoretical value so the revised creep and recovery test is capable of producing accurate internal stress. In addition, the test is simple and the process of loading and unloading is well controlled by the MTS. The entire test takes about three minutes, significantly improving the efficiency of laboratory testing.

Significant Problems, Issues and Potential Impact on Progress

The three-step loading added in the recovery phase to measure the internal stress is determined on a trial and error basis. It may not be the correct value in the first time of testing, but it can be readily corrected by observing the strain curve. For example, if the strain rate corresponding to the step

loading is greater than zero at the point, the loading should be changed to a lower level. In general, two trials are enough to produce a desired strain curve to determine the internal stress.

Work Planned Next Quarter

The measurement of the internal stress is the first step to characterize healing in damaged asphalt mixtures. The next step is to characterize the material behavior during the recovery phase of both undamaged and damaged asphalt mixtures. The material behavior of undamaged asphalt mixtures in the recovery phase serves as the reference state, and the material behavior of damaged asphalt mixtures in the recovery phase reflects the effect of healing. Once the material behaviors are characterized, a further step can be taken to quantify the healing using an energy approach.

Work Element F1c: Aging

Subtask F1c-1: Critical Review of Binder Oxidative Aging and Its Impact on Mixtures (TAMU)

Work Done This Quarter

Several oxidation mechanisms of asphalt binder were reviewed in previous quarterly report. Specifically, they are Petersen's dual-reaction free radical chain reaction (FRCR) mechanism, King's oxycyclic electron transfer initiated oxidation (ETIO) mechanism, and Herrington's inhibited free radical autoxidation (IFRA) mechanism. All mechanisms have difficulty explaining the “fast-rate plus constant-rate” scheme of binder oxidation. One possible reason is that reactions during the fast-rate period and the constant-rate period might go through different reaction pathways so that no simple mechanism is able to explain the kinetics. One way to probe this possibility is by using antioxidants. By comparing the aging kinetics of antioxidant-treated binders with control, we might see the stage when the antioxidants take effect and differentiate the oxidation mechanism for the fast-rate period. For this purpose, a literature review of antioxidants was conducted.

The search for effective antioxidants to retard binder oxidation started as early as 1960, and the study of effective and economic antioxidants is ongoing. For example, Willams et al. (2008) were investigating lignin-containing ethanol co-products as an economic performance enhancer for asphalt. Through the years, many antioxidants were examined. Mainly, they were aromatic amines, metal (lead or zinc) compounds, phenolic antioxidants, carbon black, and hydrated lime. A detailed review of antioxidants for asphalt binder is available from Apeagyei (2006).

During the evaluation of the effectiveness of antioxidants, very few people (Martin, 1968) studied the effect of antioxidants on binder oxidation chemistry. Most address the effectiveness of antioxidants based on comparison of rheological properties, typically viscosity. However, antioxidants might have changed the binder hardening in two ways, 1) by slowing down oxidation rates and 2) by making the binder softer or harder by changing the binder composition and compatibility. Therefore, for the purpose of a study of mechanism, those two effects should be studied separately.

Furthermore, while the oxidation of asphalt goes through an early fast-rate period followed by a constant-rate period, most antioxidant studies evaluated binders after RTFO and PAV aging without considering these two different reaction paths. It is possible that antioxidants only work during one of these two periods while the other is not affected. Therefore, binders should be aged and sampled during both the fast-rate and constant-rate period. This approach will provide a more detailed view of the function of antioxidants and of the nature of the two oxidation mechanisms.

Significant Results

N/A

Significant Problems, Issues and Potential Impact on Progress

There are no problems or issues.

Work Planned Next Quarter

Based on this review, an experimental design will be developed for the study of oxidation mechanisms using selected antioxidants and the experimental work will begin.

Review of the literature and work on other research projects is ongoing.

Cited References

Apeageyi, A.K., 2006, Laboratory Evaluation of Antioxidants for Asphalt Binders. Ph.D. dissertation at University of Illinois at Urbana- Champaign.

Williams, R. C., and McCready, N. S., The Utilization of Agriculturally Derived Lignin as an Antioxidant in Asphalt Binder. Center for Transportation Research and Education Final Report No. 06-260, Iowa.

Martin, K. G., 1968, Laboratory Evaluation of Antioxidants for Bitumen. *Proc. Of the Australian Road Research Board*, Vol. 4, Part 2.

Subtask F1c-2: Develop Experimental Design (TAMU)

Work Done This Quarter

No work this quarter.

Significant Results

None.

Significant Problems, Issues and Potential Impact on Progress

The planned experiments using ARC core binders is underway, as well as measurements on mixtures fabricated using other binders.

Work Planned Next Quarter

Measurements of mixture rheology and fatigue continue. Also, rheological measurements of binders extracted and recovered from these mixtures will be made as part of the effort to link binder oxidation to changes in mixture properties.

Subtask F1c-3: Develop a Transport Model of Binder Oxidation in Pavements (TAMU)

Work Done This Quarter

Measurements of Recovered Binder Properties

Measurements of the WRI test section sites awaits delivery of the field cores.

Model Validation with Preliminary Field Measurement

The previous quarter, work was reported on recent work towards an improved fundamentals-based oxygen transport and reaction model for predicting asphalt binder oxidation rates in pavements. Model elements include pavement temperature, pavement air voids characteristics (total air voids, pore sizes and distribution), asphalt binder oxidation kinetics, and oxygen diffusivity in asphalts. In this quarter, and in lieu of having WRI field cores for analysis, field oxidation rates for a number of pavements in Texas and Minnesota, determined for TxDOT project 0-6009, were compared to calculations made using the more detailed transport model developed in this ARC work. In addition, the effects of model elements including pavement temperature, air voids properties, and binder oxidation kinetics on field oxidation rates were evaluated by comparing field oxidation rates at these different pavement sites.

Table F1c-3.1 summarizes six pavement sites from Texas and Minnesota. The Texas sites range from Amarillo in the North to Laredo in the South, and to the Lufkin in the East. Most of the field cores are taken from top surface layers of pavements, but also from layers far below the surface. For example, IH35 #5 at Waco is a 4 inch rich bottom layer (high asphalt binder content), placed on a 6 inch flex base, at a depth of 16 inches below the pavement surface. (Here the number after the name of the highway indicates the pavement layer studied. If not specified in table F1c-3.1, the pavement layer is the surface layer.) The thicknesses of the various pavement layers ranged up to 4 inches but down to as little as 2 inches. The Bryan district pavement (US290) contained unmodified binders, while other pavements are SBS polymer modified. Oxidation and hardening kinetics for all the binders were measured separately for either the recovered binders from the field cores or for the same binders obtained from the manufacturer. Additionally, IH35 #5 at Waco has lowest accessible air void of 5.9 percent, while US290 at Bryan has accessible air void as high as 12.4 percent; and most of pavement layers have intermediate values from 7.3 to 7.9 percent. The ages of the

pavements range from new construction (US277) to 6 years old (Amarillo US54) at the time of the first coring date. Coring at two times provided field oxidation rates.

Also included in the study is Cell 1 from the MnRoad test site in Minnesota. The thickness of the core layer is 4.5 inches, taken from pavement surface. Oxidation reaction kinetics parameters were measured with binder recovered from the field cores. The accessible air void content for this pavement layer was 4.8 percent. Cell 1 was constructed in 1993 and cores were obtained from this MnRoad site in November 2004 and November 2008.

This collection of pavement cores covers a large variety of key elements that affect pavement oxidation, and provided data that could be used to assess the effects of pavement temperature (Texas versus Minnesota; surface layer versus bottom layer), air void properties (from a low accessible air void of 5.9 percent to a high accessible air void of 12.4 percent), and asphalt oxidation and hardening kinetics (a variety of asphalt binders) on measured or modeled oxidation rates.

Table F1c-3.1. List of field sites studied.

District (State)	Highway	Thickness (inch)	PG (modifier)	Binder Supplier	AAV (%)	Cons.	1 st Coring	2 nd Coring
Laredo (TX)	US277	2.5	70-22 (SBS)	Valero-C	7.3	2008	07/2008	09/2009
Lufkin (TX)	US69	2	70-22 (SBS)	Marlin	7.9	2003	02/2005	06/2008
Bryan (TX)	US290	2.5	64-22 (Un)	Eagle	12.4	2002	10/2005	08/2008
Waco (TX)	IH35 #5	3	70-22 (SBS)	Alon	5.9	2003	10/2005	08/2008
Amarillo (TX)	US54	2.5	70-28 (SBS)	Alon	7.3	1998	12/2004	07/2008
Laredo (TX)	IH35 #4	2	70-22 (SBS)	Valero-C	2.0	2007	--	06/2008
Metro Area (MN)	I-94	4.5	AC-120(Un)	--	4.8	1993	11/2004	11/2008

Cores taken from fields were analyzed for interconnected air voids (by X-ray CT) and total and accessible air voids (by CoreLok or SSD) first, and then sliced into 0.5 inch layers, each for separate binder extraction and recovery. The recovered binders were analyzed for oxidation by infrared spectroscopy (FT-IR) and for physical properties by dynamic shear rheometry (DSR) to provide data on asphalt binder oxidation and hardening rates in pavements.

In addition, pavement temperature, air void properties, and asphalt oxidation kinetics were characterized for these pavement cores. Then, layer-by-layer, oxidation rates were modeled as a function of time and depth in the pavement cores based on the improved oxygen transport and reaction model. One should note that model calculation provided a range, instead of a single value, of oxidation rates, depending on the upper or lower limit of P_{av} (the oxygen partial pressure in the pore) used. The higher values of P_{av} and thus the higher oxidation rates are obtained by assuming

that convective flow through the pavement pores is sufficient to maintain the oxygen partial pressure at 0.2 atm. The lower values of P_{av} and thus the lower oxidation rates are obtained by assuming that replenishment of oxygen in the pores is achieved only by diffusion of oxygen from the pavement surface.

Because of the limited number of cores that can be obtained, the relatively short time between corings (due to the project length relative to the slow field oxidation rate), and the inherent variability that tends to exist between cores, the ability to make layer-by-layer comparisons of these field oxidation measurements, especially considering the fairly modest layer-by-layer differences indicated by the model calculations, is necessarily limited. Consequently, the overall binder oxidation rates for each pavement core (rather than slice by slice comparisons) were compared using the field measurements and model calculations.

Table F1c-3.2 summarizes yearly oxidation rates (in terms of carbonyl growth) measured for these six validation cores. Maximum and minimum oxidation rates calculated from the model are also reported. The visual comparison is shown in figure F1c-3.1. The ranking of predicted oxidation rates from high to low is the same as the ranking established by field measurement except for US277 and the oxidation rates measured in the field can be quite close to the range of predicted oxidation rates that were established by the maximum and minimum oxidation rates. For example, the measured oxidation rate is only 3 percent higher than the maximum oxidation rate calculated for US290, and for US54 the measured oxidation rate is 6 percent lower than the minimum oxidation rate predicted.

Table F1c-3.2. Comparison of measured and modeled field oxidation rates.

STATES	Site	Oxidation rate modeled (CA/year)		Bulk oxidation rate measured (CA/year)
		Maximum	Minimum	
MN	Cell 1	0.0200	0.0195	0.0256
	US277-LRD	0.0465	0.0451	0.0705
	US69-LFK	0.0258	0.0255	0.0370
	US290-BRY	0.0651	0.0620	0.0671
TX	IH35-WAC #4	0.0264	0.0243	0.0340
	US54-AMR	0.1117	0.0994	0.0935

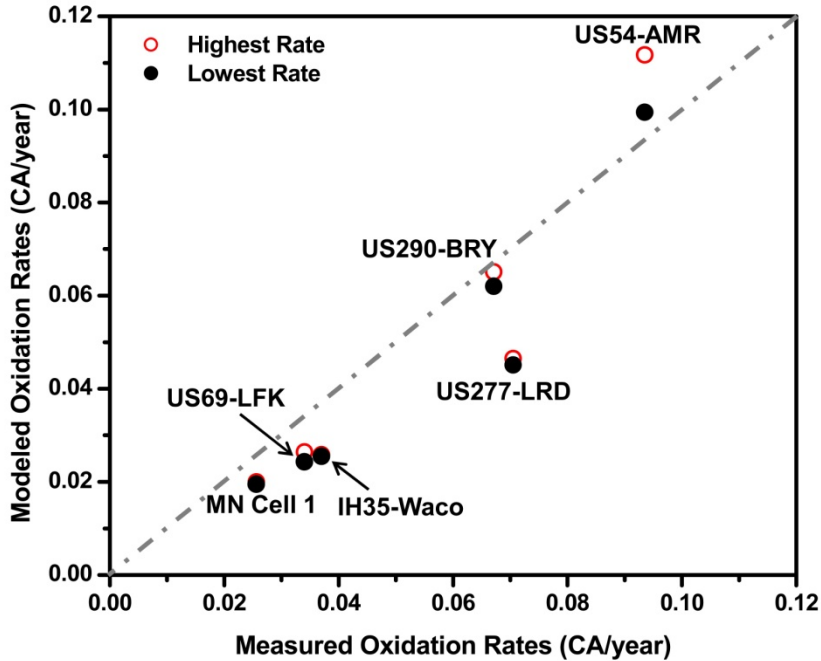


Figure F1c-3.1. Comparison of measured and modeled field oxidation rates.

On the other hand, there are exceptions. For example, for pavements from US277, US69, IH35-Waco, and MN Cell 1, the respective measured oxidation rates are 34, 30, 22, and 21 percent higher than the maximum oxidation rates predicted.

A possible explanation of these higher rates is that these pavements were all newly constructed pavements, at least relative to their oxidation rates; at the time of their first core, the Texas pavement's respective service lives were 0, 1.5, and 2 years. For MN Cell 1, the first core was taken after 11 years in the road. Oxidation of a neat asphalt binder is characterized by an initial rapid rate period that declines over time until a constant-rate period is reached. It has been estimated that the fast oxidation rate period can last as long as 2~3 years for Texas pavements, and 12 years or longer for Minnesota pavements. Thus, the asphalt binder oxidation for these pavement cores was most likely dominated by the initial rapid oxidation period, rather than the slower constant-rate reaction regime. However, in the model calculations, only the slower constant-rate reaction kinetics parameters were used to calculate the field oxidation rates, thereby likely providing a significant underestimation of the oxidation rates. The reaction rate for the constant rate period can generally be described using an Arrhenius expression for temperature variation and pressure dependence, while the reaction mechanisms are still not fully understood for initial rapid rate period. An extensive understanding of oxidation mechanisms and oxidation kinetics in this rapid oxidation period is essential to incorporating the fast reaction period into this model and to providing a more accurate prediction of oxidation rates during the first several years of service for newly constructed pavements.

In spite of this disagreement of model predictions for pavements that are largely in the fast rate oxidation period, in general this fundamentals-based model provides a very good match with field

measurements, suggesting that it captures the critical elements that affect asphalt binder oxidation in pavements.

Significant Results

Recent developments on pavement temperature modeling, oxygen diffusivity measurement, and pavement air voids characterization, coupled with a thermal and oxygen transport model in pavements, provide a good foundation for model calculations. This is a very important result that is the culmination of many years of work towards such a model.

Significant Problems, Issues and Potential Impact on Progress

The effort to obtain cores from pavement sites in different climate zones continues. Cores from such sites will provide 1) data on binder oxidation as a function of time and depth in pavements and 2) data on changes to mixture rheology and fatigue resistance that occur in response to binder oxidation.

Work Planned Next Quarter

Field cores from studied pavement sites will be continue to be collected and measured to provide more accurate data on binder oxidation as a function of time and depth in these pavements.

Field cores from sites as available from WRI will be tested to provide data on binder oxidation as a function of time and depth in pavements in different climate zones.

Oxidation mechanism and kinetics in this fast reaction period will be studied to incorporate into the improved oxygen transport and reaction model.

Model verification and validation with above mentioned pavement sites is an ongoing effort throughout the entire project.

Subtask F1c-4: The Effects of Binder Aging on Mixture Viscoelastic, Fracture, and Permanent Deformation Properties (TAMU)

Work Done This Quarter

The reader is referred to Work Elements F1b-2 and F2c.

Work Planned Next Quarter

The reader is referred to Work Elements F1b-2 and F2c.

Subtask F1c-5: Polymer Modified Asphalt Materials (TAMU)

Work Done This Quarter

A number of base asphalts and their corresponding polymer modified asphalts (PMB) were oxidized at different temperatures and at 1 atm air pressure. Samples collected at different oxidation levels were measured for oxidation level (carbonyl content) and rheological properties including low shear limiting viscosity and DSR function.

The ratios of the limiting viscosity (or DSR function) for the polymer modified binder to the limiting viscosity (or DSR function) for the base binder, are being used to analyze oxidation susceptibility and oxidation kinetics for different polymer modifiers in terms of polymer functional type.

Work Planned Next Quarter

This experiment will be continuing throughout the next quarter with additional asphalt binders and their corresponding PMB.

Decreases in this rheological ratio with oxidation at different temperatures will be analyzed for polymer oxidation susceptibility and polymer oxidation kinetics.

Work Element F1d: Healing (TAMU)

Subtask F1d-1: Critical review of the literature

Subtask F1d-2: Material selection

Subtask F1d-3: Experiment design

Subtask F1d-4: Test methods to measure properties related to healing

Subtask F1d-5a: Testing of materials and validating healing model

Subtask F1d-5b: Thermodynamic model for healing in asphalt binders

Work Done This Quarter

We have hypothesized overall healing to be due to microscopic wetting and intrinsic strength gain. In the previous quarters we reported a method to measure intrinsic strength gain as well as the influence of aging and temperature on the rate of intrinsic strength gain. In the past quarter we have started measuring overall healing in FAM as a function of rest period and level of damage. We formulated a test matrix and started tests according to this matrix.

Significant Results

We have started quantifying the overall healing in FAM specimens as a function of rest period as well as level of damage. Figure F1d.1. illustrates a typical plot from these measurements. In other words, figure F1d.1. allows the user to estimate the expected percentage of healing for a given rest period and damage level immediately preceding the rest period. Completing this experiment design

will allow us to measure and validate the healing response of materials as function of its viscoelastic properties and damage level.

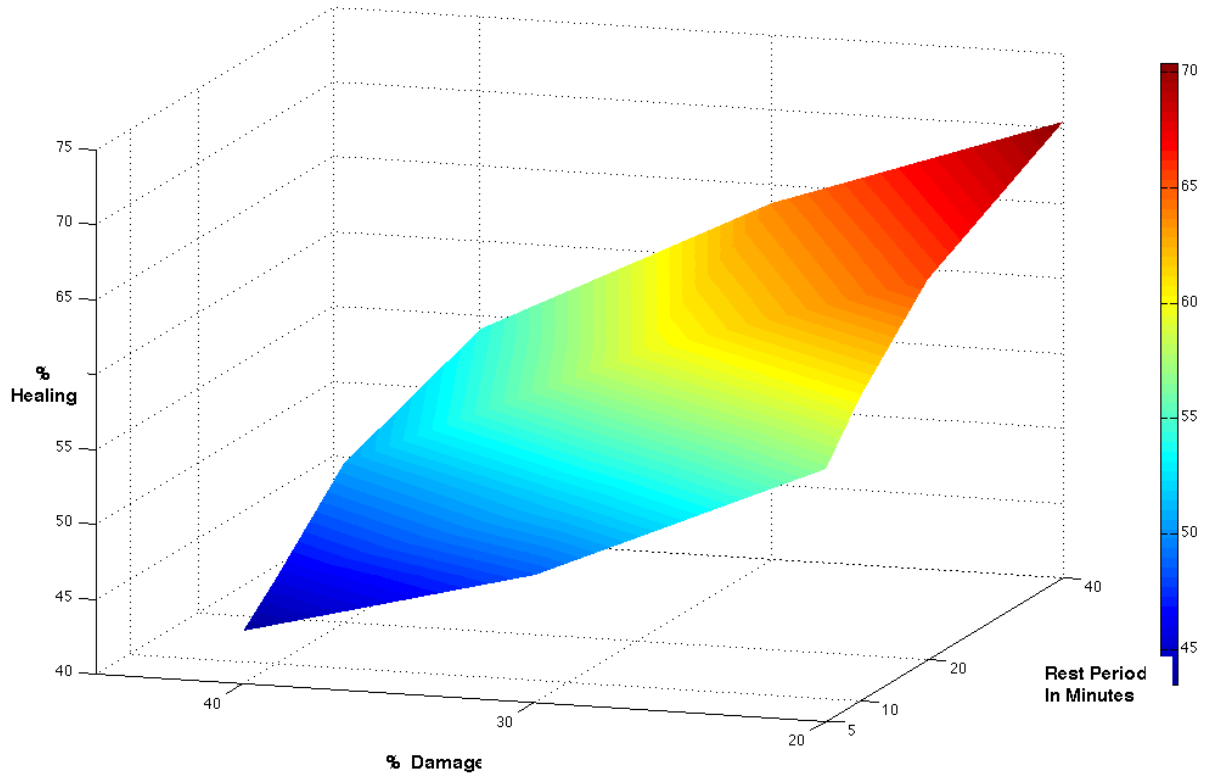


Figure F1d.1. Overall healing in FAM specimens as a function of level of damage as well as rest period

Significant Problems, Issues and Potential Impact on Progress

None.

Work Planned Next Quarter

We will continue to measure intrinsic healing as well prepare FAM specimens to measure overall healing.

Subtask F1d-6: Evaluate Relationship Between Healing and Endurance Limit of Asphalt Binders (UWM)

Work Done This Quarter

It was observed that the procedure of time sweep with rest periods, in which oscillatory ramp to the target strain amplitude is used, induced damage during the ramping step for aged binders. This observation complicated healing analysis, and thus the research team decided to adopt a different procedure. A single long rest period was adapted during a time sweep. With the use of a single rest period, the number of cycles below the target strain amplitude is insignificant compared to the total number of loading cycles, thus making the healing evaluation less influenced by the possible damage during the ramping step.

This new procedure is based on the work of Santagata et al. (2009). First, a strain-controlled time sweep is run without rest period. The number of cycles to a 35% reduction in $|G^*|$ is then calculated. Then, a time sweep is run at the same amplitude with a one-hour rest period inserted at the number of cycles corresponding to a 35% reduction in $|G^*|$ calculated from the no-rest case. A small oscillatory load (i.e., $\gamma = 0.01\%$) is applied during the rest period to measure the recovery of the binder over time. After the rest period, loading resumes until failure. Two LTPP binders at three age levels—un-aged, rolling thin film oven (RTFO)-aged, and pressure aging vessel (PAV)-aged—were tested using this procedure. Preliminary results have been repeatable and allowed for distinguishing between different binders and age levels.

Significant Results

Figure F1d-6.1 shows the normalized modulus (i.e., $|G^*|$ divided by initial $|G^*|$) versus number of loading cycles at three aging levels for binder 370901 (PG 64-22). It can be seen that fatigue life increases with binder age. However, healing is not significantly affected by aging level for this specific binder.

Figure F1d-6.2 presents results for binder 370964 (PG 76-22). It can be observed that increase in modulus which occurs with the rest period is largest for aged binders. Overall, experimental results show that the inclusion of a single long rest period leads to a significant recovery in $|G^*|$. It is important to note that after the rest period, damage proceeds following approximately the same rate as prior to the rest period, and thus the benefit of the rest period diminishes quickly. This trend of diminishing benefit raises some questions about healing effects and points out the need to reevaluate the value of healing.

Due to the fact that damage after the rest period proceeds at a similar rate as before the rest period, an increase in fatigue life was calculated as the number of cycles of loading it takes after the rest period to reach the value of $|G^*|$ just before the rest period. Results for both binders tested are presented in table F1d-6.1.

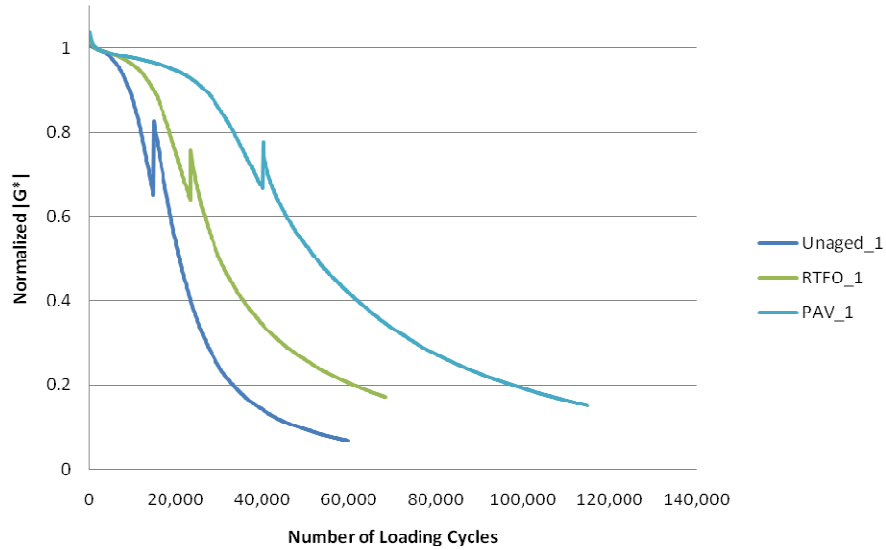


Figure F1d-6.1. Graph. Normalized $|G^*|$ versus time for binder 370901 (PG 64-22).

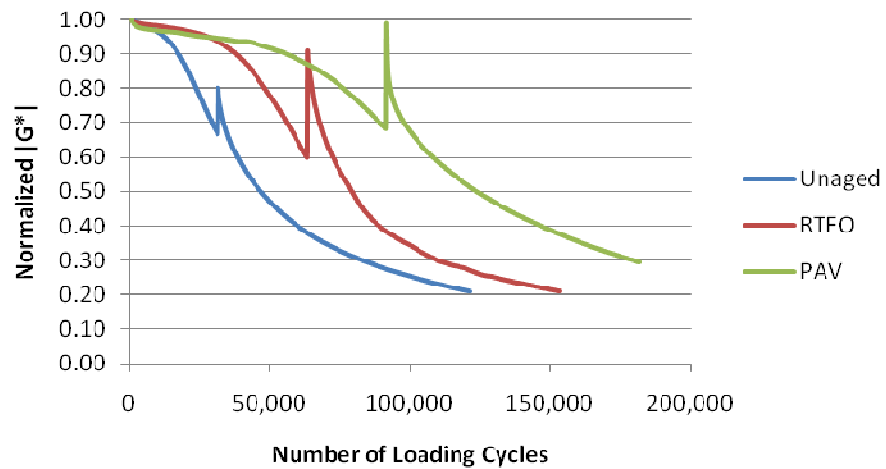


Figure F1d-6.2. Graph. Normalized $|G^*|$ versus time for binder 370964 (PG 76-22).

Table F1d-6.1. Increase in fatigue life (number of cycles) due to single rest period as a function of binder age.

	370901 (PG 64-22)	370964 (PG 76-22)
Un-aged	3,150	3,300
RTFO	2,175	8,925
PAV	2,550	7,650

Experimental results indicate that irrespective of the age level, the polymer-modified binder (370964) exhibits greater healing effect than the neat binder. Also, binder 370901 exhibits the greatest healing effect when un-aged, while binder 370964 exhibits the greatest healing effect at the RTFO age level. The neat binder (370901) shows less change in healing potential with age than the modified binder (370964).

The results collected to date indicate that the use of a time sweep with a single long rest period allows for distinguishing between the healing potential of different binders at different age levels. Additionally, preliminary results show reasonable repeatability for the test procedure.

Significant Problems, Issues and Potential Impact on Progress

None.

Work Planned Next Quarter

The research team will continue evaluating the use of a time sweep with a single long rest period using LTPP binders at different age levels. A proposal for deriving a healing potential index will be proposed and tested for repeatability.

Cited References

Santagata, E., O. Baglieri, D. Dalmazzo, and L. Tsantilis, 2009, Rheological and Chemical Investigation on the Damage and Healing Properties of Bituminous Binders. *Journal of the Association of Asphalt Paving Technologists*, 78: 567-595.

Subtask F1d-7: Coordinate with Atomic Force Microscopic (AFM) Analysis (WRI)

Work Done This Quarter

No activity this quarter.

Subtask F1d-8: Coordinate Form of Healing Parameter with Micromechanics and Continuum Damage Models (TAMU)

Work Done This Quarter

In this quarter, a systematic framework for modeling micro-damage healing in asphalt materials is developed based on the laws of thermodynamics and continuum damage mechanics. More validation of the developed model has been carried out based on data from the Nottingham database.

Significant Results

For the first time, a consistent thermodynamic framework for deriving viscoelastic, viscoplastic, and viscodamage constitutive models with micro-damage healing has been proposed. The framework

can be used to derive various models based on the knowledge of only how the material stores energy and how the material dissipates energy. Therefore, only two scalar functions (i.e., the free energy function and the rate of energy dissipation function) are needed to be identified based on experiments.

Significant Problems, Issues and Potential Impact on Progress

None

Work Planned Next Quarter

In the coming quarter the formulated micro-damage healing model will be validated against ALF experimental data. Moreover, the effect of micro-damage healing on rutting will be simulated using PANDA.

CATEGORY F2: TEST METHOD DEVELOPMENT

Work Element F2a: Binder Tests and Effect of Composition (UWM)

Work Done This Quarter

During this quarter the research team modified the selected neat binders (i.e., FH, CRM) with Elvaloy AM and radial styrene-butadiene-styrene (RSBS). For comparison purposes, the same level of modification was maintained (i.e., 0.7% Elvaloy AM, 1.5% Elvaloy AM, 2% RSBS and 4% RSBS). The amount of polyphosphoric acid (PPA) required for the Elvaloy blends was maintained at 0.17%, while 0.123% cross-linker was used for the RSBS blends. It should be noted that, previously, 0.234% cross-linker was used for 4% linear SBS (LSBS). Massive cross-linking was achieved when this amount of cross-linker was added to the 4% RSBS blends, which created workability issues.

The research team performed the following tests on these newly prepared polymer blends: high-temperature Superpave grading with the Dynamic Shear Rheometer (DSR), elastic recovery in the DSR (ER-DSR), Multiple Stress Creep and Recovery (MSCR), and Linear Amplitude Sweep (LAS). The ER-DSR tests were performed at 25 °C; the MSCR tests were performed at the base binder PG high temperature (58 °C for CRM-based binders and 64 °C for FH-based binders). The LAS tests were performed at the intermediate PG temperatures. Additionally, the team conducted preliminary tests on mastics to investigate repeatability and to verify the capabilities of the DSR geometry to test asphalt binders with fine particles.

Significant Results

The DSR tests were performed on original and rolling thin film oven (RTFO)-aged binder. The selected parameter was $|G^*|/\sin\delta$, which was determined at two temperatures from which the true grade (i.e., continuous grade) was determined. The true grade results are shown in table F2a.1.

Table F2a.1. True grade results.

Binder	True grade (TG)		HT grade
	Original	RTFO	
FH + 0.7 Elvaloy AM + 0.17 PPA	71.0	73.3	70
FH + 1.5 Elvaloy AM + 0.17 PPA	74.5	73.5	70
FH + 2 RSBS + cross-linker	74.3	74.4	70
FH + 4 RSBS + cross-linker	82.9	79.2	76
CRM + 0.7 Elvaloy AM + 0.17 PPA	62.6	64.2	58
CRM + 1.5 Elvaloy AM + 0.17 PPA	66.0	67.1	64
CRM + 2 RSBS + cross-linker	68.2	68.4	64
CRM + 4 RSBS + cross-linker	78.6	75.4	70

Comparing the results presented in table F2a.1 with the previously reported results for the binders modified with Elvaloy 4170 and LSBS, it can be noted that at the same level of modification the Elvaloy AM is less effective, while no significant differences exist between radial and linear SBS.

One of the advantages of running the elastic recovery in the DSR is the possibility of continuing to monitor the recovery of the binder. The DSR records data at 0.065-second intervals, which permits the calculation of the elastic recovery at different loading times (e.g., 750, 1800, 2700 and 3600 seconds). Table F2a.2 shows the percent elastic recovery for the tested binders at different times. Previously reported elastic recovery values for Elvaloy 4170 and LSBS are similar to the values shown in table F2a.2 for Elvaloy AM and RSBS, respectively.

Table F2a.2. Elastic recovery results at different loading time intervals.

Binder	750 s	1800 s	2700 s	3600 s
FH + 2 RSBS + cross-linker	47.6%	53.3%	53.9%	57.8%
FH + 4 RSBS + cross-linker	63.4%	69.3%	69.9%	73.5%
FH + 0.7 Elvaloy AM + 0.17 PPA	33.8%	37.8%	38.3%	41.0%
FH + 1.5 Elvaloy AM + 0.17 PPA	45.5%	50.6%	51.2%	54.6%
CRM + 2 RSBS + cross-linker	45.3%	49.9%	50.4%	53.0%
CRM + 4 RSBS + cross-linker	66.2%	72.6%	73.3%	77.4%
CRM + 0.7 Elvaloy AM + 0.17 PPA	27.0%	28.5%	28.7%	28.7%
CRM + 1.5 Elvaloy AM + 0.17 PPA	51.3%	55.9%	56.5%	58.9%

The MSCR results for the FH-based binder at 64 °C and CRM-based binder at 58 °C are shown in table F2a.3. A comparison in terms of the nonrecoverable creep compliance (J_{nr}) for the FH-based binder is shown in figure F2a.1. It can be seen that no significant difference exists between the J_{nr}

values for the binders modified with linear and radial SBS. The J_{nr} values for the binders modified with Elvaloy AM are approximately 50% higher than for the binders modified with Elvaloy 4170.

Table F2a.3. MSCR results for FH- and CRM-based binders.

Binder	FH-based Binders				CRM-based Binders			
	% Recovery		$J_{nr}, 1/kPa$		% Recovery		$J_{nr}, 1/kPa$	
	100Pa	3200Pa	100Pa	3200Pa	100Pa	3200Pa	100Pa	3200Pa
FH + 2 RSBS + cross-linker	51.77	44.77	50.09	42.56	0.52	0.62	0.45	0.53
FH + 4 RSBS + cross-linker	68.37	59.62	84.12	83.14	0.09	0.10	0.17	0.22
FH + 0.7 Elvaloy AM + 0.17 PPA	30.89	21.53	22.46	14.69	1.36	1.55	0.78	0.91
FH + 1.5 Elvaloy AM + 0.17 PPA	44.49	36.06	49.81	42.71	0.57	0.66	0.58	0.70

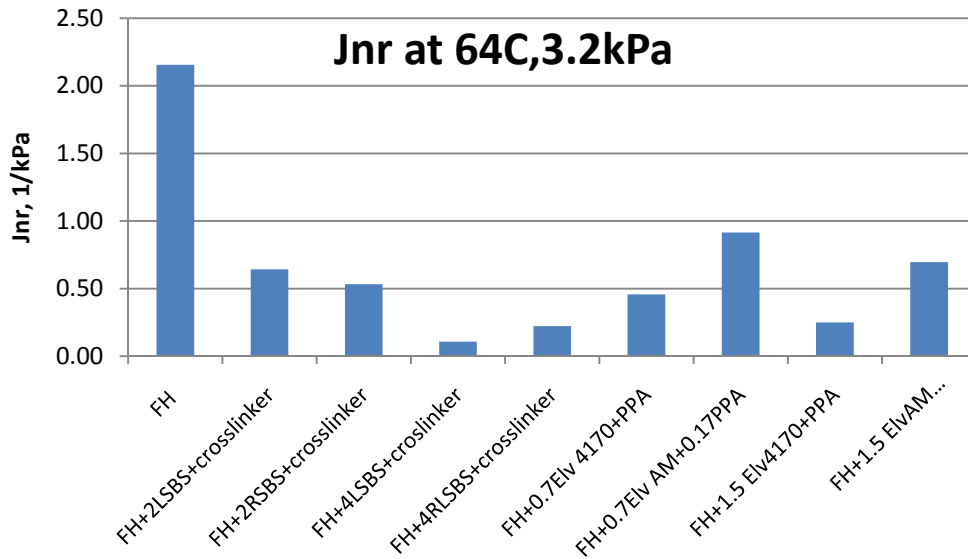


Figure F2a.1. Chart. J_{nr} at 64 °C and 3.2 kPa for FH-based binder.

Table F2a.4 shows the results from LAS testing. Note that FH modified with 0.7% and 1.5% Elvaloy AM were tested at the same temperature because 1.5% Elvaloy AM did not increase the PG of the unmodified binder, as indicated in table F2a.1. In terms of fatigue performance (e.g., number of cycles to failure (N_f)), it can be observed that the FH binders modified with RSBS and Elvaloy AM have better performance than the CRM binders modified with RSBS and Elvaloy, respectively.

Table F2a.4. LAS results.

Binder	Testing Temp.(°C)	A	B	N_r γ = 2.5%	N_r γ = 5%
FH + 2 RSBS + cross-linker	28	2.06E+07	-4.690	2.80E+05	1.08E+04
FH + 4 RSBS + cross-linker	31	4.25E+07	-4.843	5.03E+05	1.75E+04
FH + 0.7 Elvaloy AM + 0.17 PPA	28	1.68E+07	-4.697	2.26E+05	8.73E+03
FH + 1.5 Elvaloy AM + 0.17 PPA	28	2.36E+07	-4.630	3.39E+05	1.37E+04
CRM + 2 RSBS + cross-linker	22	1.09E+07	-4.681	1.49E+05	5.81E+03
CRM + 4 RSBS + cross-linker	25	2.69E+07	-4.846	3.17E+05	1.10E+04
CRM + 0.7 Elvaloy AM + 0.17 PPA	19	1.01E+07	-4.687	1.38E+05	5.38E+03
CRM + 1.5 Elvaloy AM + 0.17 PPA	22	1.86E+07	-4.687	2.53E+05	9.84E+03

Significant Problems, Issues and Potential Impact on Progress

None.

Work Planned Next Quarter

The research team will focus its efforts on preparing and testing binders modified with different mineral fillers. The materials used for mastic preparation will be carefully selected based on results from the current NCHRP 9-45 study. Fillers that showed extreme behavior in terms of Rigden voids will be selected for mastic preparation.

Work Element F2b: Mastic Testing Protocol (TAMU)

Work Done This Quarter

This work element is completed and the reader is referred to work element M1c.

Work Element F2c: Mixture Testing Protocol (TAMU)

Work Done This Quarter

Investigations are continued in this quarter on the viscoelastic and viscoplastic characterization of the asphalt mixtures by conducting the stress-controlled tests and data analysis on the laboratory fabricated asphalt mixture specimens. Specifically, the following four achievements are made:

- An experimental protocol is developed to characterize the viscoelasticity and viscoplasticity of asphalt mixtures;
- A new strain decomposition technique is proposed to separate the viscoelasticity from the viscoplasticity of asphalt mixtures;

- A parameter acquisition method is presented to obtain the material coefficients in the Perzyna-type viscoplastic strain model; and
- A data analysis tool (DAT) is programmed using the software Excel and Matlab to automatically determine the material properties from the experimental data.

Details of the achievements made in this quarter are summarized in a draft paper (Zhang et al. 2011) and briefly presented as follows:

1) An Experimental Protocol to Characterize Viscoelasticity and Viscoplasticity

1.1) Experimental Protocol

To characterize the viscoelastic and viscoplastic properties of asphalt mixtures in compression, an experimental protocol is developed that includes three tests: 1) a nondestructive creep test to obtain the undamaged creep compliance and relaxation modulus, 2) a nondestructive dynamic modulus test to obtain the undamaged complex modulus and phase angle, and 3) a destructive controlled-stress cyclic loading test to determine the viscoplastic characteristics.

The three tests are conducted on the laboratory fabricated cylindrical asphalt mixture specimens with a height of 150 mm and a diameter of 100 mm. Three vertical linear variable differential transformers (LVDTs) with a gauge length of 90 mm are mounted at 120° from each other on the lateral surface of each asphalt mixture specimen. The specimens are stored in the environmental chamber of the Universal Testing Machine (UTM) with a temperature of 40°C for at least 3 hours to reach the equilibrium temperature. The loading sequence used in the experimental protocol is shown in figure F2c.1. The creep test is firstly conducted using the UTM in which a constant compressive stress of 20 kPa is applied to the specimen for 120 sec. Then the compressive load is removed and the specimen is at rest for 1 hour. After the 1-hour rest period, the dynamic modulus test is conducted on the same specimen, in which a compressive sinusoidal stress with a maximum stress value of 35 kPa is applied to the sample for 20 cycles at a frequency of 1 Hz. The total strain at the end of both the creep test and the dynamic modulus test is controlled to less than 150 $\mu\epsilon$ which is believed to be the linear viscoelastic limit for the asphalt mixture in compression. After another 1-hour rest period, the controlled-stress cyclic loading test is performed on the same undamaged specimen, in which a sinusoidal compressive load with a minimum stress of 120 kPa and a maximum stress of 690 kPa is applied on the specimen at a frequency of 1 Hz. The total deformation is recorded using the three LVDTs until the specimen fails.

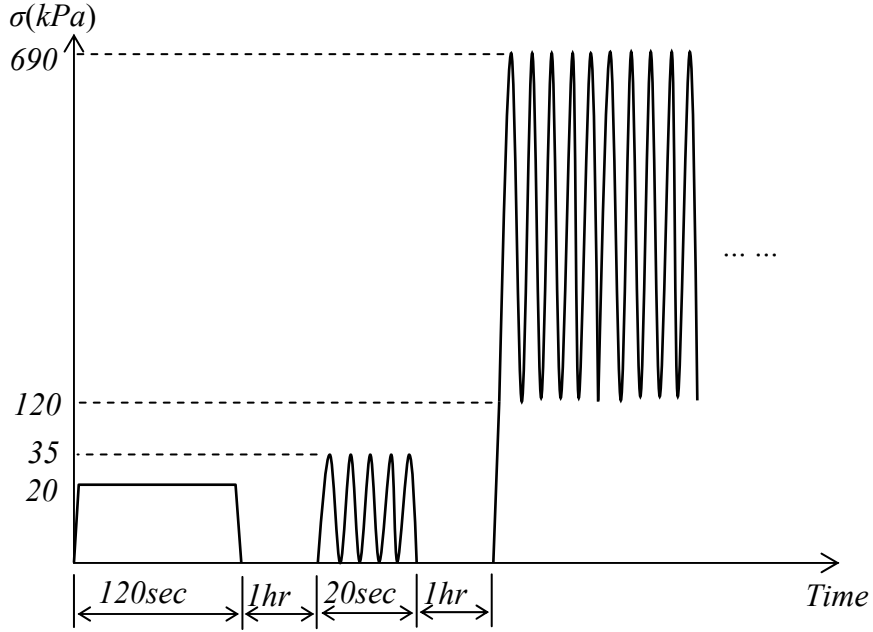


Figure F2c.1. Loading sequences in the experimental protocol (not scaled).

1.2) Viscoelasticity Characterization

To accurately characterize the viscoelastic properties of the asphalt mixture, a Prony series model including multiple Kelvin elements and one spring in series is used in this study and the relaxation modulus and the creep compliance are shown as follows:

$$E(t) = E_{\infty} + \sum_{j=1}^M E_j \exp\left(-\frac{t}{k_j}\right) \quad (\text{F2c.1})$$

$$D(t) = D_0 + \sum_{i=1}^M D_i \left[1 - \exp\left(-\frac{t}{\tau_i}\right)\right] \quad (\text{F2c.2})$$

where $E(t)$ = relaxation modulus; E_{∞} = long term equilibrium modulus; E_j = components of modulus; k_j = relaxation time; $D(t)$ = creep compliance; D_0 = instantaneous compliance; D_i = components of creep compliance; τ_i = retardation time; and M = total number of Kelvin elements. The creep compliance and relaxation modulus have the following relationship:

$$\bar{E}(s)\bar{D}(s) = \frac{1}{s^2} \quad (\text{F2c.3})$$

where $\bar{E}(s)$ and $\bar{D}(s)$ are the Laplace transforms of the $E(t)$ and $D(t)$, respectively, and $s =$ variable in the Laplace domain. Thus, by taking the inverse Laplace transform of equation F2c.3, it is possible to solve one of the relaxation modulus or the creep compliance if the other one is known. Equation F2c.3 yields $E(0)D(0) = E(\infty)D(\infty) = 1$.

In the compressive creep test, the constant stress is $\sigma = 20$ kPa and the strain is calculated using the average deformation measured from the three LVDTs divided by the gauge length of 90 mm. Then the creep compliance is directly calculated using $D(t) = \varepsilon(t)/\sigma$, which can be perfectly fitted by equation F2c.2. The relaxation modulus can be estimated using equation F2c.3 and be fitted using equation F2c.1. Examples of $D(t)$ and $E(t)$ for an asphalt mixture at 40°C are shown in figure F2c.2.

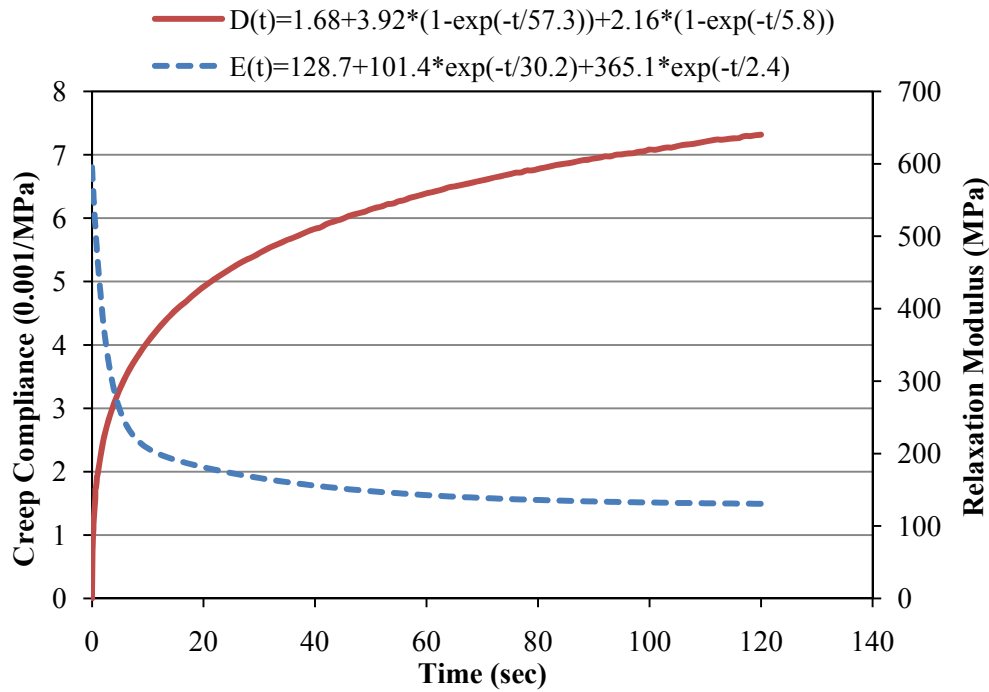


Figure F2c.2. Creep compliance and relaxation modulus of an undamaged asphalt mixture at 40°C.

In practice, the load applied to the asphalt pavement is not a static load but a dynamic load such as a moving traffic load with a short loading period, e.g. 0.01 sec to 1 sec. The loading period has an approximate relationship with the loading frequency: $t \approx 1/2\omega$. For example, a frequency of 1 Hz corresponds to a loading period of $t = 1/2\omega = 1/4\pi = 0.08$ sec. In the creep test, the measured strain data are not stable at the loading time of 0.08 sec due to the transient effect that may die out in several seconds. Therefore, the relaxation modulus or creep compliance at a very short time period may not be accurately determined using the creep test. A dynamic modulus test is needed to obtain the accurate complex modulus at a short loading time or at high frequencies. When performing the

dynamic modulus test on the same specimens that are tested in the creep test, the magnitude of the complex modulus ($|E^*|$) and the phase angle (ϕ) can be obtained at a temperature of 40°C and a frequency of 1 Hz.

1.3) Viscoplasticity Characterization

In order to characterize the viscoplastic properties of the asphalt mixture, the controlled-stress cyclic loading tests are conducted on the asphalt mixture specimens. The function of the applied load is:

$$\sigma(t) = \sigma_1 - \sigma_0 \cos(\omega t) \quad (\text{F2c.4})$$

The load in equation F2c.4 can be decomposed into two components: the creep stress σ_1 and the cyclic stress $\sigma_2 = \sigma_0 \cos(\omega t)$. The creep strain output due to the creep stress is:

$$\varepsilon_1(t) = \sigma_1 \hat{D}(t, \sigma_1) = \sigma_1 \left\{ \hat{D}_0 + \sum_{i=1}^L \hat{D}_i \left[1 - \exp\left(-\frac{t}{\hat{\tau}_i}\right) \right] \right\} \quad (\text{F2c.5})$$

where $\hat{D}(t, \sigma_1)$ = damaged creep compliance at a stress of σ_1 , a formulation similar to $D(t)$ shown in equation F2c.2 is used for $\hat{D}(t, \sigma_1)$ in equation F2c.5 but with different coefficients; \hat{D}_0 = instantaneous compliance which includes elastic response and plastic response, thus $\hat{D}_0 \neq D_0$; \hat{D}_i = components of the damaged creep compliance, and $\hat{D}_i \neq D_i$; $\hat{\tau}_i$ = retardation time of the damaged creep compliance, and $\hat{\tau}_i \neq \tau_i$, and L = total number of Kelvin elements.

The cyclic strain due to the cyclic stress $\sigma_2 = \sigma_0 \cos(\omega t)$ is expressed as:

$$\varepsilon_2(t) = \varepsilon_N \cos(\omega t - \hat{\phi}_N) \quad (\text{F2c.6})$$

where ε_N = amplitude of the cyclic strain at the N-th load cycle; and $\hat{\phi}_N$ = angle of strain lagging behind the cyclic stress at the N-th load cycle, $\hat{\phi}_N$ can be considered as the phase angle of the damaged complex modulus $\hat{E}_N^*(\omega)$ at the N-th load cycle whose magnitude is defined as:

$$\left| \hat{E}_N^*(\omega) \right| = \frac{\sigma_0}{\varepsilon_N} \quad (\text{F2c.7})$$

Based on the raw data of $\varepsilon_2(t)$, the magnitude and phase angle of the damaged complex modulus are calculated and shown in figure F2c.3 which also shows the total strain data. It is found that the

damaged complex modulus $\hat{E}_N^*(\omega)$ is time (load cycles) dependent at a constant frequency. In the primary stage, $|\hat{E}_N^*(\omega)|$ increases and $\hat{\phi}_N$ decreases; in the secondary stage, both $|\hat{E}_N^*(\omega)|$ and $\hat{\phi}_N$ remain constant. The change of $|\hat{E}_N^*(\omega)|$ and $\hat{\phi}_N$ in the primary stage may have two causes: 1) the initial transient responses which is because the dynamic loads need a period of time to disappear; and 2) the initial air voids in the asphalt mixture take a period of time to be compressed and to close, until then the asphalt mixture becomes stiffer and yields constant material properties. Both $|\hat{E}_N^*(\omega)|$ and $\hat{\phi}_N$ are assigned constant values that are measured in the secondary stage since this stage dominates the deformation of the asphalt mixture. In the tertiary stage, $|\hat{E}_N^*(\omega)|$ decreases and $\hat{\phi}_N$ increases, which are caused by the opening and propagation of cracks. The tertiary deformation is not the concern in this study since the real asphalt pavement needs to be rehabilitated once the tertiary deformation starts.

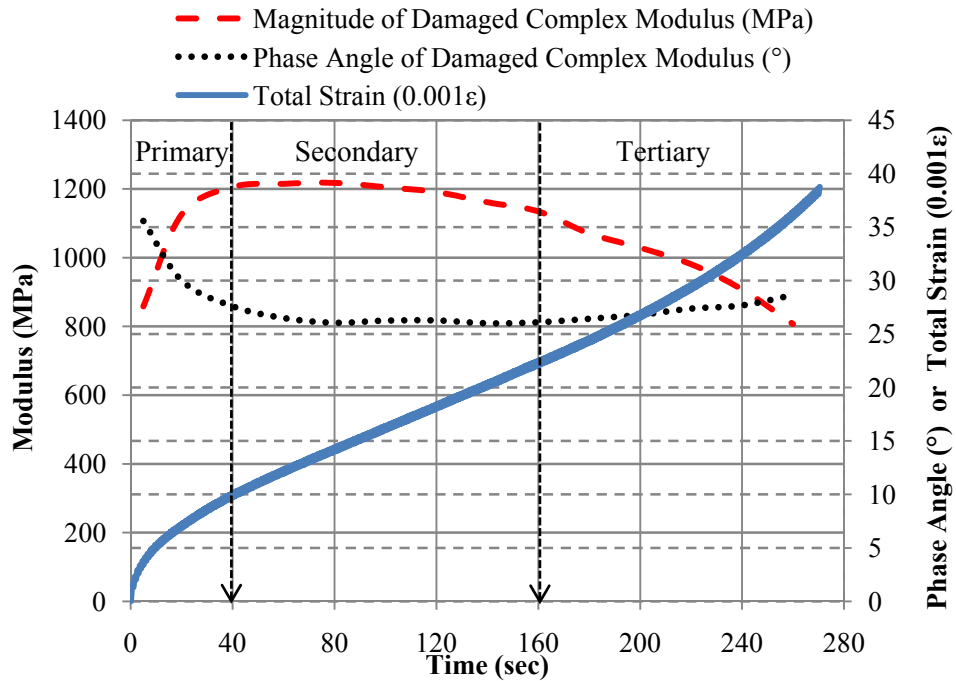


Figure F2c.3. Total strain, magnitude and phase of damaged complex modulus of an asphalt mixture at 40°C and 1 Hz.

2) Separation of Viscoplasticity and Viscoelasticity

2.1) Strain Decomposition

The strain measured in the controlled-stress cyclic loading test is the total strain (ε) which consists of the elastic (ε^e), viscoelastic (ε^{ve}), plastic (ε^p) and viscoplastic strain (ε^{vp}) in the primary and secondary deformation stages. The decomposition of the total strain is shown in equation F2c.8. The viscoplastic strain and the parameters of the viscoplasticity model can be determined when the other three strain components are deducted from the total strain.

$$\varepsilon = \varepsilon^e + \varepsilon^{ve} + \varepsilon^p + \varepsilon^{vp} \quad (\text{F2c.8})$$

A common method to perform the strain decomposition is to conduct the creep and recovery test. As shown in figure F2c.4, if the load is released at time t_0 , the instantaneously recovered strain is the elastic strain and the retarded recovered strain is the viscoelastic strain. When the recovery time is sufficiently long, the viscoelastic strain can be fully recovered and the remaining strain is the sum of the viscoplastic strain and plastic strain. However, this strain decomposition method is associated with two problems: 1) it is impossible to directly separate the strain components in the creep process of the test, and the recovery loading time that is required will increase the testing time; 2) the accumulated strain at the end of each recovery period does not necessarily consist of only the plastic strain and the viscoplastic strain but it can also include viscoelastic strain that has not fully recovered yet since a limited recovery time is used in the test. Thus, a new method is needed to accurately decompose the measured total strain.

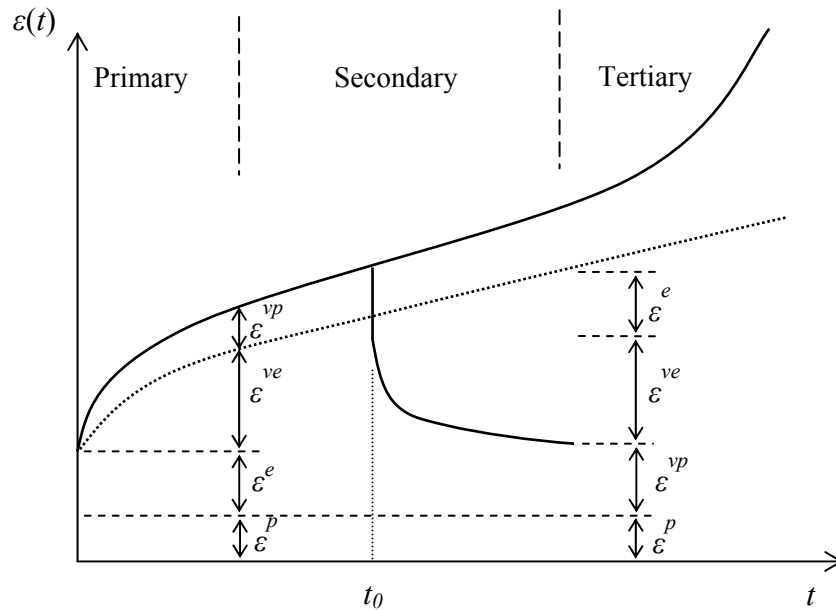


Figure F2c.4. Creep and recovery test and strain decomposition.

2.2) Calculation of Pseudo Strain

Schapery (1984) proposed the extended elastic-viscoelastic correspondence principle which states that, if the actual stress or strain is replaced with the pseudo variables, the constitutive equation for the viscoelastic material is identical to those for the elastic material. The pseudo strain is defined as:

$$\varepsilon^R(t) = \frac{1}{E_R} \int_0^t E(t-\xi) \frac{d\varepsilon(\xi)}{d\xi} d\xi \quad (\text{F2c.9})$$

where ε^R = pseudo strain; t = current time; ξ = previous time before t ; $\varepsilon(\xi)$ = measured strain history; $E(t)$ = relaxation modulus; and E_R = reference modulus which is an arbitrary constant. Based on equations F2c.9, the physical stress and the pseudo strain have a relationship as:

$$\sigma(t) = E_R \varepsilon^R(t) \quad (\text{F2c.10})$$

It is clear that a correspondence can be found between equation F2c.10 and the elastic stress-strain relationship, e.g. the Hooke's law. The advantage of this extended correspondence principle is that the effect of time on the constitutive equation of the viscoelastic material is eliminated, which brings significant convenience to the following damage analysis on the viscoelastic material.

Based on the definition of pseudo strain in equation F2c.9, the pseudo strain can be calculated in the controlled-stress cyclic loading test. The creep strain in equation F2c.5 yields the creep pseudo strain $\varepsilon_1^R(t)$ that is shown in equation F2c.11 and the cyclic strain in equation F2c.6 produces the cyclic pseudo strain $\varepsilon_2^R(t)$ that is shown in equation F2c.12.

$$\varepsilon_1^R(t) = \frac{\sigma_1}{E_R} \left\{ E_\infty \hat{D}(t) + \hat{D}_0 \Delta E(t) + \sum_{i=1}^L \sum_{j=1}^M \frac{\hat{D}_i E_j}{(1 - \hat{\tau}_i/k_j)} \left[\exp\left(-\frac{t}{k_j}\right) - \exp\left(-\frac{t}{\hat{\tau}_i}\right) \right] \right\} \quad (\text{F2c.11})$$

$$\varepsilon_2^R(t) = \frac{\sigma_0}{E_R} \frac{|E^*(\omega)|}{|\hat{E}_N^*(\omega)|} \cos(\omega t - \hat{\phi}_N + \phi) \quad (\text{F2c.12})$$

where $\Delta E(t) = E(t) - E_\infty$. Then the total pseudo strain in the controlled-stress cyclic loading test is calculated using the superposition principle as:

$$\varepsilon^R(t) = \varepsilon_1^R(t) - \varepsilon_2^R(t) \quad (\text{F2c.13})$$

2.3) Separation of Viscoelasticity and Viscoplasticity

Equations F2c.11 and F2c.12 establish a practical method to calculate the pseudo strains, in which the reference modulus needs to be determined. Many researchers employ a unity for the reference modulus which has the same unit as stress. However, the pseudo strain calculated using this method is only a relative value that does not have a physical meaning and cannot be used in the strain decomposition. Thus, a reference modulus with a physical meaning is needed in the viscoplastic analysis. The reference modulus can be determined by converting the viscoelastic problem to the elastic problem with introducing the pseudo strain, which equals to the elastic strain in the undamaged condition. Comparing equation F2c.10 with Hooke's law ($\sigma = E_0 \varepsilon^e$) and letting $\varepsilon^R = \varepsilon^e$ yields:

$$E_R = E_0 \quad (\text{F2c.14})$$

where E_0 = Young's modulus. It can be proved that by assigning the reference modulus to the Young's (elastic) modulus, the viscoelastic strain can be eliminated from the total strain in the undamaged conditions, such as in the nondestructive creep test and the nondestructive dynamic modulus test.

Introducing the pseudo strain allows the separation of the components of the total strain. By calculating the pseudo strain and defining the reference modulus as Young's modulus, the elastic strain is left in the undamaged condition while the elastic, plastic and viscoplastic strains remain in the damaged condition, that is,

$$\varepsilon^R(t) = \begin{cases} \varepsilon^e & \text{Undamaged} \\ \varepsilon^e + \varepsilon^p + \varepsilon^{vp}(t) & \text{Damaged} \end{cases} \quad (\text{F2c.15})$$

Based on equations F2c.8, F2c.15, Hooke's law and $\varepsilon^{vp}(0) = 0$, the measured total strain can be decomposed as:

$$\begin{cases} \varepsilon^e = \frac{\sigma}{E_0} \\ \varepsilon^{ve}(t) = \varepsilon(t) - \varepsilon^R(t) \\ \varepsilon^p = \varepsilon^R(0) - \varepsilon^e \\ \varepsilon^{vp}(t) = \varepsilon^R(t) - (\varepsilon^e + \varepsilon^p) \end{cases} \quad (\text{F2c.16})$$

Finally, every component of the total strain is separated from each other and can be characterized individually. For example, figure F2c.5 shows the curves of the strain components of the asphalt mixture changing with load cycles in the primary and secondary stage of the controlled-stress cyclic loading test. The sinusoidal change of each strain is not shown in figure F2c.5 since only the strain at the end of each load cycle is plotted. As can be seen from figure F2c.5, the total strain is

successfully decomposed into elastic strain, plastic strain, viscoelastic strain and viscoplastic strain. The elastic and plastic strain are independent of the load cycles while the viscoelastic and viscoplastic strain increase with load cycles and follow a power function.

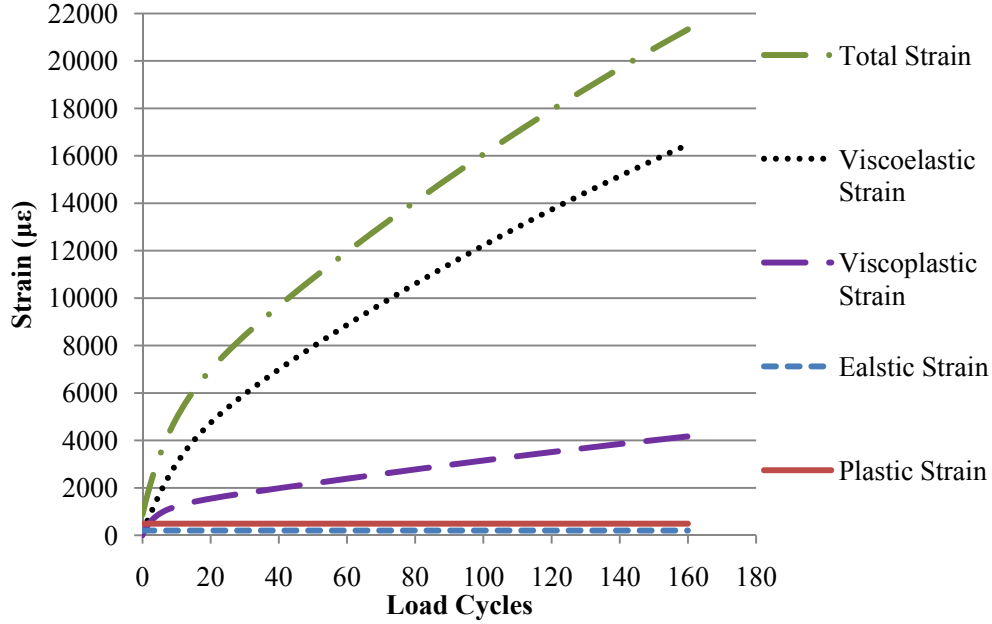


Figure F2c.5. Strain decomposition in control stress cyclic loading test.

3) Parameters Acquisition in Viscoplastic Strain Model

In previous quarterly reports, the Perzyna’s type viscoplasticity model is used and a series of method was proposed using the cohesion (C), friction angle (φ) and modified vector magnitude (Δ') to estimate the material parameters in the viscoplasticity model including the yield surface function parameters (α , κ_0 and d) and the viscoplastic potential function parameters (β and d). However, the viscoplastic parameters (Γ and n) and the strain hardening function parameters (κ_1 and κ_2) have not been determined yet. The separation of the viscoelastic strain and the viscoplastic strain makes it easier to accurately characterize the viscoplastic deformation of the asphalt mixture. The viscoplastic strain separated from the total strain in the controlled-stress cyclic loading test can be directly used to estimate the remaining parameters of the Perzyna’s type viscoplasticity model for the asphalt mixtures.

The controlled-stress cyclic loading test is a uniaxial compressive test, in which the stress at the end of each cycle is $\sigma_N = \sigma_1 - \sigma_0$. Thus, the first derivative of the viscoplastic potential function is:

$$\frac{\partial g}{\partial \sigma_N} = 1 - \frac{1}{3} \beta \tag{F2c.17}$$

The yield surface function becomes:

$$f = \left(1 - \frac{\alpha}{3}\right) \sigma_N - \kappa_1 \left\{1 - \exp\left[-\kappa_2 \cdot \varepsilon_e^{vp}(N)\right]\right\} - \kappa_0 \quad (\text{F2c.18})$$

The viscoplastic strain rate with respect to time can be transformed to the viscoplastic strain rate with respect to load cycles as follows:

$$\dot{\varepsilon}^{vp}(t) = \frac{d\varepsilon^{vp}}{dt} = \frac{d\varepsilon^{vp}}{dN} \frac{dN}{dt} = \dot{\varepsilon}^{vp}(N) \frac{\omega}{2\pi} \quad (\text{F2c.19})$$

Substituting equation F2c.17, F2c.18 and F2c.19 into Perzyna's viscoplasticity model yields:

$$\dot{\varepsilon}^{vp}(N) = \frac{2\pi}{\omega} \frac{\Gamma}{(\sigma_y^0)^n} \left[\left(1 - \frac{\alpha}{3}\right) \sigma_N - \kappa_1 \left\{1 - \exp\left[-\kappa_2 \cdot \varepsilon^{vp}(N)\right]\right\} - \kappa_0 \right]^n \left(1 - \frac{\beta}{3}\right) \quad (\text{F2c.20})$$

For the viscoplastic strain in the primary and secondary stage, the Tseng-Lynton model has been widely used to fit the strain curve as follows:

$$\varepsilon^{vp}(N) = \varepsilon_\infty^{vp} \exp\left[-\left(\frac{\rho}{N}\right)^\lambda\right] \quad (\text{F2c.21})$$

where ε_∞^{vp} = ultimate viscoplastic strain when time goes to infinity; ρ and λ = material parameters. These three parameters can be obtained by fitting equation F2c.21 to the viscoplastic strain curve obtained in equation F2c.16. Equation F2c.21 yields the first derivative of the viscoplastic strain as:

$$\dot{\varepsilon}^{vp}(N) = \lambda \rho^\lambda \varepsilon_\infty^{vp} N^{-(\lambda+1)} \exp\left[-\left(\frac{\rho}{N}\right)^\lambda\right] \quad (\text{F2c.22})$$

Substituting equations F2c.21 and F2c.22 into equation F2c.20 and using the least squares method, the parameters including Γ , n , κ_1 , and κ_2 in the viscoplastic strain model can be determined.

4) Data Analysis Tool (DAT) for Experiments

In the proposed experimental protocol, each specimen is sequentially tested in the nondestructive creep test, nondestructive dynamic modulus test and controlled-stress cyclic loading test, which produce a significant amount of data that need to be analyzed to determine the material properties. In order to save calculation time and effort, a data analysis tool (DAT) is programmed in the software Excel and Matlab to automatically calculate the material properties with inputting the raw data measured from the tests. The package of the DAT includes the following functions:

- a) Creep test data analysis: by inputting the stress, strain and time data of the nondestructive creep test into the Excel program, the creep compliance and relaxation modulus will be calculated and fitted by Matlab using equation F2c.1 and equation F2c.2, and coefficients of the models will be presented for users.
- b) Cyclic test data analysis: by inputting the load, deformation and time data of the controlled-stress cyclic loading test into the Excel program, the stress and strain in every load cycle will be calculated and then fitted by the third order Fourier transform function in Matlab. The program will determine the maximum and minimum values of the stress and strain and their corresponding time, which are used to calculate the magnitude and phase angle of the complex modulus of the damaged asphalt mixture specimen at each load cycle.
- c) Strain decomposition calculation: based on the output of the creep test data analysis, cyclic test data analysis as well as the nondestructive dynamic modulus, the pseudo strain can be automatically calculated and the strain decomposition can be performed in the DAT.

Significant Results

The viscoelastic and viscoplastic properties of asphalt mixtures are further investigated in this quarter. First, an experimental protocol is developed to characterize the viscoelasticity and viscoplasticity of the asphalt mixtures using a nondestructive creep test, a nondestructive dynamic modulus test and a controlled-stress cyclic loading test. Second, a new strain decomposition technique is proposed to separate the viscoelasticity from the viscoplasticity using the extended elastic-viscoelastic corresponding principle to calculate the pseudo strain by defining the reference modulus as the Young's modulus so the pseudo strain has a physical meaning. Third, based on the viscoplastic strain curve separated from the total strain, a parameter acquisition method is proposed to obtain the viscoplastic parameters and the strain hardening parameters in the Perzyna-type viscoplastic strain model. Finally, a data analysis tool (DAT) is programmed in the software Excel and Matlab to automatically solve for the material properties, including the creep compliance and the relaxation modulus of the undamaged asphalt mixtures, and the complex modulus and phase angle of the damaged asphalt mixtures. The programmed DAT also performs the strain decomposition automatically. The entire test and analysis sequence on a single sample requires about four hours, a significant reduction in the time required by previous method by a factor of ten or more.

Significant Problems, Issues and Potential Impact on Progress

It is necessary to verify the reliability and repeatability of the proposed experimental protocol and data analysis methods for the viscoplastic characterization of the asphalt mixtures.

Work Planned in Next Quarter

- More tests according to the proposed testing protocol will be conducted on various asphalt mixture specimens that vary in the volumetric properties, material properties and aging conditions;

- Test protocol and data analysis method will be investigated to characterize the viscoelastic fracture in the asphalt mixtures including the estimation of the anisotropic damage density and crack growth when the material is in the controlled-stress mode.

Cited Reference

Zhang, Y., R. Luo, and R. L. Lytton, 2011, Viscoelastic and Viscoplastic Characterization of an Asphalt Mixture in Compression. *Draft available.*

Work Element F2d: Structural Characterization of Micromechanical Properties in Bitumen using Atomic Force Microscopy (TAMU)

Work Done This Quarter

Tomography is carried out as needed on specimens that are used in developments of aging, healing and unified models. The reader is referred to work element F1c-3.

Significant Results

None.

Significant Problems, Issues and Potential Impact on Progress

None.

Work Planned Next Quarter

Tomography will be carried out as needed for the models development.

Work Element F2e: Verification of the Relationship between DSR Binder Fatigue Tests and Mixture Fatigue Performance (UWM)

Work Done This Quarter

The research team investigated the use of time-temperature superposition for the Linear Amplitude Sweep (LAS) test results to estimate fatigue damage at any testing temperature and loading frequency. In asphalt mixtures, it has been demonstrated that time-temperature superposition can be applied to viscoelastic continuum damage (VECD) results to predict fatigue life at any temperature and time from a single fatigue test (Daniel and Kim 2002; Kutay et al. 2008). The current VECD analysis framework for binder LAS testing must be revised for easy application of time-temperature superposition. This was accomplished by using a normalized value of the loss modulus in place of the absolute value as a material integrity parameter.

While Johnson (2010) and Kim et al. (2006) proposed using the absolute value of loss modulus as the material integrity parameter for VECD analysis, others have instead used a normalized value as

a material integrity parameter (Daniel and Kim 2002; Kutay et al. 2008). For example, Daniel and Kim (2002) used pseudo-stiffness divided by initial pseudo-stiffness in place of an absolute value. Kutay et al. (2008) also cited use of normalization to reduce sample variability. In addition to accounting for sample-to-sample variation, use of a normalized material integrity parameter allows for easy application of time-temperature superposition, since absolute values of properties vary with temperature and time.

Significant Results

Since the goal of fatigue analysis is to evaluate material degradation and not undamaged material properties, it seems reasonable to use a model that looks at the relative change in material properties with damage. Table F2e.1 includes the current analysis framework and the revised framework to allow for use of time-temperature shifting.

Table F2e.1. Comparison of current and modified VECD analysis frameworks.

CURRENT ANALYSIS FRAMEWORK	MODIFIED ANALYSIS FRAMEWORK
$\frac{dD}{dt} = \left(\frac{\partial W}{\partial D}\right)^\alpha$ <p>where D is damage, t is time, W is work performed, and α is a constant related to rate at which damage progresses</p>	$\frac{dD}{dt} = \left(\frac{\partial W}{\partial D}\right)^\alpha$ <p>where D is damage, t is time, W is work performed, and α is a constant related to rate at which damage progresses</p>
$\alpha=1 + 1/m$, where m is the slope a log-log plot of storage modulus versus frequency	$\alpha=1 + 1/m$, where m is the slope a log-log plot of storage modulus versus frequency
$W = \pi \cdot I_D \cdot \gamma_0^2 \cdot G^* \sin \delta$ <p>where I_D is the undamaged G^*, γ_0 is strain amplitude</p>	$W = \pi \cdot I_D \cdot \gamma_0^2 \cdot C$, where $I_D = \frac{ G^* \cdot \sin \delta_{initial}}{ G^* \cdot \sin \delta_{LVE}}$ $C = \frac{ G^* \cdot \sin \delta}{ G^* \cdot \sin \delta_{LVE} \cdot I_D}$, γ_0 is strain amplitude, $ G^* \cdot \sin \delta_{LVE}$ is the linear viscoelastic loss modulus at the reference temperature
$D(t) \cong \sum_{i=1}^N [\pi I_D \gamma_0^2 (G^* \sin \delta_{i-1} - G^* \sin \delta_i)]^{\frac{\alpha}{1+\alpha}} (t_i - t_{i-1})^{\frac{1}{1+\alpha}}$ <p>where t is time</p>	$D(t) \cong \sum_{i=1}^N [\pi I_D \gamma_0^2 (C_{i-1} - C_i)]^{\frac{\alpha}{1+\alpha}} (t_{Ri} - t_{Ri-1})^{\frac{1}{1+\alpha}}$ <p>where t_R is the reduced time</p>
$ G^* \sin \delta = C_0 - C_1(D)^{C_2}$ <p>where C_0 is the undamaged $G^* \cdot \sin \delta$, C_1 and C_2 are curve fit parameters</p>	$C = C_0 - C_1(D)^{C_2}$ <p>where C_0 is 1, C_1 and C_2 are curve fit parameters</p>
$N_f = A(\gamma_{max})^B$ where $B = -2\alpha$	$N_f = A(\gamma_{max})^B$ where $B = -2\alpha$
$A = \frac{f(D_f)^k}{k \left(\pi \frac{I_D}{ G^* } C_1 C_2 \right)^\alpha G^* ^{-\alpha}}$ <p>where f is the frequency, D_f is the damage at failure, and $k = 1 + (1 - C_2)\alpha$</p>	$A = \frac{f_R(D_f)^k}{k(\pi I_D C_1 C_2)^\alpha}$ <p>where f_R is the reduced frequency, D_f is the damage at failure, and $k = 1 + (1 - C_2)\alpha$</p>

The primary modification is the definition of W and I_D . The work performed is quantified using a loss modulus normalized by the initial undamaged loss modulus. I_D is the ratio between the initial undamaged loss modulus at the test temperature to the undamaged loss modulus at the reference temperature in the modified framework. Note that there is no direct relationship between the fatigue law parameter A derived from the two analysis frameworks shown in table F2e.1.

The modified formulas allow for application of time-temperature superposition through use of reduced time. However, for asphalt binders, the parameter α is also temperature-dependent. Figure F2e.1 shows a log-log relation of relaxation modulus over a wide range of relaxation times for a

typical asphalt binder. The plot appears to be nearly linear over short time scales (i.e., in which α for a single temperature is calculated), but is nonlinear over a broad time range, (i.e., over multiple temperatures). Hence, α must also be corrected when predicting fatigue law parameters at multiple temperatures.

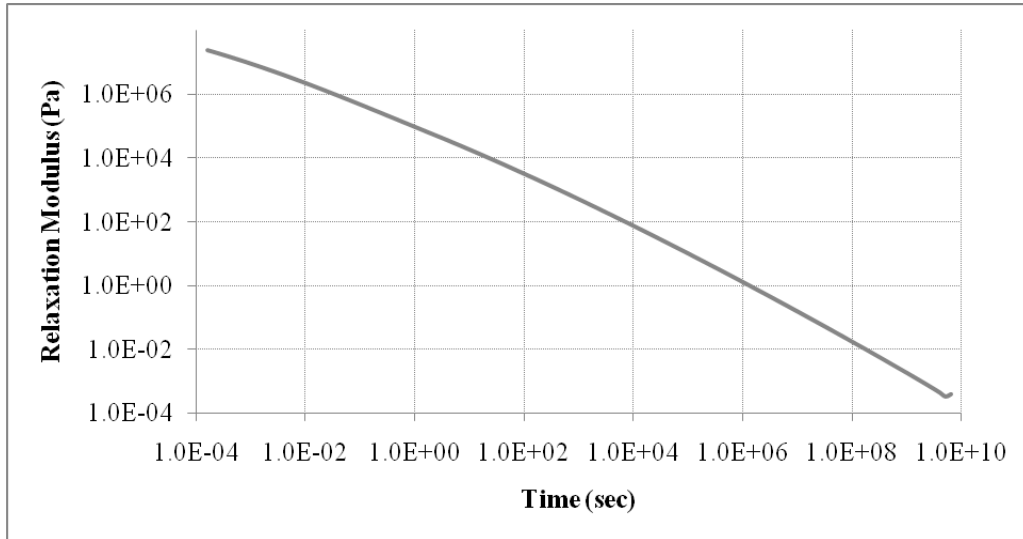


Figure F2e.1. Graph. Relaxation modulus over broad time scale.

To obtain α at the target temperature, it is recommended that a frequency sweep be conducted at the temperature fatigue results are needed (i.e., the reference temperature), in addition to the frequency sweep at the temperature at which the fatigue test was conducted. The two frequency sweeps (one at the target temperature and one at the LAS testing temperature) can be used to determine shift factors and the reduced time.

Time-temperature superposition was applied to LAS results of four LTPP binders. The binders were tested using LAS procedure at the PG intermediate grade temperature and the LTPP actual pavement intermediate temperature. The results at the intermediate PG temperature were then shifted to the intermediate pavement temperature and compared to VECD results of tests conducted at the reference temperature. The VECD material integrity (C) versus damage (D) curves were all successfully shifted to the reference temperature. Figure F2e.2 shows an example of the temperature shifting for LAS testing.

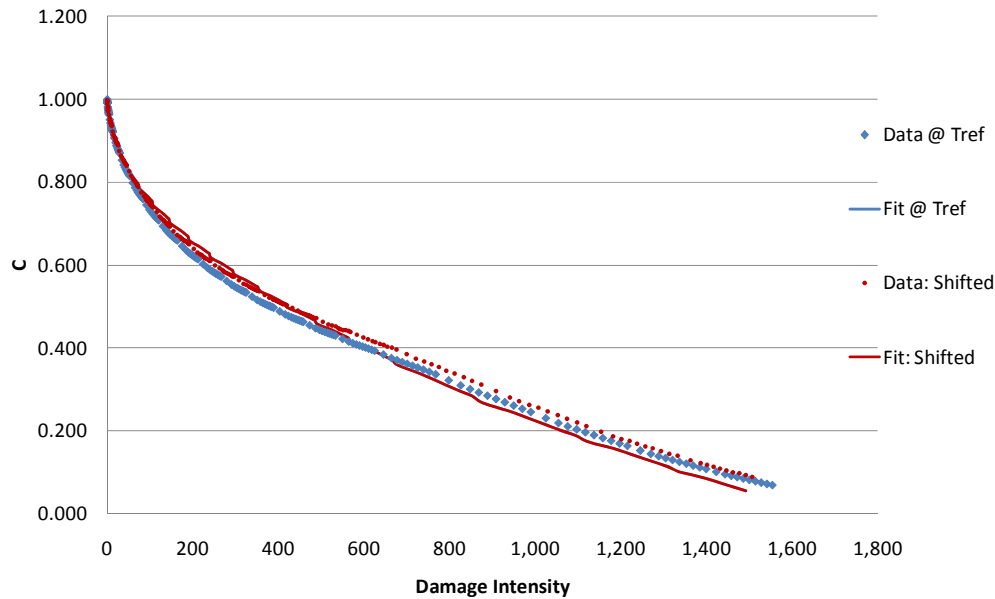


Figure F2e.2. Graph. Shifting damage curves of binder 290963 (PG 64-16).

The fatigue model parameter A predicted from time-temperature superposition does not always agree with the A calculated at the reference temperature, despite apparent unification of damage curves. Damage curves predicted using time-temperature superposition agree with the measured curves at the reference temperature, as shown in figure F2e.2. Therefore, it appears that large differences in A values are caused by the sensitivity of A to the damage curve fit parameters C_1 and C_2 .

Although curves appear very similar, there are large differences in model fit parameters that inhibit successful unification of fatigue law parameter A . Due to the sensitivity of the current power law model, a numerical solution in place of the curve fit and closed-form solution to obtain A is currently being developed to allow for accurate fatigue life prediction at multiple temperatures from a single LAS test. The parameter B depends only on α , which, as was discussed previously, can be directly estimated from a frequency sweep at the reference temperature used to obtain the time-temperature shift factor.

Significant Problems, Issues and Potential Impact on Progress

None.

Work Planned Next Quarter

The research team will investigate the use of numerical solutions for the fatigue law parameters in addition to the existing closed-form solution. The idea is to reduce the current sensitivity of fatigue life to the power law parameters C_1 and C_2 . The research team will also begin testing mastics to determine the influence of mineral filler on fatigue. The team will conduct fatigue testing of asphalt mixtures using the Indirect Tensile Test. The LAS procedure will be used for fatigue

characterization of the binders used for asphalt mixture preparation and a comparison between binder and mixture fatigue performance will be conducted.

Cited References

Daniel, J. S., and Y. R. Kim, 2002, Development of a Simplified Fatigue Test and Analysis Procedure Using a Viscoelastic Continuum Damage Model. *Journal of the Association of Asphalt Paving Technologists*, 71: 619-650.

Johnson, C. M., 2010, Estimating Asphalt Binder Fatigue Resistance using an Accelerated Test Method. Ph.D Thesis, University of Wisconsin–Madison.

Kim, Y., H. J. Lee, D. N. Little, and Y. R. Kim, 2006, A Simple Testing Method to Evaluate Fatigue Fracture and Damage Performance of Asphalt Mixtures. *Journal of the Association of Asphalt Paving Technologists*, 75: 755-787.

Kutay, M. E., N. H. Gibson, and J. Youtcheff, 2008, Conventional and Viscoelastic Continuum Damage (VECD) Based Fatigue Analysis of Polymer Modified Asphalt Pavements. *Journal of the Association of Asphalt Paving Technologists*, 77: 395-434.

CATEGORY F3: MODELING

Work Element F3a: Asphalt Microstructural Model

Subtask F3a-1. ab initio Theories, Molecular Mechanics/Dynamics and Density Functional Theory Simulations of Asphalt Molecular Structure Interactions (URI)

Work Done This Quarter

Quantum mechanics calculations to test asphaltene molecular structures have been completed. A manuscript describing changes in molecular architectures that are required to enable lower energies is nearly completed for the journal *Energy and Fuels*.

New molecules for use in model bitumens were selected that are larger and more diverse in polarity compared to prior systems that have been studied by molecular simulations. Compositions were chosen for AAA-1 (Canadian), AAK-1 (Venezuelan), and AAM-1 (West Texas Intermediate). Saturate and naphthene aromatic molecular weights are in the range of 400 to 500 g/mol for each molecule. These are 150% to 250% larger than those in prior simulations and are closer to the ranges measured in ARC size exclusion chromatography experiments. Molecular architectures were chosen that are consistent with results from mass spectrometry in geochemistry studies found in the literature. The asphaltene molecules are consistent with the most recent findings published by Mullins (2010). His proposed molecules have been changed to be consistent with our quantum mechanics results concerning low-energy asphaltene structures. The SARA balances in the model bitumens were adjusted during the quarter based on feedback within the ARC chemo-mechanics team.

Significant Problems, Issues and Potential Impact on Progress

When choosing model bitumen compositions, it was challenging to identify molecules that can contribute a sufficiently high sulfur concentration (e.g. 5.5 mass% sulfur atoms in AAA-1) while retaining realistic molecular architectures, molecular weights, and reasonable balances among asphaltene, polar aromatic, naphthene aromatic, and saturate concentrations. A model asphaltene molecule with 1 or 2 sulfur atoms in itself has a sulfur mass concentration *lower* than 5.5%, yet this is one of few compounds that is expected to contain sulfur! Atomic sulfur mass fractions of 3.6% have been achieved in the model AAA-1 and AAK-1 bitumens at this time (compared to reported concentrations of 5.5% and 6.4%) through a 290 g/mol highly aromatic resin that has a particularly high sulfur concentration and is detected in geological samples. Increasing the sulfur concentration further distorts the carbon balance further away from aliphatic:aromatic balance; the current systems already contain 39.5 and 40.9% aromatic carbon compared to 28.1 and 31.9% reported for AAA-1 and AAK-1. Within the current molecules, simultaneously increasing the sulfur concentration and decreasing the aromatic content is not possible.

Work Planned Next Quarter

Data analysis and manuscripts will be completed on a spontaneous wax formation event in a molecular simulation and on unique attributes of asphaltene chemistry that have been recognized through quantum mechanics calculations and molecular simulations. This work was delayed from the prior quarter in order to focus efforts on the composition studies and initial molecular simulations.

Subtask F3a-2. Develop algorithms and methods for directly linking molecular simulation outputs and phase field inputs (URI, NIST, VT)

No activity this quarter.

Subtask F3a-3. Obtain temperature-dependent dynamics results for model asphalts that represent asphalts of different crude oil sources (URI)

Work Done This Quarter

Monte Carlo and molecular dynamics simulations at different temperatures have been started. Results are not yet available.

An initial example of a simulation box for AAA-1 at 298 K is shown in figure F3a-3.1. Yellow/orange and blue spheres indicate sulfur and nitrogen heteroatoms. Gray and white spheres indicate carbon and hydrogen atoms. Periodic boundary conditions are in use, meaning that molecules that exit the left side of the box re-enter on the right (and similarly for the top/bottom and front/back).

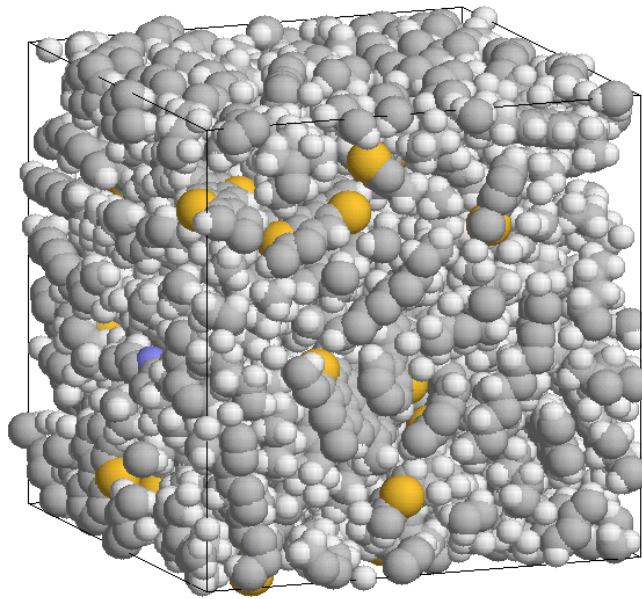


Figure F3a-3.1. Simulation box for AAA-1 at 298 K.

Significant Problems, Issues and Potential Impact on Progress

None

Work Planned Next Quarter

Molecular simulations will be conducted across a range of temperatures for the model bitumen systems. Findings for the dynamics of individual molecules within these systems will begin to be studied, and full results are anticipated in the April-to-June quarter.

Subtask F3a-4. Simulate changes in asphalt dynamics after inducing representations of chemical and/or physical changes to a model asphalt (URI)

No activity this quarter.

Subtask F3a-5. Molecular mechanics simulations of asphalt-aggregate interfaces (VT)

Subtask F3a-6. Modeling of fatigue behavior at atomic scale (VT, NIST)

Subtask F3a-7. Modeling of moisture damage (VT)

Work Done This Quarter

In this quarter, the major work focused on the experimental study of the fatigue phenomenon of asphalt concrete from a micro point of view. The experimental results will be used to validate the modeling and simulation to be performed in the next few quarters.

A Direct Tension Tester (DTT) from Interlaken Company was altered to adapt to a new lab test methodology, which is able to evaluate the performance of asphalt binder, mastics and fine mixes of asphalt concrete mixture in direct tension under cyclic loading.

Test Builder software package with the DTT system allows users to build up their own customized test procedure. A control program for a new fatigue test procedure was written which is able to apply cyclic tensile loading to asphalt binder, mastic and mixture specimens under controlled test temperature and loading rate.

A set of asphalt binder, mastic and mixture specimens were prepared and tested respectively. The loading history and the corresponding strain were recorded during the fatigue test. The effects of loading magnitude, temperature and loading rate on the performance of the asphalt binder under cyclic loading were analyzed. The mastic specimens were prepared by mixing the pure binder with quartz filler and the content of filler was controlled by the weight ratio between filler and asphalt binder. Mastic specimens containing 20%, 30% and 40% fillers were prepared and tested respectively. The effects of filler content on the performance of mastic specimen were analyzed. The mixture specimens were prepared by mixing a small size aggregate with pure binder or mastic. The content of aggregates added in the mixture is set to be 50% of the weight of asphalt binder. Two different mixture specimens were prepared: one with no fillers added in the mixture and the other with 30% fillers added in the mixture. The performance differences of the two mixture specimens were analyzed.

Finally, the test results of asphalt binder, mastics and mixture were analyzed and their relationships were discussed.

The major findings of the study are shown below:

1. Under low temperature, the asphalt binder is easy to break under cyclic loading even the loading level is lower than the tensile strength. The strain of the specimen keeps increasing as number of loading cycles increases.
2. The magnitude of the cyclic loading is the major factor to determine the final strain and number of loading a binder specimen can hold.
3. The asphalt binder becomes softer as temperature increases, both the strain level and number of loading a specimen can hold are increased when temperature is higher.
4. At -20 °C, the impacts of loading rate to the performance of asphalt binder is not as significant as loading magnitude and test temperature.
5. The introduction of filler is able to significantly improve the fatigue resistance of asphalt binder, the strain level and number of loading a mastic specimen is much larger than pure asphalt binder specimen. However, the fatigue resistance of mastic specimen is not linearly increased with the increase of content of filler. A 30% weight ratio between filler and asphalt binder is found to be a good content of filler providing longer resistance.

6. The introduction of larger size aggregates to the binder can improve the fatigue resistance of asphalt binder. However, larger size aggregates added into mastic specimen does not improve the fatigue resistance of the mastic.

Significant Problems, Issues and Potential Impact on Progress

In this quarter, the VT-NIST team has concentrated on micro-scale methods to associate the fatigue properties of asphalt binder, mastic and mixture, mainly the testing part, which will serve as comparison/validation of modeling part in the next two quarters. The problem encountered is that the NIST subcontract has not been materialized due to the DoC procedure for approving. It has been in the approval process for more than 12 months. If it cannot be approved in the next month or so, Virginia Tech will propose to release this subcontract and perform its work at Virginia Tech solely.

Work Planned Next Quarter

X-ray tomography imaging technique will be utilized to: Obtain the internal structure of the specimen; provide a tool to analyze the change of internal structure of specimen before and after test; reconstruct the internal structures of mastic and mixture specimen based on 2-D slices of scanned image; estimate the voids content of the mastic and mixture specimens.

Finite element modeling method will be utilized to simulate the fatigue process of the asphalt binder, mastic and mixture with consideration of the real internal structure of the samples. The internal structures obtained from the X-ray scanning (including Nano-CT) are mapped into the mesh of digital modeling based on Finite Element Method (F3a-6).

The materials will be subjected to moisture conditioning and tested for estimating the moisture damage effects. Molecular Dynamics modeling of fatigue and moisture damage (F3a-6, F3a-7) will be performed.

Phase field theories applications will be developed to model the asphalt microstructure evolution (F3a-2.4), characterize asphalt emulsion and phase separation process (F3a-2.5), and for modeling fatigue cracking and self-healing processes (F3a-2.6).

Subtask F3a-8. ab initio Calculations of Asphalt Molecular Structures and Correlation to Experimental Physico-Chemical Properties of SHRP Asphalts (WRI-TU Delft)

Work Done This Quarter

A literature review was conducted to identify thermodynamic theories which support phase-field modeling approaches which may be utilized to define fracture and self-healing mechanism at multiple scales in asphalt based infrastructure systems.

Healing Mechanism in Polymers

Kessler (2007) and Yuan et al. (2008) have recently published review papers on the topic of self-healing material systems. In these publications the authors consider state-of-the-art research

conducted to improve the physical and mechanical properties of polymer and polymeric coating materials by incorporating self-healing mechanisms. Yuan et al. (2008), adopts the terms extrinsic and intrinsic to describe self-healing processes with and without the addition of “pre-embedded” healing agents, respectively. Intrinsic self-healing is then defined as being an innate property of the material which requires a stimulus (usually heating) to activate the healing or repair process. Upon “stimulation” of the damaged material, physical and/or chemical interactions take place a few key examples of which include: surface rearrangements, diffusion, wetting, hydrogen bonding, melting/crystallization, and in some cases even chemical reactivity. Extrinsic healing, on the other hand, may actually involve identical types of interactions, but these materials are tailored by incorporating or “pre-embedding” a healing agent into the material itself.

A more detailed exposition on the topic of self-healing materials maybe found in van der Zwaag (2007) and Ghosh (2009). A key concept in these references is the importance of the mechanism(s) involved in fracture damage and self-healing. Similar mechanisms seem to be applicable to all different types of materials, including, biological, polymeric, metals, concrete and asphalt. van der Zwaag (2007) has considered current design principles, namely the "damage prevention" approach and a self-healing inspired “damage management” approach. Each design principle may be described by a damage function, $d\mathcal{G}[m(\rho)]/dt$, defined in the present case by a change in material strength, \mathcal{G} , of a mass element of material, $m(\rho)$, changing as a function of density and time,

$$\frac{d}{dt}\mathcal{G}[m(\rho,t)] = \begin{cases} \geq 0, & 0 < t < t_n \\ < 0, & t_i < t < t_{i+\Delta t} \end{cases} \quad (\text{F3a-8.1})$$

In the damage prevention design approach, damage can remain constant at zero (i.e., never damages), or continues to sustain damage throughout its life cycle to time, t_n . With the damage management design approach, on the other hand, damage may actually decrease over some time intervals, $t_{i+\Delta t}$, due to healing behavior of the material.

In regard to the damage management design approach, several researchers (Varley et al. 2010; Varley and van der Zwaag 2008; Yufa et al. 2009; Xua and Li 2010) have for example considered phase transformation phenomena as a mechanism which lends to material self-healing (specifically polymers in the present sited cases). Varley et al. (Varley et al. 2010; Varley and van der Zwaag 2008) considered the thermo-mechanical properties of self-healing in ionomers by studying ballistics testing. Studies showed that local frictional heating induced by the damage results in a thermally activated healing process. By considering the geometry of the damaged region of the system, as well as the viscous/elastic and phase transition temperature properties of the ionomers, these investigators could manipulate material mechanical properties. In effect it was observed that a colloidal force (self-organization) could be induced in the system by introducing dissolved salt-ions to interact with ion-functionalities of the ionomers studied to manipulate phase transition temperatures as well as viscous and elastic behavior. Further, Yufa et al. (2009) considered healing in diblock copolymer films by using nano-lithography (by AFM, Atomic Force Microscopy) as a wear testing protocol. Here, sample thin-film surfaces were scratch damaged then monitored via AFM imaging over time. With this approach, in particular, the investigators could observe changes in ordering in morphology on the surface of the film over time. Healing properties in these materials

were attributed by these authors to physico-chemical properties which corresponded to viscoelastic and plastic flow properties, and thus to relaxation processes, but also to melting and re-crystallization processes.

Irreversible Thermodynamic Framework for Fracture-Healing in Asphalt Mastics

Recently, Nosonovsky et al. (Nosonovsky 2010; Nosonovsky et al. 2009; Nosonovsky and Bhushan 2010) have considered the net entropy production in damage-healing "tribosystems" (tribiology surface wear system) in order to understand the dissipative processes. The net entropy production of a damage-healing systems is then defined by

$$\dot{S}_{net} = \dot{S}_{damage} + \dot{S}_{healing} \quad (F3a-8.2)$$

Entropy production in a system is generally defined by the sum of the conjugate-pairs of thermodynamic variables (Demirel 2007), as

$$\dot{S}_{prod} = \sum_{j=1}^N J_j X_j \geq 0 \quad (F3a-8.3)$$

Here generalized fluxes (or flows), J_j and thermodynamic forces, X_i define conjugate-pairs (e.g., temperature-entropy, pressure-volume, chemical potential-number of particles, stress-strain, etc.) of thermodynamic variables. Each flux is said to couple with all other thermodynamic forces,

$$J_i(X_i) = \sum_{j=1}^N L_{ij} X_j \quad (F3a-8.4)$$

where L_{ii} and L_{ij} are kinetic coupling coefficients based on Onsager's reciprocal relations. The net entropy production of a coupled process is thus expressed as

$$T\dot{S} = \sum_{i=1}^N \sum_{j=1}^N L_{ij} X_i X_j \geq 0 \quad (F3a-8.5)$$

Nosonovsky et al. (2010), thus suggests that the net entropy production in a damage- healing process is coupled,

$$T\dot{S}_{net} = \sum_i X_i J_i = X_d J_d + X_h J_h \quad (F3a-8.6)$$

where $X_d J_d$ and $X_h J_h$ are damage and healing force-flux terms, which couple as

$$J_d = L_{dd} X_d + L_{dh} X_h \quad (F3a-8.7)$$

and

$$J_h = L_{hd}X_d + L_{hh}X_h \quad (\text{F3a-8.8})$$

respectively, where, according Onsager's reciprocal relations, $L_{dh} = L_{hd}$. The net entropy production is thus expressed as

$$\begin{aligned} T\dot{S}_{net} &= X_d (L_{dd}X_d + L_{dh}X_h) + X_h (L_{hd}X_d + L_{hh}X_h) \\ &= L_{dd}(X_d)^2 + 2L_{dh}X_dX_h + L_{hh}(X_h)^2 \end{aligned} \quad (\text{F3a-8.9})$$

Nosonovsky et al. (2010) further suggests the net entropy production may also be expressed as a scaled system,

$$\dot{S}_{net} = \dot{S}_{macro} + \dot{S}_{meso} + \dot{S}_{nano} \quad (\text{F3a-8.10})$$

where

$$\dot{S}_{macro} = L_{dd}(X_d)^2 \quad (\text{F3a-8.11})$$

$$\dot{S}_{meso} = 2L_{dh}X_dX_h \quad (\text{F3a-8.12})$$

$$\dot{S}_{nano} = L_{hh}(X_h)^2 \quad (\text{F3a-8.13})$$

These three expressions basically suggest that nanoscopic processes associated with the "actions" of molecules which contribute to healing in a damaged system couple with the macroscopic forces associated with the damage process, and may result in ordering-disordering in the system at intermediate scales.

Thus, it is presently hypothesized that healing processes in asphalt based composite systems, i.e., mastics and pavements, may undergo a solidification step or process in addition to crack closure processes (Schapery 1989), which have already been proposed in asphalt systems (Lytton et al. 2001). Entropy production in a solidification process, (Sekerka 2011; Emmerich 2010), is derived, based on phase-field modeling approaches, as

$$\dot{S}_{prod} = \frac{d}{dt} \mathcal{S} + \int_{\mathcal{A}_{sub}} \left[\frac{\mathbf{q}_c}{T} + \varepsilon_{\varphi s}^2 \phi \nabla \varphi \right] \cdot \hat{\mathbf{n}} d^2x \geq 0 \quad (\text{F3a-8.14})$$

where an inner functional is defined by

$$\mathcal{S} = \int_{\mathcal{V}} \left[s(u, \varphi) + \varepsilon_{\varphi s}^2 |\nabla \varphi|^2 \right] d^3x \quad (\text{F3a-8.15})$$

A similar set of expressions are also give for the internal energy production rate,

$$\dot{U}_{prod} = \frac{d}{dt} \mathcal{U} + \int_{\mathcal{A}_{sub}} \left[\mathbf{q}_c + \varepsilon_{\varphi u}^2 \dot{\varphi} \nabla \varphi \right] \cdot \hat{\mathbf{n}} d^2 x = 0 \quad (\text{F3a-8.16})$$

where the inner functional is defined by

$$\mathcal{U} = \int_{\mathcal{V}} \left[u(\mathbf{r}, t) + \varepsilon_{\varphi u}^2 |\nabla \varphi|^2 \right] d^3 x \quad (\text{F3a-8.17})$$

The free energy functional is thus related to the internal energy and entropy functional as

$$\mathcal{F} = \mathcal{U} + T\mathcal{S} \quad (\text{F3a-8.18})$$

so that a free energy balance, of form $f = u + Ts$, is given by

$$\varepsilon_f^2 = \varepsilon_{\varphi u}^2 + T \varepsilon_{\varphi s}^2 \quad (\text{F3a-8.19})$$

given the variation to maximize entropy, $\delta(\mathcal{S} - \lambda \mathcal{U}) = 0$. Here, $u(\mathbf{r}, t)$ and $\varphi(\mathbf{r}, t)$ are functions of a position vector \mathbf{r} and time, t , \mathbf{q}_c , is the heat flux, and gradient effects, (internal energy, $\varepsilon_{\varphi u}^2 \dot{\varphi} \nabla \varphi$ and entropy, $\varepsilon_{\varphi s}^2 \dot{\varphi} \nabla \varphi$), integrated over $\mathcal{A} \propto \hat{\mathbf{n}} d^2 x$ and $\mathcal{V} \propto d^3 x$. The reader is referred to Sekerka (2011) and Emmerich (2010) for an exhaustive derivation of diffuse interface theory as it applies to entropy production in solidification processes.

In Subtask M1b-2: Work of Adhesion at Nano-Scale using AFM, of the present report, AFM images of fractured asphalt surfaces clearly show organized linear arrangements of sub-micron-sized particles, and other distinct features, which occur in repetitive patterns. We believe that images such as those shown in figure M1b-2.1 represent a waveform frozen in time, and that this waveform contains information about time-dependent flow properties associated with a nearly instantaneous fracture event. That is, these images present a mapping of strain localization during the fracture process. Similar patterns of strain localization (often referred to as shear banding) can be observed on the fractured faces of a broad range of ductile and quasi-brittle materials. The thermodynamic framework considered here may lend to the modeling of this type of phenomena.

Significant Problems, Issues and Potential Impact on Progress

None

Work Planned Next Quarter

Specific terms defining entropy production of processes of healing will be identified in asphalt systems to arrive at the net entropy production. Simple wear testing of asphalt thin films via AFM nano-lithography will be conducted on asphalts which differ based on differences in chemical composition and rheological properties to study "repair" rate to be compared with mechanical

measures of fracture and healing in asphalt mastic systems. These tests will be coordinated with testing conducted in Subtask M1b-2.

Cited References

Demirel, Y., 2007, *Nonequilibrium Thermodynamics: Transport and Rate Processes in Physical, Chemical and Biological Systems*. Elsevier, Amsterdam, The Netherlands.

Emmerich, M., 2010, *The Diffuse Interface Approach in Materials Science: Thermodynamic Concepts and Applications of Phase-Field Models*. Springer-Verlag Berlin Heidelberg.

Ghosh, S. K., 2009, *Self-Healing Materials: Fundamentals, Design Strategies, and Applications*. Wiley-VCH Verlag GmbH & Co. KGaA.

Helrich, C. S., 2009, *Modern Thermodynamics with Statistical Mechanics*. Springer-Verlag, Berlin, Heidelberg.

Kessler, M.R., 2007, Self-healing: A New Paradigm in Materials Design. *Journal Proceedings of the Institution of Mechanical Engineers, Part G: Journal of Aerospace Engineering*, 221(4), 479-495.

Lytton, R. L., C. W. Chen and D. N. Little, 2001, *Microdamage Healing in Asphalt and Asphalt Concrete, Volume III: A Micromechanics Fracture and Healing Model for Asphalt Concrete*, FHWA-RD-98-143. Federal Highway Administration, U. S. Department of Transportation, McLean, VA.

Nosonovsky, M., and B. Bhushan, 2010, Surface Self-organization: From Wear to Self-healing in Biological and Technical Surfaces. *Applied Surface Science*, 256, 3982-3987.

Nosonovsky, M., and S. K. Esche, 2008, A Paradox of Decreasing Entropy in Multiscale Monte Carlo Grain Growth Simulations. *Entropy*, 10(2), 49-54.

Nosonovsky, M., 2010, Entropy in Tribology: in the Search for Applications. *Entropy*, 12(6), 1345-1390.

Nosonovsky, N., R. Amano, J. M. Lucci and P. K. Rohatgi, 2009, Physical Chemistry of Self-organization and Self-healing in Metals. *Phys. Chem. Chem. Phys.*, 11, 9530-9536.

Mullins, O. C., 2010, The Modified Yen Model. *Energy Fuels*, 24: 2179-2207.

Schapery, R. A., 1989, On the Mechanics of Crack Closing and Bonding in Linear Viscoelastic Media. *International Journal of Fracture*, 39, 163-189.

Sekerka 2011, Irreversible Thermodynamic Basis for Phase Field Models. *Philosophical Magazine*, 91(1), 3-23.

van der Zwaag, S., 2007, *Self Healing Materials: An Alternative Approach to 20 Centuries of Materials Science*, Springer Series in Materials Science, Vol. 100. Springer, Dordrecht, The Netherlands.

Yuan, Y. C., T. Yin, M. Z. Rong, and M. Q. Zhang, 2008, Self Healing in Polymers and Polymer Composites. Concepts, Realization and Outlook: A Review. *eXPRESS Polymer Letters*, 2(4), 238–250.

Work Element F3b: Micromechanics Model (TAMU)

Subtask F3b-1: Model Development (TAMU, NCSU, UNL)

Work Done This Quarter

Cohesive Zone Micromechanical Model (UNL)

During this quarter we have mainly progressed towards the following activities:

- We implemented the bilinear cohesive zone model proposed by Espinosa and Zavattieri (2003) in the form of a UEL (User Element) code subroutine within a commercial finite element software, *ABAQUS*. The CZ model by Espinosa and Zavattieri (2003) appears to be more appropriate than CZ models previously implemented because it can better account for mixed-mode fracture.
- We then extended the rate-independent CZ model proposed by Espinosa and Zavattieri (2003) to incorporate rate-dependent characteristics of cohesive zone fracture.

Work progress and significance of each activity can be summarized as follows:

Implementation of the CZ model proposed by Espinosa and Zavattieri (2003)

One of the primary tasks during this quarter was the implementation of the bilinear cohesive zone model proposed by Espinosa and Zavattieri (2003) into *ABAQUS* commercial FE package in the form of a UEL (User Element) code subroutine. Figure F3b-1.1 presents a portion of the UEL subroutine.

```

if (ambda .le. amdba_cr) then

    Trac(1,1) = alpha_Tmax*T_max*(1/ambda_cr)*(delta_t_gp/
    & del_c_t)

    Trac(2,1) = T_max*(1/ambda_cr)*(delta_n_gp/
    & del_c_n)

    Trac_Jacob(1,1) = alpha_Tmax*T_max/(del_cc_n**2/del_c_n**2+
    & Csi_square*del_cc_t**2/del_c_t**2)**(1/2.)
    & /del_c_t
    Trac_Jacob(2,2) = T_max/(del_cc_n**2/del_c_n**2+Csi_square*
    & del_cc_t**2/del_c_t**2)**(1/2.)/del_c_n
    Trac_Jacob(1,2) = 0.0d0
    Trac_Jacob(2,1) = 0.0d0

elseif ((ambda .gt. amdba_cr) .and. (ambda .lt. 1.0d0)) then

    a1 = alpha_Tmax*T_max*(1-(delta_n_gp**2/del_c_n**2+Csi_square*
    & delta_t_gp**2/del_c_t**2)**(1/2.))/(1-(del_cc_n**2/del_c_n
    & **2+Csi_square*del_cc_t**2/del_c_t**2)**(1/2.))/(delta_n_gp**2/
    & del_c_n**2+Csi_square*delta_t_gp**2/del_c_t**2)**(1/2.)*
    & delta_t_gp/del_c_t

    a2 = T_max*(1-(delta_n_gp**2/del_c_n**2+Csi_square*delta_t_gp**2/
    & del_c_t**2)**(1/2.))/(1-(del_cc_n**2/del_c_n**2+Csi_square*
    & del_cc_t**2/del_c_t**2)**(1/2.))/(delta_n_gp**2/del_c_n**2+
    & Csi_square*delta_t_gp**2/del_c_t**2)**(1/2.)*delta_n_gp/
    & del_c_n

```

Figure F3b-1.1. A portion of UEL code subroutine implemented into *ABAQUS*.

We decided to implement this new bilinear model because it allows clearer definition of two different fracture modes (*i.e.*, normal and in-plane shear for 2-D simulations) and their mixity than the bilinear model implemented in the previous quarter. A short description of the newly implemented model is given below.

The non-dimensional effective displacement and effective traction for a two-dimensional case can be given by:

$$\lambda_e = \sqrt{\left(\frac{\Delta_n}{\delta_n}\right)^2 + \xi^2 \left(\frac{\Delta_t}{\delta_t}\right)^2} \quad (\text{F3b-1.1})$$

$$T_e = \sqrt{(T_n)^2 + (T_t)^2} \quad (\text{F3b-1.2})$$

where the subscript e, n, t represents effective, normal (opening), and tangential (shear sliding), respectively, λ is the non-dimensional displacement, and ξ is the parameter coupling normal and tangential fracture toughness.

Cohesive zone traction in the bilinear model increases from zero to a peak value (*i.e.*, cohesive strength) in a linear elastic fashion and then presents linear softening that accounts for progressive damage occurring in the fracture process zone. At the maximum traction, a parameter (λ_{cr}) can be identified. The non-dimensional displacement λ_{cr} is considered an important parameter in the

bilinear model, since the parameter defines initiation of damage in the fracture process zone, and also controls the pre- and post-peak slopes of the model. Another important displacement quantity, the critical displacement (δ), represents a displacement jump where complete separation occurs, inferring zero traction.

For the pre-peak region ($\lambda_e \leq \lambda_{cr}$), the normal and tangential components of the traction are given by:

$$T_n = \frac{T_{\max}}{\lambda_{cr}} \cdot \left(\frac{\Delta_n}{\delta_n} \right) \quad (\text{F3b-1.3})$$

$$T_t = \frac{\alpha T_{\max}}{\lambda_{cr}} \cdot \left(\frac{\Delta_t}{\delta_t} \right) \quad (\text{F3b-1.4})$$

where $\alpha = \xi^2 (\delta_n / \delta_t)$

For the post-peak region ($\lambda_e > \lambda_{cr}$), the normal and tangential components of the traction can be expressed as follows:

$$T_n = \frac{1 - \lambda_e}{1 - \lambda_{cr}} \cdot \frac{T_{\max}}{\lambda_{cr}} \cdot \left(\frac{\Delta_n}{\delta_n} \right) \quad (\text{F3b-1.5})$$

$$T_t = \frac{1 - \lambda_e}{1 - \lambda_{cr}} \cdot \frac{\alpha T_{\max}}{\lambda_{cr}} \cdot \left(\frac{\Delta_t}{\delta_t} \right) \quad (\text{F3b-1.6})$$

The cohesive zone fracture energy (*i.e.*, work of separation) is calculated by integrating the cohesive zone traction with respect to the separation distance. The work of separation in pure normal displacement condition (mode I fracture) and in pure shear sliding condition (mode II fracture) can be expressed by equation F3b-1.7 and equation F3b-1.8, respectively.

$$G_n = \int_0^{\delta_n} T_n d\Delta_n = \frac{1}{2} \delta_n T_{\max} \quad (\text{F3b-1.7})$$

$$G_t = \int_0^{\delta_t} T_t d\Delta_t = \alpha \frac{1}{2} \delta_t T_{\max} = \xi^2 \frac{1}{2} \left(\frac{\delta_n}{\delta_t} \right) \delta_t T_{\max} = \xi^2 G_n \quad (\text{F3b-1.8})$$

Equation F3b-1.8 provides a physical meaning for the parameter ξ .

Implementation of the rate-dependency in the CZ model

One of key elements in our modeling effort is the development and implementation of a rate-dependent cohesive zone fracture model. During this quarter, we extended the rate-independent

intrinsic bilinear cohesive zone model proposed by Espinosa and Zavattieri (2003) to a rate-dependent cohesive zone model in the form of another *ABAQUS* UEL subroutine.

Using the rate-dependent cohesive zone model, two different sets of finite element analyses simulating SCB tests were performed: (i) first, the rate-dependent mechanical behavior induced by viscoelastic bulk elements was disregarded by assuming isotropic linear elasticity for the volumetric material elements; (ii) second, the rate-dependent mechanical behavior was predicted by considering both the viscoelastic response of bulk elements and the rate-dependent fracture in the cohesive zone.

The first set of simulations was performed to verify if the newly-implemented code properly assigns different sets of cohesive zone fracture parameters corresponding to the rate of relative displacements between the two faces of each cohesive zone element. As demonstrated in figure F3b-1.2, the overall mechanical behavior of the SCB samples is clearly affected by the rate of applied loading (note that SCB_10 signifies a simulation performed at 10 mm/min loading rate) although the rate-dependent viscoelastic behavior of bulk elements was disregarded. This implies that the rate-dependent fracture implemented in the cohesive zone affects rate-dependent mechanical responses of overall mixture. Slower loading rates resulted in more compliant responses.

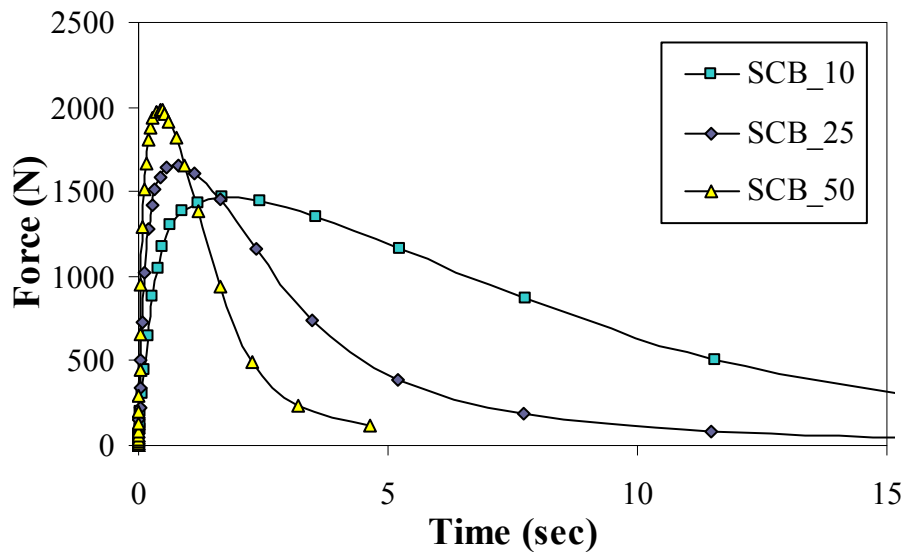


Figure F3b-1.2. Rate-dependence of fracture process considering bulk material elasticity.

The second set of simulations was conducted to validate the proposed modeling approach by including two major sources of rate-dependency together: the bulk element viscoelasticity and rate-dependent fracture process. For the model validation, SCB fracture tests conducted at different loading rates (1, 5, 10, 25, 50, 100, 200, 400, and 600 mm/min) were simulated, and results from the simulations were compared to test results. Figures F3b-1.3 and F3b-1.4 show a very good agreement between the results obtained using the rate-dependent cohesive zone model and the corresponding

SCB experimental results. This agreement indicates that the model has been successfully developed and implemented.

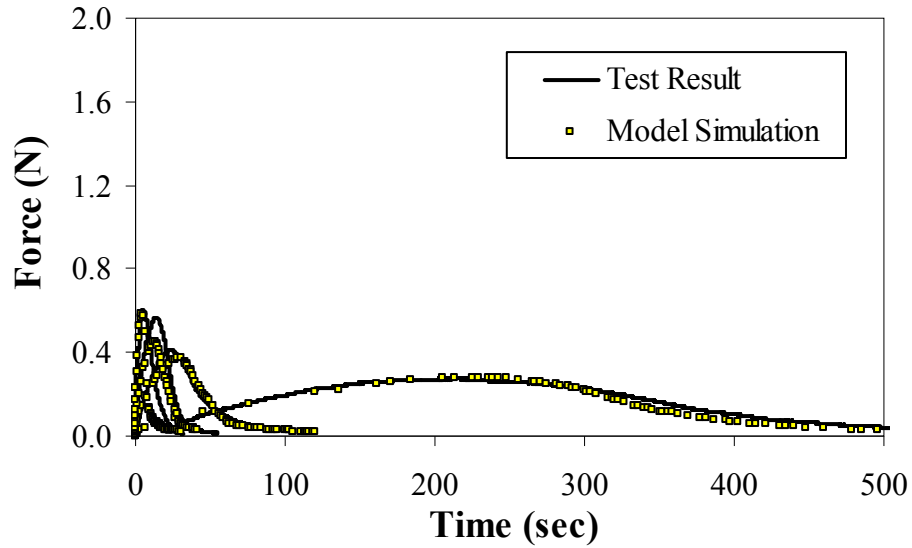


Figure F3b-1.3. Test results vs. numerical simulations for loading rates: 1, 5, 10, and 25 mm/min.

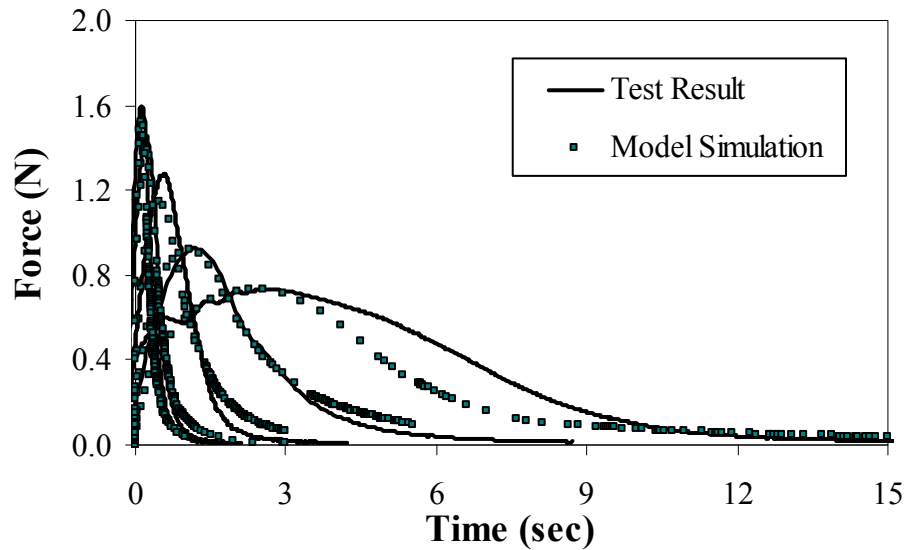


Figure F3b-1.4. Test results vs. numerical simulations for loading rates: 50, 100, 200, 400, and 600 mm/min.

Lattice Micromechanical Model (NCSU)

Efforts in the previous quarter focused on air voids and their effect on stiffness. Two shapes were chosen as the basic shapes for air voids: circular and octagonal, the latter with randomly shaped octagons that have an elongation factor of three. The stiffness of the specimens with different air void contents was predicted for both types of shape. Both shapes show a constant decrease in stiffness with an increase in air void content. However, the rate of the decrease for the octagonal shape is faster than that for the circular shape, indicating that stiffness is sensitive to the shape of the air voids. Moreover, it is expected that the strength properties will be affected significantly by the shape of the air voids. Thus, realistic modeling of the shapes of air voids was the focus of this quarter's effort.

To gain a deeper understanding of air void shapes, it is best to observe air voids as real images. X-ray tomographic images provide a good look at air void shape characteristics. To obtain such images, the full depth of the specimen is scanned (x-rayed), and a stack of gray-scale images is obtained for the whole depth of the specimen, as shown in figure F3b-1.5 (a). The x-ray tomographic images in this study were provided by Dr. Emin Kutay of Michigan Tech.

Figure F3b-1.5 (a) shows an x-ray tomographic image in which the white spots indicate the densest particles in the aggregate specimen. The intensity of the particles decreases from the white area to the black area. The black spots in the image have zero density and represent air voids. The gray areas in the image are low density areas that may or may not be considered as air voids.

It is best to convert the images to a black and white image – black being the air voids and white being everything else in the mix. In a black and white image, the boundaries of the voids are clearer and the shape characteristics are more evident than in a gray scale image. This conversion was made by applying a threshold for the gray scale of the image. A typical converted image is shown in figure F3b-1.5 (b), which shows the air void shapes with clarity. By measuring the area of the black spots in the image, the air void content of the specimen can be measured. Changing the threshold causes a change in the shape and area of the voids in the specimen. The appropriate threshold is the one that yields an air void content that approximates the field observations.

The above process has been applied for different specimens, and black and white images have been obtained. Some basic trends for the shapes have been identified, and further investigation into the shape characteristics is underway. These results will enable the virtual fabrication program to generate specimens with more realistic air void shapes than can be obtained currently. The virtual fabrication program would commence in the next quarter.

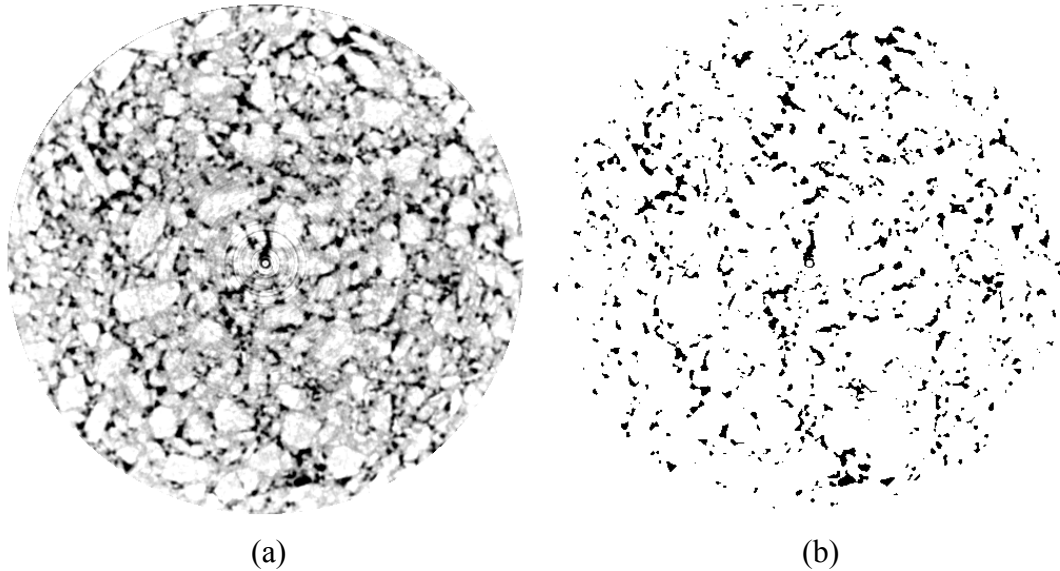


Figure F3b-1.5. a) Raw x-ray tomographic image, and b) x-ray tomographic image after applying threshold

Continuum Damage to Fracture

In this quarter, implementation of a nonlocal damage framework in a two-dimensional finite element code was completed. In parallel, the mechanism of localization is being investigated with the ultimate goal of establishing a quantitative criterion for localization that can be incorporated into the nonlocal model.

Significant Results

None

Significant Problems, Issues and Potential Impact on Progress

None

Work Planned Next Quarter

Cohesive Zone Micromechanical Model (UNL)

In the next quarter we will work on the following activities:

- Model validation and calibration: performance tests of asphalt concrete mixtures, modeling of the asphalt concrete mixture tests, and comparisons between model simulation results and experimental test results.
- Material characterization and fracture testing of ARC core materials.

Lattice Micromechanical Model (NCSU)

- Acquire the shape characteristics of the air voids from x-ray tomographic images.
- Include air voids in the virtual fabrication program.

Continuum Damage to Fracture

- Incorporate microcrack interactions and other related physical mechanisms into the nonlocal model and implement it for viscoelastic materials.
- Further investigate the quantification of the onset of localization.

Cited Reference

Espinosa, H. D., and P. D. Zavattieri, 2003, A grain level model for the study of failure initiation and evolution in polycrystalline brittle materials. part I: theory and numerical implementation. *Mechanics of Materials*, 35, 333-364.

Subtask F3b-2: Account for Material Microstructure and Fundamental Material Properties (TAMU)

Work Done This Quarter

The reader is referred to work elements F1c and F1d.

Work Element F3c: Development of Unified Continuum Model (TAMU)

Work Done This Quarter

See M4c for details on the progress in the development of the continuum-based moisture-induced damage mode. Also see F1d-8 on the development of the continuum-based micro-damage healing model. We have completed the validation of the constitutive model in PANDA using the ALF laboratory data from NCState. The data included compression creep recovery tests and extension cyclic tests.

Significant Results

We finalized the method to obtain the model parameters and demonstrated the ability of the model to describe the results of compression and extension tests at various testing conditions.

Significant Problems, Issues and Potential Impact on Progress

The process of obtaining the model parameters for the extension tests was more time consuming than we originally planned. Therefore, we fell slightly behind on conducting simulations of the structural response of the ALF sections.

Work Planned Next Quarter

We will examine two methods that have been used in the past in the simulations of fatigue tests. The objective is to determine if these methods can be used to reduce the time needed to apply loads in the structural finite element model. We will also conduct simulations to validate the model against the structural response of the various sections of the ALF experiment.

Continuum-based Model for Aging

Work Done This Quarter

In this quarter, the calibration of the developed aging model is attempted against existing experimental complex shear modulus data of two aged asphaltic mixtures (Bryan and Yoakum mixtures) documented in report FHWA/TX-05/0-4468. The viscoelastic behavior only is considered to fit the shear modulus master curves with respect to the variation of the angular frequency.

Significant Results

Close agreement has been obtained between the experimental data and the model predictions. A journal paper is under preparation to document the model development and validation.

Significant Problems, Issues and Potential Impact on Progress

None

Work Planned Next Quarter

Adding to the viscoelastic behavior of aged mixture, the viscoplastic and viscodamage behavior of aged one will be considered to calibrate the aging model parameters and to predict the realistic behavior of the aged asphalt. Moreover, 3-D rutting simulation for both unaged and aged asphalt will be carried out to investigate the long-term behavior of asphalt.

Fatigue Year 4		Year 4 (4/10-3/11)											Team			
		4	5	6	7	8	9	10	11	12	1	2	3			
Material Properties																
F1a	Cohesive and Adhesive Properties															
F1a-1	Critical review of literature															TAMU
F1a-2	Develop experiment design															
F1a-3	Thermodynamic work of adhesion and cohesion															
F1a-4	Mechanical work of adhesion and cohesion			D				F								
F1a-5	Evaluate acid-base scale for surface energy calculations															
F1b	Viscoelastic Properties															
F1b-1	Separation of nonlinear viscoelastic deformation from fracture energy under cyclic loading			M&A, F, JP				JP								TAMU
F1b-2	Separation of nonlinear viscoelastic deformation from fracture energy under monotonic loading														JP	
F1c	Aging															
F1c-1	Critical review of binder oxidative aging and its impact on mixtures															TAMU
F1c-2	Develop experiment design															
F1c-3	Develop transport model for binder oxidation in pavements					P					JP		P, JP			
F1c-4	Effect of binder aging on properties and performance												P, JP			
F1c-5	Polymer modified asphalt materials					P										
F1d	Healing															
F1d-1	Critical review of literature															TAMU
F1d-2	Select materials with targeted properties															TAMU
F1d-3	Develop experiment design															TAMU
F1d-4	Test methods to determine properties relevant to healing				D			F								TAMU
F1d-5	Testing of materials							JP								TAMU
F1d-6	Evaluate relationship between healing and endurance limit of asphalt binders							JP					P			UWM
F1d-7	Coordinate with AFM analysis	JP														WRI
F1d-8	Coordinate form of healing parameter with micromechanics and continuum damage models															TAMU
Test Methods																
F2a	Binder tests and effect of composition															
F2a-1	Analyze Existing Fatigue Data on PMA															UWM
F2a-2	Select Virgin Binders and Modifiers and Prepare Modified Binder															
F2a-3	Laboratory Aging Procedures															
F2a-4	Collect Fatigue Test Data							JP					DP, P		JP	
F2a-5	Analyze data and propose mechanisms											P				
F2b	Mastic testing protocol															
F2b-1	Develop specimen preparation procedures					F										TAMU
F2b-2	Document test and analysis procedures in AASHTO format					F										
F2c	Mixture testing protocol															
F2d	Tomography and microstructural characterization															
F2d-1	Micro scale physicochemical and morphological changes in asphalt binders														JP	TAMU
F2e	Verify relationship between DSR binder fatigue tests and mixture fatigue performance															
F2e-1	Evaluate Binder Fatigue Correlation to Mixture Fatigue Data															UWM
F2e-2	Selection of Testing Protocols			D		F										
F2e-3	Binder and Mixture Fatigue Testing															
F2e-4	Verification of Surrogate Fatigue Test								D				F, DP			
F2e-5	Interpretation and Modeling of Data						JP								M&A	
F2e-6	Recommendations for Use in Unified Fatigue Damage Model												P			
Models																
F3a	Asphalt microstructural model															WRI
F3b	Micromechanics model															
F3b-1	Model development					JP							P			TAMU
F3b-2	Account for material microstructure and fundamental material properties															
F3c	Develop unified continuum model															
F3c-1	Analytical fatigue model for mixture design															TAMU
F3c-2	Unified continuum model											JP		M&A		
F3c-3	Multi-scale modeling										JP				M&A	
	Lattice Model			DP		DP, JP										NCSU
	Continuum Damage to Fracture				DP				JP							

LEGEND

Deliverable codes

- D: Draft Report
- F: Final Report
- M&A: Model and algorithm
- SW: Software
- JP: Journal paper
- P: Presentation
- DP: Decision Point
- [x]

- Work planned
- Work completed
- Parallel topic

Deliverable Description

- Report delivered to FHWA for 3 week review period.
- Final report delivered in compliance with FHWA publication standards
- Mathematical model and sample code
- Executable software, code and user manual
- Paper submitted to conference or journal
- Presentation for symposium, conference or other
- Time to make a decision on two parallel paths as to which is most promising to follow through
- Indicates completion of deliverable x

Fatigue Year 2 - 5		Year 2 (4/08-3/09)				Year 3 (4/09-3/10)				Year 4 (04/10-03/11)				Year 5 (04/11-03/12)				Team
		Q1	Q2	Q3	Q4	Q1	Q2	Q3	Q4	Q1	Q2	Q3	Q4	Q1	Q2	Q3	Q4	
Material Properties																		
F1a	Cohesive and Adhesive Properties																	
F1a-1	Critical review of literature			JP													TAMU	
F1a-2	Develop experiment design																	
F1a-3	Thermodynamic work of adhesion and cohesion																	
F1a-4	Mechanical work of adhesion and cohesion						JP			D	F							
F1a-5	Evaluate acid-base scale for surface energy calculations													JP				
F1b	Viscoelastic Properties																	
F1b-1	Separation of nonlinear viscoelastic deformation from fracture energy under cyclic loading			D,JP	M&A				JP	I&A,F,J	JP		P	JP	M&A,D	F	TAMU	
F1b-2	Separation of nonlinear viscoelastic deformation from fracture energy under monotonic loading			JP	M&A				JP				JP		JP,M&A,D	F		
F1c	Aging																	
F1c-1	Critical review of binder oxidative aging and its impact on mixtures																TAMU	
F1c-2	Develop experiment design			D	F													
F1c-3	Develop transport model for binder oxidation in pavements		P		P,JP		P		P,JP		P	JP	P,JP		D,M&A	F		
F1c-4	Effect of binder aging on properties and performance				JP,P		JP	D	F				P,JP		JP	D	F	
F1c-5	Polymer modified asphalt materials						P				P					D	F	
F1d	Healing																	
F1d-1	Critical review of literature																TAMU	
F1d-2	Select materials with targeted properties																TAMU	
F1d-3	Develop experiment design																TAMU	
F1d-4	Test methods to determine properties relevant to healing			JP					JP	D	F						TAMU	
F1d-5	Testing of materials						JP				JP				M&A,D	JP,F	TAMU	
F1d-6	Evaluate relationship between healing and endurance limit of asphalt binders	DP				DP	JP	DP			JP		P		JP	D	F	UWM
F1d-7	Coordinate with AFM analysis									JP								WRI
F1d-8	Coordinate form of healing parameter with micromechanics and continuum damage models															JP,D	F	TAMU
Test Methods																		
F2a	Binder tests and effect of composition																	
F2a-1	Analyze Existing Fatigue Data on PMA			DP														UWM
F2a-2	Select Virgin Binders and Modifiers and Prepare Modified Binder			DP														
F2a-3	Laboratory Aging Procedures																	
F2a-4	Collect Fatigue Test Data		P		JP		P		P					P,DP,JP				
F2a-5	Analyze data and propose mechanisms				P			P				P			P	D	F	
F2b	Mastic testing protocol																	
F2b-1	Develop specimen preparation procedures		D								F							TAMU
F2b-2	Document test and analysis procedures in AASHTO format		D								F							
F2c	Mixture testing protocol			D,JP	F													
F2d	Tomography and microstructural characterization																	
F2d-1	Micro scale physicochemical and morphological changes in asphalt binders						JP				JP							TAMU
F2e	Verify relationship between DSR binder fatigue tests and mixture fatigue performance																	
F2e-1	Evaluate Binder Fatigue Correlation to Mixture Fatigue Data						DP,D	F			D	F						UWM
F2e-2	Selection of Testing Protocols																	
F2e-3	Binder and Mixture Fatigue Testing																	
F2e-4	Verification of Surrogate Fatigue Test														D	F,DP		
F2e-5	Interpretation and Modeling of Data		JP		P		JP		P		JP				M&A			
F2e-6	Recommendations for Use in Unified Fatigue Damage Model													P		D	F	
Models																		
F3a	Asphalt microstructural model							JP								M&A	F	WRI
F3b	Micromechanics model																	
F3b-1	Model development				JP				JP		JP		P	D	DP	F,SW		TAMU
F3b-2	Account for material microstructure and fundamental material properties													D		F		
F3c	Develop unified continuum model																	
F3c-1	Analytical fatigue model for mixture design															M&A,D	F	TAMU
F3c-2	Unified continuum model				JP				JP				JP	M&A	D	DP	F,SW	
F3c-3	Multi-scale modeling												JP	M&A	D		F	
	Lattice Model										DP	DP,JP						NCSU
	Continuum Damage to Fracture										DP		JP					

LEGEND

Deliverable codes

- D: Draft Report
- F: Final Report
- M&A: Model and algorithm
- SW: Software
- JP: Journal paper
- P: Presentation
- DP: Decision Point
- [x]

- Work planned
- Work completed
- Parallel topic

Deliverable Description

- Report delivered to FHWA for 3 week review period.
- Final report delivered in compliance with FHWA publication standards
- Mathematical model and sample code
- Executable software, code and user manual
- Paper submitted to conference or journal
- Presentation for symposium, conference or other
- Time to make a decision on two parallel paths as to which is most promising to follow through
- Indicates completion of deliverable x

PROGRAM AREA: ENGINEERED MATERIALS

CATEGORY E1: MODELING

Work element E1a: Analytical and Micro-mechanics Models for Mechanical Behavior of Mixtures (TAMU)

Work Done This Quarter

In this quarter, further investigation is made on the crack growth in the fine asphalt mixture (FAM) specimens and the testing and data analysis of field cores.

The crack growth in the dry FAM specimens is investigated based on the strain energy equivalence principle. In the process of loading, the FAM specimen goes through three distinct stages. Firstly, the FAM specimen stiffens because: 1) the air voids within the specimen are closed, in effect “healing” them, 2) the aggregates are drawn together, and 3) the asphalt mastic is stretched by the tensile stress that leads to a thinner film thickness. In the second stage, the cracks open again and propagate into the intact materials. In the third stage, the magnitude of the complex modulus of the FAM specimen decreases rapidly and the phase angle of the complex modulus increases dramatically, which lead to the failure of the specimen. Figure E1a.1 illustrates the three distinct stages: 1) stiffening of the FAM specimen due to the densification of aggregates, 2) crack growth into loss of the intact material, and 3) final failure stage.

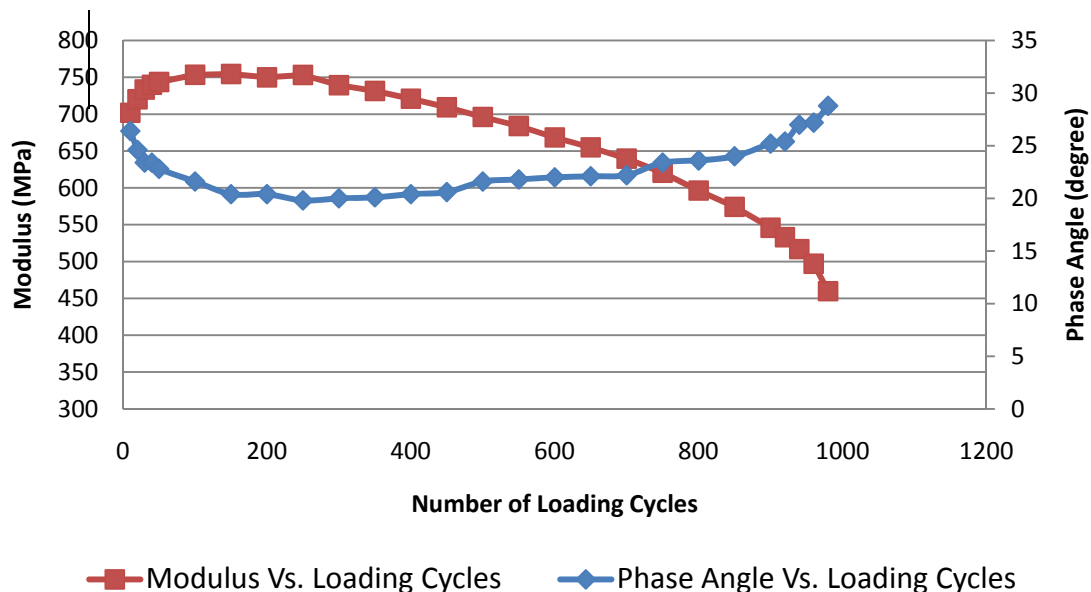


Figure E1a.1. Typical FAM specimens modulus and phase angle change under stress-controlled loading mode.

As discussed in the previous quarterly report, the crack growth of the FAM is obtained using the recoverable pseudo strain energy (RPSE) balance equation as follows:

$$RPSE^A * V = RPSE^T * V - RPSE^T * \left(\frac{2M\pi^2\bar{c}^3}{3} \right) + 2M\pi\bar{c}^2\gamma \quad (E1a.1)$$

Assuming that the crack radius and the number of cracks does not change after the first loading cycle, the RPSE balance equation is applied to the first loading cycle of the destructive repeated direct tension (RDT) test as shown in equation E1a.2:

$$RPSE_1^A * A_{AM}\bar{t} = RPSE_1^T A_{AM}\bar{t} - RPSE_1^T \left(\frac{2M\pi^2c_0^3}{3} \right) + 2M\pi c_0^2\gamma \quad (E1a.2)$$

The cumulative RPSE is then calculated as follows:

$$\begin{aligned} \sum_{i=1}^N (RPSE_i^A) V &= \sum_{i=1}^N RPSE_i^T V \\ &= -\frac{2\pi^2}{3E_{LVE}} \frac{3\cos(\phi-\varphi)}{4E_{LVE}} (\sigma_1^{T2} M_0 c_0^3 + \sigma_2^{T2} M_1 c_1^3 - \sigma_2^{T2} M_0 c_0^3 + \dots + \sigma_N^{T2} M_{N-1} c_{N-1}^3 - \sigma_N^{T2} M_{N-2} c_{N-2}^3) \\ &\quad + 2\pi\gamma (M_0 c_0^2 + M_1 c_1^2 - M_0 c_0^2 + \dots + M_{N-1} c_{N-1}^2 - M_{N-2} c_{N-2}^2) \end{aligned} \quad (E1a.3)$$

Assuming σ_i^T for two adjacent cycles are equal, the crack radius of the FAM is calculated using equation E1a.4.

$$\bar{c} = \frac{[\beta RPSE_N^T V - \alpha RPSE_N^A + 2\gamma]}{\pi M_{N-1} C_{N-1}^2} \left[\frac{2E_T}{(\sigma_N^T)^2 \pi \cos(\phi-\varphi)} \right] \quad (E1a.4)$$

$$\alpha = \frac{\sum_{i=1}^N (RPSE_i^A) V}{(RPSE_N^A) V} \quad \beta = \frac{\sum_{i=1}^N RPSE_i^T V}{RPSE_N^T V} \quad (E1a.5)$$

According to the force equilibrium condition, the force in the undamaged configuration is equal to that in the damaged configuration. Then \bar{c} is obtained as follows:

$$\sigma_N^T (A_M - M_{N-1} \pi c_{N-1}^2) = \sigma_N^A A_M \quad (E1a.6)$$

Notations of equations E1a.1 through E1a.6 are: σ = tensile stress; \bar{t} = asphalt film thickness; E_{LVE} = linear viscoelastic modulus of FAM specimen that is measured from the undamaged

RDT test; ϕ = phase angle of FAM specimen at zero loading cycle (intercept from the phase angle curve fitting of damaged FAM specimen); A_{AM} = total area of damaged asphalt mastic; ϕ = phase angle measured from the destructive RDT; \bar{c} = mean crack radius; M = number of cracks; γ = adhesive bond energy; and the superscript A and T represents “Apparent” and “True” respectively.

Using equations E1a.4, E1a.5 and E1a.6, the crack growth in the FAM dummy specimens is determined and illustrated in figure E1a.2. It is observed from figure E1a.2 that the mean crack radius linearly increases in the second stage and that the crack growth varies between specimens. The initial air void radius before loading can be obtained by extending backward the trend line to the vertical axis. These data can be analyzed further to produce the tensile Paris’ Law fracture coefficients, A and n .

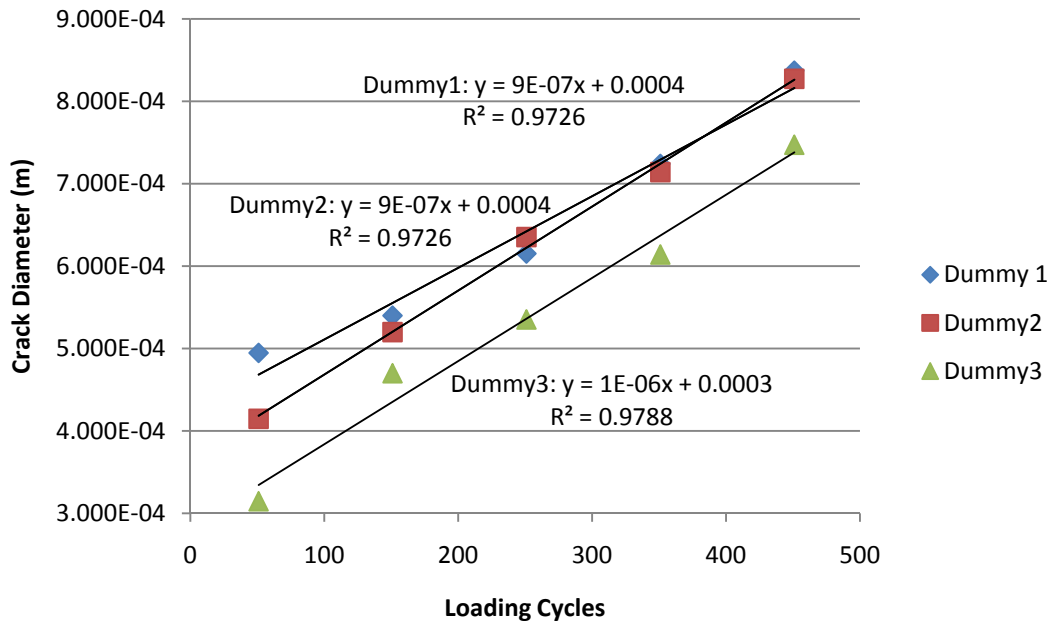


Figure E1a.2. FAM specimens crack development under stress-controlled loading mode.

In addition to the FAM test data analysis, the direct tension test data of field cores from US 277, US 82 and SH 59 in Texas are analyzed to determine the stiffness gradient with pavement depth. Field cores from both the wheel path and the shoulder in different ages are selected to analyze the effect of traffic and aging on the stiffness gradient of the field cores. A new extension-compression testing machine is used to test the specimens with a higher machine feedback frequency of 20 Hz than that of the other Material Testing System (MTS) (2 Hz). The higher feedback frequency of the new testing machine results in more accurate testing results, but it also creates a widely scattered data pattern. In order to eliminate the noise in the data sets, a new method is developed to obtain the Laplace transform of the oscillating amplitudes. Firstly, an exponential function is fitted to the strain-time output. Secondly, the difference between the output data and the fitting curve is calculated in each sampling time, as shown in figure E1a.3.

The resultant difference function is symmetric so the square of the difference function results in a saw tooth function with the same frequency as the original function as shown in figure E1a.4. Thirdly, a moving average filter is used to smooth the saw tooth function as shown in figure E1a.5. Finally, the square root of the smoothed function is calculated to determine the response function parameters such as frequency amplitude, as presented in figure E1a.6.

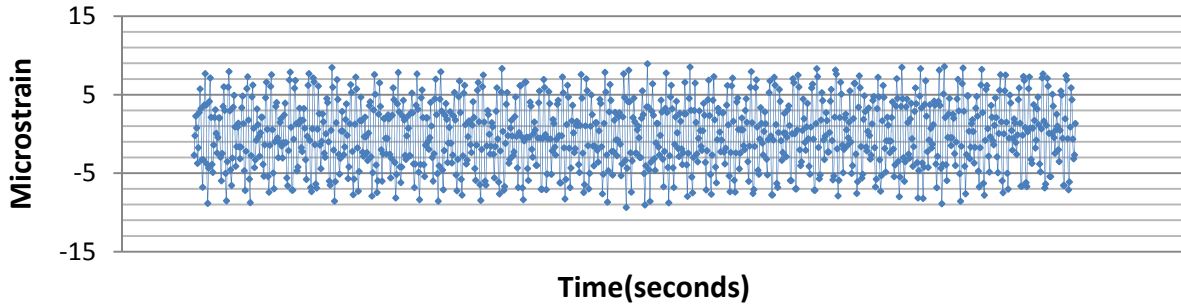


Figure E1a.3. Difference function versus time.

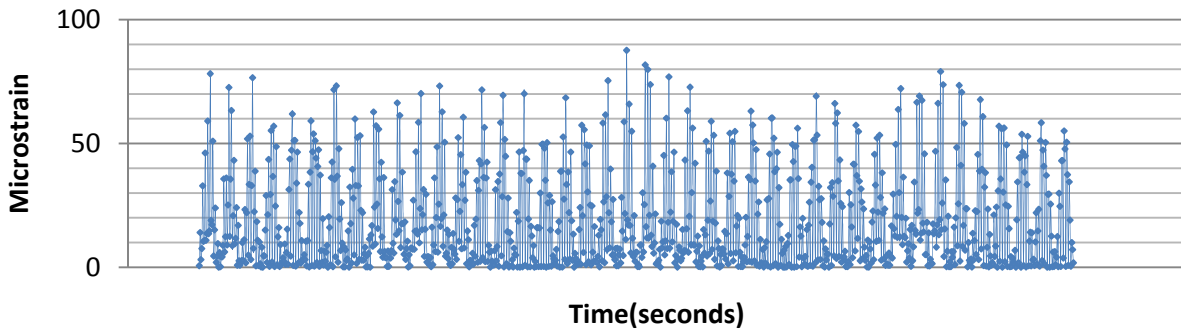


Figure E1a.4. Square of difference function versus time.

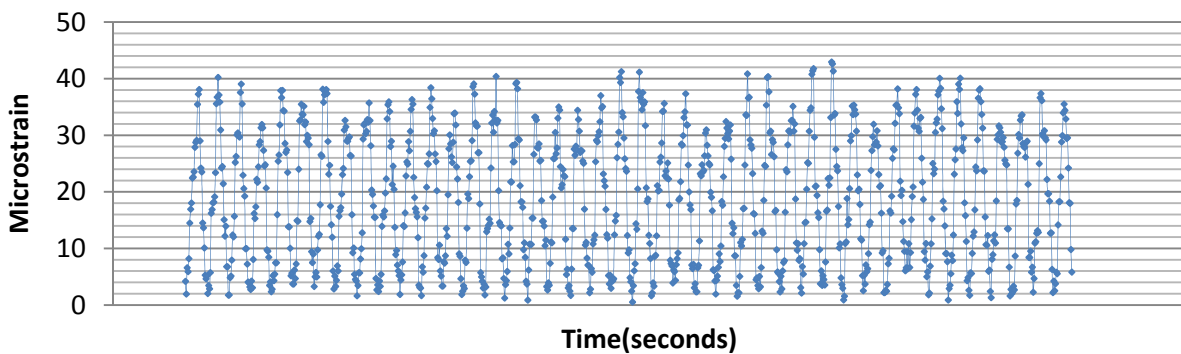


Figure E1a.5. Smoothed function using the moving average filter.

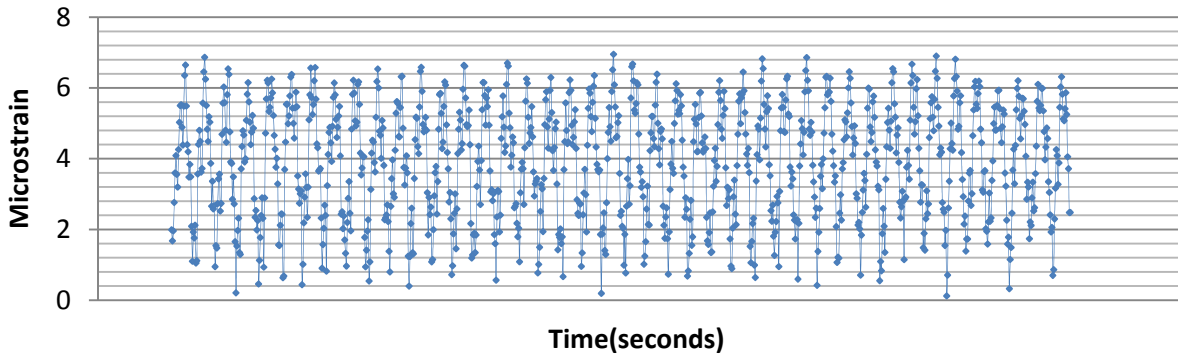


Figure E1a.6. Square root of the smoothed function.

The analysis method documented in previous quarterly reports is used to determine the stiffness gradient of each specimen in terms of two parameters, n and k . The analysis results indicate that the stiffness changes linearly with the pavement depth in the first few years after construction. The analysis is performed on data of tests at two temperatures, 10°C and 20°C . The stiffness gradient of each sample has the same pattern at the two temperatures. In some cases, a low modulus is determined at the bottom of the asphalt layer. This fact will be verified with the results of the binder extraction and X-ray CT scan. The analysis results also show that, at 10°C , the surface modulus in the wheel path increases faster with time than that in the shoulder.

According to the analyzed data, the k value has a phase angle of 180 degrees and the n value has a phase angle near zero degrees. Table E1a.1 is a summary of the gradient analysis results for the selected field cores. This table also presents comprehensive information regarding the cores including construction date, coring date, mix design properties and etc. The RWP, NBS and EBS in table E1a.1 stand for Right Wheel Path, North Bound Shoulder and East Bound Shoulder, respectively. The first number in the sample ID stands for the coring sequence and the second number indicates the replicates. For example, US82-EBS-2-5 represents for a core taken from east bound shoulder of the US 82 in the second coring period as a fifth replicate.

Table E1a.1. Summary of stiffness gradient analysis results of selected field cores.

Sample ID	Coring Location	Construction Date	Coring Date	Thickness (inches)	Binder Type	Binder Content (%)	Machine Feed-back Rate(Hz)	Test Temperature	Specimen Thickness (inches)	n	n Phase Angle	k	k Phase Angle	Modulus at Surface (ksi)	Modulus at the Bottom (ksi)
US82-EBS1-5	US82-Shoulder	Jul-08	Aug-08	3	PG 70-28	6.2	2	10C	2	1.03	0	2.1	180	515	245
US82-EBS-2-5	US82-Shoulder	Jul-08	Dec-09	3	PG 70-28	6.2	20	10C	2	1.02	0	3.04	180	555	182
US82-EBS-2-5	US82-Shoulder	Jul-08	Dec-09	3	PG 70-28	6.2	20	20C	2	1.01	0	3.04	180	348	114
US82-EBS-2-4	US82-Shoulder	Jul-08	Dec-09	3	PG 70-28	6.2	20	10C	2	0.98	0	2.97	180	541	182
SH59-RWP-1-3	SH59-Wheel Path	Jul-07	Jul-08	3	PG70-22	4.9	2	10C	2	1.23	0	2.12	180	1209	573
US-277-NBS-1-5	US277-Shoulder	Apr-08	Jul-08	3	PG70-28	4.2	20	10C	2	1.19	0	3.42	180	623	183
US-277-NBS-2-3	US277-Shoulder	Apr-08	Dec-09	3	PG70-28	4.2	20	10C	2	1.06	0	5.78	180	685	118
US-277-NBS-1-5	US277-Shoulder	Apr-08	Jul-08	3	PG70-28	4.2	20	20C	2	1.07	0	3.48	180	280	80
US-277-NBS-2-3	US277-Shoulder	Apr-08	Dec-09	3	PG70-28	4.2	20	20C	2	1.03	0	5.91	180	349	60.3
US-277-NBS-1-4	US277-Shoulder	Apr-08	Jul-08	3	PG70-28	4.2	20	10C	2	1.01	0	1.45	0	316	218
US-277-NBS-2-1	US277-Shoulder	Apr-08	Dec-09	3	PG70-28	4.2	20	10C	2	1	0	3	180	835	279
US-277-NBS-1-4	US277-Shoulder	Apr-08	Jul-08	3	PG70-28	4.2	20	20C	2	1.01	0	3.03	180	237	78.3
US-277-NBS-2-1	US277-Shoulder	Apr-08	Dec-09	3	PG70-28	4.2	20	20C	2	1.02	0	3.07	180	479	156
US-277-RWP-1-2	US277-Wheel Path	Apr-08	Jul-08	3	PG70-28	4.2	20	10C	2	1.02	0	3.94	180	509	129
US-277-RWP-2-1	US277-Wheel Path	Apr-08	Dec-09	3	PG70-28	4.2	20	10C	2	0.92	0	5.84	180	858	146
US-277-RWP-1-2	US277-Wheel Path	Apr-08	Jul-08	3	PG70-28	4.2	20	20C	2	1.03	0	3.04	180	314	103
US-277-RWP-2-1	US277-Wheel Path	Apr-08	Dec-09	3	PG70-28	4.2	20	20C	2	1.01	0	6.08	180	517	85
US-277-RWP-1-5	US277-Wheel Path	Apr-08	Jul-08	3	PG70-28	4.2	20	10C	2	1.04	0	4.24	180	683	161
US-277-RWP-2-3	US277-Wheel Path	Apr-08	Dec-09	3	PG70-28	4.2	20	10C	2	1.01	0	6.78	180	966	143
US-277-RWP-1-5	US277-Wheel Path	Apr-08	Jul-08	3	PG70-28	4.2	20	20C	2	1.02	0	5.08	180	258	51
US-277-RWP-2-3	US277-Wheel Path	Apr-08	Dec-09	3	PG70-28	4.2	20	20C	2	1.01	0	6.22	180	349	56

Significant Results

The fatigue crack growth model is established based on the Strain Energy Equivalence Principle for the FAM specimen under the controlled-stress RDT test.

Work Planned Next Quarter

The bond energy between asphalt and aggregate under different relative humidity will be evaluated.

More field cores will be analyzed to evaluate the effect of traffic and aging on the stiffness gradient with the pavement depth. The results will also be verified with the results of the binder extraction and X-ray CT scan of the same samples. The analysis method can be performed on test results of any machine with different feedback so more samples from different sources can be analyzed using this method.

A finite element model will be developed in the software ABAQUS to verify the stiffness gradient model. This model will be used to evaluate the size and geometry effects on the oscillation amplitudes of the test data.

Work element E1b: Binder Damage Resistance Characterization (DRC) (UWM)

Subtask E1b-1: Rutting of Asphalt Binders

Work Done This Quarter

Work completed during this quarter consisted of conducting Repeated Creep and Recovery (RCR) and Multiple Stress Creep and Recovery (MSCR) tests on different binders at temperatures of 46 °C, 58 °C and 70 °C. Tests were conducted at stress levels of 100 Pa and 3200 Pa for MSCR and 100 Pa, 3200 Pa and 10000 Pa for RCR. A neat FH 64-22 and three modified binders (styrene-butadiene-styrene (SBS), CBE (plastomer-modified) and ground tire rubber (GTR)) were used. Replicates were included for each binder.

Work done under other subtasks and sample preparation procedure for mastics based on the work of other researchers was finalized. Mastic preparation and testing for the neat binder is under way.

Work completed this quarter on mixtures was focused on the granite aggregate. While preparation of the bulk of the material is nearing completion, enough granite aggregate was sieved, washed and dried to produce six coarse and six fine specimens used for mixture design. The coarse mixtures were prepared at 4.0%, 4.5% and 5.0% asphalt by weight, while the fine gradation mixes included 5.0%, 5.5% and 6.0% asphalt binder. Replicates were included for each binder.

Efforts to model the binder behavior under MSCR testing was continued using the model presented in the ARC Q3 2008 report. A good fit was obtained for the neat binder; work for modified binders is under way.

Significant Results

Binder Modification

Analysis of the MSCR test results for binders indicates that modified binders vary in their nonrecoverable creep compliance (J_{nr}) and percent recovery (%R) values depending on temperature, stress level and modifier type. The plastomer modifier exhibited the best (lowest) overall J_{nr} value, and the best (highest) %R. However, it also showed the highest sensitivity to change in stress level among all binders. The sensitivity of all binders to stress increased with temperature, but for the CBE-modified binder the change was very significant. For example, as the stress is increased from 100 Pa to 3200 Pa, the plastomer (CBE)-modified binder showed a drop of about 30% to 60% in %R for tests conducted at 58 °C and 70 °C, respectively. The corresponding jump in J_{nr} is not nearly comparable.

The analysis of the RCR results showed that with increasing the stress level from 100 Pa to 3200 Pa and then 10000 Pa, the performance order of different modifiers gets reversed. At 10000 Pa, the plastomer (CBE) exhibits the worst standing in terms of J_{nr} and R% among the modifiers at 10000 Pa. This change of performance was similar to the MSCR results, but perhaps the stress level in MSCR did not go high enough to see the change of ranking of modified binders based on the J_{nr} values. Furthermore, the levels of modifications on all these binders were just enough to cause a one-grade bump in high temperature (from 64 °C to 70 °C). Further testing to clarify the stress and temperature sensitivity of the modifiers is warranted.

Figure E1b-1.1 shows an example of how the ranking of binders changes in the RCR test in terms of J_{nr} and %R when stress is changed from 3200 Pa to 10000 Pa. J_{nr} values appear similar at 3200 Pa, while very different at 10000 Pa. It should be noted, however, that despite the stress sensitivity, the J_{nr} values remain below the limit of 1.0 (1/Kpa) required by the current MSCR proposal. However, the value of %R is almost nil at the end of the RCR testing at 10000 Pa.

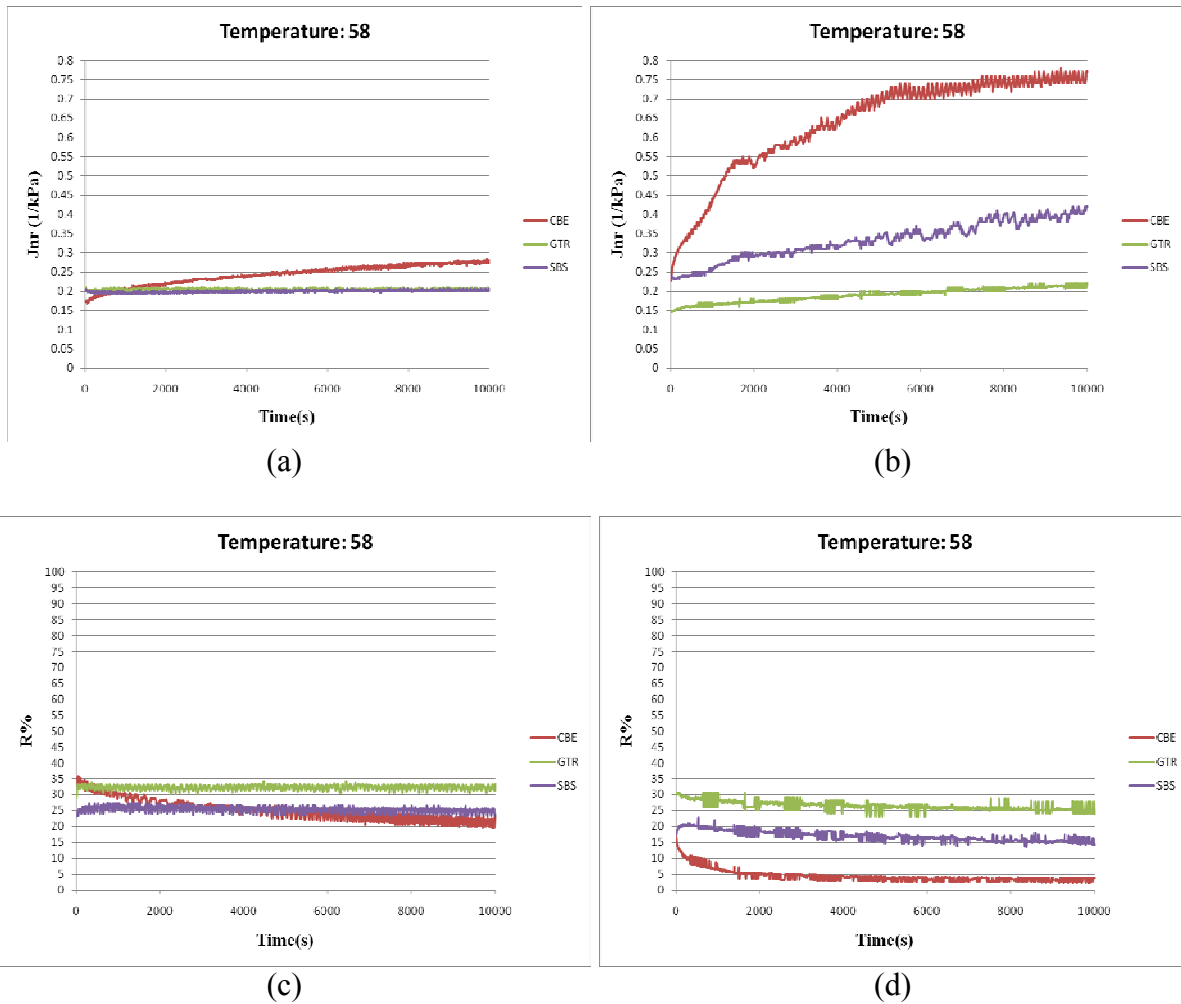


Figure E1b-1.1. Graphs. RCR results at 58 °C for all modified binders at different stress levels: (a) J_{nr} values at 3200 Pa; (b) J_{nr} values at 10000 Pa; (c) %R values at 3200 Pa; and (d) %R values at 10000 Pa.

Mixture Modification

The results of mixture design for the coarse mixtures with the granite aggregates are shown in figure E1b-1.2. It is clear that a fourth asphalt binder content prepared at a minimum of 5.5% will be needed to achieve the 96% G_{mm} at N_{design} . On the other hand, it is shown that the fine mixtures will need an additional set of replicates prepared at a lower asphalt content (4.5%). This was not anticipated, as the asphalt contents were selected based on the previous results for the limestone aggregates with almost identical gradations.

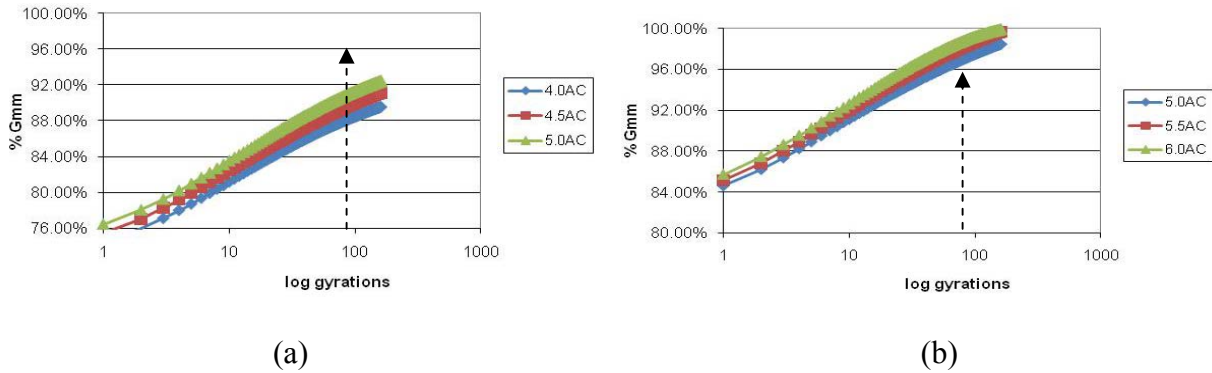


Figure E1b-1.2. Graphs. Densification curves for: (a) coarse; and (b) fine gradations of granite.

Significant Problems, Issues and Potential Impact on Progress

None.

Work Planned Next Quarter

Work for next quarter will focus on the following tasks:

- Continue MSCR binder modeling for modified binders.
- Complete RCR and MSCR testing of mastic with neat and modified binders.
- Perform analysis of mastic data.
- Complete the fourth data points to finalize the matrix.
- Conduct the RCR on the fourth data point samples at 50 psi and 150 psi, and complete imaging of internal aggregate structure for additional investigation.
- Conduct full suite of mixture testing on the granite aggregate samples for the neat binder, as well as the three modified forms of that binder (identical to tests done on the limestone mixtures during last quarter).

Subtask E1b-2: Feasibility of Determining Rheological and Fracture Properties of Asphalt Binders and Mastics using Simple Indentation Tests

Work Done This Quarter

The research team finished the modification of the indentation test. Two new components were added to the previous system: a new counterbalance system to improve contact and flexibility of loading, and an automatic data acquisition system to improve resolution of measurements. The new indentation/penetration device is shown in figure E1b-2.1.

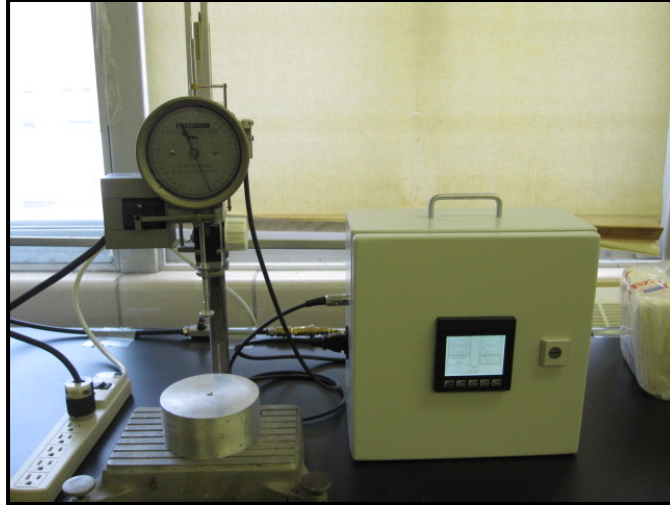


Figure E1b-2.1. Photograph. Modified indentation/penetration test.

In the device, the indenter shaft is attached to a new pulley system with counterweights to allow the shaft with the indenter to float freely. Note that the preloading or initial contact issue is minimized with the addition of the pulley system. This new pulley system is not as sensitive as the previously designed system, and it can be easily adjusted for each new test. In addition, a magnetic strip is used to record the displacement of the indenter. The magnetic strip is a set of magnets with different poles in a row, which send signals to the data acquisition system during movement of the indenter to measure displacement. The new data acquisition system saves the displacement over time on a memory card.

Significant Results

In this quarter, creep and recovery tests were performed with the modified indentation/penetration device. Figure E1b-2.2 shows an example of a creep and recovery test performed at room temperature with the new penetration system. Table E1b-2.1 shows the asphalt binders tested with the new system. Note that three different sample sizes and three replicates for each condition were tested. All tests were conducted at room temperature. The creep and recovery test used 3 minutes and 12 minutes of loading and unloading, respectively, and 50 grams of loading.

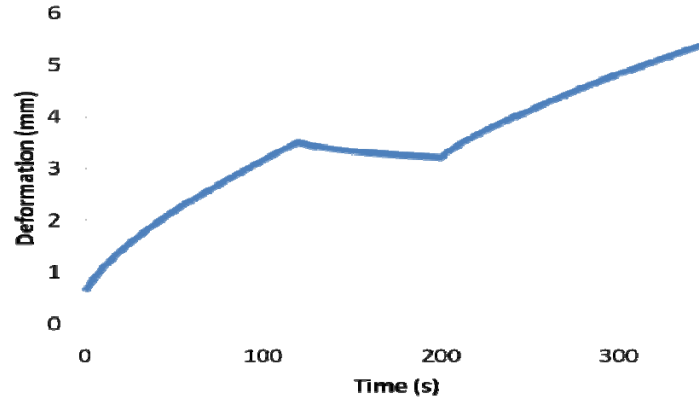


Figure E1b-2.2. Graph. Creep and recovery test with the modified indentation/penetration test.

Table E1b-2.1. Experimental matrix for indentation/penetration test.

Base Binder	Modification	Sample Height		
		5.1 cm	3.4 cm	1.7 cm
FH 64-22	Neat	X	X	X
	Styrene-Butadiene-Styrene (SBS)	X	X	X
	Plastomer (CBE)	X	X	X

Typical results for the creep and recovery test of the binders are presented in figure E1b-2.3. The effect of modification can be clearly seen in the trends shown. The modified binders (CBE and SBS) show lower displacements, which indicate the stiffening effect of the modifiers. Furthermore, the binder modified with SBS seems to have higher elastic recovery in comparison to the neat and CBE-modified binder. Size effects are observed in the creep and recovery test. Generally, smaller samples (i.e., h=1.7 cm) appear to be stiffer than the h=5.1 cm samples.

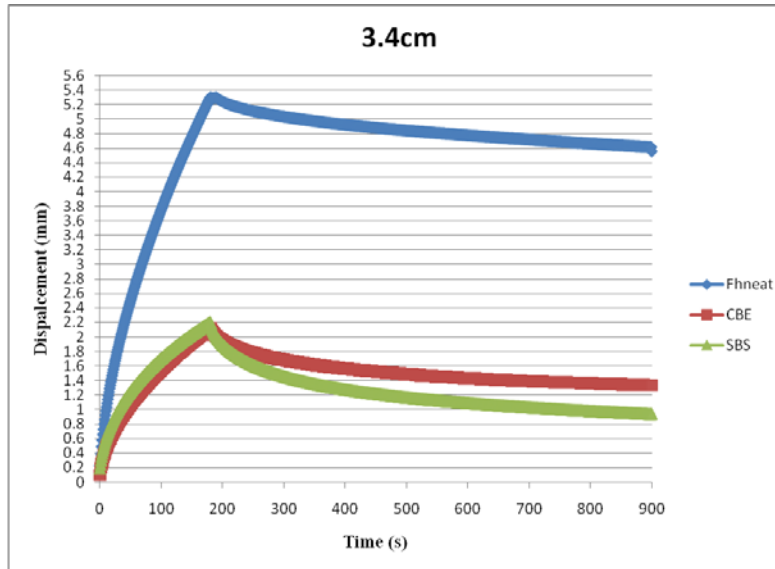


Figure E1b-2.3. Graph. Effect of modification on the indentation creep and recovery test for samples with $h=3.4$ cm.

Significant Problems, Issues and Potential Impact on Progress

The research team had difficulties establishing a repeatable procedure with the new indentation device. More specifically, the clutch used to hold/release the indentation shaft caused significant movement of the indenter at the beginning of the test. The research team is exploring changes in the test procedure to avoid the dynamic forces generated by the clutch at the beginning of the test. The team also envisions the control of temperature as another issue of the current testing procedure and is exploring ways to modify the indentation/penetration system to allow for temperature control.

Work Planned Next Quarter

Work next quarter will focus on the following tasks:

- Assess the repeatability of the modified indentation/penetration device with a new procedure that initially avoids the use of the clutch.
- Use the indentation device for creep and recovery tests with 1:9 proportion for the loading and unloading time.
- Optimize the sample geometry with finite element (FE) modeling.
- Continue the collaborative effort with the University of Minnesota on the estimation of fracture properties of asphalt binders with indentation tests at low temperatures.
- Complete test matrix of mastic samples with the modified indentation/penetration device.

Work Element E1c: Warm and Cold Mixes

Subtask E1c-1: Warm Mixes (UWM)

Work Done This Quarter

The research team began to collaborate with CECA, a subsidiary of the Arkema Group, in evaluating the effect of testing geometry on the coefficient of friction measured by the lubricity test. At the end of the study, results obtained from the UW–Madison lubricity test and a commercially available Dynamic Shear Rheometer (DSR) tribology fixture operated by CECA will be compared.

The experimental plan calls for evaluation of three binders: one control and two modified with the CECA additive at different concentrations (0.3% and 0.6%). Due to limited availability, testing temperature, speed and normal force have been held constant. Testing was completed on the DSR tribology fixture at CECA and the split samples were sent to UW–Madison for testing. Upon receipt of the samples, lubricity testing will begin. Additional mixture workability data across a range of temperatures has been collected for various warm mix asphalt (WMA) additive types and concentrations. This information will be used in future work to validate the importance of the Asphalt Lubricity Test.

Efforts related to implications of reduced aging temperatures for production of WMA focused on addressing comments on a journal paper received from the Association of Asphalt Pavement Technologists (AAPT) review panel and submission of the final document. The comments were valuable in providing suggestions for expansion of the work in both binder and mixture testing to provide a more comprehensive understanding of the impacts of reduced aging. Short-term aging at temperatures of 120 °C and 135 °C on the materials used in the AAPT paper has helped the research team to begin to better understand the relationship between aging temperature and rheological performance.

Collaborative efforts continued with University of Nevada, Reno on moisture damage testing. WMA additives and asphalt binders were collected and shipped to UNR to allow for continued work on moisture damage testing. Bitumen Bond Strength (BBS) testing at UW–Madison remains 50% complete; testing will finish in the next quarter. The research team is unaware of any Wisconsin DOT WMA field projects that were constructed in the 2010 season, thus no progress has been made on this element. The research team will discuss opportunities for research and testing on 2011 construction projects in the spring.

Significant Results

Results provided by CECA on lubricity testing using the commercial DSR tribology cell indicate no sensitivity to the presence of additive and exhibit values of coefficient of friction considerably lower than values that have been measured at 90 °C in the UW–Madison fixture for other materials. Additional information comparing the performance between the two testing devices will be available pending receipt of the CECA samples.

The evaluation of a viscosity-reducing polymer additive (VR-1) has continued, and numerous data points from both the laboratory and the field were collected. The research team is currently analyzing asphalt binder and compaction data to establish guidelines for establishing mixing and compaction temperatures. This additive is similar to other viscosity reducers in that at temperatures below its softening point, it improves asphalt binder performance. The research team plans to expand the creation of these guidelines to include other additive types.

Significant Problems, Issues and Potential Impact on Progress

Asphalt lubricity testing and WMA performance evaluation were delayed due to urgent testing needs in other work areas. This time-sensitive testing was related to the construction season; it is anticipated that the project will get back on schedule in the next quarter. The subtasks for evaluation of asphalt binder performance and mixture compaction were extended in the Gantt chart to account for additional time in development of the lubricity test and continued interest in evaluating the impacts of reduced aging on performance.

Minor delays were experienced due to lack of availability of the flow number (FN) test and lubricity test due to equipment issues. Both machines are now up and running. The research team continues to work with the UW–Madison Physics Department machine shop on the design of a self-centering lubricity fixture, but has so far been unsuccessful.

The lack of WMA field projects has delayed this subtask in the work plan at least six months due to the short construction season in Wisconsin. The research team will consider another approach to obtaining valid field information.

Work Planned Next Quarter

The following activities are planned for next quarter:

- *Lubricity testing.* Collaborative work with CECA will continue. The research team will also develop and execute a work plan for continued evaluation of the asphalt lubricity test. Specific areas of the work plan include: evaluation of reproducibility/repeatability, effect of concentration and ruggedness testing.
- *Impacts of reduced aging on performance.* Short-term aging at reduced temperatures and testing will continue. More asphalt binder sources and binder modification will be included to more fully develop the relationship between the rate of change of binder performance as a function of temperature and aging index used to develop the FHWA model that is the basis for the current production temperature minimums defined in the NCHRP 9-43 report. Potential development of a similar model using the Multiple Stress Creep and Recovery (MSCR) test results will be evaluated. Additional mixture performance testing is planned. Potential areas of expansion include: use of modified binders, additional mixture gradations, and/or additional aggregate sources. The research team will also develop a work plan for expansion of this subtask to consider the impacts of reduced aging temperatures on long-term durability.

- *Moisture damage.* The BBS testing matrix will be completed, and the research team will work with University of Nevada, Reno to discuss results of mixture testing. Preliminary results will be presented in the ARC Q1 2011 report.

Subtask E1c-2: Improvement of Emulsions' Characterization and Mixture Design for Cold Bitumen Applications (UWM)

Work Done This Quarter

This quarter the construction and performance properties of six types of emulsions were measured to evaluate the capability of tests selected for the draft Strawman specification, which was developed in conjunction with the Emulsion Task Force to differentiate between types and composition of emulsions. The tests included the Bitumen Bond Strength (BBS) test, the Multiple Stress Creep and Recovery (MSCR) test, and the stress sweep test.

Six emulsions were produced by a Wisconsin supplier: CRS-2, CRS-2L, CRS-2P, HFRS-2, HFRS-2P and HFRS-2L. These materials are representative of those used for chip sealing in the U.S. The BBS test was conducted on emulsion residues before and after moisture conditioning on aggregate and glass substrates. The moisture conditioning involved submersion in a 40 °C water bath for 24 hours. All emulsion residues were obtained using ASTM 7479 Method B, which involves recovery of a thin film of emulsion for 6 hours at 60 °C. The results from the various test methods were compared to evaluate their sensitivity to emulsion composition and types of modification.

Significant Results

The conditions for the BBS test provided in the Emulsion Task Force Strawman specification include evaluation of bond strength after 6 hours curing in an environmental chamber at 35 °C and 30% humidity. Initial testing results showed that HFRS-2 emulsion could not develop a sufficient bond after these curing conditions. Applying the relationship between moisture loss and development of emulsion properties measured in previous ARC research, and the recommendations of NCHRP Project 14-17 regarding the moisture loss, it was found that the HFRS-2 emulsion in the BBS fixture required 15 hours of curing time to allow for 85% of the moisture to evaporate from the sample. Conversely, all other emulsion types achieved approximately 85% moisture loss after 6 hours curing.

Results also suggest that substrate type influences the rate of moisture loss. After 6 hours curing on granite the average moisture loss was 87.4%, while it was 91% on the glass substrate. Based on these findings, the research team is in the process of revising the testing protocol to require that comparison of bond strength between different emulsions be based on moisture loss rather than curing time. Examples of the BBS test results at 85% moisture loss are presented in figure E1c-2.1.

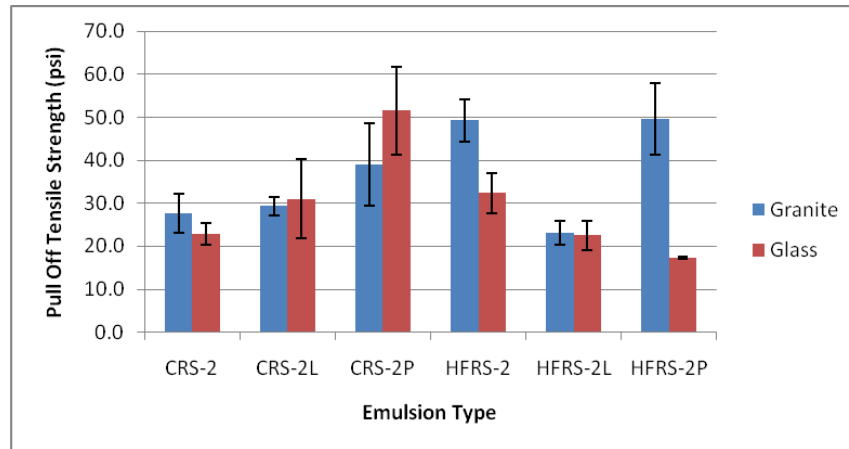


Figure E1c-2.1. Chart. Bond strength of emulsions cured at approximately 85% moisture loss on granite and glass substrates.

Results clearly show that the BBS can differentiate between emulsions based on modification and substrate type. For the cationic emulsions, use of latex and polymer modification resulted in marginally higher bond strengths, with the highest strength observed for the CRS-2P emulsion. Higher strengths were also observed for these modified emulsions after curing on the glass substrate. Conversely, no effect of modification was observed for the anionic emulsions, with lower strengths observed for the testing on the glass substrate. It should also be mentioned that all emulsions showed bond strength below the minimum of 100 psi proposed in previous ARC work (Miller et al. 2010). It is hypothesized that the variability observed for certain emulsion/substrate combinations is due to the relative low bond strengths observed for these materials. Further research is needed to investigate the relationship between moisture loss and bond strength.

BBS testing on emulsion residues cured using the ASTM 7479 Method B (6 hours at 60 °C with very thin films) exhibited much higher values of bond strength, with values ranging from 150 psi to 300 psi, indicating that considerable bond strength is developed due to the residue recovery process specified in the ASTM standard. Results of moisture conditioning were used to calculate ratios of wet-to-dry bond strength. Ratios ranged from 0.76 to 1.22, indicating that moisture susceptibility is not a primary concern in evaluation of emulsion residue properties and, in some cases, strength is gained due to moisture conditioning. It was observed that the latex- and polymer-modified emulsions for both the anionic and cationic chemistries exhibited less moisture susceptibility.

For performance-related properties, three high-temperature tests were conducted on residues of the six emulsions. The MSCR and Superpave grading tests were conducted at 52 °C and 64 °C; stress levels for the MSCR were 1.0 kPa, 3.2 kPa and 10 kPa. The stress sweep was conducted at stress levels ranging from 100 Pa to 7000 Pa at a temperature of 64 °C. Based on the results to date, the MSCR has shown the best potential as an effective specification test. Values of nonrecoverable creep compliance (J_{nr}) as a function of stress level for the MSCR test conducted at 64 °C are presented in figure E1c-2.2.

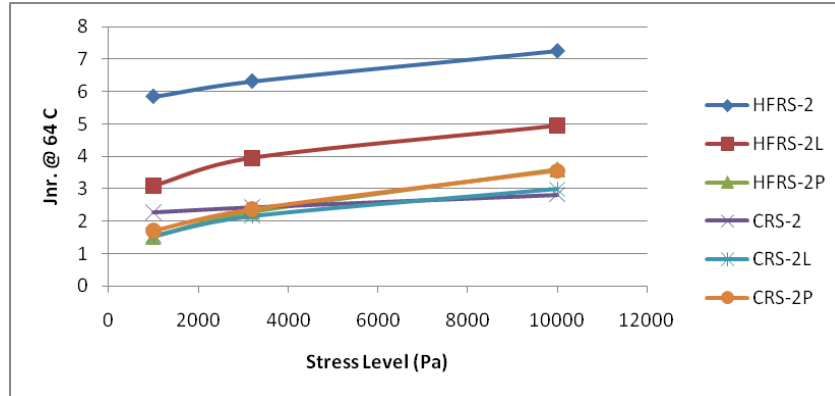


Figure E1c-2.2. Graph. Comparison of J_{nr} versus stress level for MSCR testing conducted at 64 °C for conventional and modified cationic and anionic emulsions.

Results indicate that the MSCR test is able to differentiate between performance of the high-float anionic emulsions, with the HFRS-2 and HFRS-2L exhibiting significantly more susceptibility to permanent deformation. In terms of the J_{nr} parameter, the cationic emulsions all exhibit similar performance. Furthermore, based on the slope of the J_{nr} versus stress plot, all emulsion types appear to exhibit similar stress sensitivity. The percent recovery (%R) parameter was used as an indicator of the polymer network developed due to the use of modification. The %R evaluated at a temperature of 64 °C and 3.2 kPa for the six materials evaluated is provided in figure E1c-2.3.

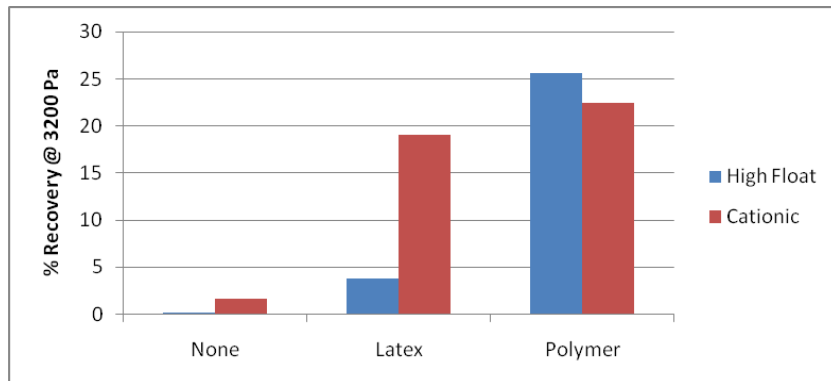


Figure E1c-2.3. Chart. MSCR results showing %R at a testing temperature of 64 °C and stress level 3.2 kPa for modified and unmodified emulsion residues.

The other candidate tests were found to be insensitive to material type, only indicating the poor performance of the HFRS-2 emulsion. Initial analysis of the stress sweep data used the reduction in complex modulus, G^* relative to G^* at 100 Pa over a range of stress levels. Up to 5.0 kPa, this analysis method was unable to differentiate materials, with the five adequately performing

emulsions exhibiting reductions in G^* ranging from 30% to 35%. Further data analysis is needed before eliminating the stress sweep as a high-temperature performance test.

Significant Problems, Issues and Potential Impact on Progress

Further investigation of the relationship between moisture loss and bond strength is needed. This issue will be investigated in subsequent quarters and should not significantly impact progress. The insensitivity of the stress sweep to material type was unexpected. Alternative data analysis methods will be investigated in the next quarter.

The Gantt chart was modified to show that a draft literature review report will be submitted next quarter rather than during this quarter. The literature review will now be included as a section in the final report for the project.

Work Planned Next Quarter

The following activities are planned for next quarter:

- *Emulsion construction properties.* Previously presented viscosity testing will be analyzed in greater detail to evaluate the potential for use of the rotational viscometer to evaluate emulsion viscosity. Additional analysis will be conducted on the BBS data to determine how moisture loss will be incorporated into recommended testing procedures. An overview of the BBS test will be given at the Asphalt Emulsion Manufacturers Association (AEMA) conference on February 24, 2011.
- *Emulsion residue performance.* A high-temperature performance test will be selected. Elastic recovery in the Dynamic Shear Rheometer (DSR) will be conducted on all emulsion residues. Intermediate- and low-temperature properties will be evaluated on both recovered and pressure aging vessel (PAV)-aged residues.
- *Cold mixes.* Initial literature review and testing related to mix design methods for cold mixes will commence. The work plan developed and initial testing results will be presented at the AEMA conference on February 24, 2011.

Cited References

Miller, T., Z. Arega, and H. U. Bahia, 2010, Correlating Rheological Properties of Emulsion Residue to Early Chip Seal Performance. Presented at the 89th Transportation Research Board Annual Meeting, Washington, D.C.

CATEGORY E2: DESIGN GUIDANCE

Work element E2a: Comparison of Modification Techniques (UWM)

Work Done This Quarter

The research team decided to include two new tests in the experimental plan for this work element: Linear Amplitude Sweep (LAS) and Bitumen Bond Strength (BBS) test. The LAS test is designed to measure the fatigue performance at intermediate temperatures, while the BBS test is designed to measure the bond strength between asphalt and aggregate as well as the asphalt binder susceptibility to moisture damage. The protocols for performing the LAS and BBS tests are described in different work elements.

The LAS tests were conducted at the intermediate PG temperatures of the base binder, determined according to the AASHTO standard MP1, as well at the intermediate PG temperature plus 10 °C. By performing the LAS test at two different temperatures, the dependence of the fatigue law parameters (i.e., A and B) on temperature is quantified. As mentioned in the ARC Q3 2010 report, the D-labeled binders were replaced with binders of the same PG but from a different supplier. Currently, the tests included in the experimental plan are being performed on these new materials.

Significant Results

An example of a stress versus strain curve from LAS testing at two different temperatures is shown in figure E2a.1. It can be observed that the LAS response significantly changes by increasing the temperature by 10 °C.

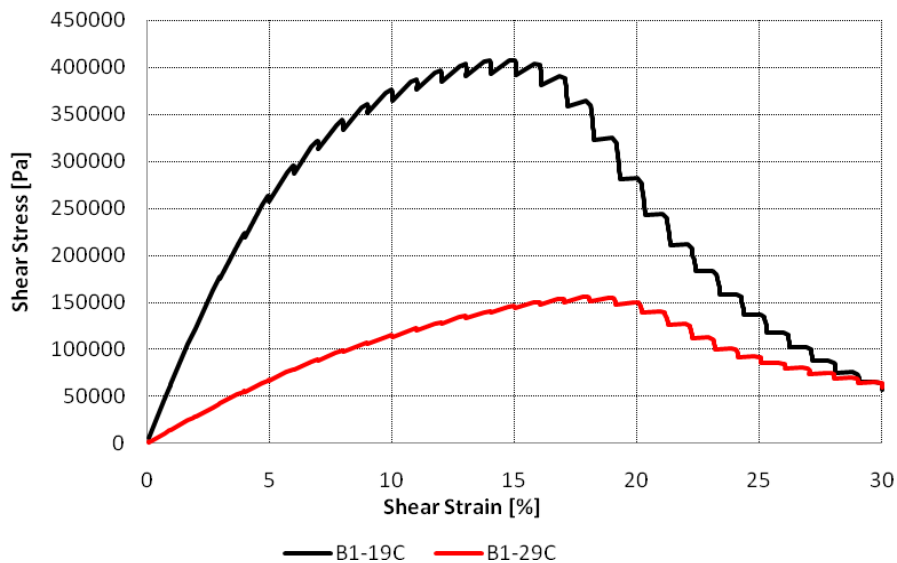


Figure E2a.1. Graph. LAS stress versus strain curve at different temperatures.

Table E2a.1 presents the fatigue law parameters for LAS testing at two different temperatures. Note that the numbers of cycles to failure (N_f) were calculated at two arbitrarily selected strain levels (i.e., 2.5% and 5%).

Table E2a.1. LAS test results.

Binder	Temp (°C)	A	B	N_f @ 2.5%	N_f @ 5%
A0	25	7.64E+06	-4.599	1.13E+05	4.66E+03
	35	1.27E+07	-4.306	2.45E+05	1.24E+04
A1	25	9.75E+06	-4.824	1.17E+05	4.14E+03
	35	1.27E+07	-4.306	2.45E+05	1.24E+04
A2	25	1.56E+07	-5.073	1.49E+05	4.42E+03
	35	18114941	-4.731	2.37E+05	8940.672
A3	25	1.50E+07	-4.926	1.65E+05	5.42E+03
	35	2.09E+07	-4.689	2.85E+05	1.11E+04
A4	25	3.95E+07	-5.260	3.18E+05	8.29E+03
	35	5.88E+07	-5.048	5.76E+05	1.74E+04
B0	19	8.46E+06	-4.720	1.12E+05	4.25E+03
	29	1.40E+07	-4.410	2.46E+05	1.16E+04
B1	19	1.89E+07	-4.887	2.14E+05	7.24E+03
	29	5.54E+07	-4.675	7.64E+05	2.99E+04
B2	19	2.85E+07	-5.045	2.81E+05	8.50E+03
	29	1.02E+08	-4.927	1.12E+06	3.67E+04
C0	19	9.95E+06	-4.738	1.30E+05	4.86E+03
	29	1.25E+07	-4.365	2.29E+05	1.11E+04
C1	19	1.29E+07	-5.028	1.29E+05	3.94E+03
	29	1.55E+07	-4.624	2.24E+05	9.08E+03
C2	19	3.25E+07	-5.222	2.71E+05	7.26E+03
	29	5.15E+07	-5.014	5.21E+05	1.61E+04
E0	25	6.37E+06	-4.576	9.62E+04	4.04E+03
	35	9.69E+06	-4.292	1.90E+05	9.69E+03
E1	25	2.01E+07	-4.793	2.49E+05	8.97E+03
	35	4.75E+07	-4.641	6.76E+05	2.71E+04
E2	25	3.28E+07	-4.921	3.62E+05	1.19E+04
	35	1.66E+08	-4.807	2.03E+06	7.25E+04

The data listed show that as the temperature increases, the fatigue law parameter A increases and parameter B decreases, consistently. Also, the number of cycles to failure increases when the temperature increases.

To give an idea of relative effect of temperature, the ratios between the values of the parameters tested at the two temperatures are presented in table E2a.2. The results indicate that the parameter A is more susceptible to temperature than parameter B . The change in B as a result of 10 °C increase in temperature is less than 10% increase. It is also noted that sensitivity to temperature is binder-specific. It can be observed that binders B1, B2, E1 and E2 are more susceptible to changes in temperature than other binders.

Table E2a.2. Change in A , B , N_f at 2.5% and N_f at 5% with temperature.

Binder	A_{PG}/A_{PG+10}	B_{PG}/B_{PG+10}	$N_{f2.5PG}/N_{f2.5PG+10}$	$N_{f5PG}/N_{f5PG+10}$
A0	0.60	1.07	0.46	0.38
A1	0.77	1.12	0.48	0.33
A2	0.86	1.07	0.63	0.49
A3	0.72	1.05	0.58	0.49
A4	0.67	1.04	0.55	0.48
B0	0.61	1.07	0.46	0.37
B1	0.34	1.05	0.28	0.24
B2	0.28	1.02	0.25	0.23
C0	0.80	1.09	0.57	0.44
C1	0.83	1.09	0.57	0.43
C2	0.63	1.04	0.52	0.45
E0	0.66	1.07	0.51	0.42
E1	0.42	1.03	0.37	0.33
E2	0.20	1.02	0.18	0.16

Significant Problems, Issues and Potential Impact on Progress

None.

Work Planned Next Quarter

In addition to the test procedures included in the experimental matrix for this work element (i.e., Binder Yield Energy Test (BYET), Multiple Stress Creep and Recovery (MSCR) test, Bending Beam Rheometer (BBR), Single-Edge Notched Bending (SENB) test and frequency sweep testing), the research group is planning to use the BBS test as an additional test procedure for all 17 binders.

Work element E2b: Design System for HMA Containing a High Percentage of RAP Materials (UNR)

Work Done This Quarter

This work element is a joint project between University of Nevada, Reno and University of Wisconsin–Madison. The PG analysis procedure developed in previous quarters was applied to additional recycled asphalt pavement (RAP) source-fresh binder combinations to demonstrate blending dependence on RAP source, fresh binder source and chemical modification. A summary report that details the analysis procedure verification results at low, intermediate and high temperatures, as well as significant results at low temperature for the above-mentioned work, was also completed.

Additional RAP/recycled asphalt shingle (RAS) combinations were tested to further verify that the proposed procedure can capture the blended binder properties of RAP and RAS mixtures. Comparison of the proposed analysis procedure with mixture binder extraction data at low temperature was also completed for a single RAP source and two fresh binder sources. Collaboration with work element E2d, Thermal Cracking Resistant Mixes for Intermountain States, using the Single-Edge Notched Bending (SENB) testing apparatus continues as variability in test samples remains high.

Under subtask E2b-5, the testing for the extracted/recovered asphalt binders from the Manitoba PTH8 field-produced and lab-produced mixtures has been completed. The blend asphalt binders' properties were backcalculated from the measured dynamic modulus using the Hirsh model and the Huet-Sayegh model and results are being analyzed.

Under subtask E2b-3, requested materials for one of the projects in UTAH have been received. Testing of the received materials has started following the experimental plan for the RAP mixing experiment listed in subtask E2b-3.

Significant Results

The procedure sensitivity to RAP source was studied by comparing the results of blending a single binder source with two different RAP sources, denoted by *MCC* and *EAP* in table E2b.1. As a second example, the same two RAP sources were blended with a different fresh binder with the same low-temperature PG (different continuous grade) at the same RAP binder replacement. The resulting analysis is summarized in table E2b.1.

Table E2b.1. Sensitivity analysis of characterization procedure to RAP source.

RAP Source	RAP Binder Percent ¹ [%]	Fresh Binder PG	Binder Continuous Grade		Grade Change Rate [°C /% RAP ²]
			Fresh Binder	Blended Binder	
MCC	17.5	76-22	-23.9	-18.4	0.31
EAP-3	17.5		-23.9	-17.7	0.36
MCC	17.5	67-22	-22.6	-17.2	0.31
EAP-3	17.5		-22.6	-18.3	0.21

¹ RAP binder replacement; RAP binder as a weight percent of total binder

² Degree change in terms of PG per percent RAP binder replacement

MCC has less of an effect on the blended binder continuous grade for fresh binder PG 76-22 compared to *EAP* (0.31 °C /% RAP for *MCC* compared to 0.36 °C /% RAP for *EAP*). This trend is reversed for the fresh binder PG 67-22 blends, where *MCC* has more of an effect on the blended binder continuous grade. Also, just as described in the binder sensitivity section, the RAP sources, in general, behave differently between binder grades.

To study whether the type of modification of fresh binders has an effect on the blending that occurs between the modified binder and RAP source, one RAP source was tested with one base binder and three modified binders. The modified binders had the same base binder in common and were modified to achieve desirable high-temperature properties. The low-temperature properties were assumed to satisfy the PG -22 requirements regardless of modification type.

Table E2b.2 demonstrates that the modified base binder (0% RAP binder replacement) does indeed satisfy the PG -22 requirements for all cases, but also influences how the modified binder reacts to the RAP binder, as seen in the differences in the *Grade Change Rate* column in table E2b.2. The implications of these results confirm earlier findings that the fresh binder-RAP blending relationship is highly dependent on both the source of RAP and composition of fresh binder. This is particularly true when modified fresh binders are used.

Table E2b.2. Sensitivity analysis of characterization procedure to fresh binder modifier.

RAP Source: HOH		RAP Binder Percent ¹ [%]	Binder Continuous Grade		Grade Change Rate [°C /% RAP ²]
Fresh Binder (Modifier)			Fresh Binder	Blended Binder	
PG 64-22 (Neat, Base Binder)		11.8	-22.3	-21.6	0.06
PG 76-22 (3.5% CBE)		11.8	-22.3	-20.7	0.14
PG 76-22 (6.0% AC-9)		11.8	-22.1	-21.5	0.05
PG 76-22 (SBS)		11.8	-24.3	-23.3	0.09

¹ RAP binder replacement; RAP binder as a weight percent of total binder

² Degree change in terms of PG per percent RAP binder replacement

SBS = styrene-butadiene-styrene.

Table E2b.3 summarizes the findings for the RAP and RAS blend presented in the ARC Q3 2010 report, as well as an additional RAP and RAS blend. The measured low-temperature continuous grade was found via actual Bending Beam Rheometer (BBR) testing, while the estimated true grade was determined by applying a linear relationship between the RAS-alone and RAP-alone tests (tested in the standard analysis procedure). The differences in continuous grade values indicate a strong linear relationship.

Table E2b.3. RAP and RAS blend testing.

Scenario 1 (presented in ARC Q3 2010 report)						
Fresh Binder	PG 58-28			RAP Source	TP	
				RAS Source	TS	
Blend	% RAP Binder¹	% RAS Binder¹	% Fresh Binder²	Binder Cont. Grade [C]		Difference [C]
				Estimated	Calculated [Linear Comb.]	
Fresh Binder	0	0	100	-30.4	-	
RAP Alone	23.9	0.0	76.1	-23.8	-	
RAS Alone	0.0	40.2	59.8	-14.4	-	
Trial 1	8.7	8.0	83.2	-26.8	-24.8	2.08
Trial 2	14.6	13.5	71.9	-21.8	-21.0	0.82

Scenario 2						
Fresh Binder	PG 64-22			RAP Source	NR	
				RAS Source	RS	
Blend	% RAP Binder¹	% RAS Binder¹	% Fresh Binder²	Binder Cont. Grade [C]		Difference [C]
				Estimated	Calculated [Linear Comb.]	
Fresh Binder	0	0	100	-22.7	-	
RAP Alone	24.7	0.0	75.3	-20.8	-	
RAS Alone	0.0	34.4	65.6	-11.3	-	
Trial 1	6.3	6.4	87.3	-18.1	-19.9	1.75
Trial 2	12.2	12.7	75.1	-14.8	-17.5	2.69

¹ Binder replacement by weight

² Weight percentage of fresh binder in the total blended binder (i.e., when no RAP or RAS materials present, 100%)

From table E2b.3, it can be concluded that the combination of RAP-alone and RAS-alone mixes for the scenarios tested is a linear relationship, and any subsequent amount of RAP or RAS binder replacement values can be reasonably estimated using only the RAP-alone and RAS-alone analysis. That is, the effect of RAP and RAS binder replacement on the low-temperature continuous grade can be assumed additive. Therefore, if RAS is to be used in conjunction with

RAP material at any unknown proportion, two blends must be created (RAP alone and RAS alone) with the selected fresh binder to estimate the combined effects.

To compare results of the method for extraction and recovery, data provided by Purdue University were used for the same RAP and binders tested in a pooled fund study. Table E2b.4 summarizes the results of the comparison. The extraction data and estimates from mortar testing procedure agree favorably for 15% and 25% RAP. Notice that most state agencies use these percentages as common cutoffs in “tiered design.” An important comment about table E2b.4 is that the mortar testing procedure provides more conservative estimates (higher estimated continuous grades) of the blended binder continuous grade when compared to the mixture extraction data for these cases.

Table E2b.4. Comparison of proposed analysis procedure with mixture extraction data.

	% RAP in Mix ¹	Cont. Grade of Blended Binder		
		Mortar Procedure	Mixture Extraction	Difference
Fresh Binder Grade PG 64-22	0	-21.4	-20.6	-0.8
	15	-18.2	-20.5	2.2
	25	-16.1	-18.6	2.5
	40	-13.0	-19.1	6.1
Fresh Binder Grade PG 58-28	0	-30.6	-	-
	25	-23.9	-26.3	2.4
	40	-20.0	-21.3	1.4

¹ Weight percentage of mix

At the time of this report this limited data set was the only extraction data available for direct comparison. More data must be collected, preferably with mixtures containing both RAP and RAS, to further validate the mortar testing procedure. This data set does, however, provide encouraging results.

Under subtask E2b-5, the PG grades of the various extracted/recovered asphalt binders from the Manitoba PTH8 field-produced and lab-produced mixtures has been completed and are shown in figure E2b.1. Overall, the recovered binders from the mixtures containing 0 and 15% RAP met the target grade for the project location of PG58-28. The recovered binders from the mixtures with 50% RAP met or exceeded the target high PG of 58°C but failed to meet the target low PG of -28°C. This observation was true for both mixtures with and without grade change. The use of softer asphalt binder (i.e. PG52-34) with the 50% RAP mix did not improve the low performance temperature of the blended asphalt binder in the mix enough to the point of meeting the target low PG.

The effectiveness of the blending chart technique with high RAP content mixtures was also evaluated. The blending chart process was used to estimate the PG of blended asphalt binders at different RAP contents following the recommendations of NCHRP project 09-12 (2004). Figure E2b.2 shows the comparison between the estimated critical temperatures from the blending chart

and the measured ones from the recovered asphalt binders. Overall a good correlation was observed between the two methods. Assuming that the grade for the recovered binder is the true value, the data show that the blending chart process could sometime underestimate or overestimate the critical temperatures by 2°C.

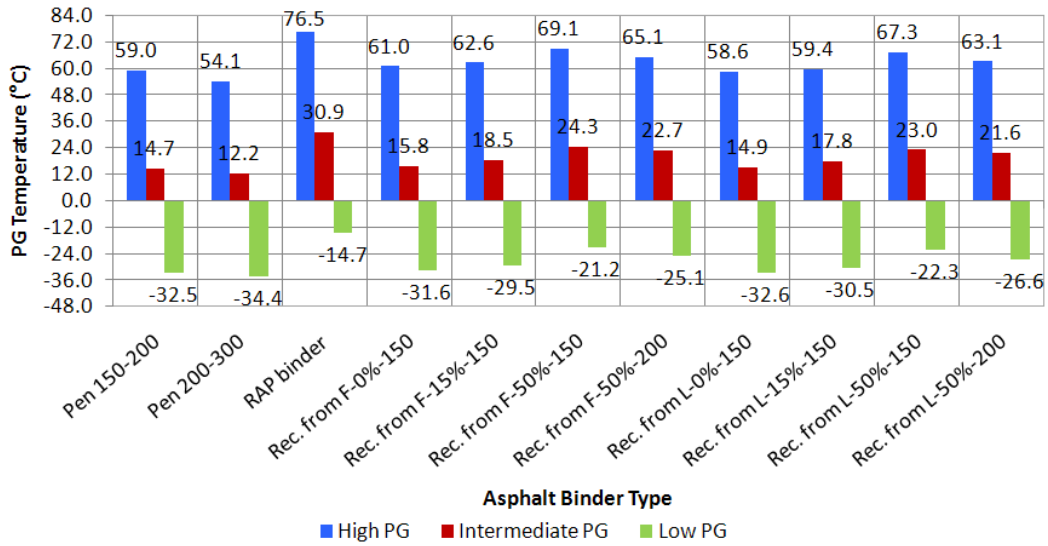


Figure E2b.1. Recovered asphalt binder grades.

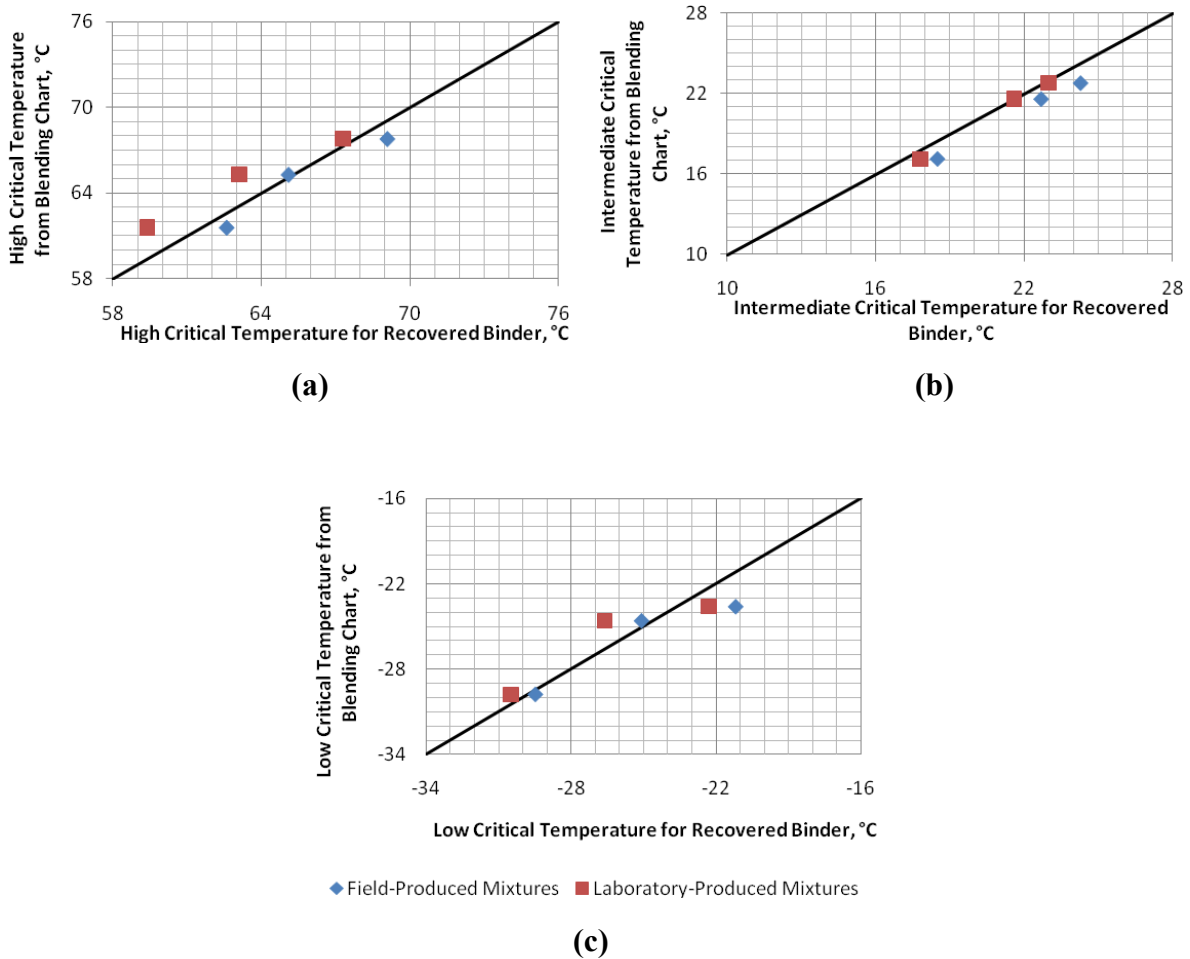


Figure E2b.2. Comparison between estimated and measured (a) high critical temperatures (b) intermediate critical temperature (c) low critical temperature.

Significant Problems, Issues and Potential Impact on Progress

Variability in fracture testing data has not allowed significant progress for this work element. Testing apparatus changes are currently being completed and testing will resume as soon as possible.

The sampling of the material from Granite Construction in UTAH for subtask E2b-3 has been delayed because of no Production of Superpave mixes. It is anticipated that material from the second source will be received by UNR this quarter. Work will start on the second source as soon as the material is received. The work progress is reflected on the Gantt chart.

Under subtask E2b-1.a, there has been some delay in the AIMS testing for the Alabama and Florida aggregates. NCAT completed the testing and data will be analyzed and report will be updated.

Work Planned Next Quarter

A work plan for workability testing of high-percentage RAP mixes to further validate the analysis procedure is currently being developed and is considered the most pertinent work to be completed. A draft standard will be completed following the workability testing to move forward with the proposed analysis procedure.

Work will continue on the evaluation of the test results for the Manitoba PTH8 RAP project.

Collect the material for the second source of the experimental plan of subtask E2b-3 “Develop a Mix Design Procedure,” and start the testing.

Cited References

National Cooperative Highway Research Program (NCHRP). Recommended Use of Reclaimed Asphalt Pavement in the Superpave Mix Design Method: Technician’s Manual. NCHRP Report 452, Transportation Research Board, National Research Council, Washington, DC, 2004.

Subtask E2b-2: Compatibility of RAP and Virgin Binders

Work Done This Quarter

The analysis of the Manitoba RAP field site samples is ongoing. Laboratory blended samples of RTFO-aged, virgin asphalt (4.25g) and laboratory extracted PTH RAP (0.75g) from the Manitoba site have been made and are ready for compatibility testing. The results will be compared to the analogous testing on the field mixes to advance our understanding of how RAP blends with virgin binder in the field and to help improve the state of the art for making these blends in the laboratory for specification or research.

In addition to the blended samples above, samples of RAP stockpiles in Iowa, California, and South Carolina have been extracted using a toluene/ethanol mixture as well as with cyclohexane. Characterization using the Asphaltene Determinator, as well as rheological measurements, has been completed and indicate some potential differences in the materials extracted with cyclohexane versus the toluene/ethanol extracted binders. These results as well as some initial AFT measurements were reported in a previous quarterly as well as in a presentation titled “Asphalt Component Compatibility – An Overview” at the RAP ETG that was recently held in Oklahoma City. The use of cyclohexane to extract the RAP and RAP-blended binders is believed to hold potential for approximating the RAP binder fractions that actually mix with virgin binder because cyclohexane has a solubility parameter similar to that of a whole asphalt. The preliminary results have led to a need for further composition analysis to pinpoint the differences in the extraction methods and the applicability of the cyclohexane extraction method as a means of determining the degree a RAP binder will blend.

Significant Results

None.

Significant Problems, Issues and Potential Impact on Progress

None.

Work Planned Next Quarter

Ongoing efforts are focused on obtaining SARA fraction comparisons as well as AFT data on the relative compatibilities. Initially, this work was held up by the delayed delivery of the new Kohler Automated Flocculation Titrimeter (AFT). The AFT has since been delivered and installed and the compatibility study will continue with the analysis of the blended materials. Initial SARA separation work was confounded by conversion of the method to a smaller column system, but has since been remedied. A full data set of SARA and AFT data for these samples should be available for the next quarterly report.

The extracted asphalts from the RAP stockpiles, initially South Carolina and California, will be blended with two, different SHRP asphalts after RTFO aging. The blends will be made at 15, 25, and 40% to determine the effect of RAP percentage on the compatibility of the entire binder system. The testing performed will include AD, SARA, AFT, and rheological methods to support the initial work performed on the Manitoba samples. This effort is ongoing, but data should be available in time for the July quarterly.

Work element E2c: Critically Designed HMA Mixtures (UNR)

Work Done This Quarter

Work continued to evaluate the applicability of the recommended deviator and confining stresses for the flow number test. Materials from FLDOT, NCDOT, TxDOT, Wisconsin and NCAT test track sections were received. Mixing and compaction temperatures for all binders have been determined. In addition, all mix designs are being verified at the reported optimum binder contents.

The work on converting the pulse duration in time domain for a given pavement response into frequency domain continued to be investigated. The Fast Fourier Transformation (FFT) is being used to convert the pavement responses from time domain to frequency domain. The concept of predominant frequency(ies), f_p , to predict all components of the pavement responses was verified for different pavement structures and conditions. In this quarter, the approach was also verified when a relatively stiff layer such as a cement-treated base is used underneath the asphalt layer. To this end, additional runs using 3D-Move were completed for two different asphalt pavement structures (thin and thick) at two temperatures (70 and 104°F) subjected to a tandem axle load at three different speeds (10, 40 and 60 mph).

The frequencies for the asphalt sub-layers as proposed by the MEPDG procedure were determined and compared to the predominant frequencies determined by the FFT analysis.

Significant Results

Consistent sets of predominant frequencies for the asphalt layer were found for the various critical pavement responses. Good approximations for the viscoelastic pavement responses were found with the use of predominant frequencies. The pavement responses obtained using predominant frequencies for the asphalt sub-layers were compared to the ones determined using the MEPDG approach ($f = 1/t$), the modified MEPDG approach ($f = 1/2t$), and the Ferry's angular frequency ($f = 1/2\pi t$). Figures E2c.1 to E2c.3 show, for a thin pavement (i.e. 4 inches) and at a temperature of 70°F, the pavement responses under tandem dual tires moving at 40 mph determined by using the aforementioned approaches to assign the loading frequencies to the various asphalt sub-layers. Similarly, figures E2c.4 to E2c.6 show the results for a thick pavement (i.e. 8 inches) at a temperature of 70°F and under moving tandem dual tires at 40 mph. In the case of 4-inch HMA layer, no significant differences were observed between the viscoelastic responses and the linear elastic responses except when the Ferry's angular frequencies were used. In the case of 8-inch HMA layer, significant deviations are observed between the viscoelastic responses and the different approaches, specifically for the tensile longitudinal strains. However, the pavement responses using the predominant frequencies were still in very good agreement with the viscoelastic responses.

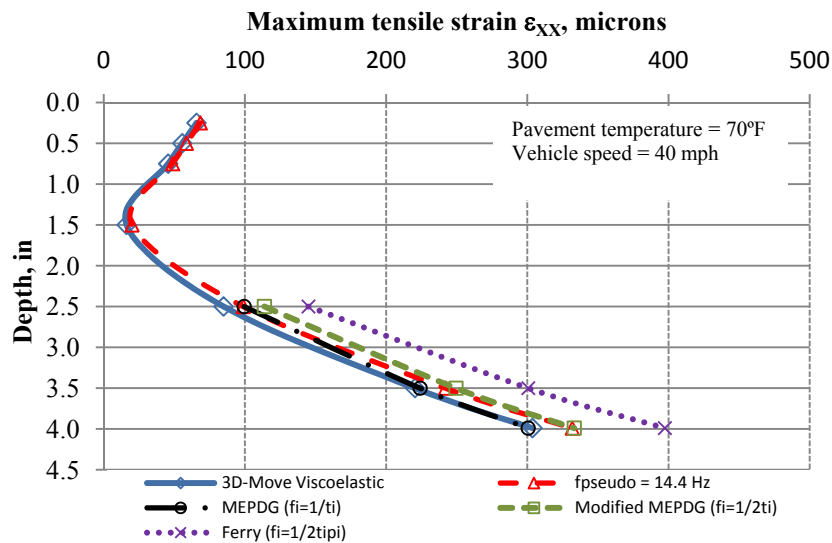


Figure E2c.1. Maximum tensile longitudinal strains at the center of the tire in the 4-inch HMA layer.

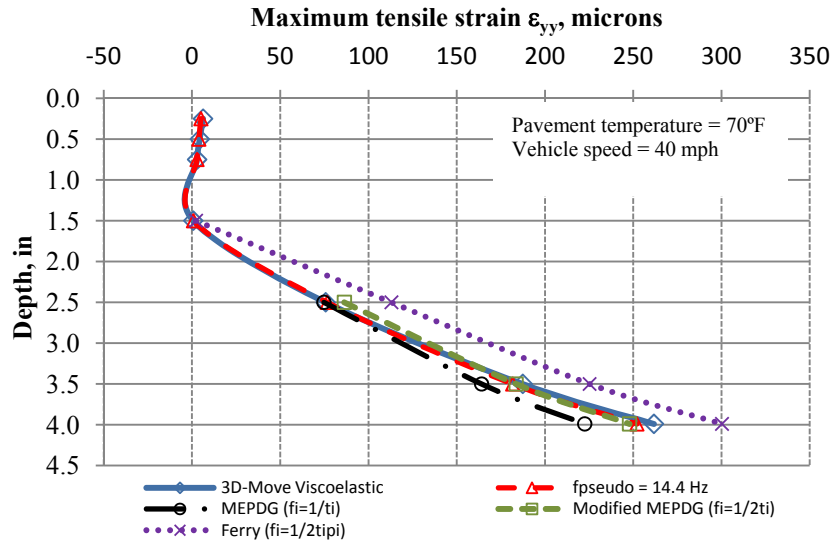


Figure E2c.2. Maximum tensile transverse strains at the center of the tire in the 4-inch HMA layer.

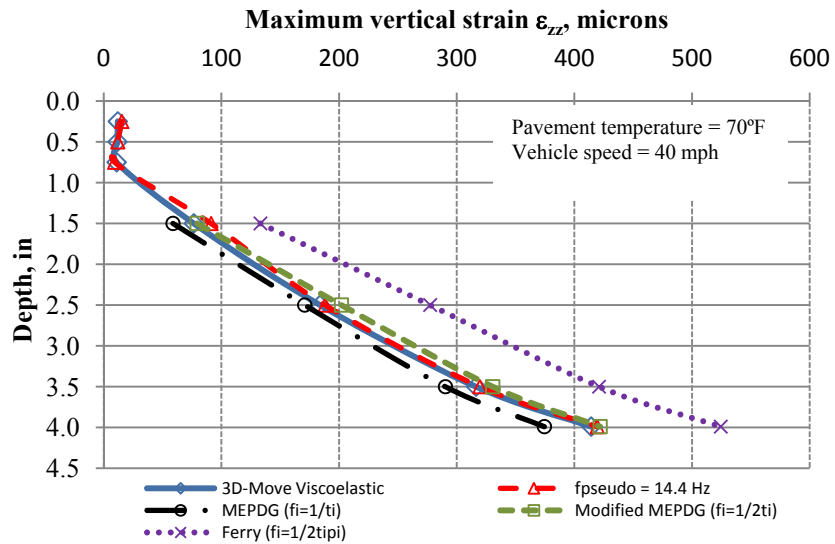


Figure E2c.3. Maximum vertical strains at the center of the tire in the 4-inch HMA layer.

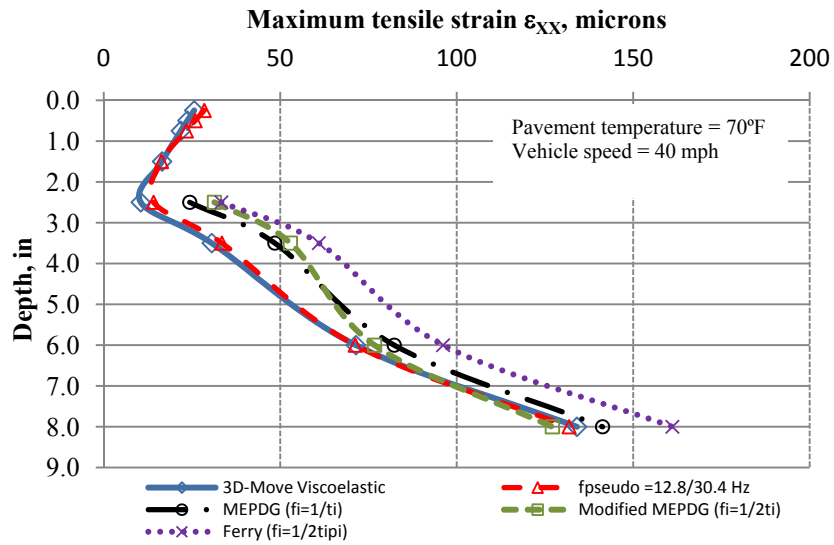


Figure E2c.4. Maximum tensile longitudinal strains at the center of the tire in the 8-inch HMA layer.

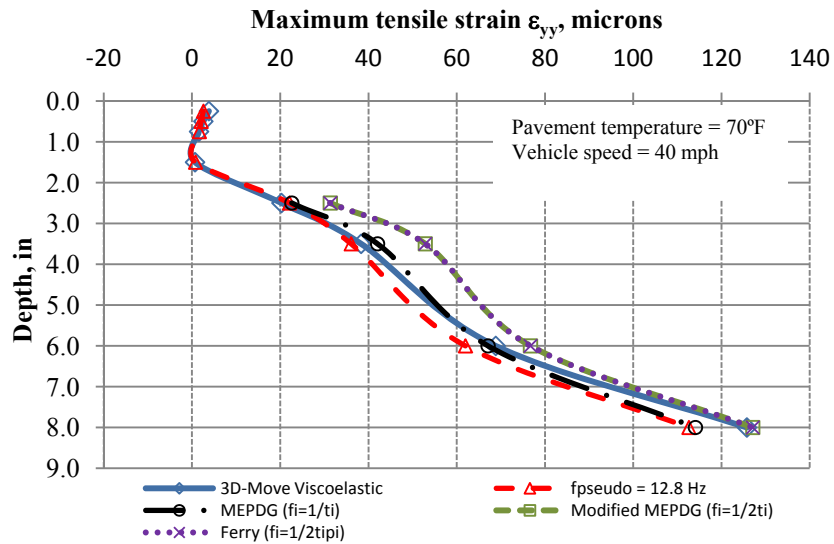


Figure E2c.5. Maximum tensile transverse strains at the center of the tire in the 8-inch HMA layer.

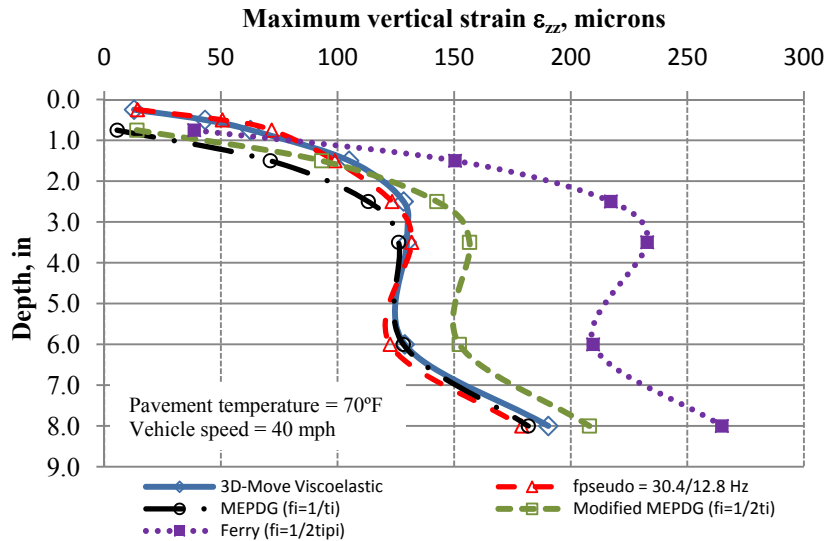


Figure E2c.6. Maximum vertical strains at the center of the tire in the 8-inch HMA layer.

Similar analyses were conducted for other cases including different temperatures, moving load speeds, and pavement structures. Overall similar findings were observed.

Significant Problems, Issues and Potential Impact on Progress

The write-ups for the figures and tables captions have delayed the submission of the subtask E2c.1 report for review.

Work Planned for Next Quarter

Continue the evaluation of the various mixtures according to the Flow Number Task Force experimental plan.

Complete the tables and figures write-ups for the report.

Continue the work on the evaluation of the predominant frequencies and present the findings at the 2011 annual meeting for the AFD80 committee in Washington D.C.

Work element E2d: Thermal Cracking Resistant Mixes for Intermountain States (UNR & UWM)

Work Done This Quarter

This work element is a joint project between University of Nevada Reno and University of Wisconsin–Madison. Based on the reviewers feedback for the submitted paper to TRB, additional work has been added to subtask E2d.1.a in which the pavement temperature distribution of various LTPP sections within and outside the intermountain region of the U.S.

will be determined. Such information will aid in the better understanding of typical warming and cooling pavement temperature rates for all sections.

The long-term oven aging of thin-film asphalt binders under Subtask E2d-3.a is complete as shown in table E2d.1. Aged binders have been shipped to University of Wisconsin-Madison and Texas A&M University. The University of Wisconsin-Madison will test the aged binders for fracture properties in the Single-Edge Notched Beam (SENB) Test and they will also measure coefficient of thermal contraction. Texas A&M has taken over the responsibility of measuring carbonyl content of the aged asphalt binders. The University of Nevada-Reno will be conducting frequency sweeps using the dynamic shear rheometer to generate mastercurves for complex modulus (G^*) and phase angle (δ) as well as determining the low shear viscosity (LSV) of the binders at a prescribed frequency of 0.00159 Hz (0.01 sec⁻¹). Furthermore, the aged binders will also be tested in the bending beam rheometer (BBR) to determine low temperature stiffness and stress relaxation properties (m-value).

Table E2d.1. Experiment testing progress.

Aging Temp (°C)	Aging Period Unit	Aging Period	Binder Type				
			PG64-22	PG64-28NV	PG64-22 +10%Lime	PG64-22 +20%Lime	PG64-22+3%SBS
135	hours	8	X	X	X	X	X
		15	X	X	X	X	X
		30	X	X	X	X	X
		44	X	X	X	X	X
100	hours	44	X	X	X	X	X
		90	X	X	X	X	X
		150	X	X	X	X	X
		240	X	X	X	X	X
85	days	7.5	X	X	X	X	X
		15	X	X	X	X	X
		25	X	X	X	X	X
		40	X	X	X	X	X
60	days	30	X	X	X	X	X
		60	X	X	X	X	X
		100	X	X	X	X	X
		160	X	X	X	X	X
50	days	60	X	X	X	X	X
		120	X	X	X	X	X
		200	X	X	X	X	X
		320	X	X	X	X	X

In this quarter, major progress was made in finalizing the unified mixture glass transition temperature (T_g) and Thermal Stress Restrained Specimen Test (TSRST) device.

In this method a specimen is produced from the Superpave gyratory sample (the gyratory compactor is accessible in most laboratories). The specimen method was slightly modified in this quarter to include sawing four prismatic beams of about 2-inch by 2-inch in cross section and about 6 inches long from 7-inch gyratory samples. Two of these beams were sawed in half to produce four 3-inch blocks. By gluing a 3-inch block to each end of the two 6-inch blocks, two 12-inch beams are produced from each gyratory sample. The advantages of this method as compared to the previous method include the production of two beams instead of one from every gyratory sample, and increasing the length of the center block by 50%, which can result in higher uniformity of stress distribution in the beam during TSRST testing.

The T_g -TSRST device, as shown in figure E2d.1, can simultaneously test two beams: an unrestrained beam, from which the change in length with temperature, and consequently the T_g , is measured, and another beam that is restrained from movement and from which the thermal stress buildup is measured. As both beams are from the same sample and both are exposed to the same temperature regime, the stress buildup, T_g , and α_l and α_g can be used to get a comprehensive picture of the low-temperature performance of the asphalt mixture.

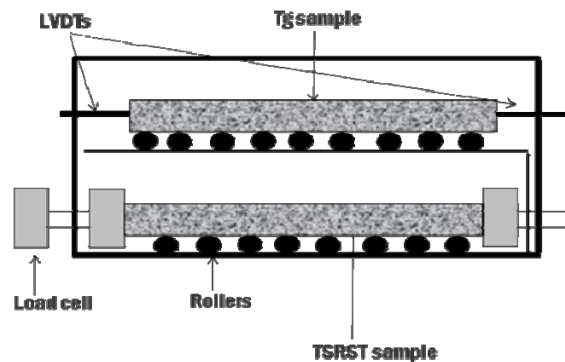


Figure E2d.1. Schematic of unified UW-Madison T_g -TSRST system.
(LVDT = linear variable differential transformer.)

Figure E2d.2 shows examples of results obtained from the T_g -TSRST testing system when temperature is decreased at the rate of $1^\circ\text{C}/\text{min}$ from 30°C to -70°C .

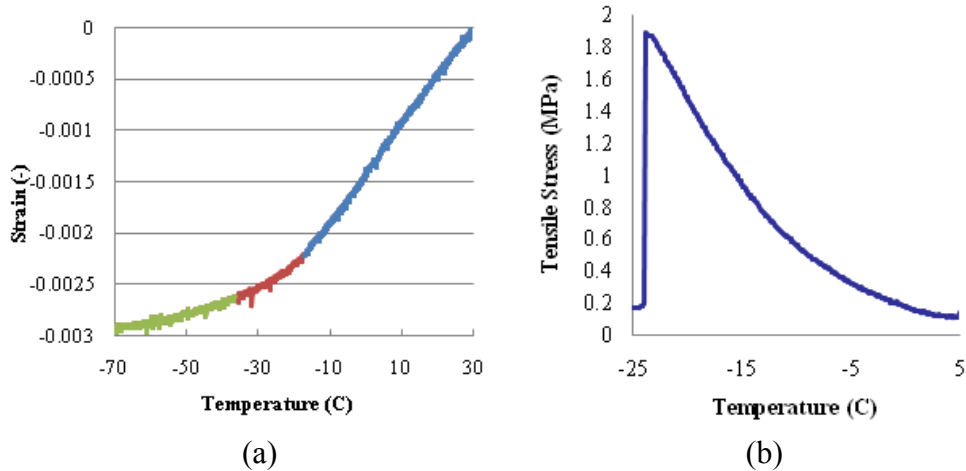


Figure E2d.2. Results obtained from the T_g -TSRST testing system: (a) typical result from a glass transition measurement of asphalt mixtures; and (b) typical result of the stress buildup to fracture in the TSRST system.

The TSRST experiment at UNR is ongoing. Particularly, the effect of cooling rate on low-temperature characteristics of cylindrical asphalt mixtures is still under investigation. The UNR team is currently investigating the effect of temperature cooling rate on TSRST specimens using the proposed cylindrical test geometry. Typical cooling rates obtained for the intermountain region of the United States obtained under Subtask E2d-1 were used. A monotonic cooling rate of 2.5°C/hr and a binary cooling rate of 3.7°C/hr followed by 0.4°C/hr were chosen for this study.

The low temperature properties of the asphalt mixtures from TSRST results (i.e. fracture temperature, fracture strength, transition temperature, and slope) were compared for the field cooling conditions and the typical cooling rate of 10°C/hr . The effect of starting test temperature on TSRST results are also currently being investigated by conducting the test at 5°C and 20°C starting temperature for cooling rates of 2.5°C/hr and 10°C/hr .

Under subtasks E2d.3.b and E2d.3.c, all of the E^* -compression samples have completed their aging durations and the entire initial E^* -compression testing has been completed. Upon completion of the E^* testing the samples are being extracted and the binder recovered for further testing. Approximately 65% of the samples have been extracted and recovered to date. A change in the location of the Fourier Transform Infrared Spectroscopy (FT-IR) testing for Carbonyl Area (CA) to Texas A&M University has improved the efficiency of that testing with approximately 40% of the CA measurements being complete. Further samples are in the process of being tested.

The TSRST specimens are all mixed and compacted and are currently going through their aging durations. Few samples have been tested, however, all of the 0 and 3 month aged samples have been cut and prepared for testing, along with nearly half of the 6 month samples. Along with the TSRST preparation, samples for the coefficient of thermal expansion, α , have also been prepared and are undergoing their respective aging as well.

Under subtask E2d-4, UNR is working on determining the relaxation modulus (E_r) for the asphalt mixture from the TSRST stress build-up measurements. The E_r will serve as an input for the asphalt mixture property in the modified viscoelastic finite element tool (VE2D) developed by TTI. The procedure for determining E_r is presented next. Since asphalt is viscoelastic material the stress and strain can be related to each other by Boltzmann principle as follows:

$$\sigma(t) = \int_0^t E(t - \tau) \varepsilon'(\tau) d\tau$$

Where σ is stress, ε' is rate of strain, E is relaxation modulus, t is time of interest and τ is variable of integration. The Boltzmann equation mathematically is convolution integral, therefore it can be rewrite in the following form:

$$\sigma(t) = \int_0^t E'(\tau) \varepsilon(t - \tau) d\tau$$

In case of induced thermal stress as the one in TSRST, the strain change with temperature gradient.

$$\varepsilon(T(t)) = \alpha(T) \Delta T = \alpha(T(t)) \times \{T(t) - T_0\}$$

Where $\alpha(t)$ is the coefficient of thermal contraction which varies with temperature. T is temperature at interested time of t and T_0 is the temperature at which no stress developed in sample.

Studies showed that α changes above and below glassy transition temperature (T_g). Thus, it can be defined as:

$$\begin{aligned} \alpha(T(t)) &= \alpha_1 \text{ for } T < T_g \\ &= \alpha_2 \text{ for } T > T_g \end{aligned}$$

The curve of thermal induced stress over time, $\sigma(t)$, is obtained from TSRST results. A polynomial function with order of three can be usually fit to the data by non-linear regression. Based on the viscoelastic principles, the relaxation modulus of asphalt mixture is determined as follows:

$$\sigma(t) = \int_0^t E'(\tau) \varepsilon(t - \tau) d\tau$$

$$\varepsilon(T(t)) = \alpha(T) \Delta T = \alpha(T(t)) \times \{T(t) - T_0\}$$

$$T(t) = C \times t + T_0$$

$$\varepsilon(t) = \alpha(t) \{Ct + T_0 - T_0\} = \alpha(t) Ct$$

$$\begin{aligned}\varepsilon(t) &= \alpha_1 C \times t \text{ for } T < T_g \\ &= \alpha_2 C \times t \text{ for } T > T_g\end{aligned}$$

For t_{T_g} is the time at which the temperature reaches the glassy transition temperature, the build-stress can be written as:

$$\sigma(t) = \int_0^{t_{T_g}} E'(\tau) \alpha_1 C (t - \tau) d\tau + \int_{t_{T_g}}^t E'(\tau) \alpha_2 C (t - \tau) d\tau$$

For $0 \leq t \leq t_{T_g}$

$$\sigma(t) = \int_0^t E'(\tau) \alpha_1 C (t - \tau) d\tau$$

$$\frac{\sigma(t)}{\alpha_1 C} = \int_0^t E'(\tau) t d\tau - \int_0^t E'(\tau) \tau d\tau$$

$$\frac{d}{dt} \left(\frac{\sigma(t)}{\alpha_1 C} \right) = t E'(t) + \int_0^t E'(\tau) \tau d\tau - t E'(t)$$

$$\frac{d^2}{dt^2} \left(\frac{\sigma(t)}{\alpha_1 C} \right) = E'(t)$$

$$E(t) - E(0) = \frac{d}{dt} \left(\frac{\sigma(t)}{\alpha_1 C} \right)$$

$$E(t) = \frac{d}{dt} \left(\frac{\sigma(t)}{\alpha_1 C} \right) + E(0)$$

For $t > t_{T_g}$

$$\sigma(t) = \int_{t_{T_g}}^t E'(\tau) \alpha_2 C (t - \tau) d\tau$$

$$\frac{\sigma(t)}{\alpha_2 C} = \int_{t_{T_g}}^t E'(\tau) t d\tau - \int_{t_{T_g}}^t E'(\tau) \tau d\tau$$

$$\frac{d}{dt} \left(\frac{\sigma(t)}{\alpha_2 C} \right) = t E'(t) + \int_{t_{T_g}}^t E'(\tau) \tau d\tau - t E'(t)$$

$$\frac{d^2}{dt^2} \left(\frac{\sigma(t)}{\alpha_2 C} \right) = E'(t)$$

$$E(t) - E(t_{T_g}) = \frac{d}{dt} \left(\frac{\sigma(t)}{\alpha_2 C} \right) - \frac{d}{dt} \left(\frac{\sigma(t_{T_g})}{\alpha_2 C} \right)$$

$$E(t) = \frac{d}{dt} \left(\frac{\sigma(t)}{\alpha_2 C} \right) - \frac{d}{dt} \left(\frac{\sigma(t_{T_g})}{\alpha_2 C} \right) + E(t_{T_g})$$

$$E(t_{T_g}) = E(t) = \frac{d}{dt} \left(\frac{\sigma(t_{T_g})}{\alpha_1 C} \right) + E(0)$$

$E(0)$ is the instantaneous elastic modulus of asphalt mixture.

Significant Results

In this quarter, the glass transition measurements of the asphalt mixtures used in MnROAD test tracks were compared and plotted against the binder T_g measurements obtained in previous quarters. This comparison is shown in figure E2d.3. Although there are differences in mix volumetrics, aggregate properties and gradation between MnROAD cells, figure E2d.3 shows that T_g values for binders and mixtures are in similar range, with the binder T_g ranging from -14 °C to -25 °C, and mixture T_g ranging from -17 °C to -27 °C.

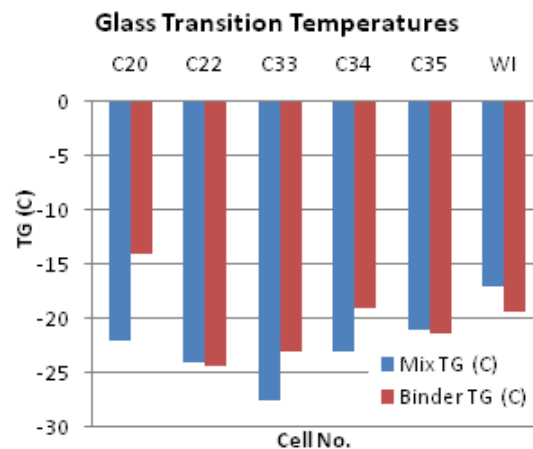


Figure E2d.3. Comparison of binder and mixture T_g .

A significant flexibility in temperature control with the new T_g -TSRST system was used to evaluate various temperature conditioning schemes that simulate field conditions. Figure E2d.4 shows the results for a scheme during which temperature was decreased to $-20\text{ }^\circ\text{C}$ and then kept constant for both the unrestrained and restrained samples at isothermal conditions for a few hours.

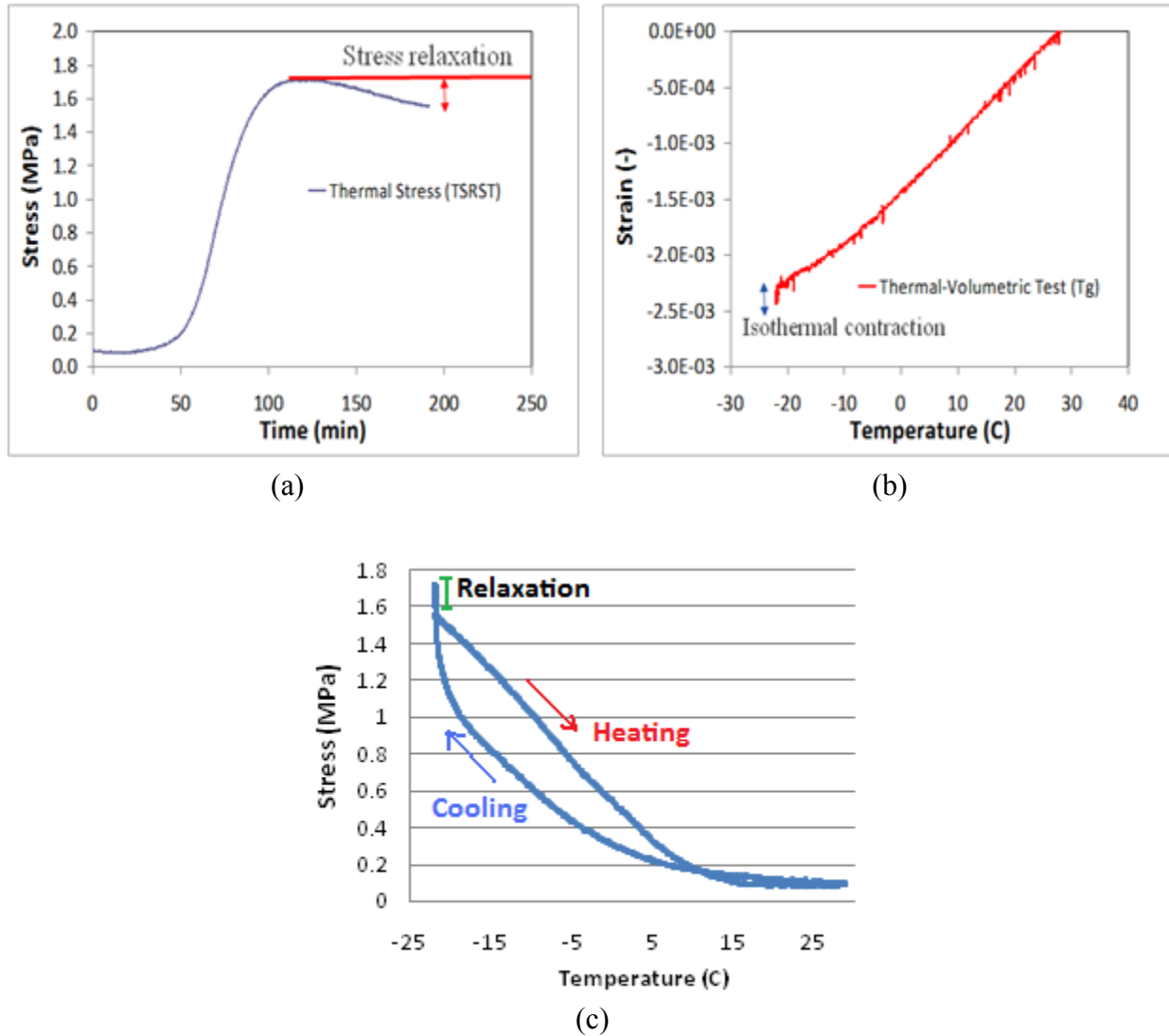


Figure E2d.4. T_g -TSRST system test results: (a) isothermal stress relaxation; (b) isothermal contraction measured for asphalt mixture; and (c) stress buildup versus temperature for full thermal cycle.

It can be seen that the unrestrained sample continued to contract at isothermal conditions. The rate seems to have a decreasing trend. This isothermal contraction has been observed in all tests, even at relatively short conditioning times of 0.5 hr. The thermal stress curve from the restrained specimen shows that the stress built up to a certain level up to the conditioning temperature.

During isothermal conditioning the stress started to gradually relax over time. It was noted that the relaxation rate seems to be decreasing in all tests and, if the current trend is to continue, stress will not relax to zero even if enough time is given for relaxation.

The stress change during a full thermal cycle in the T_g -TSRST device is shown in figure E2d.4(c). It is noted that an almost linear decrease of thermal stress during the heating portion of the test was observed (i.e., very different trend in comparison to the cooling part). However, probably the most important observation is the near-vertical curve of stress buildup when the sample reached the isothermal condition (i.e., $-20\text{ }^\circ\text{C}$). This buildup is not observed when the sample is cooled at a constant rate from room temperature to temperatures lower than the target isothermal conditioning temperature. A possible explanation for this behavior is isothermal contraction of the mixture (i.e., physical hardening at isothermal conditions).

It was observed that some of the built-up stress was relaxed when the sample was held at isothermal conditions for a few hours, as shown in figures E2d.4(a) and (c). However, this relaxation was only enough to reduce a portion of the isothermally induced built-up stress and not the stress that was built up during the cooling portion of the test, which is usually the stress measured in conventional TSRST.

This observation raises serious questions about the importance of the effect of stress relaxation for low-temperature performance of pavements. To address this, the effect of thermal cycling on the relaxation and stress buildup of mixtures was investigated. The samples were taken back to room temperature and then second and third identical thermal cycles were applied; figure E2d.5 shows the results of this test.

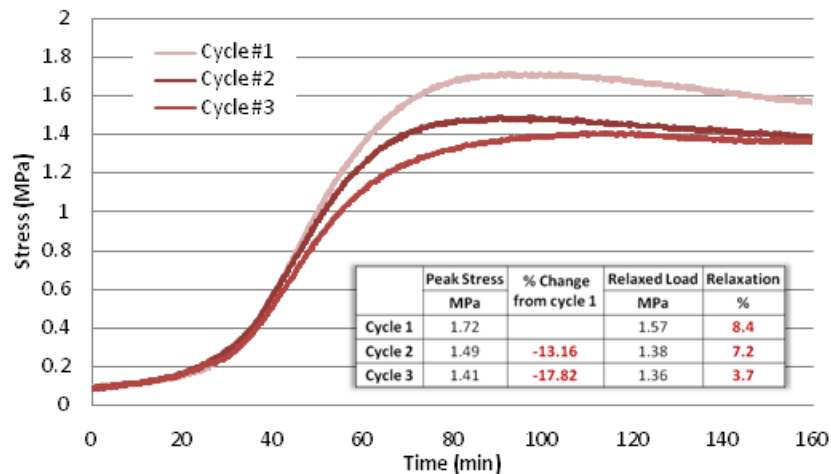


Figure E2d.5. Effect of thermal cycling on stress buildup and relaxation.

It can be seen that after the initial cycle the rate of stress buildup decreased and the sample started building up significant thermal stress at a lower temperature. Thus, in each cycle when the sample reached $-20\text{ }^\circ\text{C}$ (i.e., the isothermal conditioning temperature), it had built up less stress than the previous cycle at this temperature. Furthermore, the percent of stress relaxed at

the end of the conditioning time decreased with every cycle. It should be noted that no significant change in the glass transition and volumetric change was observed between cycles.

As mentioned in last quarter, cylindrical specimens cored from SGC samples perpendicular to the compaction direction provided good repeatability in the TSRST. The effect of cooling rates on the fracture temperature of an asphalt mixture has been evaluated. Only the monotonic cooling rate test results can be reported at this time. As discussed in the previous quarterly report, warmer fracture temperatures were observed for specimens cooled at a lower cooling rate (2.5°C/hr vs. 10.0°C/hr), however, fracture strength values were similar for the two cooling rates when the starting test temperature is 5°C. When the starting test temperature is increased to 20°C, there is a reduction in fracture strength as the cooling rate is reduced. Also, warmer fracture temperatures are also observed for lower cooling rate similar to tests conducted at a starting temperature of 5°C (table E2d.2).

Table E2d.2. Effect of monotonic cooling rates on TSRST fracture strength and temperature.

Specimen ID	Fracture Strength (psi)	Fracture Temperature (°C)
<i>Cooling Rate 2.5°C/hr</i>		
2.5°C/hr.A	162	-21.4
2.5°C/hr.B	154	-20.6
2.5°C/hr.C	160	-20.7
Average	159	-20.9
<i>Cooling Rate 10°C/hr</i>		
10°C/hr.A	281	-27.4
10°C/hr.B	282	-25.4
10°C/hr.C	187	-26.7
Average	250	-26.5

A few refinements of the TSRST test and equipment are currently being investigated which has caused some delay in this research effort. Once adjustments are made, this research effort will progress and will look into the effect of binary cooling rates on TSRST results.

Subsequent to the results obtained last quarter for subtasks E2d.3.b and E2d.3.c, which were submitted and are being presented at the TRB 2011 annual meeting, a small portion of the binder testing (Low Shear Viscosity, LSV) has since been completed.

The overall subject of the paper was to present the results of the E*-compression testing and the Carbonyl Area measurements as an indicator of the binder aging. Based upon the mixes utilized, differences in the aging rate among the two binders (neat PG64-22 and SBS modified PG64-28) as well as the differences between the aging rates between the two aggregate sources (Nevada and Colorado) were considered. The submitted manuscript included only part of the overall test matrix.

A summary of the average Low Shear Viscosity (LSV) results are depicted in the following figure E2d.6. Although only a small portion of the testing has been completed and only on the

neat PG64-22 binder, the expected results have been found. The expected result was a linear relationship between log (LSV) and CA, as can be seen in the figure. With only limited data available, the statistical analysis conducted on the findings has not yet been completed, thus no conclusions have been drawn.

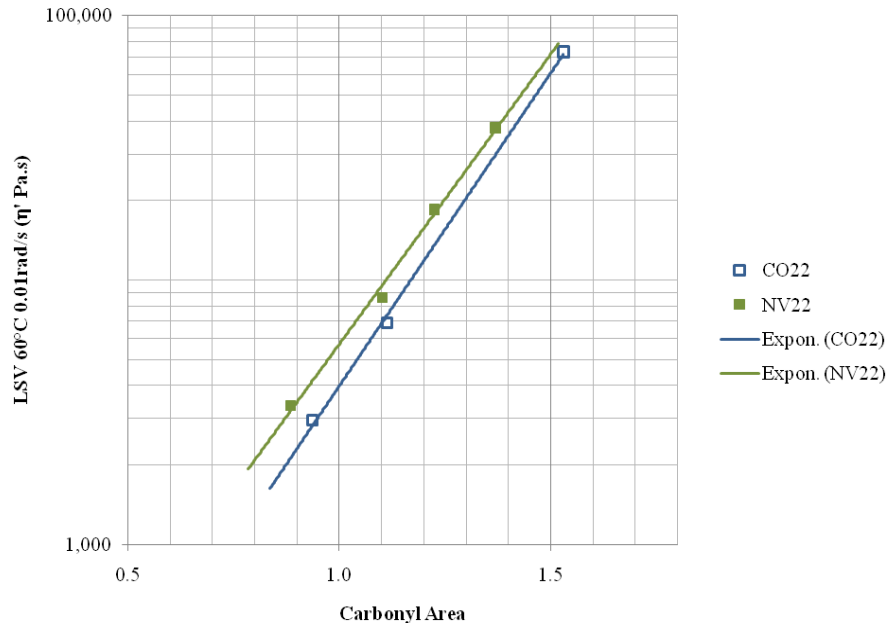


Figure E2d.6. Low shear viscosity versus carbonyl area

These findings are particularly encouraging, when considering the LSV vs CA plots are in general agreement with the analysis process being proposed for the oxidation modeling tasks taking place at Texas A&M under Dr. Glover.

Significant Problems, Issues and Potential Impact on Progress

Further progress has been made in the E*-tension area, with the previous control issues expected to be resolved by a software upgrade. A few preliminary tests have been conducted, however the results have not been thoroughly reviewed and are not yet ready for presentation.

With UNR's DSR still exhibiting some problems and being out for repair a second time, minimal binder master curves and LSV (low shear viscosity) testing has been conducted this quarter. While the DSR is out for repair additional means have been secured to allow the testing to continue. Supposedly a DSR loaner should be arriving at any time allowing the testing to get back underway. This delayed the work under Subtask E2d-4 as the findings from Subtask E2d-3 are supposed to be incorporated in the modeling system.

A few refinements of the TSRST test and equipment are currently being investigated which has caused some delay in this research effort. Once adjustments are made, this research effort will progress and will look into the effect of binary cooling rates on TSRST results.

Work Planned Next Quarter

Continue the work on subtask E2d.1.a to determine the pavement temperature distribution of the various evaluated LTPP sections. Once completed, include the information in the corresponding report.

Continue the experiment to evaluate the aging characteristics (oxidation and hardening kinetics) of asphalt binders when aged in forced convection (horizontal airflow) ovens.

Continue to evaluate the effect of cooling rate on TSRST results using the proposed cylindrical test geometry.

The research team continues to measure the behavior of asphalt mixtures at low temperatures using the newly developed unified T_g -TSRST system, focusing on the nature of the stress relaxation and contraction observed in isothermal conditions and the effect of thermal history on the stress buildup. Efforts next quarter will also focus on the development of finite element (FE) models that can help the research team understand the effect of the glass transition behavior of asphalt binder and aggregate structure on the low-temperature cracking of asphalt pavements. Single-Edge Notched Bending (SENB) testing for mastics will also begin.

Under subtasks E2d.3.b and E2d.3.c, The main focus early in the next quarter will be to significantly increase the amount of completed testing. All of the extraction/recovery testing is expected to be completed within the next two quarters, with nearly all of it being complete after the Spring of 2011. The final procedure for E^* in tension is expected to be finalized and production testing should be underway. The development of the binder master curves and LSV measurements are expected to proceed with little difficulty regardless of when UNR's DSR has been repaired. Testing on the TSRST samples are also expected to get underway as samples are available from their respective aging cycles and as the exact testing conditions are determined.

The research team will continue the work with TTI to develop a plan on how to modify the viscoelastic finite element tool (VE2D) to incorporate the findings of this work element. The research team will work on developing a subroutine that can numerically estimate the relaxation modulus from the TSRST stress build-up curve.

Work element E2e: Design Guidance for Fatigue and Rut Resistance Mixtures (AAT)

Work Done This Quarter

Hirsch Model Refinements

Laboratory work was initiated this quarter on the experiments to refine the Hirsch model. Three experiments were planned to improve the Hirsch model: (1) curing time experiment, (2) limiting modulus experiment, (3) stress dependency experiment. Each of these experiments addresses a specific aspect of the Hirsch model and dynamic modulus testing. The curing time experiment addresses whether specimen aging significantly affects measured dynamic modulus values. The limiting modulus experiment address whether the limiting minimum modulus is a HMA is significantly affected by the modulus of the aggregate used in the mixture. Finally, the stress dependency experiment address the effect of stress level on the limiting minimum modulus of HMA.

Last quarter final experimental designs for these experiments were completed. This quarter the materials needed for the experiment were located and most of them were procured. The experiment includes eight aggregates and three binders. Sufficient quantities of the three binders and six of the eight aggregates were procured. Specimen preparation was initiated.

Resistivity Model Refinements

The objective of this work is to refine the rutting model developed in NCHRP Projects 9-25 and 9-31 to better address modified binders by using data from the multiple stress creep recovery tests to characterize the binders. A final experimental design for the resistivity model refinements was developed based on the aggregates selected for the Hirsch model refinement. It includes nine binders with high temperature grade ranging from PG 58 to PG 82. Five of the binders are polymer modified, one is air blown, and three are neat. Eighteen mixtures will be tested. A total of 34 binder/mixture/temperature combinations will be used in the testing. The binders and aggregates for this experiment have been procured.

Fatigue Model Refinements

Further work on continuum damage fatigue modeling was performed last quarter. Perhaps most significantly a good predictive method for estimating the value of α was developed. This approach is based upon the concept of mixture R -value, or R_{mix} . This parameter is analogous to the R -value used in the Christensen-Anderson and CAM models for characterizing asphalt binder master curves, and is calculated using the following equation:

$$R_{mix} = \log 2 \times \frac{\log \left[\frac{4.4 \times 10^6}{|E^*|} \right]}{\log \left(1 - \frac{\delta}{90} \right)} \quad (\text{E2e.1})$$

Where 4.4×10^6 represents the typical limiting or "glassy" modulus for hot-mix asphalt (HMA) and δ is the phase angle in degrees. Figure E2e.1 is a plot of α as a function of R_{mix} for the NCHRO 9-25/31 fatigue data. It appears that R_{mix} can be directly used a surrogate for α . Although this relationship is not perfect, it should be pointed out that the limiting modulus is an assumed typical value, and that the value of δ was estimated from modulus data at two temperatures and the shift factor of the asphalt binders.

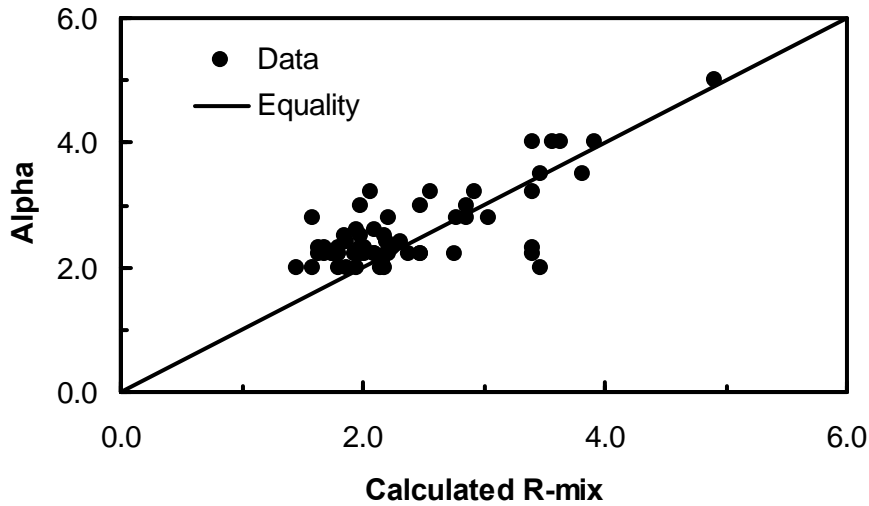


Figure E2e.1. Plot of α as a function of R_{mix} for NCHRP 9-25/31 fatigue data.

A further refinement in the analysis was made after it was realized that analysis of the 9-25/31 fatigue data was in fact iterative in nature—estimation of the initial modulus values is in part dependent upon the empirical models used to estimate α , K_1 and K_2 . Therefore, a second round of analysis was performed in which improved equations for K_1 and K_2 (those reported in the previous Quarterly Progress Report) were used in analyzing the fatigue data. This resulted in an improved data set which was then analyzed statistically to develop second-generation equations for K_1 and K_2 that were even more accurate. In review, the basic equation for damage ratio C is

$$C = \frac{1}{1 + \left(\frac{N_R}{K_1}\right)^{K_2}} \quad (\text{E2e.2})$$

Where

- N_R = reduced cycles
- K_1 = location parameter for the damage function
- K_2 = shape parameter for the damage function

Reduced cycles are calculated from initial modulus, applied strain, the continuum damage parameter (and material property) α , the shift factor $a(T)$ and the number of loading cycles. The second-generation empirical equations for K_1 and K_2 are as follows:

$$\log \left[\frac{K_1}{a(T)} \right] = 5.627 + 1.066 \left[2R_{mix} \log \left(\frac{|E^*|}{E_R} \right) \right] \quad (\text{E2e.3})$$

$$\log K_2 = -1.172 + 0.0569 \log a(T) - 0.0569 \log R_{mix} + 0.145 \log |E^*| \quad (\text{E2e.4})$$

Where $a(T)$ is the shift factor relative to the reference temperature (20°C) and E_R is the reference modulus (1×10^6 lb/in²). The r-squared values for these equations is significantly improved over the previous versions—76 % and 60 % for the models for K_1 and K_2 , respectively.

With the predictive equations for α , K_1 and K_2 , it is now potentially possible to predict the fatigue behavior of a wide range of mixtures based upon composition alone. This is done by applying the Hirsch model to estimate value for $|E^*|$ and δ , calculating R_{mix} from these data and using it as a surrogate for α , and then using equations E2e.3 and E2e.4 to estimate K_1 and K_2 . To evaluate whether this approach is feasible and whether it produces reasonable results, the ALF Phase I fatigue data was analyzed in this fashion. Layered elastic analysis (LEA) was used to estimate strains 1 cm from the surface and slightly outside the tire edge. This strain was then used to calculate reduced cycles and the damage ratio C at the point where 25 m of cracking was observed in the test sections. The results are shown in figures E2e.2 and E2e.3 below. Figure E2e.2 shows the damage ratio C at failure (25 mm total crack length) as a function of temperature relative to the glass transition temperature, as determined from fitting the Christensen-Anderson model for the two binders. Figure E2e.3 shows the predicted and measured cycles to failure for the ALF fatigue experiment. The results are very good, especially when it is considered that the fatigue data was estimated from mixture composition and binder properties, and the analysis itself was done using LEA. It should be pointed out that data from the PG 9/19°C/100 mm thick section was not included in the analysis since the FHWA ALF report indicated that data for this section was suspect. Also, the two sections at 9°C and 200 mm thickness did not fail up to the maximum loading of 400,000 cycles. The predicted cycles to failure for these sections—220,000 and 830,000—were very large and were reasonably consistent with the observed behavior.

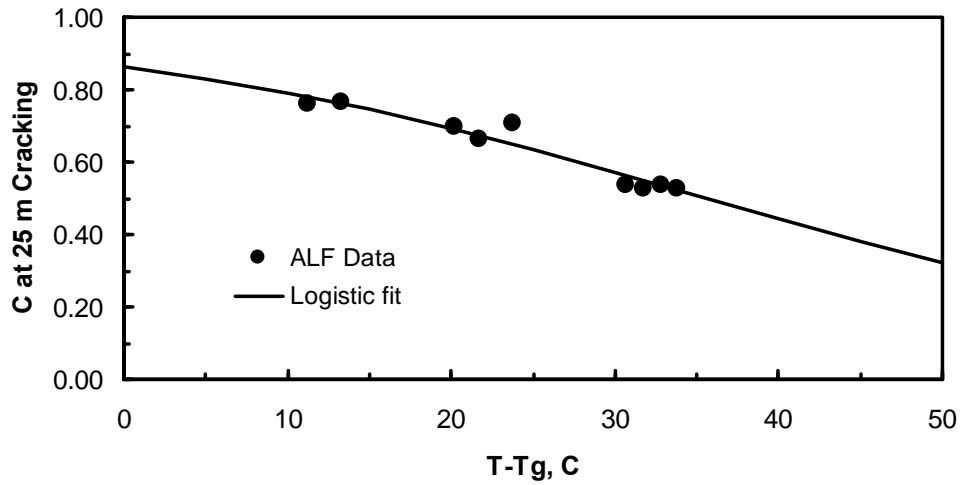


Figure E2e.2. Damage ratio C at 25 mm cracking as a function of temperature relative to glass transition for ALF Phase I fatigue data.

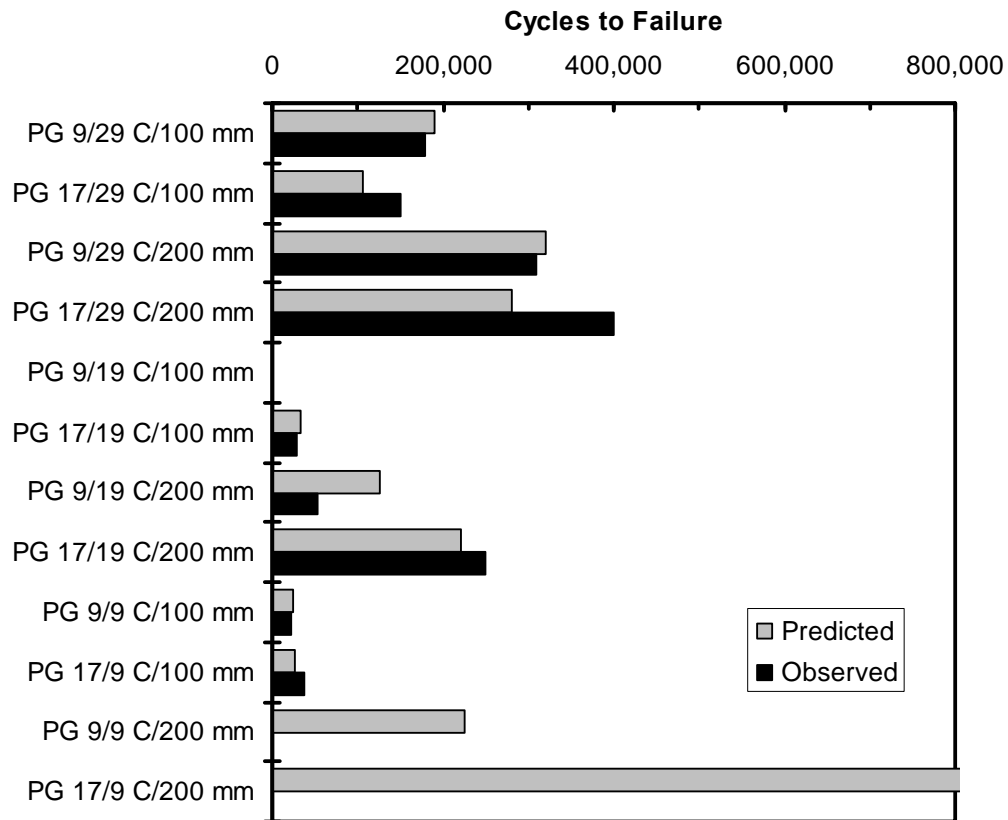


Figure E2e.3. Predicted and observed cycles to failure for ALF Phase I fatigue data.

Code Provide Binder Intermediate Temperature Grade/Test Temperature/HMA Thickness.

The results of this analysis are very significant. It strongly suggests that the proposed general function for HMA damage curves is in fact correct, and that this function can be estimated reasonably well based upon mixture composition and/or modulus values. It furthermore demonstrates that a continuum damage approach can be combined with LEA to provide a simple for effective approach to designing HMA pavements to resist fatigue cracking. A third important aspect of this analysis was that the best results were obtained not by using the strains at the bottom of the HMA layer, but by using strains at a point just below and outside of the tire edge. This demonstrates the importance of top-down fatigue cracking, and also demonstrates a simple approach to addressing this type of failure.

An attempt was made to perform a similar analysis on the ALF Phase II fatigue experiment, but measured binder properties could not be found in the various papers, reports and presentations on this experiment. Binder properties estimated from specification test data were used, but this did not work well. It is hoped measured binder data (master curves) can be located for the mixes used in the Phase II experiment so that the analysis described above can be verified using a second set of data.

A revised fatigue experiment was developed based on the results of the analyses completed in the last two quarters. This fatigue experiment will use selected mixtures from the Hirsch model and resistivity model refinement experiments.

Work Planned Next Quarter

Laboratory work will proceed for the Hirsch model, resistivity model, and continuum damage fatigue model refinements. Analysis of the data from these experiments will proceed concurrently with the laboratory testing.

Significant Problems, Issues and Potential Impact on Progress

The laboratory experiments in this Work Element are behind schedule. Materials have been procured and laboratory work has been initiated. These experiments will be completed during 2011.

Engineered Materials Year 4	Year 4 (4/2010-3/2011)												Team
	4	5	6	7	8	9	10	11	12	1	2	3	
(1) High Performance Asphalt Materials													
E1a: Analytical and Micro-mechanics Models for Mechanical behavior of mixtures													TAMU
E1a-1: Analytical Micromechanical Models of Binder Properties				P							P		
E1a-2: Analytical Micromechanical Models of Modified Mastic Systems				P							P		
E1a-3: Analytical Models of Mechanical Properties of Asphalt Mixtures				P, JP			JP (2)		JP (2)		P	JP	
E1a-4: Analytical Model of Asphalt Mixture Response and Damage											P		
E1b: Binder Damage Resistance Characterization													UWM
E1b-1: Rutting of Asphalt Binders													
E1b-1-i: Literature review													
E1b-1-ii: Select Materials & Develop Work Plan													
E1b-1-iii: Conduct Testing				DP									
E1b-1-iv: Analysis & Interpretation									JP				
E1b-1-v: Standard Testing Procedure and Recommendation for Specifications							P					DP	
E1b-2: Feasibility of determining rheological and fracture properties of asphalt binders and mastics using simple indentation tests (modified title)													UWM
E1b-2-i: Literature Review													
E1b-2-ii: Proposed SuperPave testing modifications													
E1b-2-iii: Preliminary testing and correlation of results								JP					
E1b-2-iv: Feasibility of using indentation tests for fracture and rheological properties											P	D	
E2a: Comparison of Modification Techniques													UWM
E2a-1: Identify modification targets and material suppliers													
E2a-2: Test material properties											P		
E2a-3: Develop model to estimate level of modification needed and cost index													
E2a-4: Write asphalt modification guideline/report on modifier impact over binder properties							JP						
E2c: Critically Designed HMA Mixtures													UNR
E2c-1: Identify the Critical Conditions													
E2c-2: Conduct Mixtures Evaluations											JP		
E2c-3: Develop a Simple Test													
E2c-4: Develop Standard Test Procedure													
E2c-5: Evaluate the Impact of Mix Characteristics													
E2d: Thermal Cracking Resistant Mixes for Intermountain States													UWMUNR
E2d-1: Identify Field Sections													
E2d-2: Identify the Causes of the Thermal Cracking													
E2d-3: Identify an Evaluation and Testing System							JP				P		
E2d-4: Modeling and Validation of the Developed System							JP					P	
E2d-5: Develop a Standard													
E2e: Design Guidance for Fatigue and Rut Resistance Mixtures													AAT
E2e-1: Identify Model Improvements													
E2e-2: Design and Execute Laboratory Testing Program													
E2e-3: Perform Engineering and Statistical Analysis to Refine Models													
E2e-4: Validate Refined Models													
E2e-5: Prepare Design Guidance													
(2) Green Asphalt Materials													
E2b: Design System for HMA Containing a High Percentage of RAP Material													UNR
E2b-1: Develop a System to Evaluate the Properties of RAP Materials			P				JP				P		
E2b-2: Compatibility of RAP and Virgin Binders													
E2b-3: Develop a Mix Design Procedure											D		
E2b-4: Impact of RAP Materials on Performance of Mixtures													
E2b-5: Field Trials							JP						
E1c: Warm and Cold Mixes													UWM
E1c-1: Warm Mixes													
E1c-1-i: Effects of Warm Mix Additives on Rheological Properties of Binders													
E1c-1-ii: Effects of Warm Mix Additives on Mixture Workability and Stability							JP						
E1c-1-iii: Mixture Performance Testing													
E1c-1-iv: Develop Revised Mix Design Procedures													
E1c-1-v: Field Evaluation of Mix Design Procedures and Performance Recommendations													
E1c-2: Improvement of Emulsions' Characterization and Mixture Design for Cold Bitumen Applications													UWMUNR
E1c-2-i: Review of Literature and Standards													
E1c-2-ii: Creation of Advisory Group													
E1c-2-iii: Identify Tests and Develop Experimental Plan													
E1c-2-iv: Develop Material Library and Collect Materials													
E1c-2-v: Conduct Testing Plan							JP				P		
E1c-2-vi: Develop Performance Selection Guidelines							JP				P	F	
E1c-2-vii: Validate Performance Guidelines													
E1c-2-viii: Develop CMA Mix Design Guidelines													
E1c-2-ix: Develop CMA Performance Guidelines													

Deliverable codes
D: Draft Report
F: Final Report
M&A: Model and algorithm
SW: Software
JP: Journal paper
P: Presentation
DP: Decision Point

Deliverable Description
Report delivered to FHWA for 3 week review period.
Final report delivered in compliance with FHWA publication standards
Mathematical model and sample code
Executable software, code and user manual
Paper submitted to conference or journal
Presentation for symposium, conference or other
Time to make a decision on two parallel paths as to which is most promising to follow through

Work planned
Work completed
Parallel topic

Engineered Materials Year 2 - 5	Year 2 (4/08-3/09)				Year 3 (4/09-3/10)				Year 4 (04/10-03/11)				Year 5 (04/11-03/12)				Team
	Q1	Q2	Q3	Q4	Q1	Q2	Q3	Q4	Q1	Q2	Q3	Q4	Q1	Q2	Q3	Q4	
(1) High Performance Asphalt Materials																	
E1a: Analytical and Micro-mechanics Models for Mechanical behavior of mixtures																	
E1a-1: Analytical Micromechanical Models of Binder Properties			P, JP	JP	P	P	JP		P		P	P	JP	D, JP	F		
E1a-2: Analytical Micromechanical Models of Modified Mastic Systems			P, JP	JP	P	P			P		P	P	JP	D	F, SW, M&A		
E1a-3: Analytical Models of Mechanical Properties of Asphalt Mixtures	P	P, JP	P, JP	JP	P	P	M&A		P, JP(3)	JP (2)	P, M&A	P	JP(2)	D, JP	F, SW, M&A		
E1a-4: Analytical Model of Asphalt Mixture Response and Damage			P, JP	JP	P	P					P	P		D	F, SW, M&A		
E1b: Binder Damage Resistance Characterization																	
E1b-1: Rutting of Asphalt Binders																	
E1b-1-1: Literature review																	
E1b-1-2: Select Materials & Develop Work Plan	DP, P		P														
E1b-1-3: Conduct Testing			P			JP		P	DP								
E1b-1-4: Analysis & Interpretation			JP	P	JP					JP							
E1b-1-5: Standard Testing Procedure and Recommendation for Specifications									P		DP	P	D	JP	F		
E1b-2: Feasibility of Determining rheological and fracture properties of asphalt binders and mastics using simple indentation tests (modified title)																	
E1b-2i: Literature Review																	
E1b-2ii: Proposed SuperPave testing modifications or new testing devices					D												
E1b-2iii: Preliminary testing and correlation of results					P					JP							
E1b-2iv: Feasibility of using indentation tests for fracture and rheological properties						JP		P				P, D	F				
E2a: Comparison of Modification Techniques																	
E2a-1: Identify modification targets and material suppliers				DP		DP											
E2a-2: Test material properties								P				P					
E2a-3: Develop model to estimate level of modification needed and cost index																	
E2a-4: Write asphalt modification guideline/report on modifier impact over binder properties										JP							
E2c: Critically Designed HMA Mixtures																	
E2c-1: Identify the Critical Conditions			JP	D, F		JP	D	F					JP				
E2c-2: Conduct Mixtures Evaluations							D										
E2c-3: Develop a Simple Test														D, F	JP		
E2c-4: Develop Standard Test Procedure														D, F			
E2c-5: Evaluate the Impact of Mix Characteristics																D, F	
E2d: Thermal Cracking Resistant Mixes for Intermountain States																	
E2d-1: Identify Field Sections			D, F	D, F	D	F											
E2d-2: Identify the Causes of the Thermal Cracking																	
E2d-3: Identify an Evaluation and Testing System					DP	JP	DP, D			JP		P	JP				
E2d-4: Modeling and Validation of the Developed System										JP		P				D, F	
E2d-5: Develop a Standard																D, F	
E2e: Design Guidance for Fatigue and Rut Resistance Mixtures																	
E2e-1: Identify Model Improvements																	
E2e-2: Design and Execute Laboratory Testing Program																	
E2e-3: Perform Engineering and Statistical Analysis to Refine Models														P, D, F			
E2e-4: Validate Refined Models														JP			
E2e-5: Prepare Design Guidance															M&A	P, D, F	
(2) Green Asphalt Materials																	
E2b: Design System for HMA Containing a High Percentage of RAP Material																	
E2b-1: Develop a System to Evaluate the Properties of RAP Materials			JP		P	D	D, F	D		P	JP	P					
E2b-2: Compatibility of RAP and Virgin Binders															D, F	JP	
E2b-3: Develop a Mix Design Procedure								D				D			D, F	JP	
E2b-4: Impact of RAP Materials on Performance of Mixtures																D, F	
E2b-5: Field Trials										JP						D, F	
E1c: Warm and Cold Mixes																	
E1c-1: Warm Mixes																	
E1c-1i: Effects of Warm Mix Additives on Rheological Properties of																	
E1c-1ii: Effects of Warm Mix Additives on Mixture Workability and Stability	P		D	F, DP							JP						
E1c-1iii: Mixture Performance Testing							JP		P, DP	DP, P							
E1c-1iv: Develop Revised Mix Design Procedures																	
E1c-1v: Field Evaluation of Mix Design Procedures and Performance Recommendations															JP	D, P, F	
E1c-2: Improvement of Emulsions' Characterization and Mixture Design for Cold Bitumen Applications																	
E1c-2i: Review of Literature and Standards			JP, P, D	F		D1	D3	D6									
E1c-2ii: Creation of Advisory Group																	
E1c-2iii: Identify Tests and Develop Experimental Plan				P, DP		D1		D4									
E1c-2iv: Develop Material Library and Collect Materials																	
E1c-2v: Conduct Testing Plan							JP	D5	P		JP		P				
E1c-2vi: Develop Performance Selection Guidelines										JP		P, F					
E1c-2vii: Validate Guidelines							D2							JP		P, F	
E1c-2viii: Develop CMA Mix Design Procedure																	
E1c-2ix: Develop CMA Performance Guidelines															JP	D, P, F	

Deliverable codes
D: Draft Report
F: Final Report
M&A: Model and algorithm
SW: Software
JP: Journal paper
P: Presentation
DP: Decision Point

Deliverable Description
Report delivered to FHWA for 3 week review period.
Final report delivered in compliance with FHWA publication standards
Mathematical model and sample code
Executable software, code and user manual
Paper submitted to conference or journal
Presentation for symposium, conference or other
Time to make a decision on two parallel paths as to which is most promising to follow through

Work planned
Work completed
Parallel topic
Delayed

PROGRAM AREA: VEHICLE-PAVEMENT INTERACTION

CATEGORY VP1: WORKSHOP

Work element VP1a: Workshop on Super-Single Tires (UNR)

This work element is complete.

CATEGORY VP2: DESIGN GUIDANCE

Work element VP2a: Mixture Design to Enhance Safety and Reduce Noise of HMA (UWM)

Work Done This Quarter

Efforts this quarter focused on resolving equipment issues, conducting preliminary acoustic absorption data using the Kundt tube, and conducting texture measurements on a trial field section. Research personnel addressed the issue of laser travel rate in the stationary laser profilometer (SLP) by adding a small motor to the test frame to ensure a constant travel speed of the laser along the frame. An added control box allows the user to set travel speed of the laser, which ranges from approximately 0.02 m/s to 0.18 m/s. Researchers also resolved Kundt tube calibration issues by working with Italian software technicians.

Researchers tested various materials to generate acoustic absorption measurements with the Kundt tube. Following acquisition of an appropriately sized coring bit, open- and dense-graded HMA samples were cored and tested. Results obtained from these tests are compared to reference materials. These preliminary results will be used to determine the effectiveness of further acoustic testing.

Calibration of the Circular Track Meter (CTM) and Dynamic Friction Tester (DFT) devices, currently on loan from FHWA, allowed for testing field sections. These tests enable International Friction Index (IFI) relationships to be developed in order to characterize pavement surface texture. Researchers also used other test methods, including the volumetric sand-patch technique and British Pendulum Tester (BPT) to characterize pavement surface texture.

Significant Results

Preliminary acoustic data collected using the Kundt tube show differences between mixtures in values of the acoustic absorption coefficient (α). Figure VP2a.1 depicts alpha values for open- and dense-graded HMA samples and compares these results to alpha values for two foam materials and the empty tube using a moving average filtration. Both HMA samples exhibit a characteristic increase in alpha value between frequencies of 500 Hz and 700 Hz, with the open-graded mix sample exhibiting higher peak alpha amplitudes than the dense-graded mix sample.

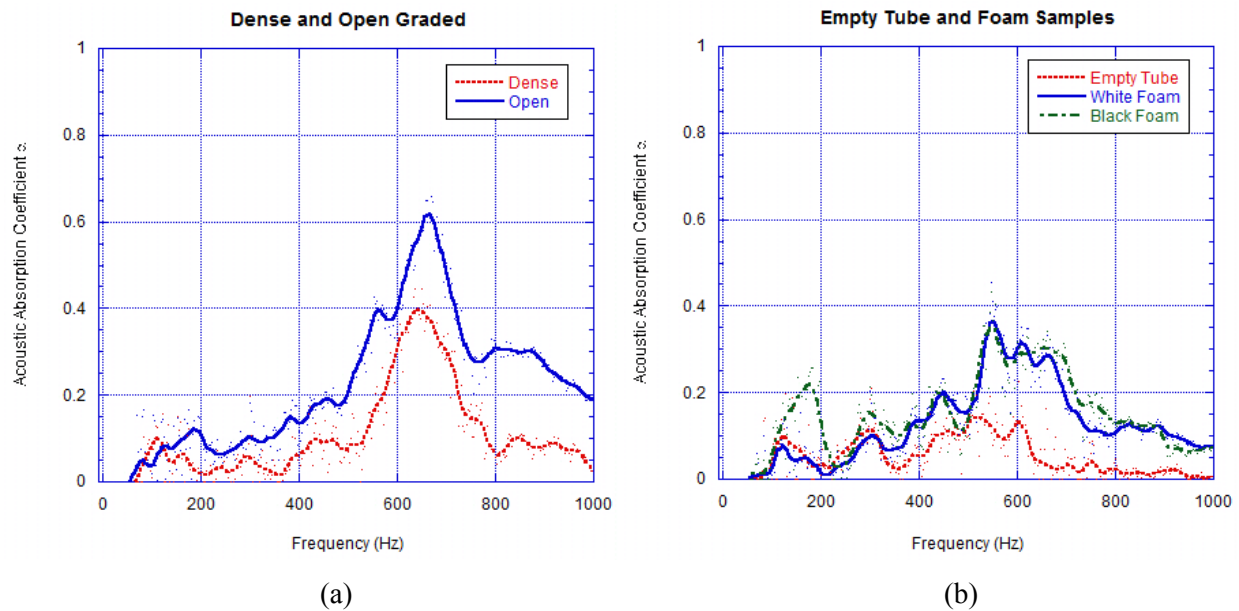


Figure VP2a.1. Graphs. Filtered acoustic absorption results for: (a) dense- and open-graded mixtures; and (b) two foam materials and the empty tube.

Table VP2a.1 compares the peak amplitude response for these samples to the response from two foam materials. Results suggest that the open-graded HMA sample is indeed absorbing more of the acoustic wave, evident in the higher alpha values. Frequencies for peak absorption coefficient appear to be similar between like materials. Dense-graded samples also exhibit less dispersion than the open-graded samples.

Table VP2a.1. Comparison of peak alpha amplitudes for HMA and foam materials.

Sample	Open-Graded HMA		Dense-Graded HMA		Foam 1		Foam 2	
	f (Hz)	α	f (Hz)	α	f (Hz)	α	f (Hz)	α
1	659	0.667	650	0.481	547	0.389	547	0.423
2	669	0.673	669	0.427	547	0.521	547	0.440

Field testing yielded data needed to characterize surface texture. CTM testing follows the ASTM E2157 standard (ASTM 2009b). Table VP2a.2 presents results obtained from the CTM device following initial calibration and trial testing. Mean profile depth (MPD) values are consistent across locations with an acceptable coefficient of variation (COV) value less than 5%. CTM values are used in the IFI calculation to estimate the slip speed S_p . Likewise, DFT testing follows the ASTM E1911 standard (ASTM 2009a).

Table VP2a.2. MPD values (in mm) obtained using the CTM device.

Section	Mean (mm)	St. Dev.	COV
1	1.261	0.011	0.9%
2	1.180	0.005	0.4%
3	1.186	0.002	0.2%
Total	1.209	0.045	3.7%

DFT results are presented in table VP2a.3 for the trial location. Combining CTM and DFT results according to the ASTM E1960 standard (ASTM 2007) allows for tabulation of the IFI. Table VP2a.4 displays tabulated IFI values for the trial location.

Table VP2a.3. Friction values obtained using the DFT device.

Section 1				Section 2				Section 3			
Speed (km/hr)	Mean	St. Dev.	COV	Speed (km/hr)	Mean	St Dev	COV	Speed (km/hr)	Mean	St Dev	COV
0	0.735	0.029	3.9%	0	0.799	0.046	5.8%	0	0.801	0.031	3.9%
20	0.691	0.043	6.2%	20	0.726	0.039	5.4%	20	0.732	0.039	5.3%
40	0.714	0.042	5.9%	40	0.712	0.037	5.1%	40	0.720	0.038	5.2%
60	0.674	0.038	5.6%	60	0.688	0.035	5.0%	60	0.696	0.025	3.6%
80	0.139	0.008	6.0%	80	0.156	0.012	7.5%	80	0.151	0.017	11.6%

Table VP2a.4. IFI calculations for the trial section.

Section	F(60)	Regression Coefficients		
		A	B	R ²
1	0.451	0.45	0.0038	0.98
2	0.472	0.47	0.0035	0.97
3	0.476	0.47	0.0035	0.97

For the sake of comparison, researchers employed two additional test methods to characterize field texture. The ASTM E965 standard (ASTM 2006) describes a volumetric sand-patch technique that is widely regarded as the gold standard for measuring surface texture. Despite simplicity, the test is prone to high variability. This sand-patch method gives an indication of mean texture depth (MTD). The second rudimentary test procedure employed in field testing is the BPT. The test method is described in the ASTM E303 standard (ASTM 2008) and gives an indication of a pavement's frictional characteristics. Table VP2a.5 presents data from these test methods. While British Pendulum Number (BPN) values do not directly relate to DFT measurements, sand-patch values can be related to CTM values. CTM values produce results similar to those obtained by the sand-patch method.

Table VP2a.5. BPT and sand-patch field data.

Section	British Pendulum Number (BPN)			Sand Patch (mm)		
	Mean	St. Dev.	COV	Mean	St. Dev.	COV
1	84.3	0.957	1.1%	1.19	0.056	4.7%
2	78.3	1.258	1.6%	1.24	0.064	5.1%
3	82.5	4.203	5.1%	1.24	0.046	3.7%

Significant Problems, Issues and Potential Impact on Progress

Because field testing cannot continue during the winter months due to low temperatures and snow, field testing will be delayed until the climate warms. Subsequent field testing will link field evaluation methods to laboratory evaluation methods. This winter period will be used to develop a field guide for technicians to follow during testing, so that when the weather is amenable field sections may be efficiently tested.

Work Planned Next Quarter

Activities planned in the next quarter include:

- Assembling an analysis package for field measurements, which will allow technicians to efficiently conduct field testing throughout the state once the weather warms. Such an analysis package will allow for rapid evaluation of field techniques for comparison to proposed laboratory test procedures.
- Calculating IFI values for laboratory samples measured using the SLP and BPT for comparison to IFI values obtained using DFT and CTM devices in the field.
- Developing and executing a test matrix for acoustic absorption measurements to study the relationships between tire-pavement noise and skid response, which will allow researchers to model the effects of mix characteristics on the acoustic response.
- Continuing collaborative efforts with international experts in the field of noise and friction.
- Investigating the effect of laser measuring rate, linear speed and spot diameter on the MPD response for the SLP.
- Beginning to develop guidelines to optimize noise reduction, safety and user costs.

Cited References

ASTM, 2006, ASTM E965, Standard Test Method for Measuring Pavement Macrotexture Depth Using a Volumetric Technique, American Society for Testing and Materials, West Conshohocken, PA.

ASTM, 2007, ASTM E1960, Standard Practice for Calculating International Friction Index of a Pavement Surface, American Society for Testing and Materials, West Conshohocken, PA.

ASTM, 2008, ASTM E303, Standard Test Method for Measuring Surface Frictional Properties Using the British Pendulum Tester, American Society for Testing and Materials, West Conshohocken, PA.

ASTM, 2009a, ASTM E1911, Standard Test Method for Measuring Paved Surface Frictional Properties Using the Dynamic Friction Tester, American Society for Testing and Materials, West Conshohocken, PA.

ASTM, 2009b, ASTM E2157, Standard Test Method for Measuring Pavement Macrottexture Properties Using the Circular Track Meter, American Society for Testing and Materials, West Conshohocken, PA.

CATEGORY VP3: MODELING

Work element VP3a: Pavement Response Model to Dynamic Loads (UNR)

Work Done This Quarter

Continued the work on the *3D-Move Analysis* software to make it a menu-driven software. Different models for specifying the master curve of the viscoelastic material (i.e. asphalt layer) have been incorporated into *3D-Move*. Figure VP3a.1 shows the input window of the asphalt material properties. The top of the figure shows all the options for the Master Curves. They have been subdivided into two categories according to the approach used: (1) Laboratory Data and (2) Model Equation. While the first category requires laboratory-measured material data, the second category uses equations for which model constants need to be specified. Except for the Huet-Sayegh Model using laboratory data, all of the following options were completed and incorporated into *3D-Move Analysis* software in this quarter:

- Laboratory Data
 1. Symmetrical Sigmoidal Function (MEPDG)
 2. Non-Symmetrical Sigmoidal Function
 3. Symmetrical Sigmoidal Function (AMPT)
 4. Huet-Sayegh Model (Under Construction)
 5. User Input (Interpolation)
- Model Equation
 1. Witczak Model
 2. Huet-Sayegh

Work is still underway to integrate MEPDG and VESYS performance models in *3D-Move*. Figure VP3a.2 shows the window for selecting the performance models and distresses to be evaluated. As an example, figures VP3a.3 and VP3a.4 show the input parameters for the

MEPDG and VESYS fatigue models, respectively. Pavement performance evaluation requires the knowledge of the maximum pavement responses at specific depths throughout the pavement. Extensive analyses for different pavement structures, material properties and loading configurations have been conducted using the *3D-Move Analysis* software in attempt to determine the critical locations for the various pavement responses that are essential for the pavement performance evaluation. The critical locations for various loading configurations (i.e. single, dual, dual tandem and tridem) and uniform tire contact pressure distributions (i.e. circular, rectangular, square and elliptical) have been determined. Those critical locations aided in eliminating unnecessary response points which optimized the run time of the software with the performance analysis option. This feature has already been implemented into the 3D-Move as preset pavement response points.

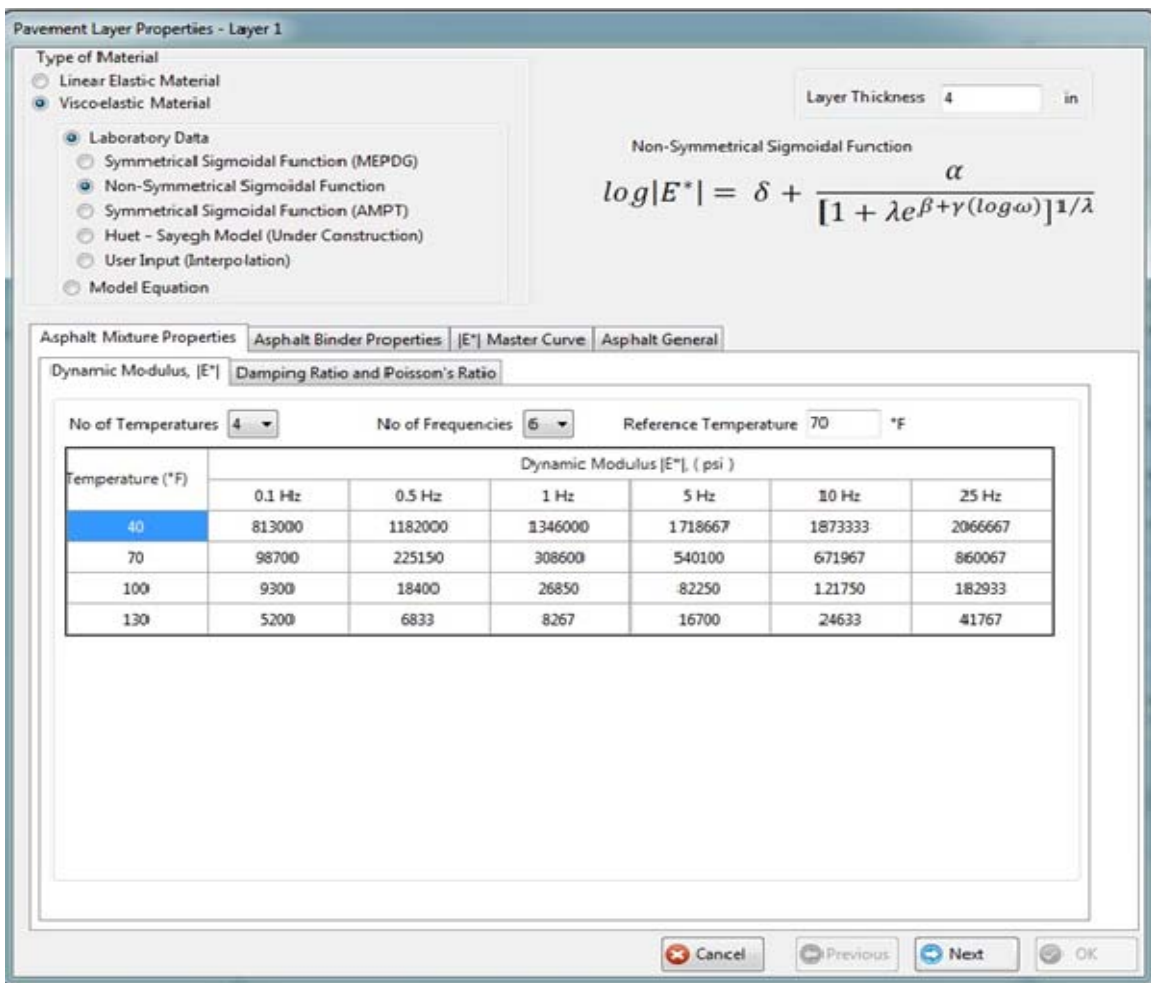


Figure VP3a.1. Non-symmetrical sigmoidal function option – dynamic modulus input.

Performance Models

MEPDG Models [Info](#)

	Limiting Values	Reliability
<input checked="" type="checkbox"/> AC Top Down Cracking (ft/mile)	2000	90
<input checked="" type="checkbox"/> AC Bottom Up Cracking (%)	25	90
<input checked="" type="checkbox"/> AC Rutting (in)	0.25	90
<input checked="" type="checkbox"/> Base/Sub base Rutting (in)	0.20	90
<input checked="" type="checkbox"/> Subgrade Rutting (in)	0.30	90

VESYS Models [Info](#)

<input type="checkbox"/> Fatigue Cracking (ft/mile)		
<input type="checkbox"/> Layer Rutting (in)		
<input type="checkbox"/> System Rutting (in)		
<input type="checkbox"/> Roughness		

Generate Response Points Cancel OK

Figure VP3a.2. Performance models.

Performance Model - MEPDG

MEPDG Models

AC Top Down Cracking | AC Bottom Up Cracking | AC Rutting | Base/ Subbase Rutting | Subgrade Rutting

$$N_f = 0.00432 \cdot C \cdot \beta_{f1} k_1 \cdot \left(\frac{1}{\epsilon_t}\right)^{\beta_{f2} k_2} \cdot \left(\frac{1}{E}\right)^{\beta_{f3} k_3}$$

$$C = 10^M$$

$$M = 4.84 \left[\frac{V_b}{V_a + V_b} - 0.69 \right]$$

N_f - Number of repetitions to fatigue cracking
 ϵ_t - Horizontal tensile strain at the critical location (in/in)
 E - Stiffness of the material (psi)
 V_a - Air Voids (%)
 V_b - Effective Binder Content (%)

Volumetric Properties

Effective Binder Content (V_b) 3 %
 Air Voids (V_a) 7 %

Analyse Type

Special Analysis
 National Calibration
 State/ Regional Calibration
 Typical Agency Values

Regression Coefficients

k_1 0.007566 β_{f1} 1
 k_2 3.9492 β_{f2}
 k_3 1.281 β_{f3}

Cancel Previous Next OK

Figure VP3a.3. MEPDG performance models.

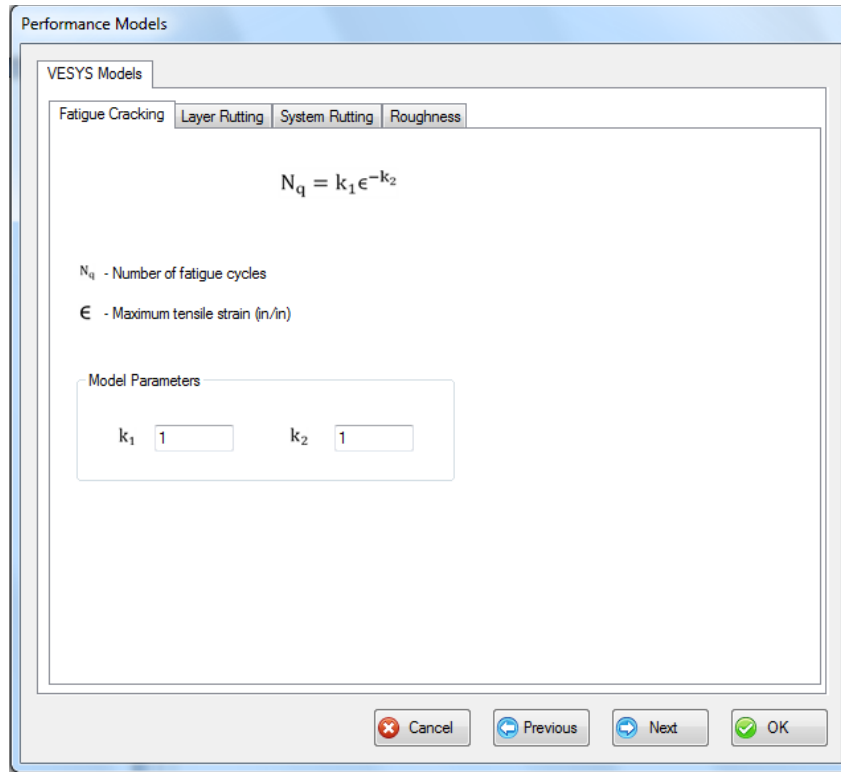


Figure VP3a.4. VESYS performance models.

For example, figure VP3a.5 shows the coordinates of the preset critical locations that are pertinent to the selected loading configuration, tire contact stress area, pavement structure, and failure modes. Those preset critical locations are automatically generated response points that cannot be deleted by the user. However, additional number of response points can be added by the user whenever desired. Similar analyses are being conducted for non-uniform contact stress distributions.

Assisted user's with issues ranging from usage questions, concepts clarifications, and bugs. The two major bugs reported by users were:

- Error in creating the Load and Materials file
- Error in creating the Master Curve

The *3D-Move Analysis* software developing team worked on fixing the reported bugs. Further details are presented below in the significant results section.

As mentioned in the last quarter, the effect of stress distributions and patterns as well as braking condition on pavement responses has been evaluated. The data has been analyzed and findings are summarized in the Master thesis: “Impact of Contact Stress Distribution and Pattern on Asphalt Pavement Performance Using 3D-Move Analysis Software.” Pavement responses were evaluated under the following stress distributions and patterns.

- Uniform pressure circular contact area
- Uniform pressure elliptical contact area
- Uniform pressure square contact area
- Non-uniform stress distribution

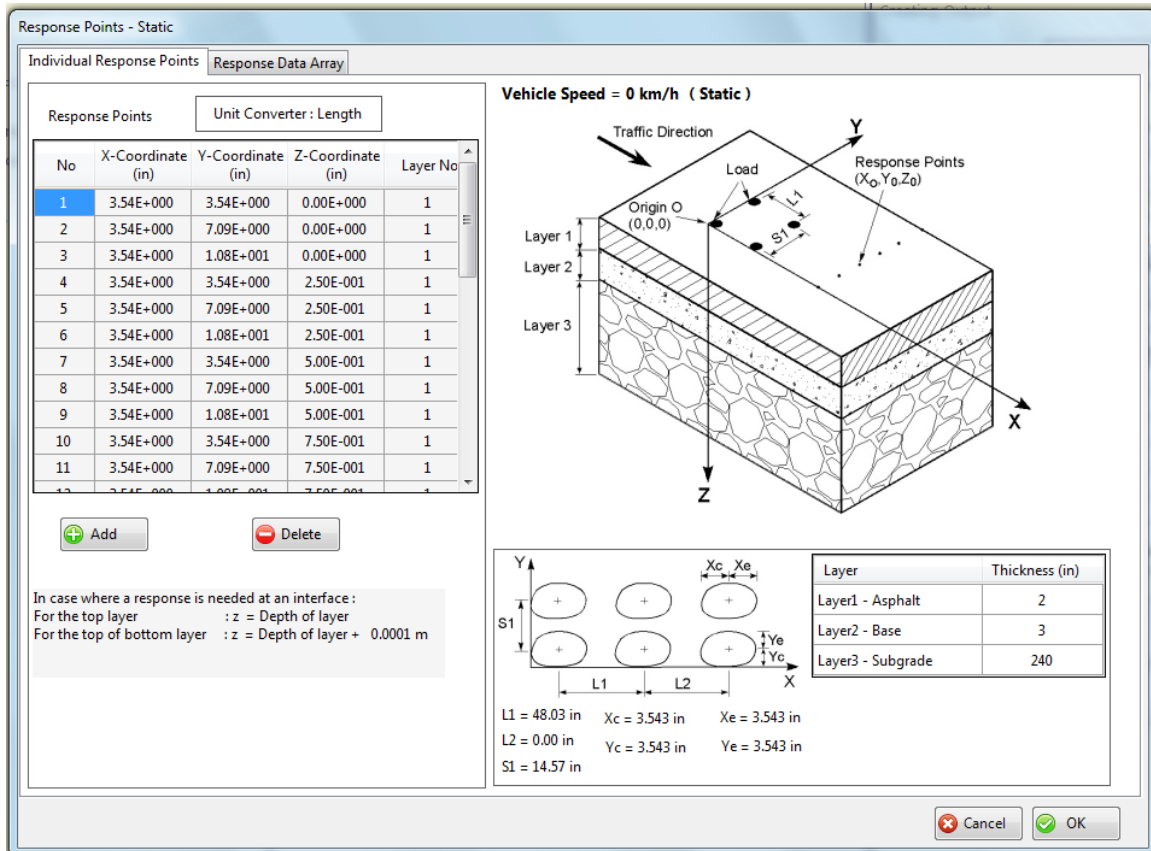


Figure VP3a.5. Response points window.

Significant Results

As an illustration, Master Curve development associated with Non-Symmetrical Sigmoidal Function and Symmetrical Sigmoidal Function (AMPT) are discussed in this report.

The bottom part of the figure VP3a.1 shows the inputs for the Non-Symmetrical Sigmoidal Function option. The principle advantage of Non-Symmetrical Sigmoidal Function over the symmetrical function is that greater flexibility exists in fitting non-symmetric master curve data. The inputs for this Master Curve option are dynamic modulus data, phase angle data, Poisson's ratio and binder data. Figure VP3a.1 shows the input window for dynamic modulus data. Next inputs are damping ratio and Poisson's ratio. Damping ratio can be given as a constant value or calculated from phase angle data (figure VP3a.6). As in Symmetrical Sigmoidal Function (MEPDG), this type of Master Curve also requires binder data. Binder data can be input in the

window shown in figure VP3a.7. Once these inputs are provided the program will generate the Master Curve. Figures VP3a.8 and VP3a.9 show the Master Curve generated for Non-Symmetrical Sigmoidal Function option at both the reference and analysis temperatures, respectively. To generate the Master Curve for this method, 3D-Move uses principal axis optimization methods.

Another option used in 3D-Move to generate the Master Curve is Symmetrical Sigmoidal Function (AMPT). The advantage of this method is that A and VTS values are not required to generate Master Curve. Instead of that, it requires VMA and VFA data. The bottom part of the figure VP3a.10 shows the inputs for the Symmetrical Sigmoidal Function (AMPT). The 3D-Move uses Levenberg-Marquardt optimization method to develop the Master Curve. Figure VP3a.11 shows the Master Curve generated for Symmetrical Sigmoidal Function (AMPT).

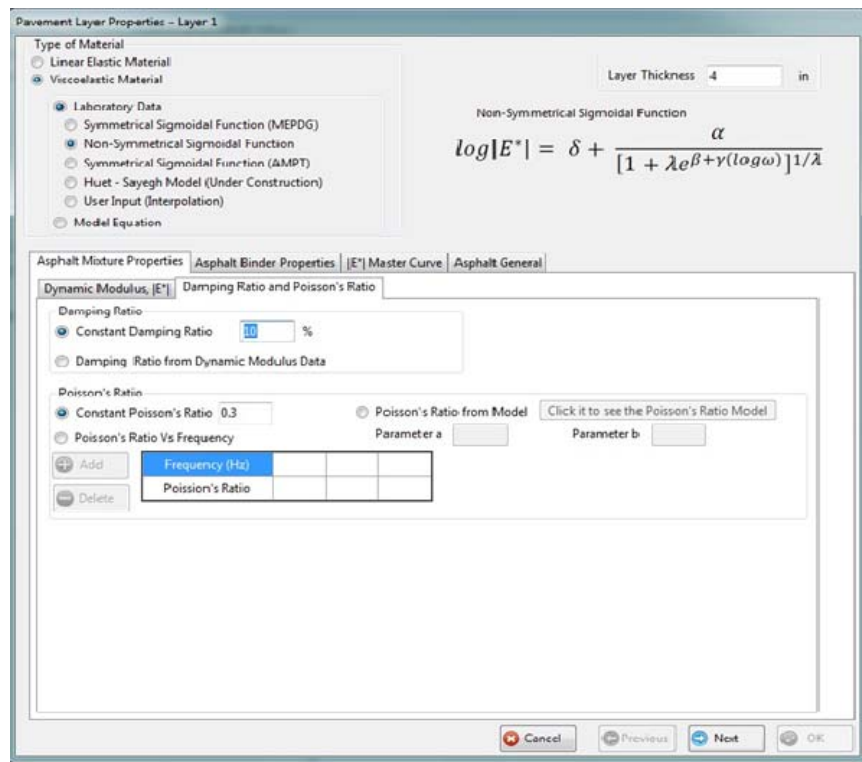


Figure VP3a.6. Non-Symmetrical Sigmoidal Function – Damping ratio and Poisson’s ratio input.

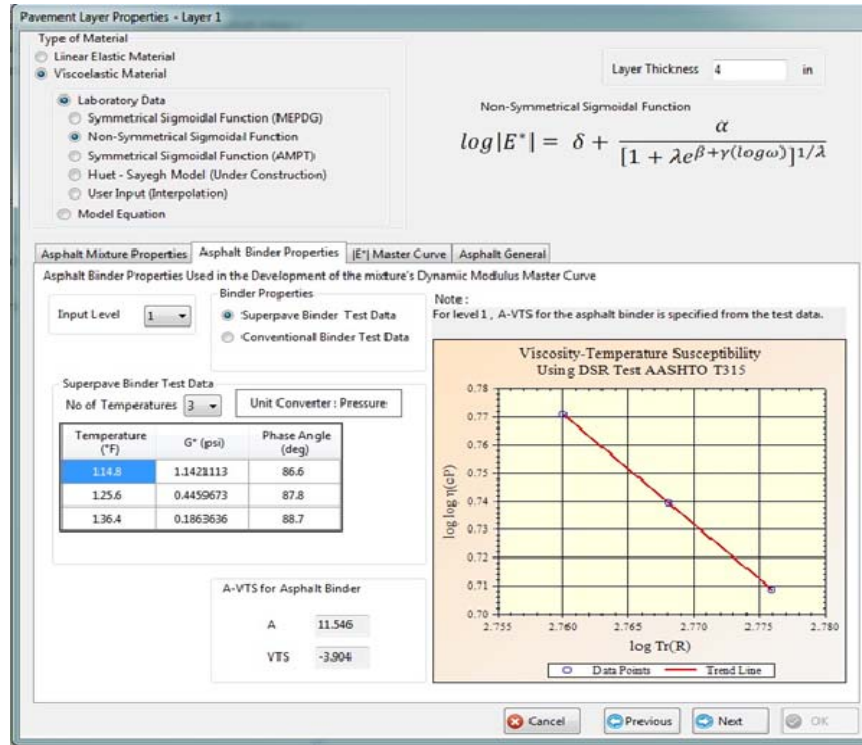


Figure VP3a.7. Non-Symmetrical Sigmoidal Function – Binder data input.

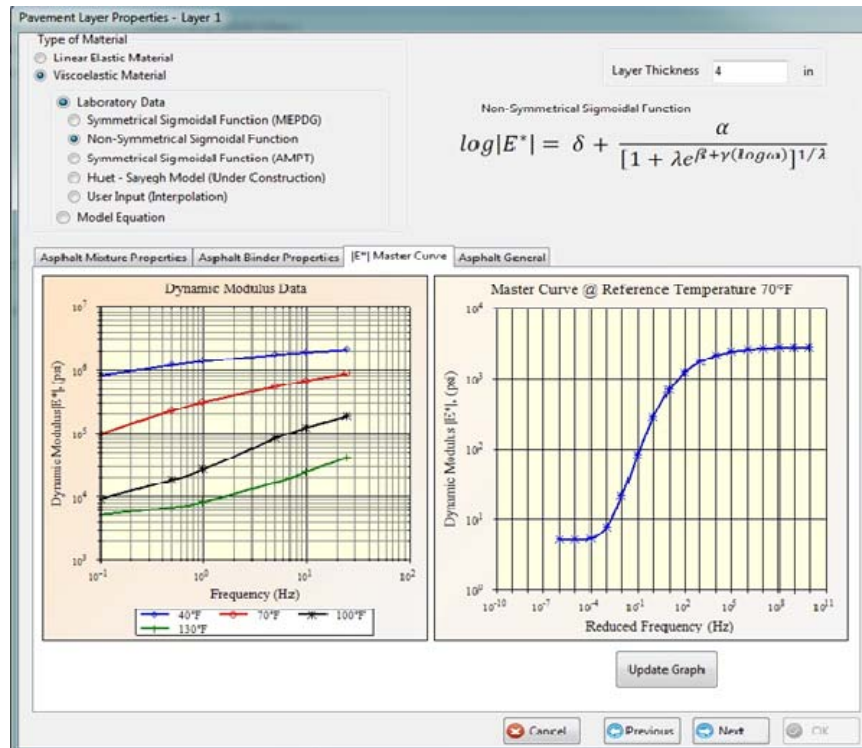


Figure VP3a.8. Non-Symmetrical Sigmoidal Function – Master curve for reference temperature.

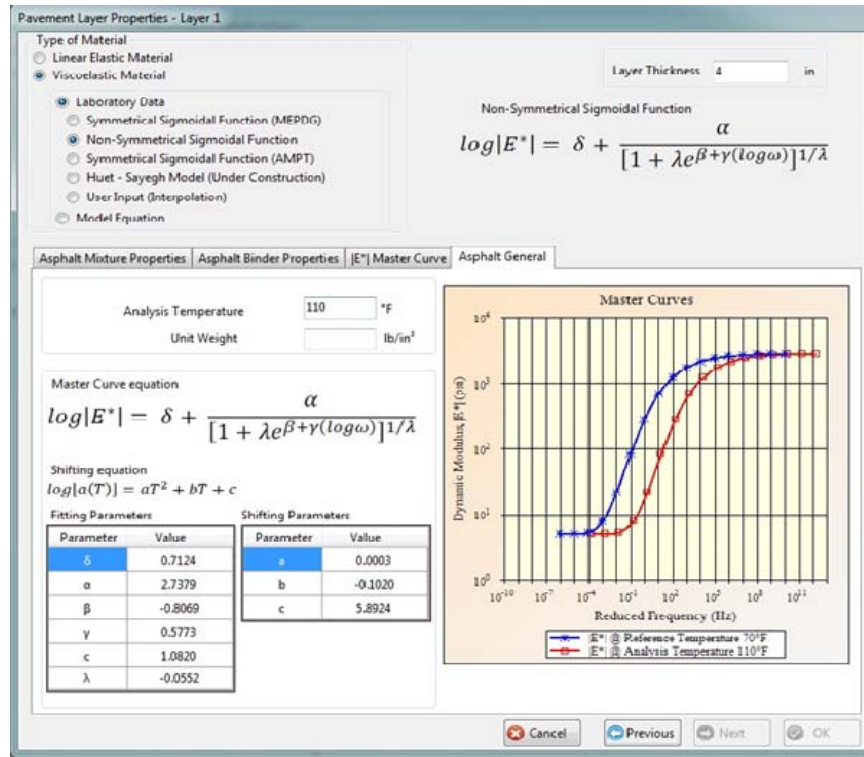


Figure VP3a.9. Non-Symmetrical Sigmoidal Function – Master curve for analysis temperature.

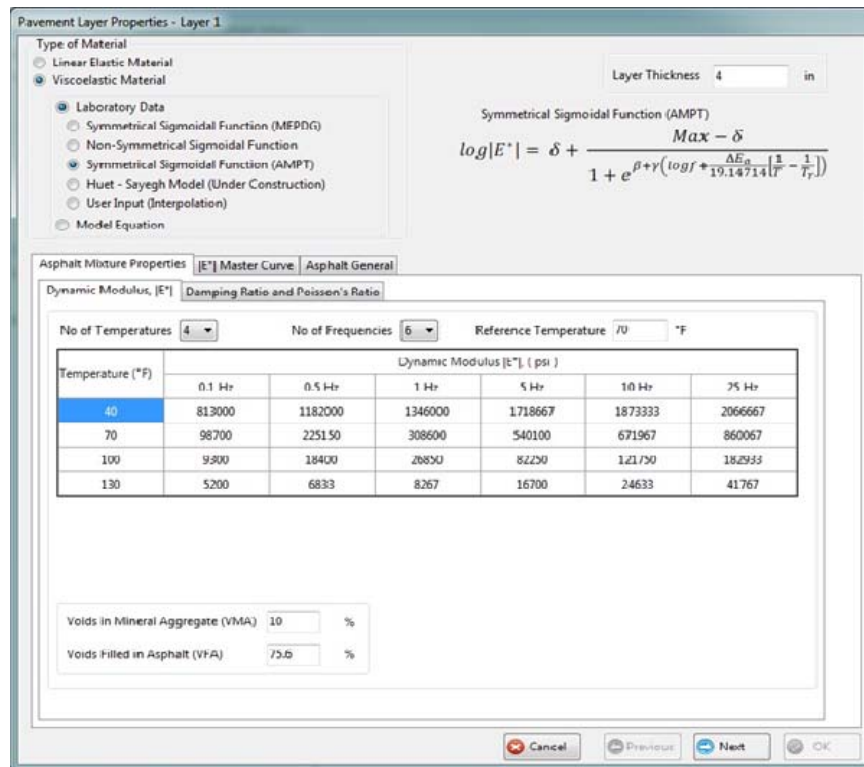


Figure VP3a.10. Symmetrical Sigmoidal Function (AMPT) – Dynamic modulus input.

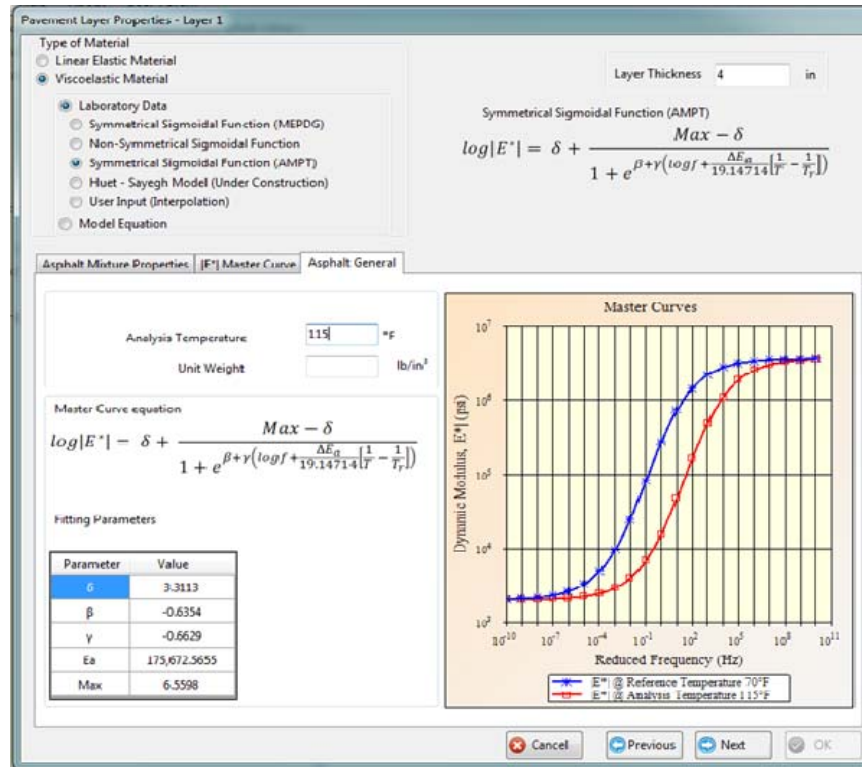


Figure VP3a.11. Symmetrical Sigmoidal Function (AMPT) – Master curve for reference temperature.

In this quarter, two major bugs were reported by *3D-Move Analysis* users and are discussed below:

Error in creating the Load and Materials file

One of the major bugs reported by some users is the error in creating the loading and materials data files as shown figure VP3a.12. This warning message was displayed while analyzing the problem in *3D-Move Analysis* ver. 1.2.

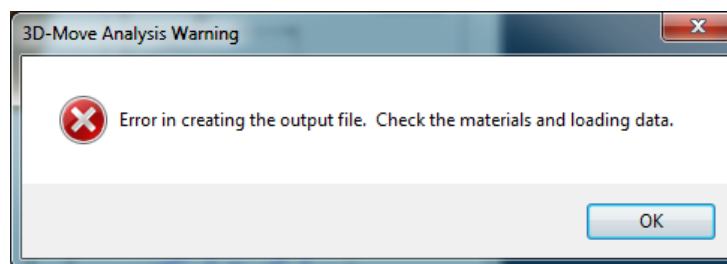


Figure VP3a.12. Warning message.

Usually, the *3D-Move Analysis* software creates many data files such as loading file, materials files, input files and output files. The program creates and saves the “loading data” and “materials data” files in temporary files so that they will be called back later on for the calculation process of the pavement responses. It was found that the warning message was displayed due to following two reasons:

- i. Error in creating the files in temporary directory in some of the computers.
- ii. Though files were created in temporary directory, program could not access those files in some computers due to the long file name and long path name.

This bug has been fixed in the newer version, will be released very soon, by assigning the appropriate file name and directory for the temporary files.

Error in creating the Master Curve

Another bug reported by some users is the error in developing a master curve. It was noticed that progress of master curve development was stopped at the 30% level when running the *3D-Move Analysis* in a 64 bit Windows operating system as shown in figure VP3a.13.

This error was due to the 32 bit and 64 bit compatibility issues. Furthermore *3D-Move Analysis* uses a 3rd party tool to develop the master curve. This tool is incorporated in *3D-Move analysis* as a dynamic link library (DLL) file. Whenever E* master curve is to be developed, program itself will call this DLL file to develop the master curve. The DLL file was created in 32 bit environment. But *3D-Move Analysis* ver. 1.2 was built to run as 32bit software in 32bit Windows operating system (OS) and 64bit software in 64bit Windows OS. That is why, when running the *3D-Move Analysis* in 64bit Windows OS, program will not support to run 32 bit DLL. This bug has been fixed in the newer version which will be released very soon.

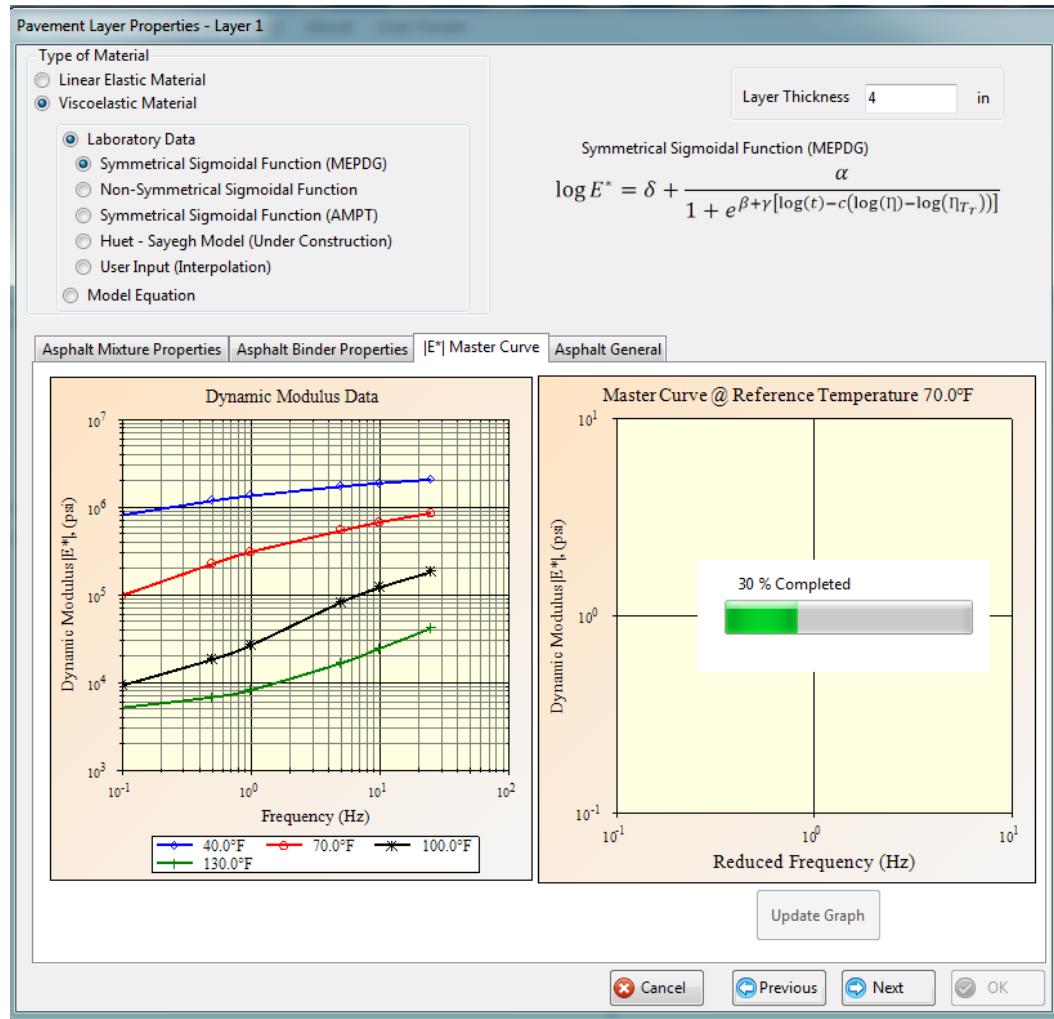


Figure VP3a.13. Window for developing E* master curve

The impact of the contact stress distributions and patterns on pavement responses and pavement performances were assessed based on the fatigue and rutting performance of asphalt pavements using the *3D-Move Analysis* Software. Four contact stress distributions were analyzed: non-uniform, uniform circular, uniform ellipse and uniform square. Three pavement structures were analyzed: thin, intermediate and thick. Two HMA mixtures, one is soft (Lockwood Source) and the other one is stiff (Sloan Source) in term of stiffness, were evaluated in this study. Pavement responses such as tensile strains at the bottom of the asphalt layer and vertical strain in the middle of the asphalt sub-layers were determined at the braking and non-braking condition. For the braking condition, the longitudinal shear stresses were estimated by multiplying the vertical stress distributions by the coefficient of friction at the tire pavement interface. Based on the generated data, the following preliminary conclusions can be made:

- A significant difference was observed between pavement critical responses computed with the non-uniform and uniform contact stress distributions.

- The non-uniform contact stress distribution resulted in lower maximum longitudinal tensile strains at the bottom of the HMA layer when compared to the uniform circle and uniform square contact stress distributions.
- The non-uniform contact stress distribution resulted in lower maximum transverse tensile strains at the bottom of the HMA layer when compared to the other three uniform contact stress distributions regardless of the asphalt layer thickness and mix type.
- The non-uniform contact stress distribution produced the lowest maximum vertical strains at all depths considered in the analysis.
- The uniform elliptical contact stress distribution produced lower longitudinal tensile strains at the bottom of the HMA layers for all cases, but it produced higher transverse tensile strains at the bottom of the HMA layers.
- For all three pavement structures, all uniform contact stress distributions produced very similar values for maximum vertical strains at the bottom of the HMA layer. The difference between the maximum vertical strains produced by the non-uniform and uniform contact stress distributions at a given depth reduces with depth below two inches from the surface. This indicates that the impact of the contact stress distribution is confined within the top 2 to 4 inches of the HMA layer.
- The difference among the maximum vertical strains produced by the non-uniform and uniform contact stress distributions at the bottom of the HMA layer reduces with the increase in the asphalt layer thickness.

Significant Problems, Issues and Potential Impact on Progress

The 3D-Move Analysis verification plan was postponed to solve the issues and bugs raised by the users, It is anticipated that a version 1.3 of the software be released in the next quarter that will address the various bugs.

Work Planned Next Quarter

Continue working on the 3D-Move model to make it a menu-driven software. Continue working on the performance evaluation subroutine. Continue to solve any issues and bugs that users may encounter. Release a version 1.3 of the software in the next quarter.

Work out the details for the *3D-Move Analysis* software verification plan in order to evaluate the potential for errors, bugs, and difficulties involved in using the software for pavement analysis purposes. UNR, with the help of FHWA, will solicit users to participate in the verification plan. It is anticipated that the list of participants will include:

- at least three representatives of public agencies,
- at least three representatives of academic researchers,
- at least three representatives of private industries, and
- at least one representative of FHWA.

Evaluate the accuracy of estimating the non-uniform contact stress distribution at a given load level from measured contact stress distributions using the linear interpolation/extrapolation.

Vehicle-Pavement Interaction Year 4	Year 4 (4/2010-3/2011)											Team	
	4	5	6	7	8	9	10	11	12	1	2		3
(1) Workshop													
VP1a: Workshop on Super-Single Tires													UNR
(2) Design Guidance													
VP2a: Mixture Design to Enhance Safety and Reduce Noise of HMA													UWM
VP2a-1: Evaluate common physical and mechanical properties of asphalt mixtures with enhanced frictional skid characteristics													
VP2a-2: Evaluate pavement macro- and micro-textures and their relation to tire and pavement noise-generation mechanisms													
VP2a-3: Develop a laboratory testing protocol for the rapid evaluation of the macro and micro-texture of pavements													
VP2a-4: Run parametric studies on tire-pavement noise and skid response						JP							
VP2a-5: Establish collaboration with established national laboratories specialized in transportation noise measurements. Gather expertise on measurements and analysis													
VP2a-6: Model and correlate acoustic response of tested tire-pavement systems						JP	P						
VP2a-7: Proposed optimal guideline for design to include noise reduction, durability, safety and costs													P
(3) Pavement Response Model Based on Dynamic Analyses													
VP3a: Pavement Response Model to Dynamic Loads													UNR
VP3a-1: Dynamic Loads													
VP3a-2: Stress Distribution at the Tire-Pavement Interface													
VP3a-3: Pavement Response Model										JP			
VP3a-4: Overall Model										SW			

Deliverable codes

- D: Draft Report
- F: Final Report
- M&A: Model and algorithm
- SW: Software
- JP: Journal paper
- P: Presentation
- DP: Decision Point

Deliverable Description

- Report delivered to FHWA for 3 week review period.
- Final report delivered in compliance with FHWA publication standards
- Mathematical model and sample code
- Executable software, code and user manual
- Paper submitted to conference or journal
- Presentation for symposium, conference or other
- Time to make a decision on two parallel paths as to which is most promising to follow through

	Work planned
	Work completed
	Parallel topic

Vehicle-Pavement Interaction Years 2 - 5

	Year 2 (4/08-3/09)				Year 3 (4/09-3/10)				Year 4 (04/10-03/11)				Year 5 (04/11-03/12)				Team
	Q1	Q2	Q3	Q4	Q1	Q2	Q3	Q4	Q1	Q2	Q3	Q4	Q1	Q2	Q3	Q4	
(1) Workshop																	
VP1a: Workshop on Super-Single Tires																	UNR
(2) Design Guidance																	
VP2a: Mixture Design to Enhance Safety and Reduce Noise of HMA																	
VP2a-1: Evaluate common physical and mechanical properties of asphalt mixtures with enhanced frictional skid characteristics				DP													UWM
VP2a-2: Evaluate pavement macro- and micro-textures and their relation to tire and pavement noise-generation mechanisms				DP													
VP2a-3: Develop a laboratory testing protocol for the rapid evaluation of the macro and micro-texture of pavements		M&A															
VP2a-4: Run parametric studies on tire-pavement noise and skid response						JP		D		JP							
VP2a-5: Establish collaboration with established national laboratories specialized in transportation noise measurements. Gather expertise on measurements and analysis																	
VP2a-6: Model and correlate acoustic response of tested tire-pavement systems										JP, P							
VP2a-7: Proposed optimal guideline for design to include noise reduction, durability, safety and costs													P				
(3) Pavement Response Model Based on Dynamic Analyses																	
VP3a: Pavement Response Model to Dynamic Loads																	
VP3a-1: Dynamic Loads			JP														UNR
VP3a-2: Stress Distribution at the Tire-Pavement Interface																	
VP3a-3: Pavement Response Model						SW, v. β					JP		SW, JP				
VP3a-4: Overall Model										SW			D	F			

Deliverable codes

- D: Draft Report
- F: Final Report
- M&A: Model and algorithm
- SW: Software
- JP: Journal paper
- P: Presentation
- DP: Decision Point

Deliverable Description

- Report delivered to FHWA for 3 week review period.
- Final report delivered in compliance with FHWA publication standards
- Mathematical model and sample code
- Executable software, code and user manual
- Paper submitted to conference or journal
- Presentation for symposium, conference or other
- Time to make a decision on two parallel paths as to which is most promising to follow through

	Work planned
	Work completed
	Parallel topic

PROGRAM AREA: VALIDATION

CATEGORY V1: FIELD VALIDATION

Work element V1a: Use and Monitoring of Warm Mix Asphalt Sections (WRI)

Work Done This Quarter

The monitoring sections at the Manitoba WMA site were established and the initial monitoring was conducted. Construction of the WMA sections was completed in July 2010. The first annual monitoring of the Manitoba RAP sections was conducted during the same trip. Manitoba Infrastructure and Transportation (MIT) personnel provided the traffic control and coring equipment and personnel. MIT personnel also conducted Falling-Weight Deflectometer (FWD) testing and longitudinal profiling of the WMA sections. The cooperation and interest of MIT continues to be outstanding.

Significant Results

None.

Significant Problems, Issues and Potential Impact on Progress

None.

Work Planned Next Quarter

No WMA pavement site monitoring is planned for the first quarter of 2011.

Work element V1b: Construction and Monitoring of Additional Comparative Pavement Validation Sites (WRI)

Work Done This Quarter

The first annual monitoring of the Manitoba RAP sections was conducted in October 2010. Manitoba Infrastructure and Transportation (MIT) personnel provided the traffic control and coring equipment and personnel. MIT personnel also conducted Falling-Weight Deflectometer (FWD) testing and longitudinal profiling of the both the WMA and RAP sections. No distress has occurred at the Manitoba RAP site after one year of service.

The Arizona comparative pavement site was monitored in December 2010. Differential performance of the different asphalt sources continues in approximately the same level as previously reported only pavement distress continues to increase in all sections. Core samples were obtained for continuation of the WRI aging study and also for mechanical testing.

Significant Results

None.

Significant Problems, Issues and Potential Impact on Progress

None.

Work Planned Next Quarter

No comparative pavement site monitoring is planned for the first quarter of 2011.

CATEGORY V2: ACCELERATED PAVEMENT TESTING

Work element V2a: Accelerated Pavement Testing including Scale Model Load Simulation on Small Test Track (WRI)

Work Done This Quarter

No activity this quarter. This work element was included in order to accommodate any accelerated testing that may occur during the project.

Significant Results

None.

Significant Problems, Issues and Potential Impact on Progress

None.

Work Planned Next Quarter

No accelerated (field) testing is planned.

Work element V2b: Construction of Validation Sections at the Pecos Research & Testing Center (WRI)

This work element is included to indicate that this may be a possibility for accelerated pavement testing for ARC research because it is a facility in the TAMU system.

CATEGORY V3: R&D VALIDATION

Work element V3a: Continual Assessment of Specifications (UWM)

Work Done This Quarter

The research team focused on several tasks this quarter. Through coordination with the Western Cooperative Test Group (WCTG), loose mix samples were received from a number of projects in which known modified binders were tested by WCTG. These mixtures are to be used in performance testing, which includes flow number, dynamic modulus and indirect tension fatigue tests. Of the 10 loose mix samples identified by WCTG for analysis, the research team has obtained seven samples. Of the seven samples, researchers have tested three mixes for flow number and dynamic modulus. Results from laboratory mixture testing will be related to concurrent round-robin binder testing administered by WCTG and the performance of mixtures placed in the field.

WCTG round-robin binder testing began in October 2010 and will continue through June 2011. Standard PG and PG-Plus binder tests, as well as other tests recently developed at UW–Madison, are used to characterize these binders. The Significant Results section presents data for all WCTG binders tested in 2010 and highlights the specifications and test methods that are being effectively deployed to laboratories.

Researchers continued to collaborate with WCTG and the Rocky Mountain Asphalt User Producer Group (RMAUPG) in efforts to evaluate PG-Plus specifications. The annual meeting of RMAUPG, held in October 2010, provided a forum for researchers to present current progress and reiterate ongoing strategies to evaluate specifications. Discussions held during the meeting identified several potential next steps.

Significant Results

Results from round-robin binder testing provide insight into the current efficacy of PG and PG-Plus specifications. Table V3a.1 details the number of labs participating in monthly binder testing and lists the PG grades tested. Participation in monthly testing is on a volunteer basis, thus the number of participating labs varies month to month. PG grades represent common grades used in practice and correspond to binders used in field projects. Of the nearly 70 labs represented in WCTG binder testing, over one-third of these labs participate on a regular basis. Note that for binder 510, two samples A and B were mistakenly distributed to labs rather than the standard single sample. As a result, binder 510 is treated as two binders in the analysis.

Table V3a.1. Summary of number of labs participating in WCTG binder testing.

Binder Code	Labs Responding	PG Grade
510A	15	70-22
510B	13	70-22
511A	40	64-28
512A	43	76-28
513A	19	64-22
514A	42	70-28
515A	24	64-34
516A	25	76-22

Table V3a.2 summarizes the list of test procedures and statistical results generated for standard PG tests. The statistics listed represent coefficients of variation (COV) calculated for the set of binders tested in one month by all participating labs. For example, in the case shown in table V3a.2, approximately 20 labs provided data for testing each of the eight binders listed in table V3a.1. The COV values vary by binder type; therefore, the maximum, minimum, average and median values of the COV for each binder test result are listed in the table.

Table V3a.2. Statistics for COV values of PG specifications.

Test	Maximum	Minimum	Average	Median
Viscosity, 20 rpm	11.4%	2.6%	5.6%	3.8%
Viscosity, 1 rpm	15.3%	5.0%	10.8%	11.5%
G*, Unaged	18.2%	2.1%	5.9%	3.0%
G*, RTFO @ PG Temp.	35.2%	4.4%	11.1%	6.4%
G*, RTFO @ PG - 6 °C Temp.	33.3%	3.6%	11.5%	6.2%
G*, PAV @ Intermediate Temp.	22.1%	4.8%	9.8%	9.1%
BBR Stiffness, 1 hr	13.6%	2.9%	7.3%	5.8%
BBS Stiffness, 24 hr	15.7%	3.8%	7.4%	6.5%
BBR m-Value, 1 hr	3.0%	1.5%	2.2%	2.1%
BBR m-Value, 24 hr	4.2%	1.4%	2.5%	2.2%
DTT Stress	26.3%	1.1%	13.5%	12.1%
DTT Strain	67.3%	24.1%	40.5%	36.8%
Maximum	67.3%	24.1%	40.5%	36.8%
Minimum	3.0%	1.1%	2.2%	2.1%

RTFO = rolling thin film oven. PAV = pressure aging vessel. BBR = Bending Beam Rheometer.
BBS = Bitumen Bond Strength. DTT = Direct Tension Test.

Table V3a.3 summarizes the PG-Plus test methods used by the group and the statistical results generated. It is clear that the COV values for the PG-Plus tests are much higher than the PG test results. With the exception of the elastic recovery test, very large COV values are reported, which raises serious concerns about the traditional PG-Plus tests as well as the more recently proposed Multiple Stress Creep and Recovery (MSCR) test. These large differences in COV

values as a function of binders suggest that additional measures are needed to reduce variability. The highest variability observed is for the MSCR test, for which the nonrecoverable creep compliance (J_{nr}) is considered at two stress levels and two temperatures.

Table V3a.3. Statistics for COV values of PG-Plus specifications.

Test	Maximum	Minimum	Average	Median
Ductility, Unaged	59.2%	9.2%	21.5%	15.2%
Ductility, RTFO	92.3%	13.4%	34.1%	17.0%
Toughness, Unaged	25.0%	9.3%	15.6%	14.3%
Tenacity, Unaged	79.5%	8.9%	33.3%	20.8%
Jnr, 3.2 kPa @ PG Temp.	131.5%	5.2%	39.1%	29.9%
Jnr, 3.2 kPa @ PG - 6 °C Temp.	42.0%	6.9%	23.6%	27.1%
Jnr, 10 kPa @ PG Temp.	105.7%	54.8%	72.5%	64.8%
Jnr, 10 kPa @ PG - 6 °C Temp.	113.3%	56.7%	74.7%	71.6%
% Rec, 3.2 kPa @ PG Temp.	64.8%	4.1%	28.4%	15.9%
% Rec, 3.2 kPa @ PG - 6 °C Temp.	67.4%	0.8%	15.9%	10.0%
% Rec, 10 kPa @ PG Temp.	61.7%	21.7%	41.9%	44.9%
% Rec, 10 kPa @ PG - 6 °C Temp.	188.2%	9.6%	43.7%	20.1%
% Elastic Recovery, 25 °C	17.0%	1.0%	6.4%	1.9%
Maximum	188.2%	56.7%	74.7%	71.6%
Minimum	17.0%	0.8%	6.4%	1.9%

% Rec = percent recovery.

During any given month, labs participating in binder testing contribute a collective set of data for a number of binders from which COV values for each test are calculated. Thus, results in tables V3a.2 and V3a.3 represent compiled results for the eight binders listed in table V3a.1. Low values of COV suggest that standardized test methods are well integrated into labs and do not vary by binder type, while high maximum COV values indicate that further investigation is needed to understand and reduce variability between labs for some binders.

Significant Problems, Issues and Potential Impact on Progress

As research personnel continue to analyze round-robin binder testing results, the publication of a related journal paper originally scheduled for November 2010 will be submitted and presented in ARC program Year 5. The Gantt chart for this work element has been updated to reflect this change.

Work Planned Next Quarter

The following activities are planned for the next quarter:

- *Mixture testing.* Efforts will focus on continuing compaction and testing of WCTG loose mix samples for dynamic modulus, fatigue and flow number. The research team anticipates having mixture testing data for eight samples by the end of the next quarter,

which will allow mixture test results to be linked to binder test results and eventually to field sections.

- *Binder testing* will continue through the next quarter on a monthly basis. Standard binder tests, PG-Plus tests and other tests being proposed by UW–Madison will be used to evaluate WCTG round-robin binders.
- *Monthly conference calls* will continue with the WCTG board to define research priorities and examine how testing protocols may be improved, including identifying sources of error and variability in PG-Plus testing, particularly for the MSCR test method.

Work element V3b: Validation of the MEPDG Asphalt Materials Models Using New MEPDG Sites and Selected LTPP Sites (UNR, UWM)

Subtask V3b-1: Design and Build Sections (Start Year 1, Year 2, and Year 3)

Subtask V3b-2: Additional Testing (Start Year 2, Year 3, and Year 4)

Work Done This Quarter

None

Significant Results

None

Significant Problems, Issues and Potential Impact on Progress

Only two agencies have committed to the construction of MEPDG sites: the Washoe RTC in northern Nevada in 2008, The South Dakota DOT in 2009/2010. The researchers are facing significant hesitation from the DOTs to use the MEPDG to design and construct HMA pavements. The level of this work element has been reduced.

Work Planned Next Quarter

None

Subtask V3b-3: Select LTPP Sections (Start Year 1 thru Year 5)

Work Done This Quarter

In this quarter, the research team completed testing 25 binders from the LTPP program using the Linear Amplitude Sweep (LAS) procedure at intermediate pavement temperatures. In the previous quarter, the LAS testing results for some LTPP binders did not show a clear relationship with field cracking data reported in the LTPP database. In an attempt to better represent field conditions, the LTPP binders were retested at the pavement intermediate temperature (IT) rather

than the PG intermediate grade. Retesting was conducted on all LTPP binders with a PG intermediate grade more than three degrees above or below the pavement IT defined based on weather data. Additionally, traffic data were incorporated in the correlation between laboratory and field measurements by normalizing cracked area by traffic.

Testing temperature is extremely important in the LAS test. The research team is currently working in the F2e work element on the implementation of a framework to take into account the effect of temperature on the fatigue law parameters A and B . The comparison between laboratory fatigue testing and field performance of LTPP binders indicates the importance of testing the binders at the intermediate measured pavement temperature rather than at the intermediate PG grade temperature if validation of LAS procedure with field performance must be addressed.

Significant Results

Table V3b-3.1 presents the analysis of the LAS results and fatigue field performance for the LTPP binders with the inclusion of traffic information.

Table V3b-3.1. LAS results for LTPP binders.

SHRP ID	PG grade	Climate Type	Fatigue Cracking/m ²	Traffic kESAL	Cracking /Traffic	Pavement IT (°C)	A ₃₅	B
090902	PG 64-28	WF	3.6	1072	3.36E-03	23	4.05E+06	-4.80
090903	PG 64-22	WF	5.1	1075	4.74E-03	23	3.29E+06	-4.70
090960	PG 58-28	WF	4.2	1076	3.90E-03	23	1.13E+06	-4.39
090962	PG 58-28	WF	6.9	1076	6.41E-03	23	1.71E+06	-4.31
120902	PG 64-16	WN	0.01	8361	1.20E-06	35.4	2.37E+06	-4.49
290963	PG 64-16	WF	91.5	1165	7.85E-02	24.8	1.37E+07	-5.42
300903	PG 64-22	DF	0.01	970	1.03E-05	17	5.76E+06	-5.28
310902	PG 58-22	DF	65.5	365	1.79E-01	25.4	1.27E+06	-4.67
310903	PG 64-28	DF	175.5	377	4.66E-01	25.4	2.36E+06	-4.86
340901	PG 64-22	WF	49.5	3518	1.41E-02	25	6.41E+06	-4.73
340902	PG 58-28	WF	11.4	3509	3.25E-03	25.2	1.88E+06	-4.47
340961	PG 78-28	WF	250.1	3513	7.12E-02	28	1.28E+07	-5.13
350902	PG 64-22	DN	19	6964	2.73E-03	33.1	1.81E+06	-4.80
350903	PG 58-22	DN	1.2	6971	1.72E-04	33.1	5.55E+05	-4.41
370901	PG 64-22	WN	37.7	2483	1.52E-02	30.7	5.03E+06	-4.55
370902	PG 64-22	WN	47.2	2490	1.90E-02	30.7	4.31E+06	-4.54
370903	PG 70-22	WN	83	2484	3.34E-02	30.7	3.81E+06	-4.65
370960	PG 76-22	WN	73.1	1867	3.92E-02	31	5.93E+06	-4.52
370962	PG 76-22	WN	0.01	1873	5.34E-06	31	4.96E+07	-4.69
370963	PG 64-22	WN	12.7	1877	6.77E-03	30.7	5.54E+06	-4.65
370964	PG 76-22	WN	51.1	1879	2.72E-02	31	4.49E+08	-5.00
370965	PG 70-22	WN	17.7	1880	9.41E-03	30.7	5.11E+06	-4.72
04B901	PG 76-10	DN	4.4	17981	2.45E-04	39.1	2.25E+06	-4.47
04B903	PG 70-10	DN	436.2	17973	2.43E-02	39.1	8.15E+05	-4.09
89A902	PG 52-40	WN	0.8	308	2.60E-03	14.4	5.99E+06	-5.46

DF = dry-freeze. WN = wet-nonfreeze. WF = wet-freeze. DN = dry-nonfreeze.
 kESAL = thousands of equivalent single-axle loads.

As shown in table V3b-3.1, there are some sections with very high cracking of 400+ linear m/m², and there are sections with no cracking at all. The traffic volume also varies significantly, from almost 18 million ESALs to less than 400,000 ESALs.

The initial analysis of the correlations of fatigue cracking normalized for traffic volume and the cycles to failure of binders at various strain levels estimated from LAS results do not show clear trends. It is expected that the analysis will continue next quarter with consideration given to

pavement structure and ranking of binders and performance. Analysis will also include careful evaluation of outliers and unique binders such as the PG 52-40, which shows the highest B value and a very low A_{35} value, and the PG 76-10, which has less than 5 linear m/m² cracking with almost 18 million ESALs.

Significant Problems, Issues and Potential Impact on Progress

None.

Work Planned Next Quarter

The research team will collect low-temperature cracking performance data from the LTPP database for the available binders. LTPP binders will be tested using the recently developed Single-Edge Notched Bending (SENB) test and comparison with field performance will be conducted.

Subtask V3b-5: Review and Revisions of Materials Models (Start Year 2, Year 3, Year 4, and Year 5)

The reader is referred to subtask V3b-1.

Subtask V3b-6: Evaluate the Impact of Moisture and Aging (Start Year 3, Year 4, and Year 5)

The reader is referred to subtask V3b-1.

Work Element V3c: Validation of PANDA (TAMU)

Work Done this Quarter

Please refer to the details presented in work elements M4c, F1d-8, and F3c. These work elements outline what has already been accomplished in validating the constitutive models that are implemented in PANDA as well as the validation work that will be carried out in the coming quarter.

We have developed the experimental setup that will be used to carry out the ARC 2x2 matrix validation plan. The experimental setup allows measuring radial and axial deformation under compression loading at different confining stresses and temperatures. The extension tests will be carried out at NCState.

Significant Results

See the significant results sections in work elements M4c, F1d-8, and F3c.

Significant Problems, Issues and Potential Impact on Progress

See the significant results sections in work elements M4c, F1d-8, and F3c.

Work Planned Next Quarter

Focus will be placed on validation of PANDA using the ARC 2x2 matrix validation plan and on the structural simulations of the ALF sections.

Work Element V3d: Engineered Properties Testing Plan (TAMU)

Work Done this Quarter

The work completed this quarter relates to work described in Work Elements F1b-2, F2c, and E1a.

Work Planned Next Quarter

Please refer to Work Elements F1b-2, F2c, and E1a.

Validation Year 4	Year 4 (4/2010-3/2011)												Team	
	4	5	6	7	8	9	10	11	12	1	2	3		
(1) Field Validation														
V1a: Use and Monitoring of Warm Mix Asphalt Sections														WRI
V1b: Construction and Monitoring of additional Comparative Pavement Validation sites														WRI
(2) Accelerated Pavement Testing														
V2a: Accelerated Pavement Testing including Scale Model Load Simulation on small test track (This work element will include all accelerated pavement testing)														WRI
V2b: Construction of validation sections at the Pecos Research & Testing Center														WRI
(3) R&D Validation														
V3a: Continual Assessment of Specification														UWM
V3a-1: Evaluation of the PG-Plus practices and the motivations for selecting the "plus" tests.								P						
V3a-2: Detailed analysis of all PG-Plus tests being proposed or in use today, documentation of benefits and costs of these tests, and comparison with new tests														
V3a-3: Development of protocols for new binder tests and database for properties measured					P									
V3a-4: Development of specification criteria for new tests based on field evaluation of construction and performance				P								JP		
V3a-5: Interviews and surveys for soliciting feedback on binder tests and specifications		P												
V3b: Validation of the MEPDG Asphalt Materials Models and Early Verification of Technologies Developed by ARC using new MEPDG Sites and Selected LTPP sites														UNR/UWM/ WRI
V3b-1: Design and Build Sections														UNR
V3b-2: Additional Testing (if needed)														
V3b-3: Select LTPP Sites to Validate New Binder Testing Procedures					DP	JP					P			UWM
V3b-4: Testing of Extracted Binders from LTPP Sections														
V3b-5: Review and Revisions of Materials Models														
V3b-6: Evaluate the Impact of Moisture and Aging														
V3c: Validation of PANDA														TAMU
V3d: Engineered Properties Testing Plan					P	JP(2)	P			JP	P			TAMU

Deliverable codes
D: Draft Report
F: Final Report
M&A: Model and algorithm
SW: Software
JP: Journal paper
P: Presentation
DP: Decision Point

Deliverable Description
Report delivered to FHWA for 3 week review period.
Final report delivered in compliance with FHWA publication standards
Mathematical model and sample code
Executable software, code and user manual
Paper submitted to conference or journal
Presentation for symposium, conference or other
Time to make a decision on two parallel paths as to which is most promising to follow through

Work planned
Work completed
Parallel topic

Validation Years 2 - 5	Year 2 (4/08-3/09)				Year 3 (4/09-3/10)				Year 4 (04/10-03/11)				Year 5 (04/11-03/12)				Team
	Q1	Q2	Q3	Q4	Q1	Q2	Q3	Q4	Q1	Q2	Q3	Q4	Q1	Q2	Q3	Q4	
(1) Field Validation																	
V1a: Use and Monitoring of Warm Mix Asphalt Sections																	WRI
V1b: Construction and Monitoring of additional Comparative Pavement Validation sites																	WRI
(2) Accelerated Pavement Testing																	
V2a: Accelerated Pavement Testing including Scale Model Load Simulation on small test track																	WRI
V2b: Construction of validation sections at the Pecos Research & Testing Center																	WRI
(3) R&D Validation																	
V3a: Continual Assessment of Specification																	UWM
V3a-1: Evaluation of the PG-Plus practices and the motivations for selecting the "plus" tests.		P	D,F														
V3a-2: Detailed analysis of all PG-Plus tests being proposed or in use today, documentation of benefits and costs of these tests, and comparison with new tests				P	D												
V3a-3: Development of protocols for new binder tests and database for properties measured						JP			P								
V3a-4: Development of specification criteria for new tests based on field evaluation of construction and performance					D		P	P			JP	P			JP		
V3a-5: Interviews and surveys for soliciting feedback on binder tests and specifications								P				P			D	F	
V3b: Validation of the MEPDG Asphalt Materials Models and Early Verification of Technologies Developed by ARC using new MEPDG Sites and Selected LTPP sites																	UNR/UWM
V3b-1: Design and Build Sections																	
V3b-2: Additional Testing (if needed)																	
V3b-3: Select LTPP Sites to Validate New Binder Testing Procedures						DP		P		JP, DP		P			D	F	
V3b-4: Testing of Extracted Binders from LTPP Sections																	
V3b-5: Review and Revisions of Materials Models																	
V3b-6: Evaluate the Impact of Moisture and Aging																	
V3c: Validation of PANDA																	TAMU
V3d: Engineered Materials Testing Plan										P(2)	JP	P					TAMU

Deliverable codes

- D: Draft Report
- F: Final Report
- M&A: Model and algorithm
- SW: Software
- JP: Journal paper
- P: Presentation
- DP: Decision Point

Deliverable Description

- Report delivered to FHWA for 3 week review period.
- Final report delivered in compliance with FHWA publication standards
- Mathematical model and sample code
- Executable software, code and user manual
- Paper submitted to conference or journal
- Presentation for symposium, conference or other
- Time to make a decision on two parallel paths as to which is most promising to follow through

- Work planned
- Work completed
- Parallel topic

PROGRAM AREA: TECHNOLOGY DEVELOPMENT

Work element TD1: Prioritize and Select Products for Early Development (Year 1) (AAT, WRI)

This work element has been completed.

Work element TD2: Develop Early Products (Year 3) (AAT, WRI)

Work Done This Quarter

Table TD2.1 summarizes the progress on the Products for Early Development. Work has been completed at WRI on the test method for Determination of Polymer in Asphalt. AAT completed a Draft AASHTO Standard for simplified continuum damage fatigue testing, but the procedure is being revised significantly based on the findings of the analyses being conducted in the continuum damage fatigue model refinement in Work Element E2e. Completion of the Draft AASHTO Standards for the other early technology development products were delayed to permit the research team to focus on other work. Table TD2.1 includes revised completion dates for these products.

Table TD2.1. Summary of progress on early development products.

Product	ARC Research Program	Format	Estimated Completion Data	ARC Partner	Draft AASHTO Standard?
Simplified Continuum Damage Fatigue Analysis for the Asphalt Mixture Performance Tester	Prior	Test Method	9/30/2011	AAT	Yes
Wilhelmy Plate Test	Prior	Test Method	Completed	TTI	Yes
Universal Sorption Device	Prior	Test Method	Completed	TTI	Yes
Dynamic Mechanical Analysis	Prior	Test Method	Completed	TTI	Yes
Automated Flocculation Titrimetric Analysis	Prior	Test Method	Completed	WRI	No (ASTM)
Determination of Polymer in Asphalt	Prior	Test Method	Completed	WRI	Yes

Work Planned Next Quarter

Work will continue of the five Products for Early Development listed in Table TD2.1 with estimated completion dates of 12/31/2010.

Significant Problems, Issues and Potential Impact on Progress

None.

Work element TD3: Identify Products for Mid-Term and Long-Term Development (Years 2, 3, and 4) (AAT, WRI)

This work element has been completed.

Work Element TD4: Develop Mid-Term and Long-Term Products (Years 3, 4, and 5) (AAT, WRI)

Work Done This Quarter

Dr. Bonaquist met with FHWA staff to review the mid-term and long-term technology development products. This review produced numerous comments on the products that the research team is currently responding to.

Work Planned Next Quarter

The research team will respond to the FHWA comments on the mid-term and long-term technology development products by January 31, 2011. Further work on these products will continue next quarter as revised based on the responses to the FHWA comments.

Significant Problems, Issues and Potential Impact on Progress

None.

PROGRAM AREA: TECHNOLOGY TRANSFER

CATEGORY TT1: OUTREACH AND DATABASES

Work element TT1a: Development and Maintenance of Consortium Website (Duration: Year 1 through Year 5) (UNR)

Work Done This Quarter

The ARC website was maintained and updated. The ARC quarterly technical progress report, July 1- September 30, 2010, was uploaded to the ARC website. The following references were updated:

- List of Publications and Conference Proceedings under the “Publications” webpage.
- List of Presentations and Posters under the “Outreach” webpage.

The 3D-Move Discussion Group Forum was also maintained.

Significant Results

None

Significant Problems, Issues and Potential Impact on Progress

None

Work Planned Next Quarter

Continue maintaining and updating the ARC website. Update the list of Publications and Conference Proceedings. Update the list of Presentations and Posters and the list of Theses and White Papers. Post information and new releases for 3D-Move. Maintain the 3D-Move Discussion Group Forum.

Work element TT1b: Communications (Duration: Year 1 through Year 5) (UNR)

Work Done This Quarter

None

Significant Results

None

Significant Problems, Issues and Potential Impact on Progress

None

Work Planned Next Quarter

Prepare and publish the eighth ARC Newsletter.

Work element TT1c: Prepare Presentations and Publications (All)

Presentations

Bahia, H., and R. Velasquez, “Understanding the Cause of Low Temperature Physical Hardening of Asphalt Binders.” Presented at the 55th Canadian Technical Asphalt Association Conference, Edmonton, Alberta, Canada, November 2010.

Clopotel, C., E. Mahmoud, and H. Bahia, “Modification of the Elastic Recovery Test and its Relationship to Performance Related Properties of Modified Asphalt Binders.” 90th Transportation Research Board Annual Meeting, accepted for poster presentation.

Hajj, E. Y., Updates on Laboratory Testing of RAP Mixtures from Manitoba Test Sections. Presented to the FHWA Expert Task Group on Recycled Asphalt Pavement (RAP), Oklahoma City, Oklahoma, October 26, 2010.

Han, Rongbin, Xin Jin, Yuanchen Cui, and Charles J. Glover. “Oxygen Diffusivity in Asphalts and Mastics,” presented at the 47th Annual Petersen Asphalt Research Conference, July 14, 2010.

Hanz, A., E. Mahmoud, and H. Bahia, “Asphalt Lubricity Test Evaluation and Relationship to Mixture Workability.” 90th Transportation Research Board Annual Meeting, accepted for presentation.

Jin, Xin, Rongbin Han, and Charles J. Glover. “A Fast-Rate - Constant-Rate Oxidation Model for Asphalt Binders,” presented at the 47th Annual Petersen Asphalt Research Conference, July 14, 2010.

Kalberer, Eric W., P. Michael Harnsberger, and A. Troy Pauli, “Reclaimed Asphalt Pavement Mixing and Compatibility” presented at the RAP Expert Task Meeting, October 26-27, 2010, Oklahoma City, OK.

Miller, T., and K. McKinney, “Asphalt Research Consortium Task Force Update: Current Efforts to Improve Specifications.” Presented at the Rocky Mountain Asphalt User Producer Group Annual Meeting, Colorado Springs, Colorado, October 13, 2010.

Prapaitrakul, Nikornpon, Rongbin Han, Xin Jin, and Charles J. Glover. “Transport Model Calculations of Asphalt Binder Oxidation in Pavements,” presented at the 46th Annual Petersen Asphalt Research Conference, July 14, 2009.

Prapaitrakul, Nikornpon, Rongbin Han, Xin Jin, and Charles J. Glover, "A Transport Model of Asphalt Binder Oxidation in Pavements," presented at the 3rd International Conference on Asphalt Materials, Qingdao, Shandong Province, China, August 6, 2009.

Publications

Clopotel, C., and H. Bahia, 2010, "Importance of Elastic Recovery in the DSR for Binders and Mastics." *Seventh International Conference on Road and Airfield Pavement Technology*, submitted.

Hajj, E. Y., A. Ullao, R. Siddharthan, and P. E. Sebaaly, 2011, "Estimation of Stress Conditions for the Flow Number Simple Performance Test," *Transportation Research Record*, 2181, TRB, Washington, D.C., pp. 67-78.

Hajj, E. Y., A. Ullao, R. Siddharthan, and P. E. Sebaaly, 2010, "Characteristics of the Loading Pulse for the Flow Number Performance Test," *J. of the Association of Asphalt Paving Technologists*, AAPT, Vol. 79, pp. 253-294.

Han, Rongbin, Xin Jin, Charles J. Glover. "Modeling Pavement Temperature for Use in Binder Oxidation Models and Pavement Performance Prediction," in press, *Journal of Materials in Civil Engineering*.

Han, R., Jin, X., and Glover, C.J., "Oxygen Diffusivity in Asphalts and Mastics," submitted to *Petroleum Sci. and Technol.*, December 2010.

Hanz, A., E. Mahmoud, and H. Bahia, 2010, "Impacts of WMA Production Temperature on Binder Aging and Mixture Flow Number." *86th Association of Asphalt Pavement Technologists Annual Meeting*, accepted.

Harnsberger, P. M., 2010, Half and Half. One year later, a mat with 50-percent RAP looks really good. *Better Roads*, December 2010, 18-21.

Harnsberger, P. M., M. J. Farrar, S-C. Huang, and R. E. Robertson, "Comparative Field Performance Using Asphalts from Multiple Crude Oil Sources." Submitted to *Transportation Research Board*, November 2010, accepted for presentation.

Hintz, C., R. Velasquez, C. Johnson, and H. Bahia, 2010, "Modification and Validation of the Linear Amplitude Sweep Test for Binder Fatigue Specification." *90th Transportation Research Board Annual Meeting*, accepted.

Hintz, C., R. Velasquez, Z. Li, and H. Bahia, 2010, "Effect of Oxidative Aging on Binder Fatigue Performance." *86th Association of Asphalt Pavement Technologists Annual Meeting*, accepted.

Jin, X., and Glover, C.J., “The Effect of Air temperature on Pavement Temperatures and Asphalt Oxidation Rates,” *Journal of Materials in Civil Engineering*, submitted December 2010.

Moraes, R., R. Velasquez, and H. Bahia, 2010, “Measuring Effect of Moisture on Asphalt-Aggregate Bond with the Bitumen Bond Strength Test.” *90th Transportation Research Board Annual Meeting*, accepted.

Pauli, A. T., R. W. Grimes, A. G. Beemer, J. J. Miller, J. D. Beiswenger, J. E. MacNaughton, T. F. Turner, and J. F. Branthaver. Morphology of Asphalts, Asphalt Chromatographic Fractions and Model Wax-doped Asphalts Studied in Thin-films by Atomic Force Microscopy. *International Journal of Pavement Engineering*. (Accepted for publication).

Prapaitrakul, Nikornpon, Rongbin Han, and Charles J. Glover (2009). “A Transport Model of Asphalt Binder Oxidation in Pavements,” *Road Materials and Pavement Design*, vol 10 Special Issue, p. 95-113.

Schmets, A., N. Kringos, T. Pauli, P. Redelius, T. Scarpas, 2010, On the Existence of Wax-induced Phase Separation in Bitumen. *International Journal of Pavement Engineering*, 11(6), 555–563.

Schuster, W. C., J. M. Wolf, and F. P. Miknis, 2010, Phosphorus-31 NMR Studies of MnRoad Test Track Cells. Submitted to *Road Materials and Pavement Design*, September 2010, in review.

Sui, C., M. J. Farrar, P. M. Harnsberger, W. H. Tuminello, and T. F. Turner, “A New Low-temperature Performance Grading Method Using 4 mm Parallel-plates on a DSR.” Submitted to Transportation Research Board, November 2010, accepted for presentation.

Velasquez, R., H. A. Tabatabaee, and H. U. Bahia, 2010, “Low Temperature Cracking Characterization of Asphalt Binders by Means of the Single-Edge Notch Bending (SENB) Test.” *86th Association of Asphalt Pavement Technologists Annual Meeting*, accepted.

Zhang, Y., R. Luo, and R. L. Lytton, 2010, Microstructure-Based Inherent Anisotropy of Asphalt Mixtures. Submitted to *Journal of Materials in Civil Engineering*, American Society of Civil Engineers (ASCE).

Work element TT1d: Development of Materials Database (Duration: Year 2 through Year 5) (UNR)

Work Done This Quarter

The following list describes the work items completed or in progress this quarter:

- Bulk Editor
- Validation Sites
- File Management

- Property Sorting and Copying
- Component Material Filter and other Enhancement to Materials Management.
- Production Database Migration

Significant Results

Property Measures – Bulk Editing

As discussed in the last report, the database now includes multi-dimensional properties, allowing the user to specify one or two additional dimensions for a property, along with default values. The last report demonstrated a template for the measure entry form for these properties, but the ability to create, edit, and delete the data was not fully implemented. This form is now complete; its function and feedback features mirroring those of the simple properties on the bulk entry form. While this interface is designed to appear similar to the bulk editing features demonstrated in last report, the programming presented specific challenges that precluding simple duplication of previous efforts. Therefore, this module required significant development time. In addition, groups of measures can be copied based on a particular test run using a feature described as replicant measures. This requested feature allows repeated measures to be created for the same property of a given material, which may vary over time or other conditions. This feature augments the default behavior of the form, which automatically generates a single field for each property. As discussed in the previous report, the ability to replicate all measures for a material is provided through the creation of multiple” test runs”. Figure TT1d.1 shows part of the user interface to create replicant measures.

PAV_DT_FAILURE_STRESS	<input type="text" value="0"/>	kPa	<input checked="" type="checkbox"/>	<input type="text" value="9/9/2010"/>	<input type="checkbox"/>
PAV_DT_FAILURE_STRAIN	<input type="text"/>	%	<input type="checkbox"/>	<input type="text"/>	<input type="checkbox"/>
SPECIFIC_GRAVITY	<input type="text"/>		<input type="checkbox"/>	<input type="text"/>	<input checked="" type="checkbox"/>
SPECIFIC_GRAVITY	<input type="text"/>		<input type="checkbox"/>	<input type="text"/>	<input type="checkbox"/>
<input type="button" value="Copy Date To Selected"/> <input type="button" value="Create Replicant for Selected"/> <input type="button" value="Delete Selected"/> <input type="button" value="Update Group"/>					

Figure TT1d.1. Bulk Editor – Replicant measures.

Validation Sites

The implementation of validation sites is complete and has been integrated with the concept of a test run so that materials used in a validation site can be traced back to their origin.

File Management

Significant progress has been made on the file management subsystem. In the initial design, we anticipated that a few files and reports would be uploaded to supplement the data recorded in the database. However, subsequent discussions revealed that many support files would be uploaded to the system. In addition, these files would need to be linked to multiple research results. As a result, the file management sub system has been reengineered.

Initially, the file upload system was flat. In other words, all uploaded files were stored in a single directory (folder). This implementation was not sufficient to store the number of files expected to be uploaded. Thus, a component was developed allowing users to create folders on the server to store files and group them based on a particular research topic or work item. The implementation of this directory management system is complete. The preceding change required that the indexing system used to reference files be updated. The implementation of this indexing system is complete.

The final component of the file upload system requires that links be created to files such that multiple links can point to the same file. Development of this final component is underway and will be completed this quarter along with the relevant help pages.

Property Sorting and Copying

Part of the planned work for this quarter was the creation of a new form to aid the data administrator in controlling how properties are applied to materials and displayed on the measure editing forms. This work is complete. The form displays properties corresponding to a particular material type. The form is made up of repeating grids such that there is one grid per material. The buttons on the form allow properties to be copied such that the same set of properties is duplicated from one material category to another. A Help page was also created for this form. Figure TT1D.2 shows the Property Sorting and Copying form.

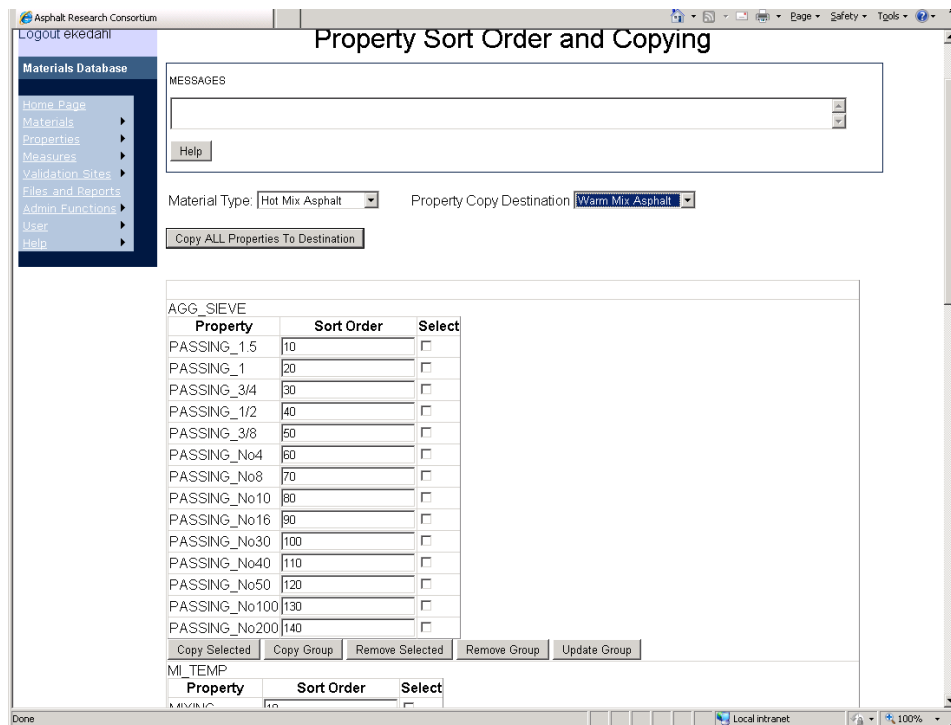


Figure TT1d.2. Property Sorting and Copying form.

Component Material Filter

A feature requested by the ARC team was the ability to view all of the materials that contain a specific component material. For example, one might wish to see the results of every application (use) of a particular binder. This capability was achieved by adding a second material selector embedded in the primary selector for choosing a component material by which to filter. This second selector has the same filtering tools as the primary selector so as to allow navigation of any number of records. To avoid confusion and clutter, this filter and other filters are hidden until their corresponding boxes are checked. In addition, the help page was revised significantly to account for the form's changes and expanded features. Figure TT1d.3 shows the revised Material form with the Component Material Filter displayed.

The screenshot shows a web form with a header containing three checkboxes: Work Tasks, Validation Sections, and Component Material. Below this is a section titled "Select Component Material" enclosed in a red border. This section contains four dropdown menus: Material Type (set to "Binder"), Material Category (set to "[ALL]"), Primary Organization (set to "University of Nevada, Renc"), and Supplier (set to "[ALL]"). Below the dropdowns are two checkboxes: Work Tasks and Validation Sections. A "Refresh Material List" button is positioned below these checkboxes. At the bottom of the red-bordered section is a list of material codes: BI 0011 UNR (McA), BI 0051 UNR (highlighted with a mouse cursor), BI 0052 UNR (PAR), BI 0063 UNR, and BI 0066 UNR.

Figure TT1d.3. Revised Materials form.

All materials have a primary organization attached, but it was agreed that certain core materials should not be associated with a particular organization, and should be clearly distinguishable. The option to assign "ARC" as a primary organization has been added. This "primary organization" will automatically append "CORE" to a material wherever it is displayed, and will allow simple retrieval of core materials through all filtering tools. Figure TT1d.4 shows the pseudo "ARC" organization.

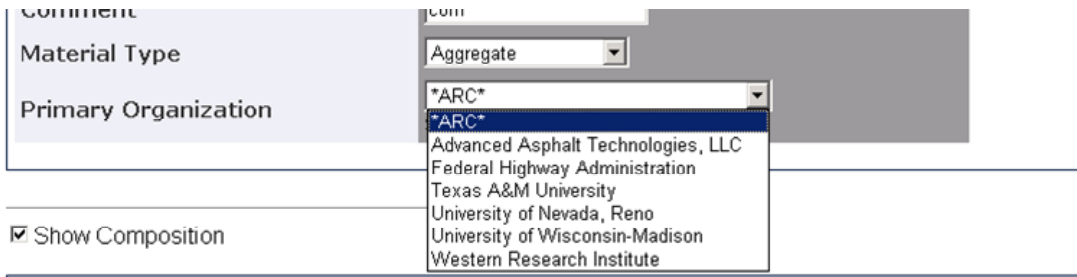


Figure TT1d.4. Pseudo-organization.

An addition to the database structure was required to meet the need for associating materials which have the same composition but differ by mix type. This feature will allow easy comparison of properties for these materials. Figure TT1d.5 shows the new mix type feature.

Show Mix Type and Material Grouping

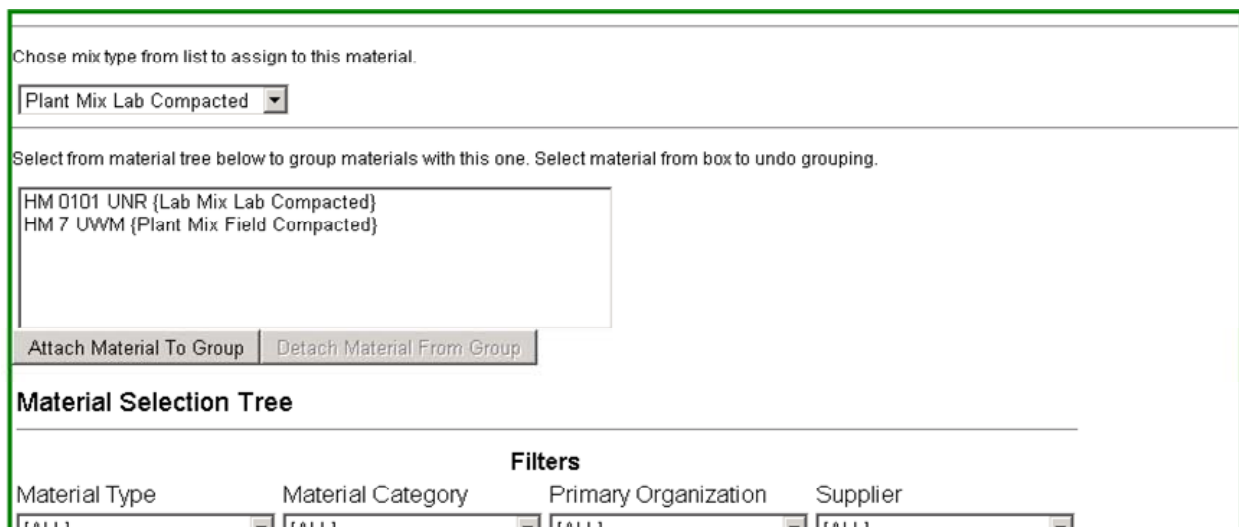


Figure TT1d.5. Mix Type and Material Grouping.

Production Database Migration

At this point in the development process, the database schema is relatively static. Minor modifications might be necessary to extend a feature or fix usability. Thus, during this quarter, the production database has been installed and most test data deleted. Entry of production data is underway.

In addition, both the test and production versions of the ARC database were migrated to a new larger machine so as to improve overall performance. The end users of the system will not see any effect from these changes other than improved performance.

Measure Browser

With the database and data entry components essentially complete, we are now developing tools for flexible data retrieval for use by consortium members and by the general public. The existing measure editing forms already allow for retrieval of results for a given material, but another utility is needed to compare results across properties.

The measure viewer form will allow retrieval of measures with maximum flexibility and filtering power. Every measure in the database can be analyzed at once, or the results can be filtered by virtually any dimension. Because each measure has a flag for "Final Results," the user has the option to retrieve only the most meaningful data. Optional summary statistics give a quick overview, and the user can drill down to the specifics of each measure. A number format selector allows the display to be adjusted, with 3 decimal places being the default.

This form and the measure editing form can have their features restricted and simplified for use by the public. However, another more specialized form for public consumption may also be desired once it becomes clear how the data may best be shared. See work planned for the next quarter.

Also under consideration is a material comparison utility which could facilitate direct comparison of the results of 2 or more materials, e.g., mix type variants of materials with the same composition, or materials sampled at different times.

Significant Problems, Issues and Potential Impact on Progress

None

Work Planned for Next Quarter

We feel that the implementation of the database is nearly complete allowing users to enter all research results. Our work plan for the next quarter is made up of four primary goals:

- The first involves fixing any small bugs found as a result of acceptance testing.
- The second is to design the system that will be seen by the general public to access the data created by the consortium researchers. This development is underway with the measure browser, which is currently under construction.
- The third is to conduct a database teleconference training. A tentative date for the training is February 24, 2011. It is anticipated that the teleconference training will precede the database workshop planned to take place in Reno Nevada around April, 2011.
- The fourth is to develop training materials for the upcoming spring 2011 workshop.

Work element TT1e: Development of Research Database (Duration: Year 2 through Year 5) (UNR)

Work Done This Quarter

Uploaded the quarterly technical progress report to the ARC website. Updated the “Publications” and “Outreach” web pages.

Significant Results

None.

Significant Problems, Issues and Potential Impact on Progress

None.

Work Planned Next Quarter

Upload the ARC quarterly technical progress report to the ARC website. Publish the ARC newsletter on the ARC website.

Work Element TT1f: Workshops and Training (UNR lead)

Work Done This Quarter

No activity this quarter.

Significant Results

None

Significant Problems, Issues and Potential Impact on Progress

None

Work Planned Next Quarter

Database training via Teleconference.




Technology Transfer Year 4	Year 4 (4/2010-3/2011)											Team	
	4	5	6	7	8	9	10	11	12	1	2		3
(1) Outreach and Databases													
TT1a: Development and Maintenance of Consortium Website													UNR
TT1b: Communications													UNR
TT1c: Prepare presentations and publications													UNR
TT1d: Development of Materials Database													UNR
TT1d-1: Identify the overall Features of the Web Application													
TT1d-2: Identify Materials Properties to Include in the Materials													
TT1d-3: Define the Structure of the Database													
TT1d-4: Create and Populate the Database													
TT1e: Development of Research Database													UNR
TT1e-1: Identify the Information to Include in the Research Database													
TT1e-2: Define the Structure of the Database													
TT1e-3: Create and Populate the Database													
TT1f: Workshops and Training													UNR

Deliverable codes

D: Draft Report
 F: Final Report
 M&A: Model and algorithm
 SW: Software
 JP: Journal paper
 P: Presentation
 DP: Decision Point

Deliverable Description

Report delivered to FHWA for 3 week review period.
 Final report delivered in compliance with FHWA publication standards
 Mathematical model and sample code
 Executable software, code and user manual
 Paper submitted to conference or journal
 Presentation for symposium, conference or other
 Time to make a decision on two parallel paths as to which is most promising to follow through

 Work planned
 Work completed
 Parallel topic

Technology Transfer Years 2 - 5

	Year 2 (4/08-3/09)				Year 3 (4/09-3/10)				Year 4 (04/10-03/11)				Year 5 (04/11-03/12)				Team
	Q1	Q2	Q3	Q4	Q1	Q2	Q3	Q4	Q1	Q2	Q3	Q4	Q1	Q2	Q3	Q4	
(1) Outreach and Databases																	
TT1a: Development and Maintenance of Consortium Website																	UNR
TT1b: Communications																	UNR
TT1c: Prepare presentations and publications																	ALL
TT1d: Development of Materials Database																	UNR
TT1d-1: Identify the overall Features of the Web Application																	
TT1d-2: Identify Materials Properties to Include in the Materials Database																	
TT1d-3: Define the Structure of the Database																	
TT1d-4: Create and Populate the Database							SW, v, β	SW									
TT1e: Development of Research Database																	UNR
TT1e-1: Identify the Information to Include in the Research Database																	
TT1e-2: Define the Structure of the Database																	
TT1e-3: Create and Populate the Database																	
TT1f: Workshops and Training																	UNR

Deliverable codes

D: Draft Report
 F: Final Report
 M&A: Model and algorithm
 SW: Software
 JP: Journal paper
 P: Presentation
 DP: Decision Point

Deliverable Description

Report delivered to FHWA for 3 week review period.
 Final report delivered in compliance with FHWA publication standards
 Mathematical model and sample code
 Executable software, code and user manual
 Paper submitted to conference or journal
 Presentation for symposium, conference or other
 Time to make a decision on two parallel paths as to which is most promising to follow through

 Work planned
 Work completed
 Parallel topic